DEVELOPMENT OF THE HOLOCENE CAÑADA HONDA FOSSIL REEF, DOMINICAN REPUBLIC: SHORT AND LONG-TERM RESPONSES TO HIGH SEDIMENTATION

By

David N. Cuevas Miranda

A thesis submitted in partial fulfillment of the requirements for the degree of

Doctor in Philosophy

in

MARINE SCIENCES

(Geological Oceanography)

UNIVERSITY OF PUERTO RICO-MAYAGÜEZ CAMPUS

2010

Approved by:

Paul M. Yoshioka, Ph.D. Member, Graduate Committee	Date
Ernesto Weil, Ph.D. Member, Graduate Committee	Date
Wilson Ramírez Martínez, Ph.D. Member, Graduate Committee	Date
Dennis K. Hubbard, Ph.D. Member, Graduate Committee	Date
Clark E. Sherman, Ph.D. President, Graduate Committee	Date
Fernando Gilbes Santaella, Ph.D. Representative of Graduate Studies	Date
Nilda E. Aponte, Ph.D. Chairperson of the Department	Date

ABSTRACT

The Holocene Cañada Honda (CH) fossil reef, located in southwestern Dominican Republic, provides a unique opportunity to examine a well-preserved fossil coral reef that thrived in a high-sedimentation environment between 9,000 to 5,000 years ago. Assessments of coral species abundance, morphology, age, and distribution, as well as characterization of reef sediment, were made to determine the paleoenvironment of reef accretion. Also, measurements of coral growth rates from the corals *Montastraea faveolata* and *Siderastrea siderea* were conducted and comparisons made with growth rate data of these same species from modern coral reefs throughout the Caribbean. Evidence for high sedimentation comes from the relatively high abundance of sediment-tolerant coral species, the tendency of these to form almost monospecific stands, and the propensity of individual colonies to grow as encrusting, dome-shaped, platy-like forms resulting in the development of ragged-margins or the so-called "stack of pancakes" morphology. Sediment incorporated into coral skeletons supports the idea of siltation stress during the accretion of the reef. Calibrated radiocarbon ages of fossil corals range from 9,256±137 to 6,737±94.5 BP. Correlation of radiocarbon ages with well-established Holocene sea-level curves indicates that most corals on this reef developed at depths between 10m to 12m. Measured growth rates in *Siderastrea siderea* (0.2-0.4 cm/yr) and *Montastraea faveolata* (0.09-0.44 cm/yr) are relatively low compared with growth rates from modern reef sites, indicating reduced light intensity caused by turbidity and coral growth at depths near 12 m. Reef sediment is characterized by more than 85% carbonate material. A significant portion of the carbonate is allochtonous and was derived from nearby Neogene limestones. The reef was able to survive under high-sedimentation conditions because the high carbonate content of incoming terrigenous sediment would have allowed better light penetration and probable sporadic storms that would have provided intervening low-sedimentation periods during which reef corals could respond and grow back, keeping-up with sedimentation. This study illustrates, once again, the presence of highly resilient coral communities under multiples conditions of natural disturbance.

RESUMEN

El arrecife de coral fósil del Holoceno en la localidad de Cañada Honda (CH), en el suroeste de la República Dominicana, ofrece una oportunidad única de examinar un arrecife de coral bien preservado que prosperó en un ambiente de alta sedimentación entre 9,000 a 5,000 años atrás. Se realizó una evaluación de la abundancia de especies de corales, su morfología, edad, distribución así como caracterización del sedimento para de esta forma determinar el paleoambiente de acreción del arrecife. También se midieron las tasas de crecimiento en corales de las especies *Montastraea faveolata* y *Siderastrea siderea* las cuales fueron posteriormente comparadas con las tasas de crecimiento de estas mismas especies pero en ambientes modernos de todo el Caribe. La evidencia de alta sedimentación se indica por la alta abundancia de especies tolerantes a la sedimentación, la tendencia de éstas a formar agrupaciones casi monoespecíficas y su crecimiento en forma de domo o plato incrustrado que con el tiempo asemeja una "pila de panqueques". Se encontró sedimento incorporado dentro del esqueleto de varios corales lo cual demuestra niveles elevados de estrés en el desarrollo del arrecife de CH. Datación calibrada de corales fósiles con radiocarbono indica edades entre 9,256±137 a 6,737±94.5 BP. Correlación de las edades de radiocarbono con curvas de nivel del mar indica que la mayoría de los corales en CH crecieron en profundidades entre 10m y 12m. Las tasas de crecimiento en *Siderastrea siderea* (0.2-0.4 cm/año) y *Montastraea faveolata* (0.09-0.44 cm/año) son relativamente bajas comparadas con las tasas de crecimiento en arrecifes modernos y sugieren que los mismos crecieron en aguas turbias y a profundidades cerca de los 12m donde la intensidad de luz es menor. El sedimento del arrecife se caracteriza por contener más de 85% $CaCO_3$, la mayoría de origen terrígeno proveniente de las calizas del Neógeno adyacentes a la Cuenca de Enriquillo. El arrecife de CH pudo sobrevivir bajo condiciones de alta sedimentación debido al alto contenido de $CaCO_3$ del sedimento terrígeno que permitió una mejor penetración de luz y al hecho de que los eventos de precipitación pudieron haber sido esporádicos permitiendo así el crecimiento y proliferación de los corales durante los periodos de baja sedimentación. De esta manera el arrecife pudo continuar a pesar de la alta sedimentación y el rápido crecimiento del nivel del mar. Una vez más se demuestra la existencia de sistemas de arrecifes bajo múltiples condiciones naturales de disturbio y con comunidades altamente duraderas.

To Almighty God, who gives me the inspiration, the strength and courage to persevere. To my lovely wife Esther, my son David José and daughters Karina and Mariana who always trust in me. I also dedicate this to my nation, the one that lives deep within the roots of my soul. Yes, it is possible!

Acknowledgements

During the development of my graduate studies in the University of Puerto Rico several persons and institutions collaborated directly and indirectly with my research. Without their support it would be impossible for me to finish my work. That is why I wish to dedicate this section to recognize their support. First, my entire family and friends which one way or another is always there for me. I am deeply grateful with the staff of the Puerto Rico Seismic Network who provided a job and financial support for me and my family throughout most of this quest. This study has been funded by doctoral fellowships from the NASA-Puerto Rico Space Grant, AGEP and EPSCoR programs from the Resource Center for Science and Engineering (RCSE) of the University of Puerto Rico (NSF Grant No. 0302696) and a graduate student grant from the southeastern section of the Geological Society of America, as well as from the Center for Research and Development of UPR-Mayagüez, and the Sea Grant College Program at UPR-Mayagüez. Special thanks to the Faculty of Arts and Sciences, the Department of Marine Sciences, the Department of Geology at UPR-Mayagüez, the Petroleum Research Fund, the American Chemical Society and the Sociedad Dominicana de Geología (SODOGEO) that have provided funding for travel, facilities and technical equipment for much of the analyses completed and to Dr. Jack Morelock which kindly provided useful reef data from SW Puerto Rico. I am also very grateful to my advisors and members of the thesis committee for their constructive criticism and advice. Also, the staff of Hospital San Antonio in Mayagüez that helped with the X-ray radiographies, Jessica Oram, Timmons Erickson, Allicia Davis and all the students from Oberlin College for their assistance in the field, Mónica del Coro, Vanessa Rosario, Viviana Díaz and Elisa Torres for laboratory analyses at UPR-Mayagüez, the Secretaría de Estado y Ambiente of the Dominican Republic and all the staff of Hotel Iguana in La Descubierta, Dominican Republic.

TABLE OF CONTENTS

1.0 Statement of the problem 1
- 1.1 Coral reefs in decline 1
- 1.2 Objectives 6

2.0 Study site 8
- 2.1 Enriquillo Basin 8
- 2.2 Modern Reefs, Southwestern Puerto Rico 12

3.0 Methodology 14
- 3.1 Community structure analyses 14
  - 3.1.1 Stratigraphy/community structure over time 14
  - 3.1.2 Chain or paleoreef surface transect-Community structure at a point in time 16
- 3.2 Coral sample analyses 18
  - 3.2.1 Coral Growth Rates 18
  - 3.2.2 Radiocarbon dates 18
  - 3.2.3 Petrographic analyses of corals 21
- 3.3 Sediment analyses 21
  - 3.3.1 Sediment composition 21
  - 3.3.2 Sediment characterization 23
    - 3.3.2.1 X-Ray Diffraction Analyses 24
    - 3.3.2.2 Constituent grain analyses 25
- 3.4 Comparison with modern reefs 25

4.0 Results 27
- 4.1 Community structure 27
  - 4.1.1 Cañada Honda Fossil Reef 27
  - 4.1.2 Coral cover along paleoreef surface 30
  - 4.1.3 Coral morphologies 32
  - 4.1.4 Comparison of coral abundances with modern coral reefs 33
- 4.2 Coral growth rates 37
- 4.3 Petrographic analyses of corals 41
- 4.4 Radiocarbon ages 42
- 4.5 Sediment analyses 46
  - 4.5.1 Sediment composition 46
  - 4.5.2 Sediment grain size 46
  - 4.5.3 XRD analyses 49
  - 4.5.4 Constituent grain characterization 53

5.0 Discussion 56
- 5.1 The Cañada Honda Fossil Reef Development 56
- 5.2 Lessons from Cañada Honda in terms of applicability to modern reef studies 67

TABLE OF CONTENTS

6.0 Summary and conclusions 72

7.0 Literature Cited 74

Appendix A. X-Ray Powder Diffraction Data.. 81

LIST OF TABLES

Table 1	Taphonomical criteria developed to determine if fossil corals were alive or dead at the time of burial	17
Table 2	Distribution (% counts) of coral species and sediment in Cañada Honda	28
Table 3	Coral species parameters calculated from Cañada Honda and the different coral zones	28
Table 4	Summary of data collected (%) along chain-transects over paleoreef surface	31
Table 5	Summary of coral morphology distribution along Cañada Honda (% counts)	34
Table 6	Relative coral species abundances (%) from Cañada Honda and modern reefs (spatially averaged) in SW Puerto Rico	35
Table 7	Results of measurements of coral growth rates from Cañada Honda	38
Table 8	Some coral growth rate data for *Montastraea annularis*, *Montastraea faveolata* and *Siderastrea siderea* in the Caribbean	39
Table 9	Petrographic descriptions of thin-sections from corals sampled in Cañada Honda	43
Table 10	Summary of calibrated radiocarbon ages from coral samples in Cañada Honda	45
Table 11	Results of sediment composition analyses from Cañada Honda reef sediment and Las Clavellinas	47
Table 12	Grain size in sediment samples from CH and Las Clavellinas	48
Table 13	Summary of XRD results on whole samples of reef sediment from Cañada Honda	50
Table 14	Summary of XRD results on sieved reef sediment samples from CH and Las Clavellinas	51
Table 15	Summary of constituent grain abundances (%) from reef sediment from Cañada Honda and sediment from Las Clavellinas	55

LIST OF FIGURES

Figure 1.1 (A) Map of the Caribbean region with location of Hispaniola. (B) Map of the Enriquillo Lake area showing location of the Cañada Honda fossil reef. Black-colored areas represent land below present sea level. Dashed line represents location of the Enriquillo Fault Zone (EFZ) 4

Figure 1.2 Photograph of a portion of the Cañada Honda outcrop showing a sedimentary horizon. These deposits are characterized by reworked bivalve, gastropod and coral fragments (mostly *Madracis* sp.) and can be traced tens of meters throughout the outcrop 5

Figure 2.1 North-South cross section across Hispaniola showing major morphotectonic features of the island (from Draper et al. 1994). The Enriqillo-Plaintain Garden Fault Zone (EPGFZ) is still active and was responsible for the January 12, 2010 (Mw 7.0) earthquake in Haiti.......... 9

Figure 2.2 Tectonic map of the Northern Caribbean Plate Boundary (from Mann et al. 2002). EPGF= Enriquillo-Plantain Garden Fault 9

Figure 2.3 Simplified north-South cross-section across the Enriquillo Basin illustrating the general geology of the area with emphasis on the characteristic terrigenous sedimentation from high-relief mountains........ 10

Figure 2.4 Google Earth image of northern shore of Lago Enriquillo near Cañada Honda. The white line highlights the drainage path and the limits of an alluvial fan 11

Figure 2.5 Photograph (looking North) of a portion of the Las Clavellinas outcrop showing alternating beds of *Acropora cervicornis* and fluvial sand and silt. Location of sediment sample LCS-4 is shown (yellow dot).............. 11

Figure 2.6 Map of the coastline of southwestern Puerto Rico summarizing the conclusions of coral reef areas (Modified from Morelock et al. 2001). Lower coral cover characterizes reef impacted by elevated sedimentation (Añasco, Mayagüez, Guayanilla, Ponce) 13

Figure 3.1 Photograph of quadrat used along the vertical transects. Constituents were counted at 100 intersections of a ten-by-ten cm grid within a meter-square PVC frame placed on the vertical exposures....................... 15

Figure 3.2 Photograph illustrating placement of meter-squared quadrats along vertical transects over exposed fossil reef wall in Cañada Honda............ 15

LIST OF FIGURES

Figure 3.3 Photograph of a portion of the Cañada Honda reef outcrop illustrating a surface buried by detritus generated over a short period of time. This provides a "time line" that can be used to make spatial comparisons with measurements on modern reefs. The "chain method" was employed to collect quantitative data along a synchronous paleoreef surface 17

Figure 3.4 Cross-section of the Cañada Honda fossil reef (modified from Hubbard et al. 2005) showing location of transects and corals sampled for growth rate (closed circles and squares) and radiocarbon analyses (stars). Facies determinations are based on the spatial distribution of coral species and their relative abundances within the counted quadrats... 19

Figure 3.5 Negative images of X-Ray radiographs from three of the corals analyzed. White line represents axis where growth measurements were obtained. A) *M. faveolata* sample M2-11; B) *S. siderea* sample MZ-12; C) *M. faveolata* sample PZ-01. High-density bands are dark colored 20

Figure 3.6 Cross-section of the Cañada Honda fossil reef (modified from Hubbard et al. 2005) showing location of transects and location of sediment samples. Facies determinations are based on the spatial distribution of coral species and their relative abundances within quadrats 22

Figure 3.7 Photograph of a portion of the Las Clavellinas outcrop showing sequence of sand and silt underlying a bed of *A. cervicornis*. Two of the sediment samples samples are shown by yellow hexagons 23

Figure 4.1 Cross-section of the Cañada Honda fossil reef (modified from Hubbard et al. 2005) showing location of transects and corals sampled for growth rate analyses. Facies determinations are based on the spatial distribution of coral species and their relative abundances within counts 29

Figure 4.2 Distribution of major coral species with elevation (below MSL) along the Cañada Honda fossil reef 29

Figure 4.3 Coral cover distribution throughout paleoreef surface 32

LIST OF FIGURES

Figure 4.4 Coral cover by species in “live” and “dead” assemblages on paleoreef surface 32

Figure 4.5 Dominant coral morphologies from the Cañada Honda fossil reef 34

Figure 4.6 Comparison of major coral species abundances from Cañada Honda and southwestern Puerto Rico 36

Figure 4.7 (A) Negative image of the X-Ray radiography of coral sample Pz-01 showing thin denser bands that correspond to thin sediment layers shown on photograph of the same sample (B) 40

Figure 4.8 Depth range and growth rate data for *Montastraea annularis* and *Montastraea faveolata* from the Caribbean and Cañada Honda. HS refers to data gathered from high sedimentation sites. Gray rectangle was placed to emphasize the range of values from Cañada Honda. Note that all samples from Cañada Honda have growth rates similar to rates reported for Caribbean reefs in greater than 12m of water 40

Figure 4.9 Depth range and growth rate data for *Siderastrea siderea* from the Caribbean and Cañada Honda. HS refers to data gathered from high sedimentation sites. Gray rectangle was placed to emphasize the range of values from Cañada Honda 41

Figure 4.10 Thickness of coral bands against radiograph from sample Pz-01 (*M. faveolata*). Notice reduced growth (thickness) where sediment bands occur. Below is a microphotograph of the bands showing location of sediment (black) 44

Figure 4.11 Correlation of calibrated radiocarbon ages from Cañada Honda with the corrected Holocene sea-level curve of Toscano and Macintyre (2003). The vertical difference between the elevation of the sample and sea level at the time it was alive (example in red for M1-5) yields the paleodepth of the coral 45

Figure 4.12 Relative average abundance (%) of constituent grains in CH reef sediment 53

Figure 4.13 Relative abundances of sediment, bivalve and coral fragments in Cañada Honda sediment samples 54

LIST OF FIGURES

Figure 5.1 Model for the formation of ragged margins in coral colonies and the development of the so-called “stack of pancakes” morphology in CH due to the occurrence of multiple high-sedimentation events (From Hubbard et al. 2005) 59

Figure 5.2 Sedimentary processes within the paleo-Enriquillo Bay illustrating a general model for the mineralogy of sediment based on provenance 62

1.0 Statement of the problem

1.1 Coral reefs in decline

Over the past three decades, a decline in reef coral abundance and diversity has been observed globally (Hughes, 1994; Hughes and Connell, 1999). Increased ocean temperatures are commonly mentioned as responsible for widespread and longstanding coral bleaching episodes and the recurrence of coral diseases (Carpenter et al., 2008), while increased atmospheric CO_2 concentrations reduce seawater pH and carbonate ion concentrations inhibiting the potential of corals and other marine calcifiers to produce skeletons (Kleypas et al., 2001; Fabry et al., 2008). These effects are locally exacerbated by overfishing, excessive nutrients from discharges of sewage and industrial waste into the ocean, and high terrestrial sediment-runoff and resuspension caused by increased coastal and agricultural development (Cortés and Risk, 1985; Edinger et al., 1998; 2000). The latter effects have contributed to widespread coral mortality, reduced coral cover and diversity, explosion in the number of bioeroders, out-competition by macroalgae, shading, smothering, and reduce coral growth (Hughes, 1994; Hughes and Connell, 1999).

There is still a major debate regarding the specific roles that anthropogenic and natural disturbances play in the current trend of reef decline. The majority of studies come from modern reef sites, many of them affected to a great extent by anthropogenic disturbance (e.g. Cortés and Risk, 1985; Scoffin, 1986; Edinger et al., 1998, 2000). However, is possible that even the earliest detailed studies on modern reefs come from already disturbed sites (Jackson, 1997). Another complication is that the short and long-term response of already stressed coral reefs is non-linear and it may take decades to observe recovery, if any. Thus, it is imperative to document changes in coral reef structure over longer periods of time (i.e. centennial to millennial) in order to make a comparable distinction between natural disturbances and anthropogenic-related disturbances. It is necessary that such record can be traced back before anthropogenic factors began to influence the site. The fossil record provides very useful information that can shed light on how coral reefs varied and responded to natural changes prior to anthropogenic-induced disturbances. If fine-scale changes documented over the past twenty to thirty years are shown to be unique, then human impact comes as a reasonable explanation. Otherwise, human interference must be considered in the context of longer-term, natural changes.

This kind of approach has been implemented in several studies (e.g. Aronson et al., 1998 and 2002) where it was found that most of the changes observed in coral reefs for the past three decades are unique at least in the last 4,000 years. Other studies from the southern Caribbean have found a persistence of the coral community structure over several thousands years in fossil reefs as old as 500,000 years BP (Pandolfi and Jackson, 2006). In a different study, this time from the Great Barrier Reef in Australia, Smithers and Larcombe (2003) reported that inner reef systems have been influenced by fine-grained terrigenous sedimentation their entire history (1,200 calibrated years before present) and even with the increase in sedimentation after European settlement, the reefs hold a diverse community with coral cover above 50% (Perry et al., 2008). These are just examples of the numerous studies around the world where fossil reef data have been gathered allowing the establishment of a pre-anthropogenic baseline from which modern comparisons can be made.

There are, nonetheless, some pitfalls that if not considered properly could lead to erroneous interpretations of the fossil reef information. These problems arise from the nature of the fossil reef and the way data is gathered. For example, there is plenty of data that can be obtained from Pleistocene terraces (e.g. Pandolfi and Jackson, 2006). Due to their age, however, there is the potential for substantial diagenesis which is a source for larger isotopic-age errors and alteration of the original character and composition of reef sediment. On the other hand, Holocene reefs are much younger and the diagenetic potential is much less than their Pleistocene counterparts. The character of the sediment and skeletal material may still be unaltered and more accurate radiometric ages can be obtained. However, because most Holocene reefs are still below sea level, data comes from boreholes which results in lower spatial resolution and potential loss of material during the drilling process. In addition, there are Pleistocene coral species that became extinct prior to the Holocene, thus differences in community structure can be revealed. This is particularly evident in the Caribbean where coral species such as the organ-pipe *Montastraea* and *Styllophora* spp. which were common in the Pleistocene, but are no longer found in the Holocene (Budd, 2000; Pandolfi and Jackson, 2001). Additional things to consider about fossil reefs are that they only represent what is preserved, which is only a fraction of the whole universe of marine organisms present in coral reefs. Furthermore, a particular transect in a fossil reef might not corresponds to the particular "snapshot" that characterizes the living coral reef (Pandolfi, 2002). On the contrary, multiple timelines can be represented in a single layer of a fossil reef. It is a "temporally averaged fossil community, an amalgam of multiple single populations in living reefs" (Pandolfi, 2002).

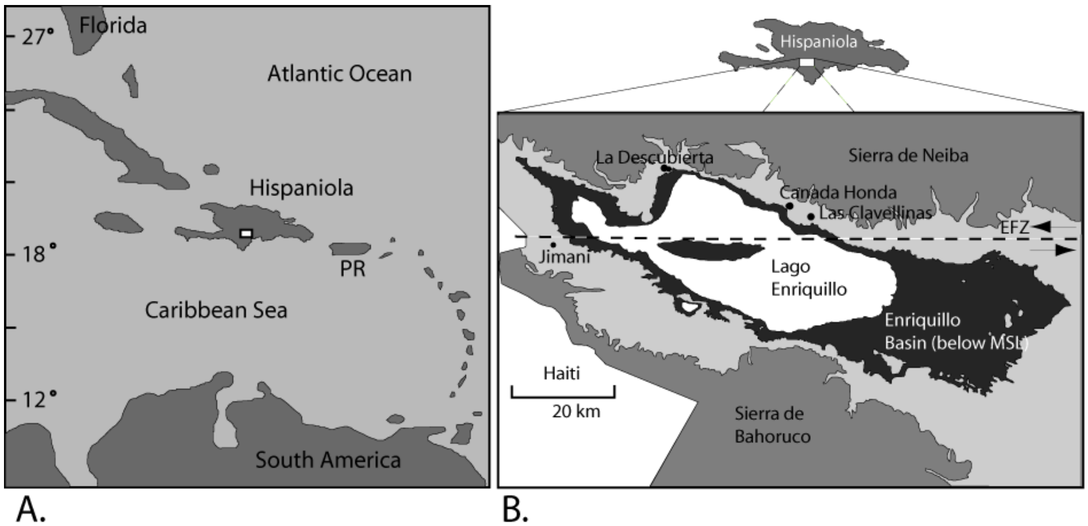

Figure 1.1 (A) Map of the Caribbean region with location of Hispaniola. (B) Map of the Enriquillo Lake area showing location of the Cañada Honda fossil reef. Black-colored areas represent land below present sea level. Dashed line represents location of the Enriquillo Fault Zone (EFZ).

Although most modern sites under high terrestrial runoff reflect substantial coral degradation, other sites (e.g. Great Barrier Reef) reveal adaptations of the reef coral organisms to such detrimental conditions (Smithers and Larcombe, 2003; Perry et al., 2008). Most of these sites occur in areas with a long history of terrestrial sedimentation prior to European settlement (Perry et al., 2008) or where terrestrial sedimentation is not accompanied by high nutrients levels (Edinger et al., 2000). Thus, it is known that coral reefs can develop in sites with high terrestrial runoff. Several questions remain. Why are most modern coral reef sites under high terrestrial runoff generally highly deteriorated? How can we separate natural versus anthropogenically induced sedimentation? Are there "good" fossil analogues?

This study is based on the subaerially exposed Cañada Honda (CH) fossil coral reef in southwestern Dominican Republic (Figure 1.1). It provides a unique opportunity to

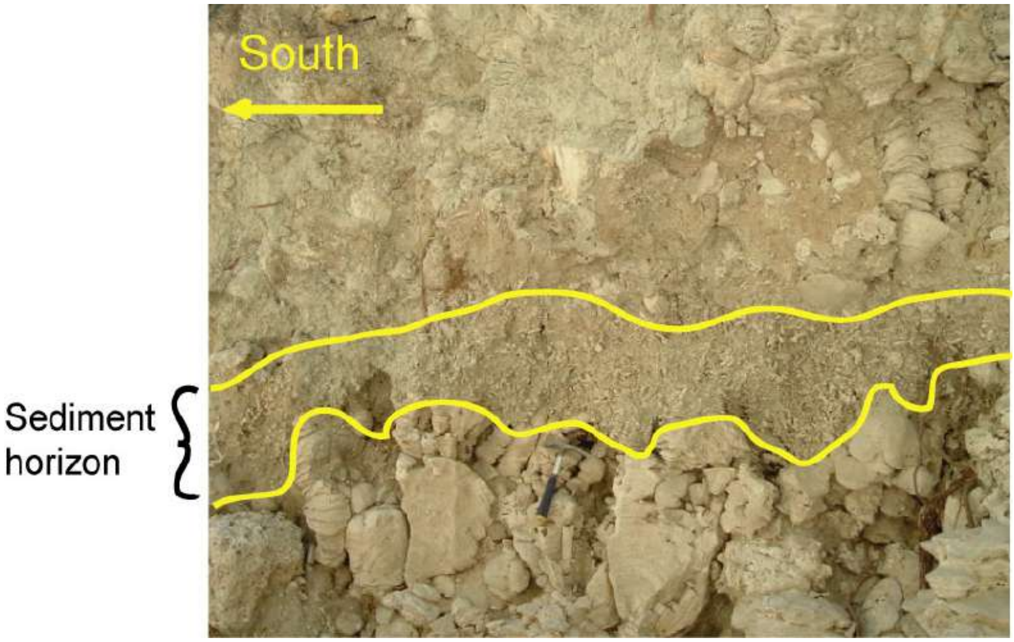

Figure 1.2 Photograph of a portion of the Cañada Honda outcrop showing a sedimentary horizon. These deposits are characterized by reworked bivalve, gastropod and coral fragments (mostly *Madracis* sp.) and can be traced tens of meters throughout the outcrop.

obtain information from a fossil reef with the spatial resolution of a Pleistocene reef (e.g. terraces on Barbados), but with the preservation that can be obtained from a Holocene fossil reef. The Cañada Honda fossil reef is remarkably well-preserved and displays subaerial exposures of shallow-water reef environments dated between 10,000 to 4,500 years ago (Taylor et al., 1985). The young age (Holocene) and the relatively dry climate have resulted in excellent preservation of original aragonitic skeletal mineralogy of fossil corals (Greer, 2001); and the high surrounding hills and restricted setting argue for a high sediment environment, as pointed out by Mann et al. (1984), Taylor et al. (1985) and Stemann and Johnson (1992). This provides a unique opportunity for comparing a reef that developed under conditions of natural stress and disturbance to modern reefs that have been subjected to anthropogenically inducesd stress.

Additionally, some stratigraphic timelines have been identified (Figure 1.2). These are exposed as sedimentary layers tens of meters long that are composed of reef debris and sediment probably deposited during one or several storm events or any other disturbance capable of producing rapid downslope sediment transport. These "event beds" were deposited on paleoreef surfaces, permitting the use of chain-transects along the surface in a similar way that is used to survey the surface in a modern reef, and therefore, allows direct comparisons between surface roughness, coral species abundance, colony size and coral cover.

1.2 Objectives

The main objectives of this study are:

1) To gather detailed information about coral community structure, species distribution and morphology as well as characteristics of sedimentary processes of the Cañada Honda fossil reef.
2) To compare the coral community structure of Cañada Honda and its sedimentary processes with that in modern counterparts. (i.e. Are the characteristics in Cañada Honda similar or different to modern living reefs?)
3) To determine if there is evidence in the fossil coral community structure or coral skeletons (e.g. reduced growth, incorporated sediment) of siltation stress.
4) To determine how a naturally sediment-stressed reef like Cañada Honda developed and its implications to our understanding of recent reef decline.

To achieve these objectives, assessments of the species composition, coral morphologies and diversity were made in Cañada Honda using field quadrat-transects placed along vertical transects up the exposed reef walls. This method also allowed determination of the general stratigraphy of the fossil reef. Coral species abundance from Cañada Honda was compared to coral abundance on from modern reefs in Southwestern Puerto Rico. Paleo-coral cover was also measured along paleoreef surfaces (chain-transects) along with measurements of coral growth rates and identification of sediment incorporated into coral skeletons. Depth of reef coral development and reef accretion were obtained from calibrated radiocarbon dates from coral samples. To help characterize sedimentary processes, sediment texture and composition were measured in samples obtained from the fossil reef as well as potential sources in the adjacent uplands. This information was used to recreate a complete history of the Cañada Honda fossil reef and to better understand how natural stress conditions (high sedimentation and/or nutrients) contributed to its development over 6,000 years of pre-anthropogenic time.

2.0 Study site

2.1 Enriquillo Basin

The Cañada Honda fossil coral reef is located on the northern shore of Lago Enriquillo, in the Enriquillo Valley of southwestern Dominican Republic (Figure 1.1). The basin is a fault-bounded, east-west trending ramp (Figure 2.1) that formed during subsidence following Late Miocene to Pliocene compression in which the Sierra de Neiba to the North and the Sierra de Bahoruco to the South were overthrust against the basin (Mann et al., 2002). After collision with the southern tip of the Bahamas Platform at the end of the Pliocene, fault movement reorganized from mostly North-South compression to mostly oblique slip. Today, the area is characterized by mostly left-lateral strike-slip movement (Mann et al., 2002) along the Enriquillo-Plantain Garden Fault Zone (EPGFZ) which is a major fault system within the complex Northern Caribbean Plate Boundary Zone (Figure 2.2).

Rising sea level flooded the valley around 10,000 years ago, marking the initiation of transgressive deposits (varying from brackish, fresh-water deposits to open-marine). Around 5,000 to 4,000 years ago, fluvial deposits from Río Yaque Del Sur gradually isolated the formerly open bay until it became completely separated from the Caribbean Sea. Subsequent evaporation formed Enriquillo Lake and exposed the fossil reefs and the valley (Mann et al., 1984). The formation of Lago Enriquillo marked the end of coral reef development and the transition to lacustrine environment (Guerard et al., 2004). Today the lake is approximately 40 m below mean sea level. While alluvium has covered much of the reef's upper surface, gullies and ravines cut by sheet flow and rivers flowing into the lake have created spectacular vertical exposures.

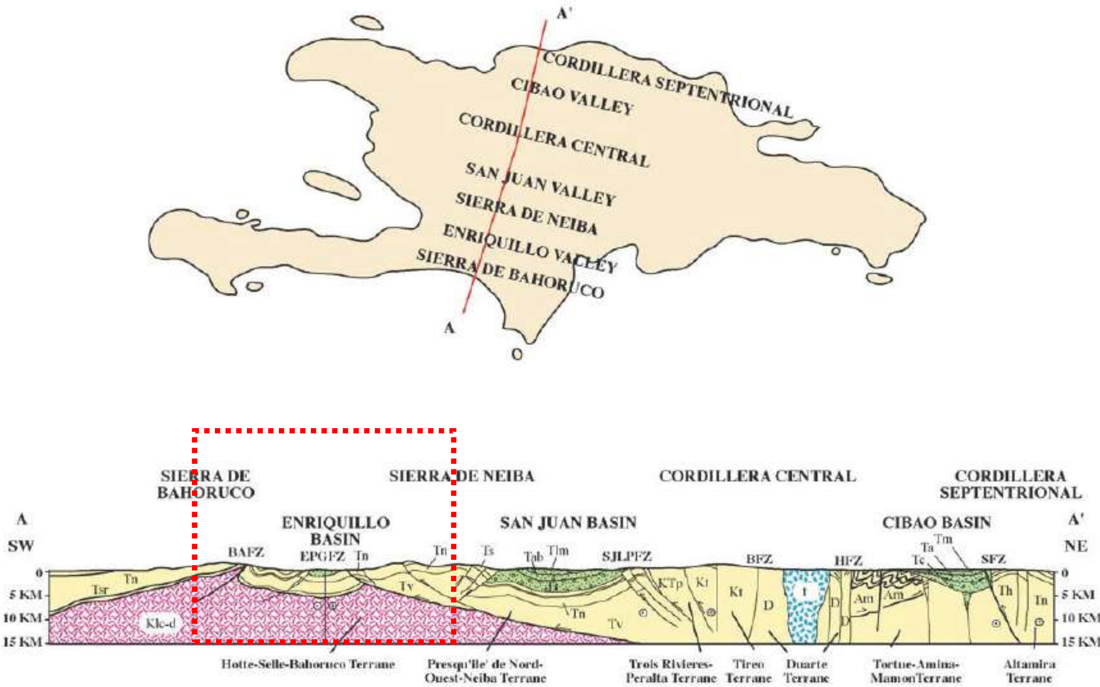

Figure 2.1 North-South cross section across Hispaniola showing major morphotectonic features of the island (from Draper et al., 1994). The Enriquillo-Plantain Garden Fault Zone (EPGFZ) is still active and was responsible for the January 12, 2010 (7.0 Mw) earthquake in Haiti.

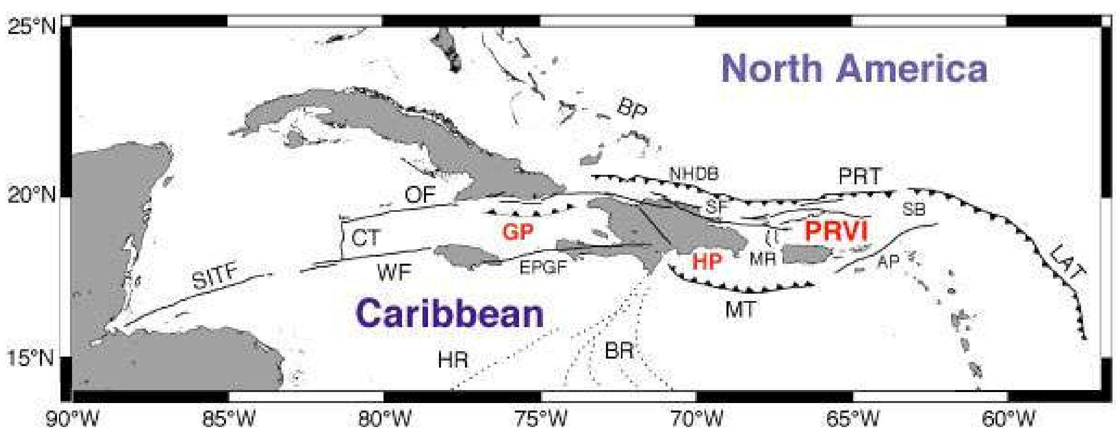

Figure 2.2 Tectonic map of the Northern Caribbean Plate Boundary (from Mann et al., 2002). EPGF= Enriquillo-Plantain Garden Fault.

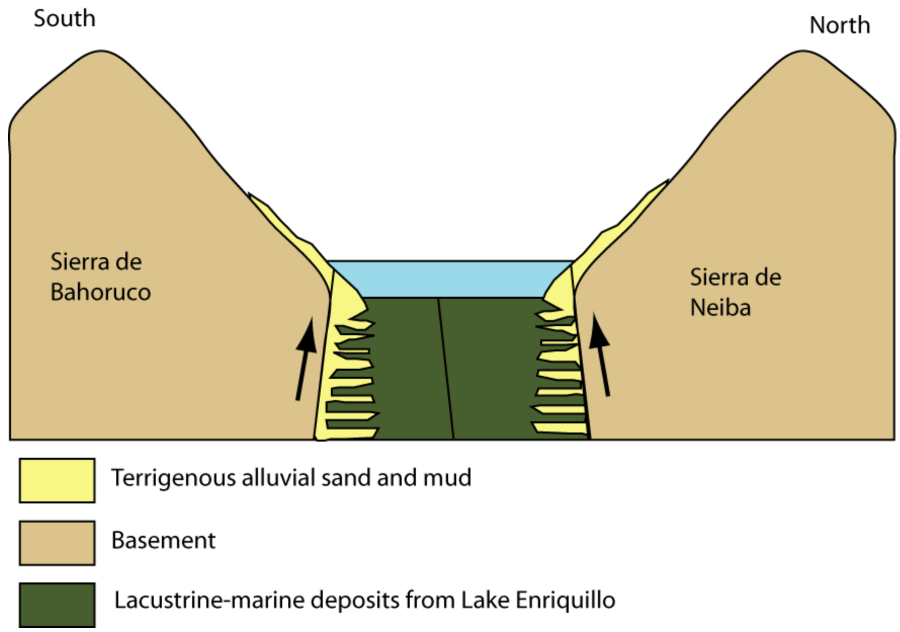

Figure 2.3 Simplified North-South cross-section across the Enriquillo Basin illustrating the general geology of the area with emphasis on the characteristic terrigenous sedimentation from such high-relief mountains.

Previous studies by Mann et al. (1984), Taylor et al. (1985) and Stemann and Johnson (1992) state the importance of high sediment influx in the development of these reefs. The ancient "Enriquillo Bay" occurred in a restricted environment (85-km long and 12-km wide) resulting in limited wave action (Mann et al., 1984). This fact is supported by the large volumes of the stag-horn coral *Acropora cervicornis* which is characteristic of protected environments (Geister, 1977) and the complete absence of the elk-horn coral *Acropora palmata* which depends on the action of the waves to remove sediment (Hubbard and Pocock, 1972). In addition, the bay is bounded on the north and south by elevated mountain ranges of abrupt topographic relief which provides large amounts of sediment that accumulated within the embayment (Figure 2.3). Aerial and satellite images of the Enriquillo Basin reveal the presence of numerous alluvial fan systems that

Figure 2.4 Google Earth image of northern shore of Lago Enriquillo near Cañada Honda. The white lines highlight the drainage path and the limits of an alluvial fan.

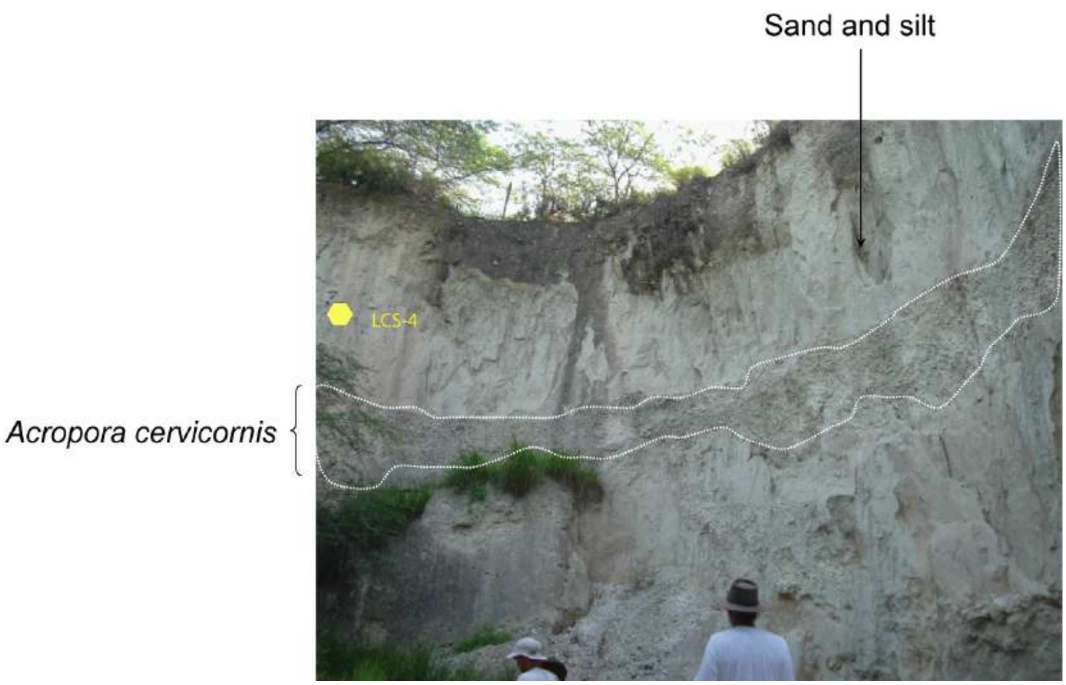

Figure 2.5 Photograph (looking North) of a portion of the Las Clavellinas outcrop showing alternating beds of *Acropora cervicornis* and fluvial sand and silt. Location of sediment sample LCS-4 is shown (yellow dot).

terminate at the lake (Figure 2.4). Alternating beds of *A. cervicornis* and fluvial sand can be seen in the Las Clavellinas outcrop (Figure 2.5) are further evidence of the tremendous terrestrial sedimentation that occurred and still occurs today in the area. Finally, Stemann and Johnson (1992) documented low-diversity assemblages of large colonies of *Siderastrea siderea* and *Stephanocoenia intersepta* in the Enriquillo fossil reefs. This particular assemblage is characteristic of reefs under siltation stress (Cortés and Risk, 1985). In the latter study, Stemann and Johnson (1992) described three statistically discrete biofacies which included an *Acropora cervicornis* facies, the low-diversity assemblage of *Siderastrea siderea* and *Stephanocoenia intersepta,* and a higher diversity assemblage (or mixed zone) consisting of *Montastraea* spp., *Colpophyllia* spp. and *Agaricia* spp.

2.2 Modern reefs, Southwestern Puerto Rico

One of the purposes of this study was to compare the information from Cañada Honda with similar data from modern coral reefs in southwestern Puerto Rico (Morelock et al., 2001), in particular the coral reefs from the west coast (Añasco, Mayagüez Bay and Cabo Rojo) and the southwestern coast from Parguera to Ponce (Figure 2.6). The coral reefs from Añasco, Mayagüez and Cabo Rojo as well as the nearshore reefs in Ponce are influenced by high-terrestrial runoff and sediment resuspension (Morelock et al., 1983; Acevedo et al., 1989) whereas those from Parguera and offshore Guánica have less terrestrial influence (Morelock et al., 2001; Ballantine et al., 2008). Coral reefs off La Parguera, especially those near the shelf-edge have the most abundant and diverse species assemblage of all communities in SW Puerto Rico (Morelock et al., 2001; Ballantine et al., 2008) with coral cover up to 40% (Figure 2.6) The reef sediment off La Parguera is almost entirely $CaCO_3$, although nearshore areas receive terrestrial sediment runoff in the form of sheet flows during occasional rains (Morelock et al., 1994). In contrast, the reefs from western Puerto Rico, Guayanilla and Ponce have a history of degradation from elevated terrestrial runoff and sediment resuspension leading to coral cover that is now below 10% (Figure 2.6) and a substratum covered with fleshy macroalgae (Acevedo et al., 1989; Morelock et al., 2001).

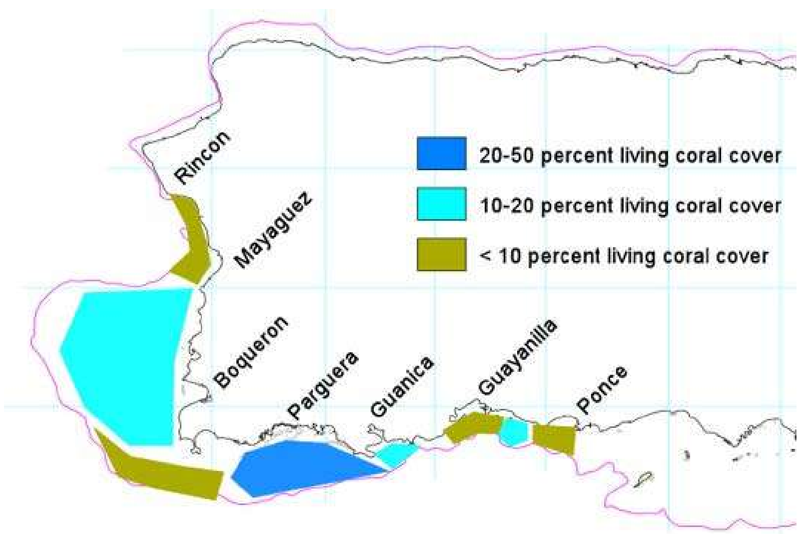

Figure 2.6 Map of the coastline of southwestern Puerto Rico summarizing the conclusions of coral reef areas (Modified from Morelock et al., 2001). Lower coral cover characterizes reef impacted by elevated sedimentation (Añasco, Mayagüez, Guayanilla and Ponce).

3.0 Methodology

3.1 Community structure analysis

3.1.1 Stratigraphy/Average community structure over time

Variations in the stratigraphy and coral assemblages exposed in the canyon walls were studied using 67 quadrats along 18 vertical transects (Figure 3.1 and 3.2). Quadrats were placed sequentially along up the exposed reef cliffs (Figure 3.2). Quadrats consisted of a meter-square PVC frame which was subdivided into a 10 x 10 cm grid that provided 100 grid-intersection points. Each point was counted as sediment or fossil. Sites were selected to provide a regularly-spaced collection of well-exposed sections throughout the lower canyon. An effort was made to not bias placement on especially large or well preserved colonies.

Coral morphology was also noted for each coral. These were grouped into five categories: platy, hemispherical (domal), conical, columnar and branching. Some of these morphologies are associated with reduced light penetration and turbidity caused by high sedimentation (James and Bourque, 1992; Van Woesik and Done, 1997). Davis et al. (2008) has proposed that these coral morphologies are largely related to the intensity of sediment stress (burial rate) and the resistance of particular species to sediment stress.

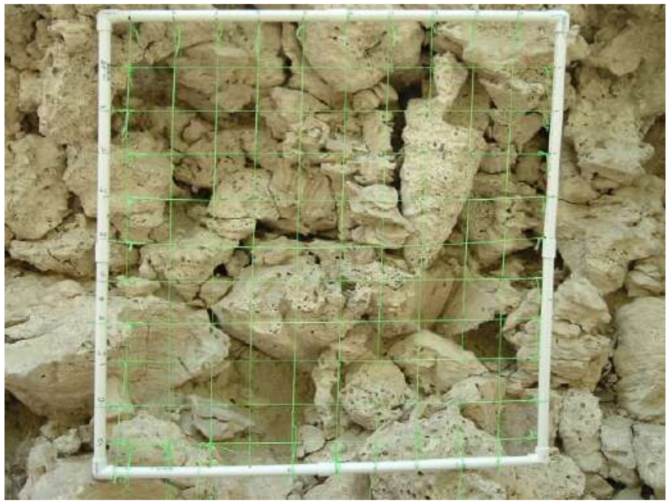

Figure 3.1 Photograph of quadrat used along vertical transects. Constituents were counted at 100 intersections of a ten-by-ten cm grid within a meter-square PVC frame placed on the vertical exposures.

Figure 3.2 Photograph illustrating placement of meter-squared quadrats along vertical transects over exposed fossil reef wall in Cañada Honda.

3.1.2 Chain or paleoreef surface transects – Community structure at a point in time

Although vertical transects can provide important information about of the overall reef community, direct comparison with a modern reef in terms of coral coverage requires the identification of an equivalent paleoreef surfaces[1]. In Cañada Honda these occur underneath sediment horizons that represent one or several events of rapid burial of the reef. One single sediment horizons extends for nearly 100 meters in lower Cañada Honda and consists of reworked bivalve, gastropod and coral fragments (mostly *Madracis* sp.) presumably derived from upslope (Figure 3.3). Corals below this horizon are often tipped down slope, suggesting that such sedimentation events were associated with debris flows. For each transect, a chain or measuring tape was placed along the paleoreef surface following its topography beneath the sediment horizon. Individual measurements were taken over a horizontal distance of one meter along the paleoreef surface (Figure 3.3). This hopefully allows a more direct comparison between surface roughness, coral species abundance, colony size and coral cover along fossil versus modern reefs. Twenty five meter-long transects were measured in the fossil reef. In addition to information on species occurrences, taphonomic criteria were developed (Table 1) allowing estimations of "live" versus "dead" coral at the instant of burial. Primary characteristics that were used include: calyx preservation, the degree of bioerosion on the coral surface and presence of encrusters in the coral surface.

[1] A major difference is that the chain-transect in a modern reef would be conducted over the same elevation whereas in the CH fossil reef the chain-transect occurs at different elevations due to the orientation of the outcrop. This could introduce some issues at the time of comparisons with modern reefs since several coral facies or environments can be crossed in the transects. This is not a big issue in CH since the measured paleoreef surface is confined within the massive coral subzone.

Lescinsky (2004) showed that when a coral colony dies and is exposed, it will take only few weeks to be covered by encrusters and macroborers. Thus, only pristine or very slightly modified colonies were classified as “live”.

Table 1. Taphonomical criteria developed to determine if fossil corals were alive or dead at the time of burial.

Coral surface description	Inferred condition at burial
1. Pristine polyp structure	Live
2. Light surface abrasion, internal polyp structure is good	Live
3. Significant interior loss, presence of encrusters	Dead
4. No polyp internal structure, only gross shape, presence of encrusters	Dead
5. Polyp is very difficult to distinguish, presence of encrsuters	Dead

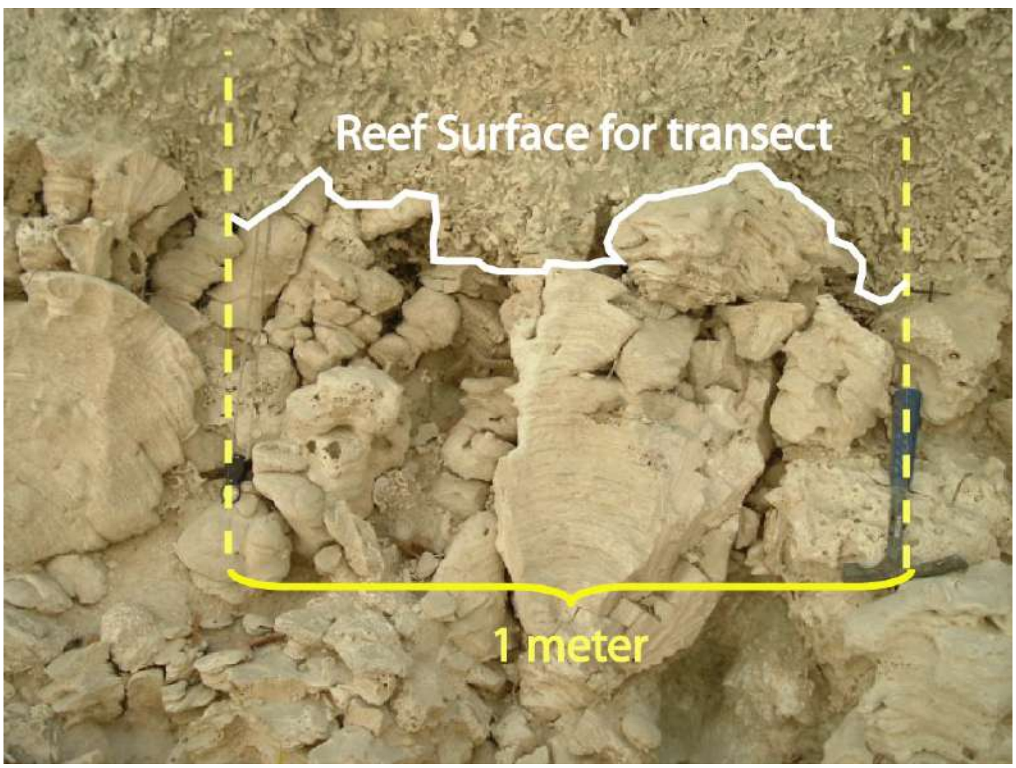

Figure 3.3 Photograph of a portion of the Cañada Honda reef outcrop illustrating a surface buried by detritus generated over a short period of time. This provides a “time line” that can be used to make spatial comparisons with measurements on modern reefs. The “chain method” was employed to collect quantitative data along a synchronous paleoreef surface.

3.2 Coral samples analyses

3.2.1 Coral Growth Rates

Growth rate analyses focused on the corals *Montastraea faveolata* and *Siderastrea siderea* which are the two most abundant massive coral species in the Cañada Honda fossil reef. Abundant data are also available for these species on modern reefs. Samples were identified and all the pertinent field information (photography, elevation[2], location) was recorded (Figure 3.4). To determine growth rates, corals were cut into 3-5 mm wide slices. The central slab of the colony, where the maximum growth occurs, was polished and X-rayed to reveal annual growth bands (Figure 3.5). The X-radiographs were scanned and the distance between successive high and low density growth bands were measured using Coral XDS 3.0 software (Kohler, 2003).

3.2.2 Radiocarbon Dates

Seven of the coral specimens analyzed for growth rates were chosen for radiocarbon dating. The samples were selected according to their location on the Cañada Honda reef in order to obtain coral ages at different elevations throughout the outcrop (Figure 3.4). Using well established Holocene sea-level curves (e.g., Toscano and Macintyre, 2003) and surveyed sample locations, radiocarbon ages were used to (a) constrain paleodepths of the corals at their time of growth and (b) provide an idea of reef accretion through time. Prior to radiocarbon analyses, coral samples were ultrasonically cleaned in distilled water. Aliquots of the samples were analyzed by X-Ray Powder Diffraction (XRD) to make sure no alteration/contamination of the original aragonite mineralogy

---

[2] Elevation data were acquired from several surveys conducted by Dennis K. Hubbard, Wilson Ramírez and students from the Department of Geology at Oberlin College from 2003 to 2007.

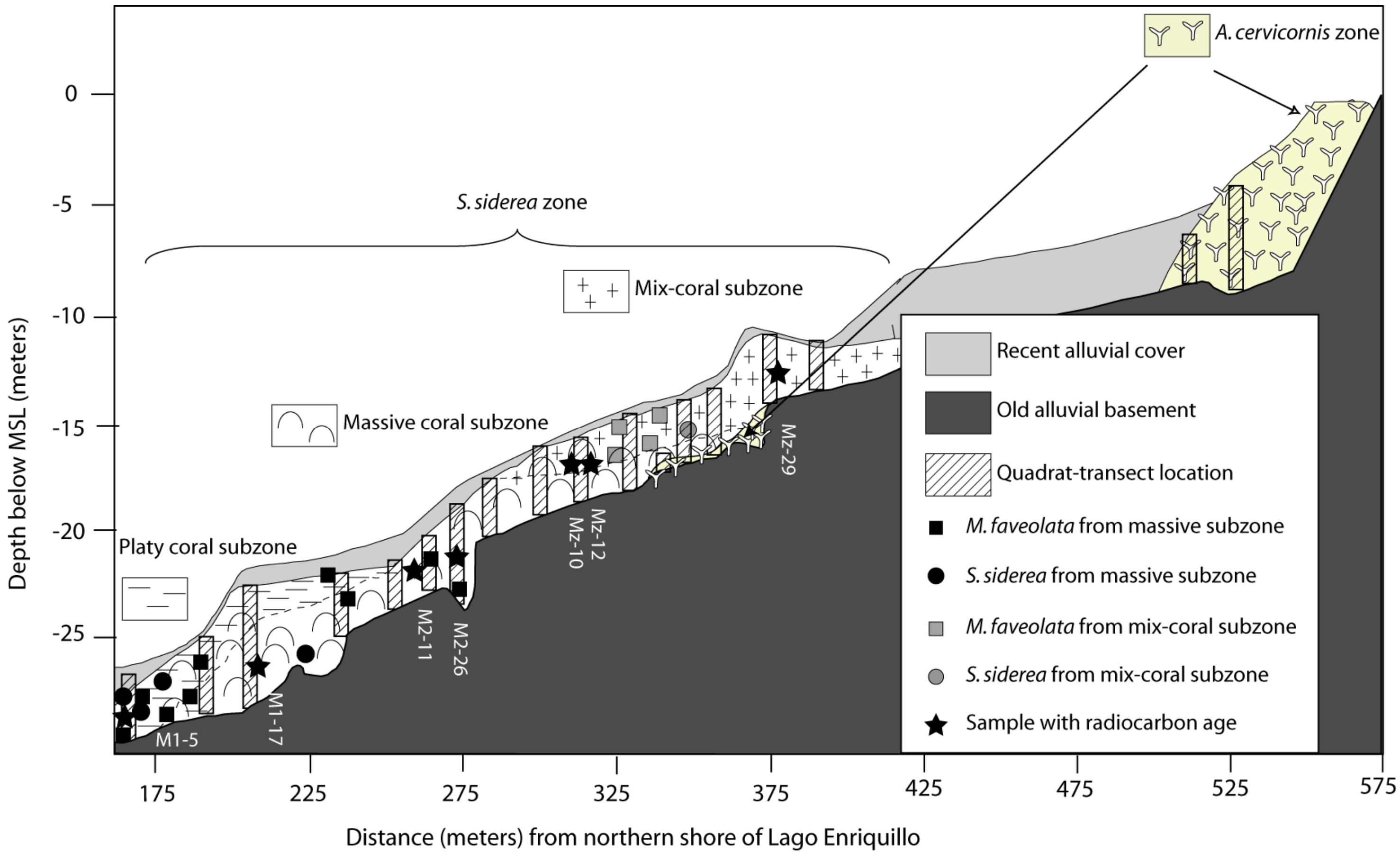

Figure 3.4 Cross-section of the Cañada Honda fossil reef (modified from Hubbard et al., 2005) showing location of transects and corals sampled for growth rate (closed circles and squares) and radiocarbon analyses (stars). Facies determinations are based on the spatial distribution of coral species and their relative abundances within the counted quadrats.

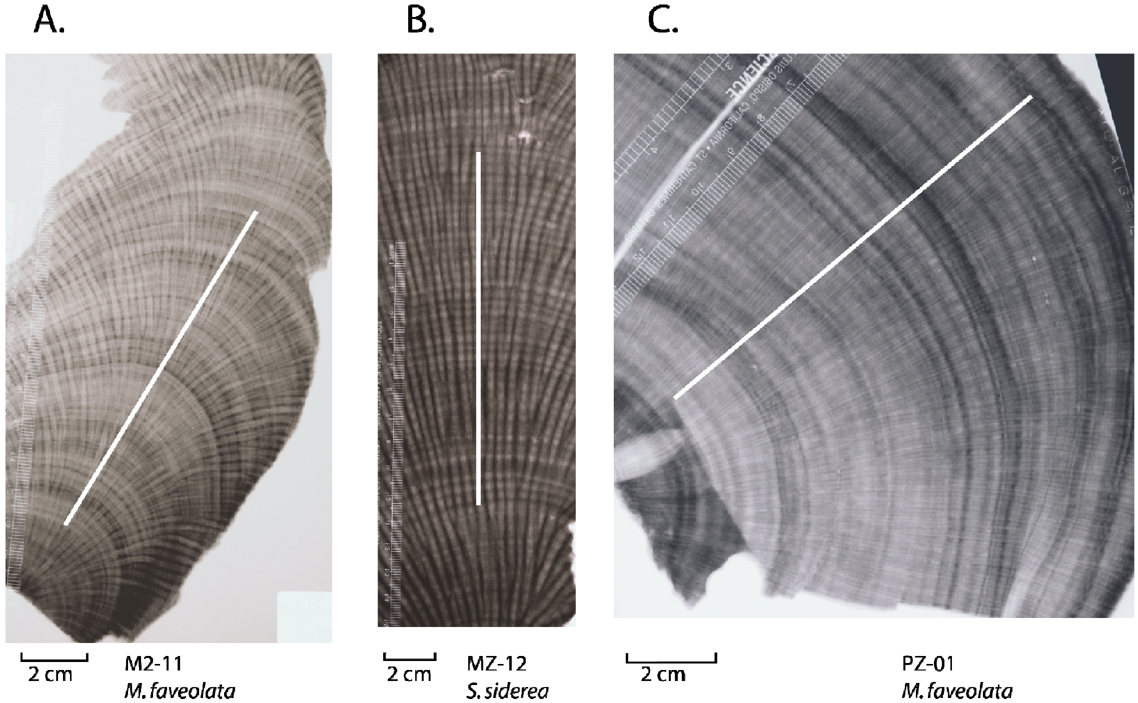

Figure 3.5 Negative images of X-Ray radiographs from three of the corals analyzed. White line represents axis where growth measurements were obtained. A) *M. faveolata* sample M2-11; B) *S. siderea* sample MZ-12; C) *M. faveolata* sample PZ-01. High-density bands are dark colored.

existed (Appendix A). XRD analyses were carried out at the XRD facilities of the Geology Department at the University of Puerto Rico in Mayagüez. Radiocarbon analyses were conducted at the National Ocean Sciences AMS Facility of the Woods Hole Oceanographic Institution in Massachusetts, USA. The ^{14}C reservoir effect for the Northern Caribbean, calculated as 425 ±52 yr (Broecker and Olson, 1961) was subtracted from the conventional (^{13}C corrected) ^{14}C ages; the values were then converted to calendar years BP (1950) using the *marine04.14c* calibration data set of Hughen et al. (2004) via the CALIB program (Stuiver and Reimer, 1993) version 5.1.

3.2.3 Petrographic analyses of corals

Twelve coral samples (including samples where linear extension was already determined) were chosen for petrographic analyses. Samples were cut and impregnated with epoxy resin under a vacuum and thin-sections were made from the portions that contained thin bands of sediment incorporated into the skeleton. The focus was on the internal structure of the coral skeleton where sediment particles had been incorporated in the hope of developing a diagnostic for siltation stress as pointed out by Barnard et al. (1974) and Cortes and Risk (1985).

3.3 Sediment analyses

3.3.1 Sediment composition

Sediment samples collected along vertical transects (Figure 3.6) were used to compare the reef sediment composition with the coral abundance and coral growth data. Nineteen sediment samples from the Cañada Honda fossil reef were analyzed for this study. In addition, four sediment samples from a fluvio-deltaic sequence overlying the Holocene fossil coral reef from Las Clavellinas (Figures 2.5 & 3.7) were analyzed to determine the composition of allochtonous terrigenous sediment that reached the former Enriquillo Bay. Analyses determined the relative organic, carbonate siliciclastic contents. A portion of each dry sample was weighed and Sodium Hypochlorite (i.e. Clorox) added to remove organic matter (Rapp et al., 2007). Samples were washed with distilled water, dried in an oven at 100˚C and weighed again to determine the percent of organic matter removed by the Clorox. This process was repeated again with a solution of 10% Hydrochloric Acid (HCl) to remove $CaCO_3$ from the samples (Rapp et al., 2007).

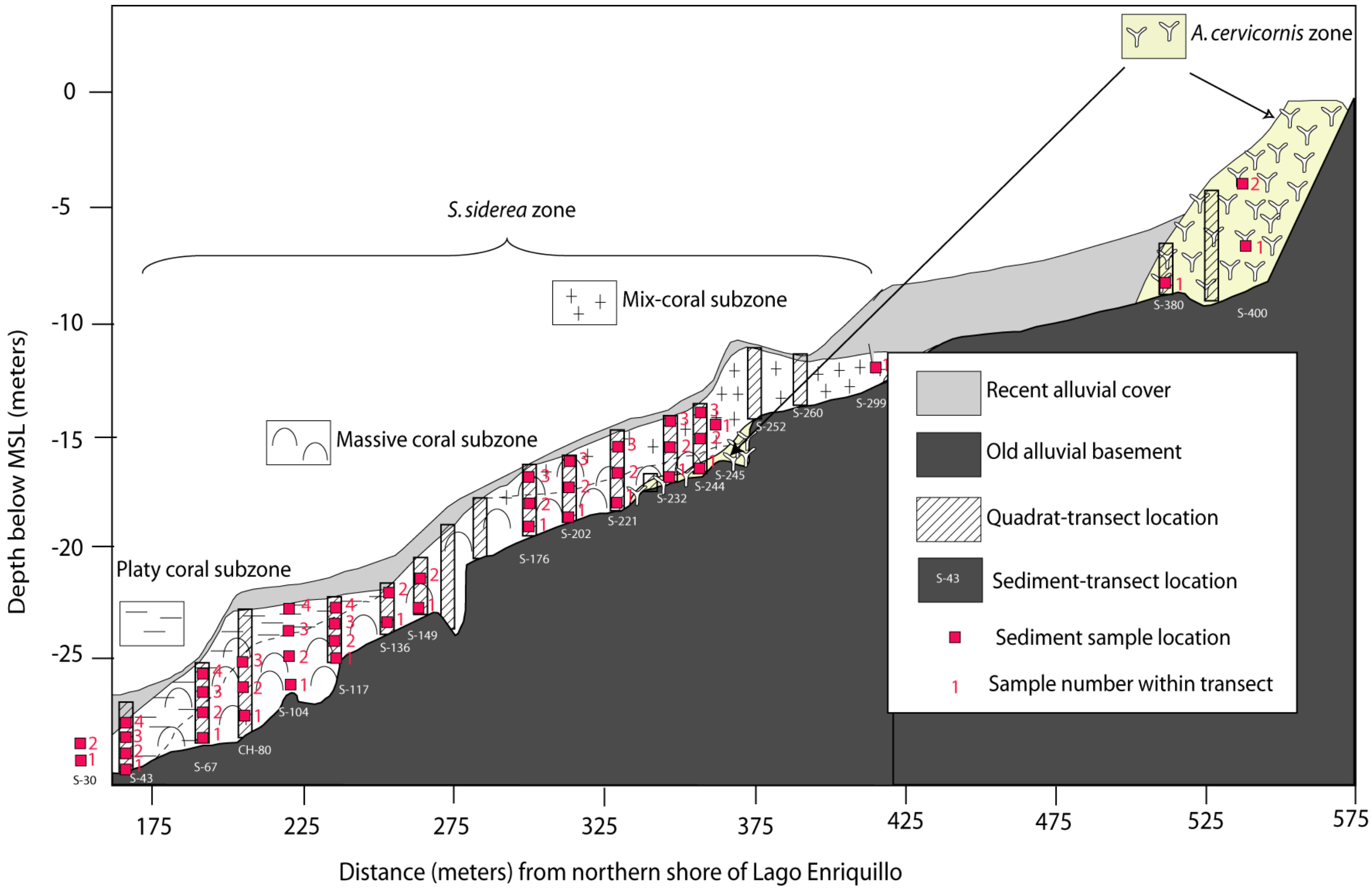

Figure 3.6 Cross-section of the Cañada Honda fossil reef (modified from Hubbard et al., 2005) showing location of transects and location of sediment samples. Facies determinations are based on the spatial distribution of coral species and their relative abundances within quadrats.

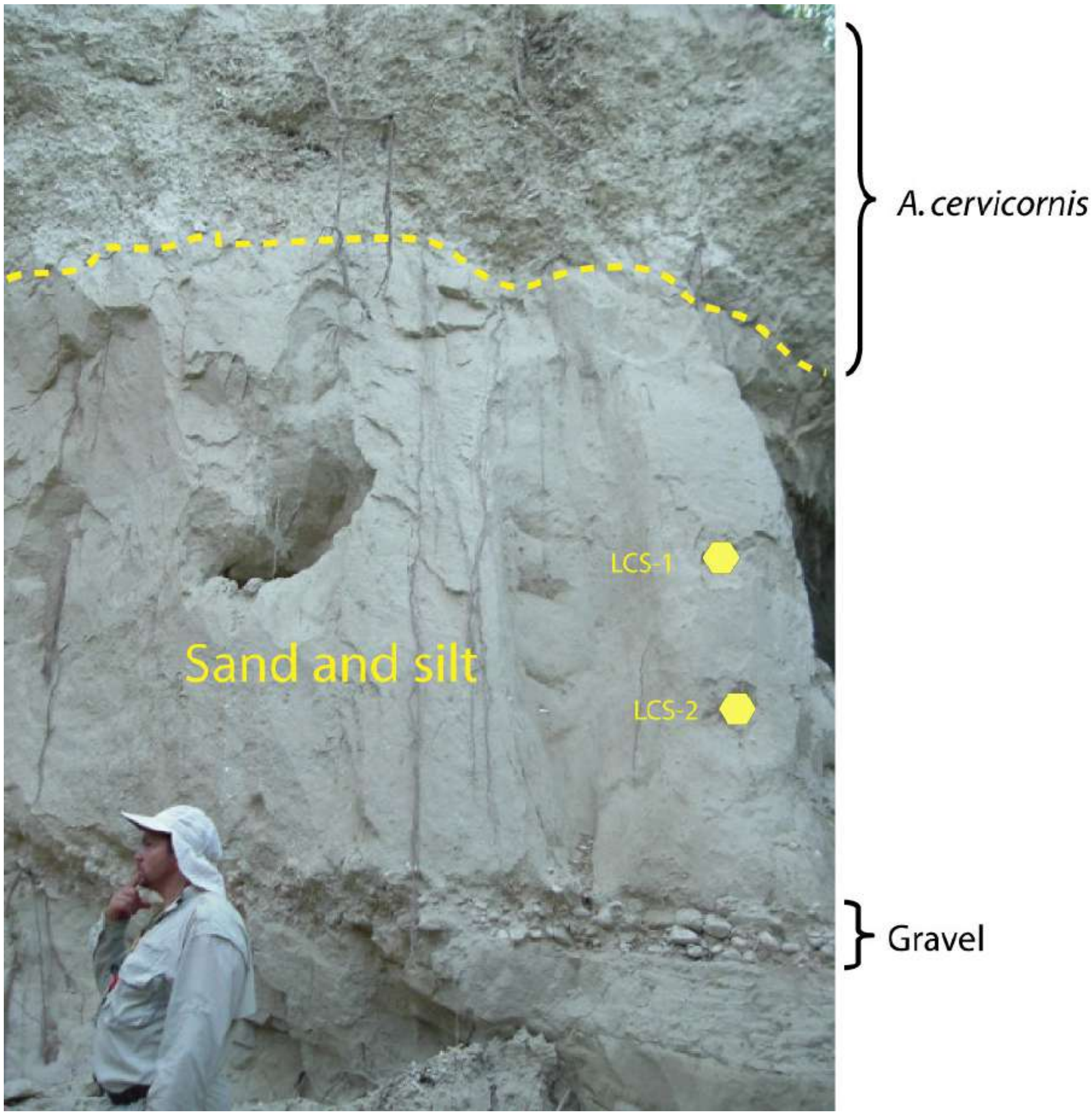

Figure 3.7 Photograph of a portion of the Las Clavellinas outcrop showing sequence of sand and silt underlying a bed of *A. cervicornis*. Two of the sediment samples are shown by yellow hexagons.

3.3.2 Sediment characterization

Sediment samples, including those samples from the fluvio-deltaic sequence in Clavellinas (Figure 3.7) were studied. Analyses consisted of determination of mineralogy (calcite, high-Mg calcite, aragonite, quartz and/or clays using X-Ray Diffraction), grain size (standard sieving techniques) and examination of the constituent grains of the sediment. Samples were disaggregated by soaking them into a 5% water-softener solution (e.g. Calgon; Abrantes et al., 2005) for at least one day and wet-sieved through a 63-μ screen. A subsample of each fraction was washed, dried and separated for further XRD analyses. For petrographic analyses, a subsample of the >63-μ fraction was washed, dried and impregnated with epoxy resin under a vacuum, and made into and thin-sections. Additional details are provided below.

3.3.2.1 X-Ray Diffraction Analyses

XRD analyses were performed on nineteen reef sediment samples from Cañada Honda. Mineral phases were identified throughout the 4-80 2θ-scale to get a general idea of the dominant mineral phases within the sediment. Shifts in the position of the aragonite peaks were quantified to determine the concentration of magnesium in the calcite. The latter is based on the relative 2θ position of the analytical aragonite peaks relative to the 2θ position of the theoretical aragonite peak. The offset in the 2θ will help determine the molar % of magnesium in the calcite (Bischoff et al., 1993) and therefore determine if the peak corresponds to low-Mg calcite (1-4 mol% Mg) or high-Mg calcite (12-15 mol% Mg). XRD analyses were also conducted on the the portion coarser than 63-μ, as well as the mud portion of each sample (<63-μ). This was done to detect any differences in mineralogy due to grain size alone. In addition, these XRD analyses were repeated only on the 2θ-range from 22 to 32 degrees allowing better visualization of individual peaks. Sediment samples from the Las Clavellinas site (fluvial sediment) were also analyzed using this procedure. On the latter samples, XRD analyses were also conducted on the acid-insoluble portion of each sample over the whole 2θ-range.

The goal f these XRD analyses is to provide estimates of allochtonous sediment input from the Neogene limestones (i.e. low-Mg calcite) that bound the Enriquillo basin relative to the sediment originated from the reef itself (mostly of aragonite and high-Mg calcite). Although some mollusk shells are made of low-Mg calcite, their contribution in modern reef systems is small (Flügel, 2004).

3.3.2.2 Constituent grain analyses

Twenty thin-sections were made from sediment samples from Cañada Honda and Las Clavellinas (18 from Cañada Honda and 2 from the fluvial sediment samples from Las Clavellinas). Grains were identified and point-counted (300 counts per sample). Constituent grain examination was conducted using a petrographic microscope and similar to those employed by Ginsburg (1956), Swinchatt (1965), Pandolfi et al. (1999) and Lidz and Hallock (2000).

3.4 Comparison with modern reefs

The coral abundance data from Cañada Honda were compared with similar data gathered from Southwestern Puerto Rico (Morelock et al., 2001). The latter is one of the few datasets of reefs from almost the entire Southwestern coast of Puerto Rico that compares reefs in high-terrestrial runoff settings (e.g. Mayagüez Bay) to "healthy" reefs (e.g. Parguera) using the same sampling method (i.e. photoquadrats). Data in Morelock et al. (2001) is presented in terms of coral cover and abundances. For this study, comparisons only focused on the relative abundances of coral species (spatially averaged) due to the different perspectives when studying a living coral reef (i.e. instantaneous snapshot of reef the surface versus the time-averaged community in a fossil coral reef). In addition, coral growth rate measurements from Cañada Honda were compared with modern coral growth rate measurements already gathered from the greater Caribbean.

4.0 Results

4.1 Community structure

4.1.1 Cañada Honda Fossil Reef

Twenty-two Scleractinian coral species were identified in the Cañada Honda fossil reef (Table 2). The most abundant species throughout the entire reef is the massive coral *Siderastrea siderea* (~47.4% of the coral counts), followed by *Montastraea faveolata* (8.7%), *Undaria agaricites* (7.7), *Colpophyllia natans* (5.8%), *Montastraea franksi* (4.1%), and *Acropora cervicornis* (3.9%). Based on the spatial distribution of coral species and their relative abundances, the Cañada Honda fossil reef can be divided into two major zones (Figure 4.1). The first, a zone of branching *A. cervicornis*, dominates throughout the upper reef outcrop (~0 to -15m elev.) in the upper portions of the Cañada Honda reef (Figures 4.1-4.2), although significant pockets can be found at approximately -20m. In this shallow zone, the coral species *A. cervicornis* has an abundance of 37.9% followed by *M. annularis* (20%) and *U. tenuifolia* (11%). The second is a zone of mostly massive corals in which *S. siderea* ranges from 50% to 70%. It is divided into the following three subzones in ascending order (-35 to -15 m elev.): (1) a platy coral subzone; (2) a low diversity assemblage or massive coral subzone; and (3) a high diversity assemblage or mixed-corals subzone (Figure 4.1). A similar pattern of coral species distribution was obtained by Stemann and Johnson (1992).

Table 2. Distribution (% counts) of coral species and sediment in Cañada Honda

Coral species	C. Honda*	*A. cervicornis* zone	*S. siderea* zone: Mixed-coral subzone	*S. siderea* zone: Massive coral subzone	*S. siderea* zone: Platy coral subzone
Siderastrea siderea	47.4	10.6	49.8	69.7	50.0
Montastraea faveolata	8.7	0.0	6.0	11.5	14.6
Stephanocoenia intersepta	1.3	0.0	0.1	2.9	1.7
Madracis spp.	0.8	0.4	0.7	0.8	1.3
Dichocoenia stokesi	1.3	1.3	0.8	3.1	0.4
Colpophyllia natans	5.8	1.0	10.3	8.7	1.3
Agaricia lamarcki	2.1	0.0	3.9	0.0	4.0
Undaria agaricites	7.7	6.7	8.5	0.0	15.3
Acropora cervicornis	3.9	37.9	0.0	0.4	0.1
Oculina diffusa	0.4	0.0	0.3	0.9	0.0
Porites porites	3.9	4.8	8.2	0.1	2.9
Siderastrea radians	0.5	0.0	0.6	0.4	0.7
Helioceris cucullata	0.7	0.2	0.1	0.3	2.0
Mussa angulosa	0.1	0.0	0.1	0.0	0.2
Manicinia aerolata	0.2	0.0	0.3	0.2	0.2
Eusmilia fastigiata	3.2	1.0	8.4	1.0	1.7
Montastraea annularis	2.0	20.0	0.0	0.0	0.0
Montastraea franksi	4.1	3.5	0.0	0.0	0.0
Montastraea cavernosa	2.3	0.0	0.4	0.0	3.1
Porites astreoides	0.3	1.5	0.3	0.1	0.3
Undaria tenuifolia	1.5	11.0	1.2	0.0	0.2
Scolymia spp.	0.0	0.0	0.0	0.1	0.0
Other ‡	1.8	1.1	0.8	1.2	0.9
Sediment	22.62†	29.3	19.5	22.9	25.5

*out of 4871 coral counts

‡ Refers to unrecognizable, highly damaged coral colonies

†Based on a total of 6295 which is the total number of counts in the quadrats

Table 3. Coral species parameters calculated from Cañada Honda and the different coral zones

	S	N
C. Honda Reef	22	4783
A. cervicornis zone	13	480
Mix subzone	18	1322
Massive subzone	15	1386
Platy subzone	18	1202

S- Number of species N-Number of counts

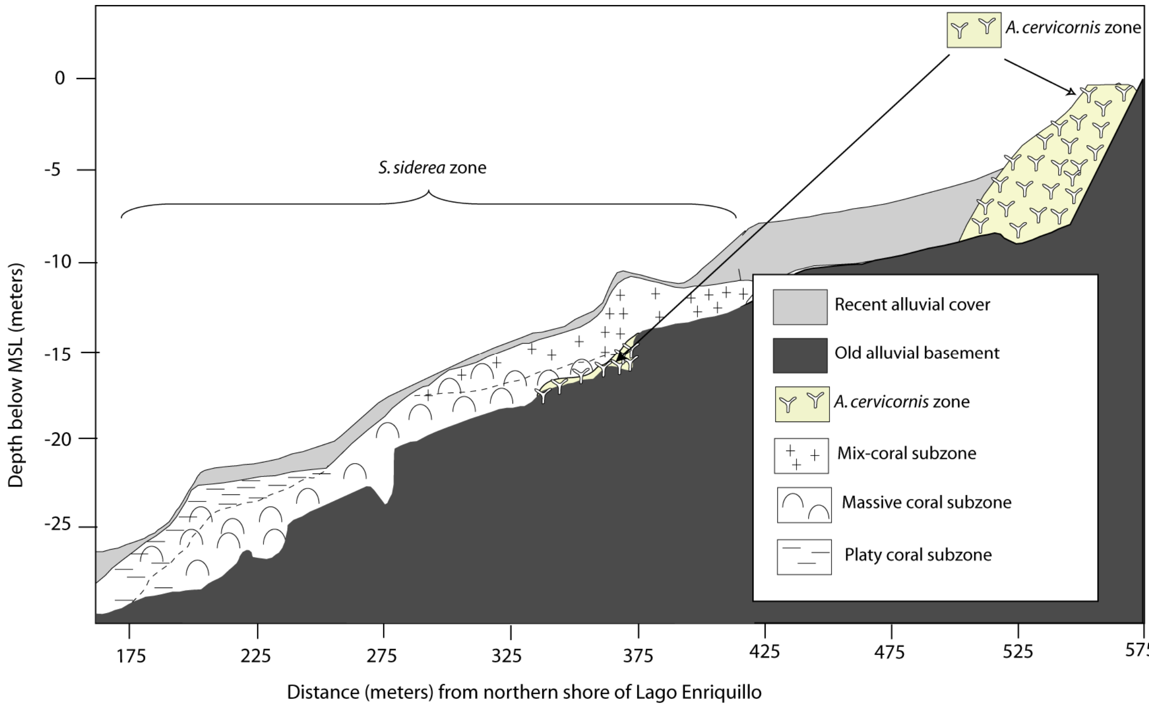

Figure 4.1 Cross-section of the Cañada Honda fossil reef (modified from Hubbard et al., 2005) showing facies and subfacies distribution. Facies determinations are based on the spatial distribution of coral species and their relative abundances within counts.

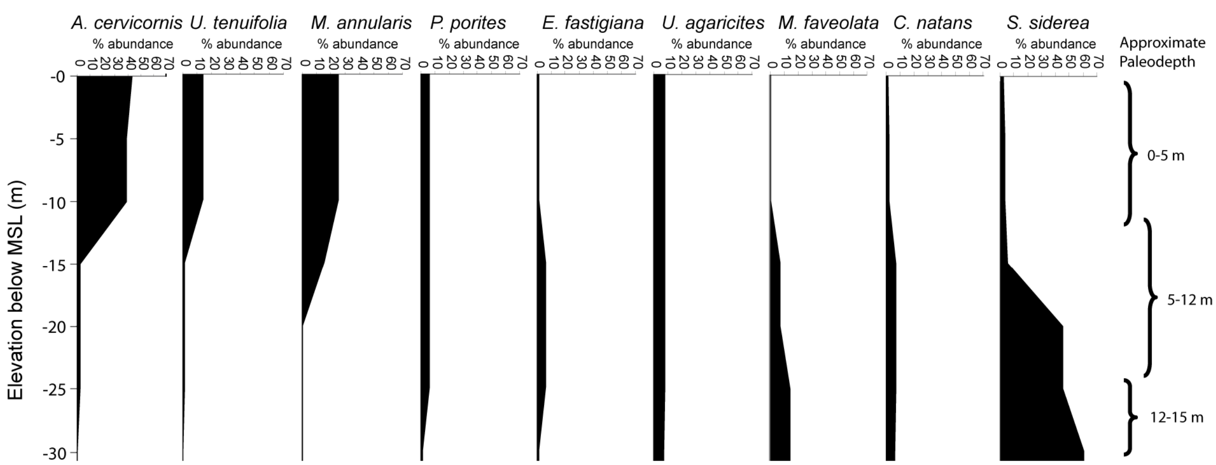

Figure 4.2 Distribution of major coral species with elevation (below MSL) along the Cañada Honda fossil reef.

The platy and mixed-coral subzones have the highest number of species (18: Table 3). In the platy coral subzone, *S. siderea* abundance is ~50%, followed by *M. faveolata* (14.6%) with corals from the genera *Agaricia* spp. and *Undaria* spp. also being common (Table 2). The platy coral subzone is characterized by platy and encrusting corals. In the mixed-coral subzone *S. siderea* abundance is ~49%, and the branching corals *E. fastigiata* (8.4%) and *P. porites* (8.2%) as well as the lettuce coral *U. agaricites* (8.5%) and *C. natans* (10.3%) are important species members in this subzone (Table 2). In the massive coral subzone, *S. siderea* (69.7%), *M. faveolata* (11.5%) and *C. natans* (8.7%) comprise ~90% of the coral counts (Table 2) and at least 15 coral species were found (Table 3).

4.1.2 Coral cover along paleoreef surface

A total of 25 1-m chain-transects were measured along the paleoreef surface beneath a *Madracis* layer within the massive coral subzone (Table 4). The substratum within individual 1-m sections is dominated by corals, most intervals having over 90% coral and averaging 88.7 % (Table 4). The "live" coral cover varies from 0 to 81% with an average of 37.7% (Table 4). If the data from all transects is considered as a whole, it can be seen that only three coral species, *M. faveolata, Siderastrea* spp., and *S. intersepta*, account for almost 97% of the "live" coral cover measured along the paleoreef surface (Figure 4.3). Furthermore, "live" coral cover is as high as 40%, while "dead" coral cover is approximately 50% and sediment cover is approximately 10% (Figure 4.3). The massive coral *M. faveolata* dominates in the "live" coral assemblage, while *Siderastrea* spp. dominates in the "dead" coral assemblage (Figure 4.4). If total coral

Table 4. Summary of data collected (%) along chain-transects over paleoreef surface

	"Live" corals						
Transect No.	*Siderastrea* spp.	*M. faveolata*	*S. intersepta*	other species	Sediment cover	Coral present	Living coral
1	10.6	19.4	0.0	18.1	2.5	97.5	48.1
2	0	46.2	0.0	14.3	0.8	99.2	46.2
3	0	56.7	0.0	0.0	3.1	96.9	56.7
4	0	42.5	0.0	0.0	5.9	94.1	42.5
5	0	29.4	0.0	0.0	0.0	100.0	29.4
6	43.5	28.5	0.0	0.0	13.8	86.2	71.9
7	31.9	39.5	8.1	0.0	0.0	100.0	79.5
8	0.0	0.0	0.0	0.0	0.0	100.0	0.0
9	0.0	0.0	10.4	28.6	0.0	100.0	38.9
10	9.2	0.0	0.0	4.6	2.3	97.7	13.8
11	25.8	36.6	0.0	2.2	19.4	80.6	64.5
12	20.9	26.6	20.9	0.0	17.1	82.9	68.4
13	24.5	0.0	0.0	0.0	0.0	100.0	24.5
14	0.0	48.1	0.0	0.0	0.0	100.0	48.1
15	33.2	22.4	0.0	0.0	0.0	100.0	55.6
16	0.0	14.4	0.0	1.4	34.9	65.1	15.8
17	0.0	34.7	19.2	0.0	8.2	91.8	53.9
18	0.0	81.0	0.0	0.0	3.6	96.4	81.0
19	0.0	25.7	13.2	0.0	9.9	90.1	38.8
20	0.0	12.6	0.0	0.0	21.7	78.3	12.6
21	0.0	0.0	0.0	0.0	100.0	0.0	0.0
22	0.0	10.1	0.0	0.0	14.4	85.6	10.1
23	0.0	8.3	0.0	0.0	18.6	81.4	8.3
24	0.0	0.0	0.0	0.0	6.0	94.0	0.0
25	34.3	0.0	0.0	0.0	0.0	100.0	34.3
Avg.	9.3	23.3	2.9	2.8	11.3	88.7	37.7

cover from both "live" and "dead" assemblages is considered, the abundances of *M. faveolata* and *Siderastrea* spp. are similar (Figure 4.4).

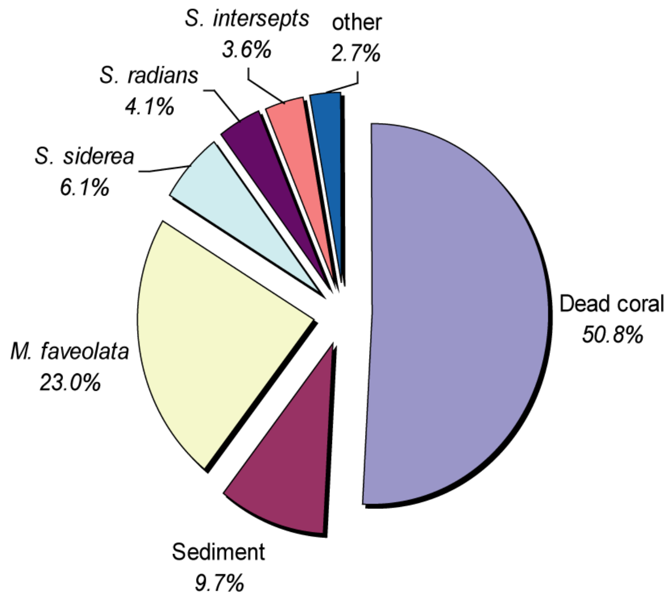

Figure 4.3 Coral cover distribution throughout paleoreef surface (global data, not averaged)

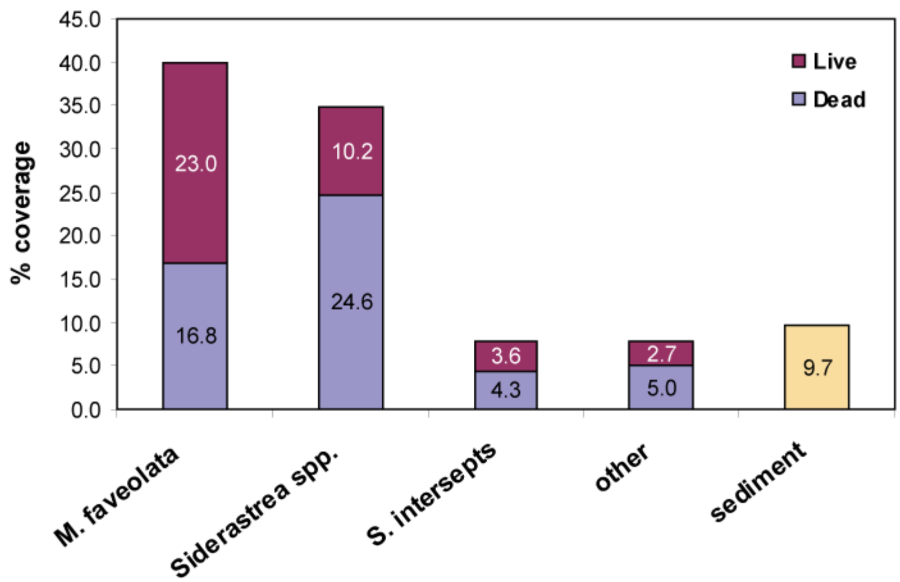

Figure 4.4 Coral cover by species in "live" and "dead" assemblages on paleoreef surface (global data, not averaged).

4.1.3 Coral morphologies

Coral morphologies were grouped into five categories: platy, hemispherical, conical, columnar and branching (Figure 4.5 and Table 5). The dominant morphology in the Cañada Honda fossil reef is hemispherical (34.9%), followed by conical (20.5%), branching (16.8%), platy (16.4%) and columnar (11.4%). Most of these morphologies are associated with reduced light penetration and turbidity caused by high sedimentation (James and Bourque, 1992; Van Woesik and Done, 1997). In addition, 51% of the counts from the massive coral morphologies (i.e. hemispheres, columns and cones) have ragged margins (Figure 4.5 and Table 5) indicative of sedimentation rates equal or almost equal to the coral growth rates (James and Bourque, 1992). An important observation is that many colonies associated with ragged margins seem to concentrate growth upwards with time, a potential indication of high sedimentation rates as suggested also by Davis et al. (2008). Davis et al. (2008) considered all colonies with ragged margins as a single morphological group (i.e. columns), but the results are similar to this study.

4.1.4 Comparison of coral abundances with modern coral reefs

Coral species abundances from vertical transects in Cañada Honda were compared with data from modern reefs in Southwestern Puerto Rico. The coral community in Cañada Honda is characterized by the vast abundance of the coral species *S. siderea* (48%) compared with less than 12% in the modern reef sites throughout SW Puerto Rico (Table 6). In addition, species of the *M. annularis* complex, which is a common member of the community structure in most modern reefs (Table 6), has a total abundance of only 15.1% in Cañada Honda. Another attribute of the Cañada Honda community structure is the complete absence of the genera *Diploria, Mycetophyllia* and *Meandrina*, which are common reef corals in modern reefs throughout the Caribbean.

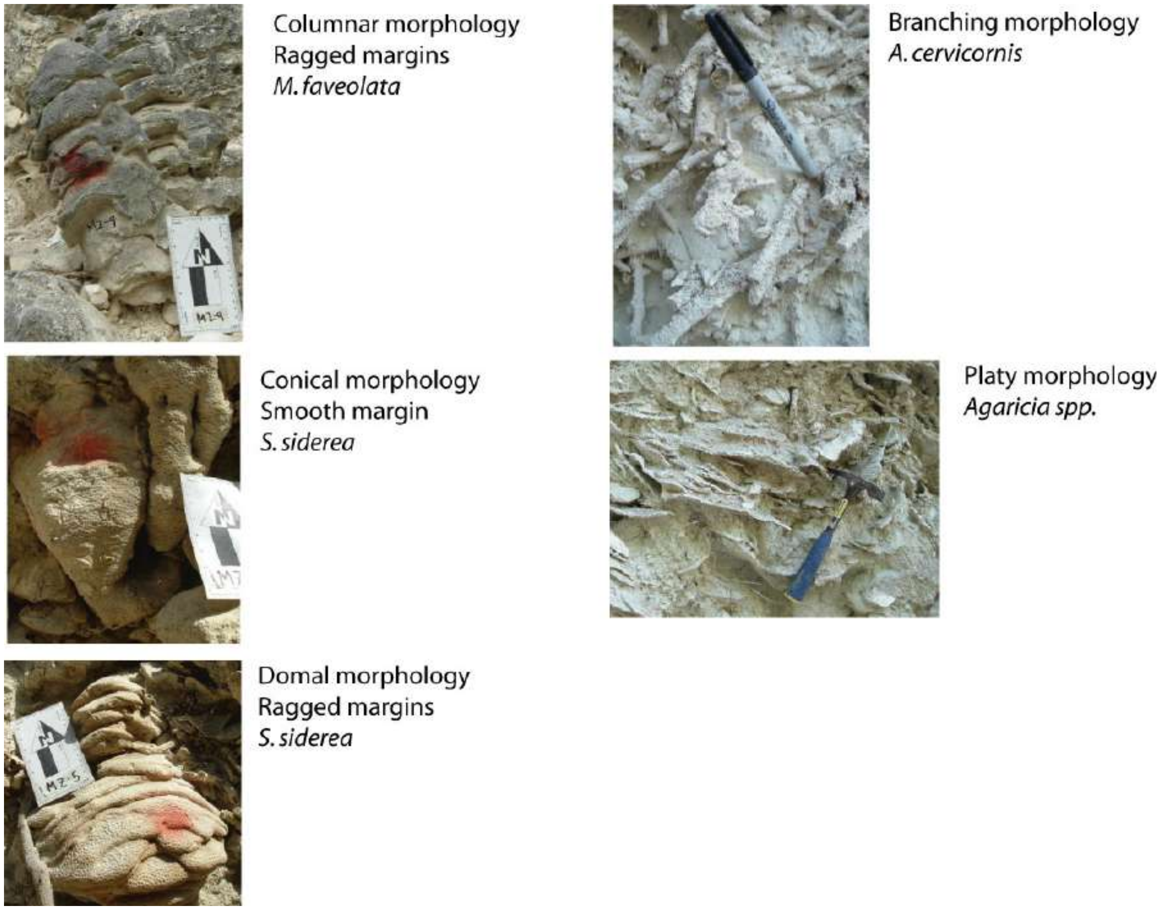

Figure 4.5 Dominant coral morphologies from the Cañada Honda fossil reef

Table 5. Summary of coral morphology distribution along Cañada Honda (% counts)

	Branching	Platy	Cones	Columns	Hemispheres/ Domes
Smooth	16.8	16.4	10.5	8.6	13.7
Ragged	-	-	10.0	2.8	21.2
Total (%)	16.8	16.4	20.5	11.4	34.9

Table 6. Relative coral species abundances (%) from Cañada Honda and modern reefs (spatially averaged) in SW Puerto Rico (Modern coral abundances from Morelock et al., 2001)

Species	C. Honda	Mayaguez Bay	Cabo Rojo Shelf	Parguera Inner and Mid-shelf	Parguera Outer shelf	Guánica	Guayanilla-Peñuelas	Ponce
Siderastrea spp.	48.8	6.5	5.5	6.0	2.8	4.9	5.2	12.4
M. annularis complex	15.1	32.8	28.2	40.3	45.5	44.9	28.1	17.1
S. intersepta	1.3	1.4	0.2	1.5	0.2	0.3	0.2	0.6
Madracis spp.	0.9	3.6	0.8	0.3	0.7	1.3	1.1	1.0
D. stokesi	1.4	0.6	0.2	0.0	0.0	0.4	0.4	2.1
C. natans	5.9	4.2	2.8	4.2	1.7	3.6	2.5	0.2
A. lamarcki	2.1	2.3	22.2	1.3	2.0	4.8	12.5	0.0
Undaria spp.	9.3	7.8	4.2	11.5	23.3	11.0	20.3	17.5
A. cervicornis	3.9	0.0	0.0	3.8	0.6	0.4	0.0	0.3
O. diffusa	0.4	0.0	0.0	0.0	0.0	0.0	0.0	0.0
P. porites	3.9	2.2	3.3	2.5	0.1	1.6	0.0	3.5
H. cucullata	0.8	0.9	0.7	0.3	0.4	0.2	0.7	0.0
M. angulosa	0.1	0.1	0.0	0.4	0.0	0.0	0.0	0.0
M. aerolata	0.2	0.0	0.0	0.0	0.0	0.0	0.0	0.0
E. fastigiata	3.2	0.0	0.7	0.3	0.1	0.0	0.0	0.0
M. cavernosa	2.4	16.7	20.3	9.2	10.0	12.1	16.2	27.4
P. astreoides	0.3	9.8	4.4	5.9	6.1	6.3	5.9	6.5
Scolymia spp.	0.0	0.0	0.0	0.0	0.0	0.0	0.0	0.0
A. palmate	0.0	0.0	0.0	2.5	0.0	0.0	1.5	0.0
M. meandrites	0.0	5.0	2.3	1.2	1.7	2.8	2.4	3.3
Diploria spp.	0.0	3.8	4.0	7.0	3.6	4.0	2.2	4.2
Mycetophyllia spp.	0.0	1.2	0.2	1.6	1.2	1.4	0.5	0.9
S. bourboni	0.0	0.0	0.0	0.2	0.0	0.0	0.1	1.8
I. rigida	0.0	0.0	0.0	0.0	0.0	0.0	0.3	0.0
D. cylindrus	0.0	1.2	0.0	0.0	0.0	0.0	0.0	1.4

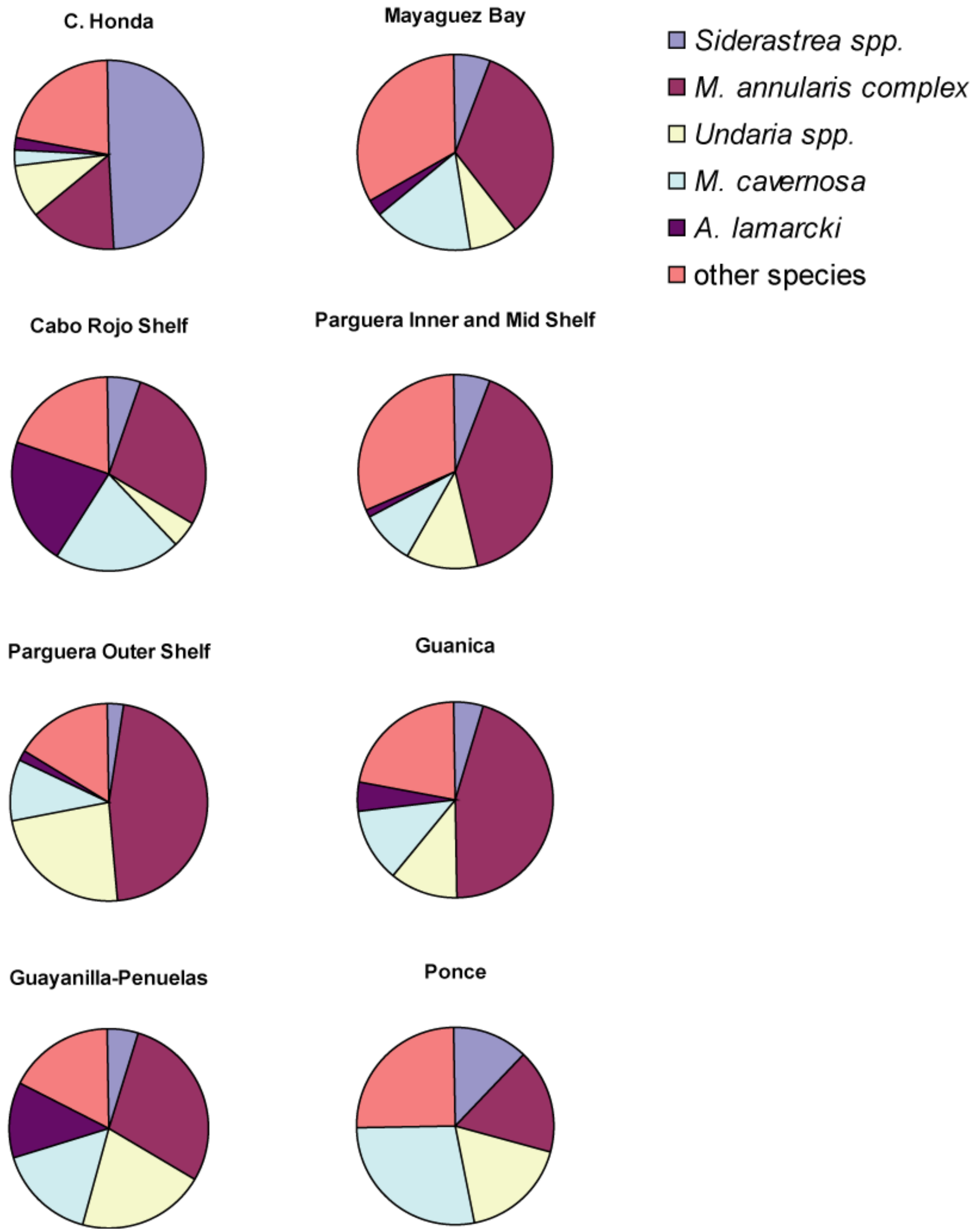

Figure 4.6 Comparison of major coral species abundances from Cañada Honda and southwestern Puerto Rico

4.2 Coral Growth Rates

Twenty-five coral colonies were analyzed to determine annual growth rate. For the massive coral *M. faveolata*, annual growth rates ranged from 0.09 to 0.44 cm/yr (Table 7). In coral colonies of *S. siderea*, annual growth rate varied from 0.2 to 0.4 cm/yr. During sample preparation it was noted that some coral colonies contained bands of sediment incorporated into the skeleton (Figure 4.7). In such bands, growth rate is very low. This is especially true for *M. faveolata* colonies. These bands were not so obvious on the *S. siderea* colonies. Table 8 shows a compilation of modern coral growth rate data from several sites in the Caribbean, including sites recognized as having siltation stress. The approximate depth at which the coral samples were taken is included, because it is well known that in addition to sediment stress, coral growth rates are also depth dependent. Annual growth rates of modern *M. annularis* and *M. faveolata* from around the Caribbean are typically higher than those of fossil *M. faveolata* from Cañada Honda. In contrast, growth rates of fossil *S. siderea* from Cañada Honda are similar to most growth rate data from the Caribbean. However, if the data from Table 8 are clustered within different depth ranges and then graphically plotted against the coral growth rate values obtained from Cañada Honda (Figure 4.8), it can be observed that fossil *M. faveolata* from Cañada Honda fall also within the range of modern coral growth beyond 12 m (Figure 4.8). Depth-related patterns for *S. siderea* are less apparent for modern reefs (Figure 4.9) and the similarities to the Cañada Honda corals are, therefore, expected.

TABLE 7. Results of measurements of coral growth rates from Cañada Honda

Coral sample	Location from Lago Emriquillo	Elevation MSL (± 1m)	N	Mean annual extension (cm/yr)	Error (2σ)	Site description
Montastraea faveolata						
Pz-01	160.0 m	-34.0 m	31	0.340	0.042	Platy coral subzone
M1-5	169.4 m	-33.0 m	28	0.091	0.013	Massive coral subzone
M1-10	181.1 m	-32.0 m	35	0.280	0.037	Massive coral subzone
M1-13	189.0 m	-32.0 m	31	0.248	0.019	Massive coral subzone
M1-30	275.0 m	-27.0 m	27	0.286	0.004	Massive coral subzone
M2-6	172.5 m	-32.0 m	22	0.363	0.024	Massive coral subzone
M2-10	272.0 m	-27.0 m	31	0.175	0.017	Massive coral subzone
M2-11	265.6 m	-28.0 m	107	0.142	0.014	Massive coral subzone
M2-17	191.5 m	-31.0 m	19	0.313	0.045	Massive coral subzone
M2-21	235.0 m	-27.0 m	12	0.278	0.062	Massive coral subzone
M3-8	233.5 m	-26.0 m	35	0.189	0.032	Massive coral subzone
M3-18	327.0 m	-20.0 m	21	0.299	0.055	Massive coral subzone
M3-20	343.0 m	-18.0 m	16	0.213	0.053	Massive coral subzone
Mz-10	322.6 m	-23.0 m	8	0.351	0.079	Mixed-coral subzone
Mz-14	335.8 m	-22.0 m	15	0.305	0.049	Mixed-coral subzone
Mz-16	345.2 m	-21.0 m	15	0.410	0.035	Mixed-coral subzone
Mz-29	382.5 m	-17.0 m	17	0.437	0.042	Mixed-coral subzone
Siderastrea siderea						
M1-17	204.2 m	-32.0 m	15	0.382	0.042	Massive coral subzone
M1-22	225.0 m	-31.0 m	17	0.269	0.033	Massive coral subzone
M2-1	170.7 m	-33.0 m	42	0.256	0.020	Massive coral subzone
M2-2	174.6 m	-34.0 m	8	0.400	0.092	Massive coral subzone
M2-26	275.0 m	-26.0 m	16	0.304	0.036	Massive coral subzone
Mz-12	322.8 m	-23.0 m	43	0.335	0.024	Mixed-coral subzone
Mz-21	357.6 m	-21.0 m	9	0.246	0.034	Mixed-coral subzone
Pz-02	160.0 m	-34.0 m	24	0.222	0.031	Platy coral subzone

TABLE 8. Some coral growth rate data for *Montastraea annularis**, *Montastraea faveolata* and *Siderastrea siderea* in the Caribbean

Coral species	Location	Depth (m)	Annual extension (cm/yr)	Authors of study
M. annularis	St. Croix, USVI	2 m	0.66-0.83	Gladfelter et al., 1978
M. annularis	St. Croix, USVI	10 m	0.70-0.89	Gladfelter et al., 1978
M. annularis	Jamaica	3-10 m	0.699-1.015	Fairbanks and Dodge, 1979
M. annularis	Barbados	3 m	0.828-1.313	Fairbanks and Dodge, 1979
M. annularis	Bermuda	3 m	0.388	Fairbanks and Dodge, 1979
M. annularis	St. Croix, USVI	<12 m	0.7-0.9	Hubbard and Scaturo, 1985
M. annularis	SW Puerto Rico‡	4-8 m	0.63-0.97	Torres and Morelock, 2002
M. annularis	Costa Rica‡	<10 m	0.53	Cortés and Risk, 1985
M. annularis	Yucatán	<10 m	~0.48-0.60	Cruz-Piñón et al., 2003
M. annularis	St. Croix, USVI	12-18 m	0.3-0.7	Hubbard and Scaturo, 1985
M. annularis	St. Croix, USVI	>18 m	≤0.2	Hubbard and Scaturo, 1985
M. faveolata	East Flower Banks, G. of Mexico	<10 m	0.75	Dokken et al., 2003
M. faveolata	West Flower Banks G. of Mexico	<10 m	0.54	Dokken et al., 2003
M. faveolata	Belize	<10 m	0.85-1.4	Gischler and Oschmann, 2005
M. faveolata	Yucatán	<10 m	~0.6-0.72	Cruz-Piñón et al., 2003
M. faveolata	Tobago	2-11 m	0.973-1.103	Moses and Swart, 2006
M. faveolata	Tobago	14 m	0.321-0.330	Moses and Swart, 2006
S. siderea	Tobago	4 m	0.452	Moses and Swart, 2006
S. siderea	St. Croix, USVI	~6-12 m	0.26-0.31	Hubbard and Scaturo, 1985
S. siderea	Costa Rica‡	<10 m	0.52	Cortés and Risk, 1985
S. siderea	Grand Cayman	<10 m	1.24	Cortés and Risk, 1985
S. siderea	SW Puerto Rico‡	4-8 m	0.35-0.43	Torres and Morelock, 2002
S. siderea	Belize	<10 m	0.8	Gischler and Oschmann, 2005
S. siderea	St. Croix, USVI	~18-40 m	0.14-0.25	Hubbard and Scaturo, 1985

* Early studies considered considered *M. faveolata* as a morphotype of *M. annularis*. These were later separated after the study of Knowlton et al. (1992). Although *M. annularis* was not part of the present investigation, some studies suggest similarities in growth rate with *M. faveolata* (e.g. Cruz-Piñón et al., 2003).
‡ Contain sites described as having siltation stress.

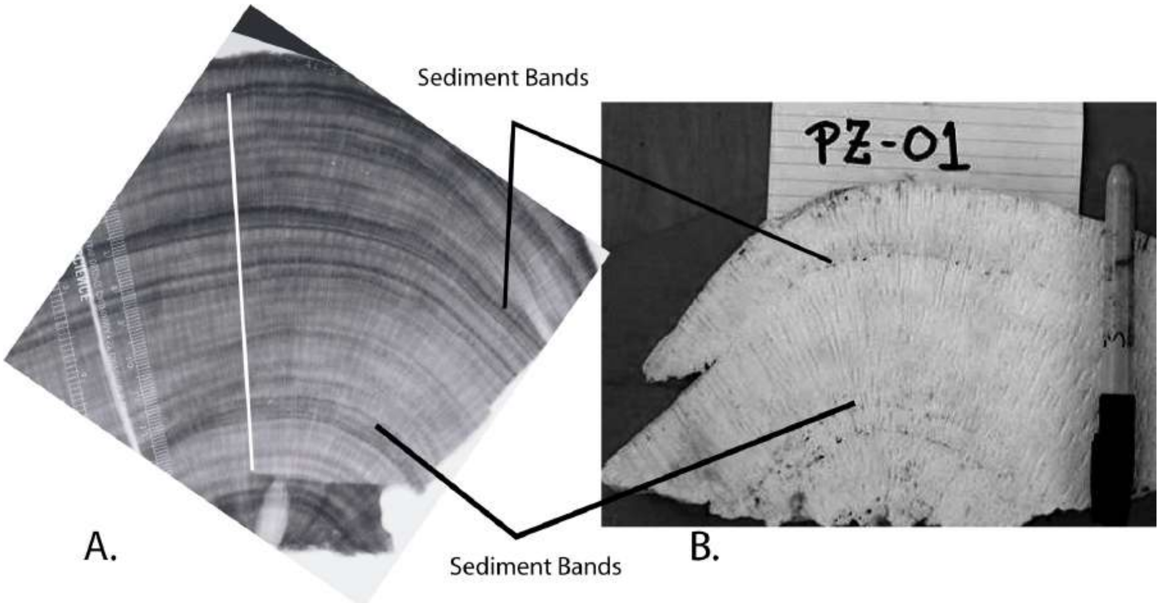

Figure 4.7 (A) Negative image of the X-Ray radiography of coral sample Pz-01 showing thin denser bands that correspond to thin sediment layers shown on photograph of the same sample (B)

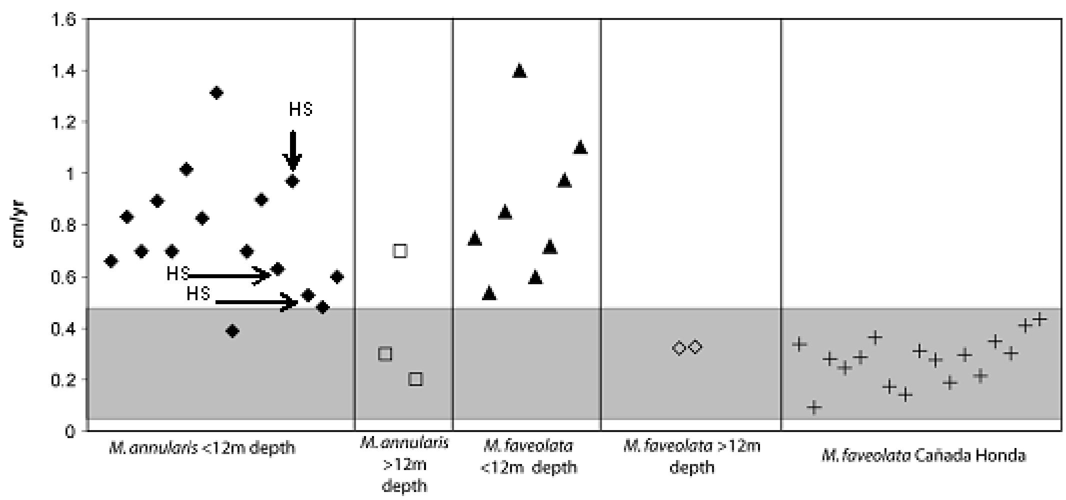

Figure 4.8 Depth range and growth rate data for *Montastraea annularis* and *Montastraea faveolata* from the Caribbean and Cañada Honda. HS refers to data gathered from high sedimentation sites. Gray rectangle was placed to emphasize the range of values from Cañada Honda. Note that all samples from Cañada Honda have growth rates similar to rates reported for Caribbean reefs in greater than 12m of water.

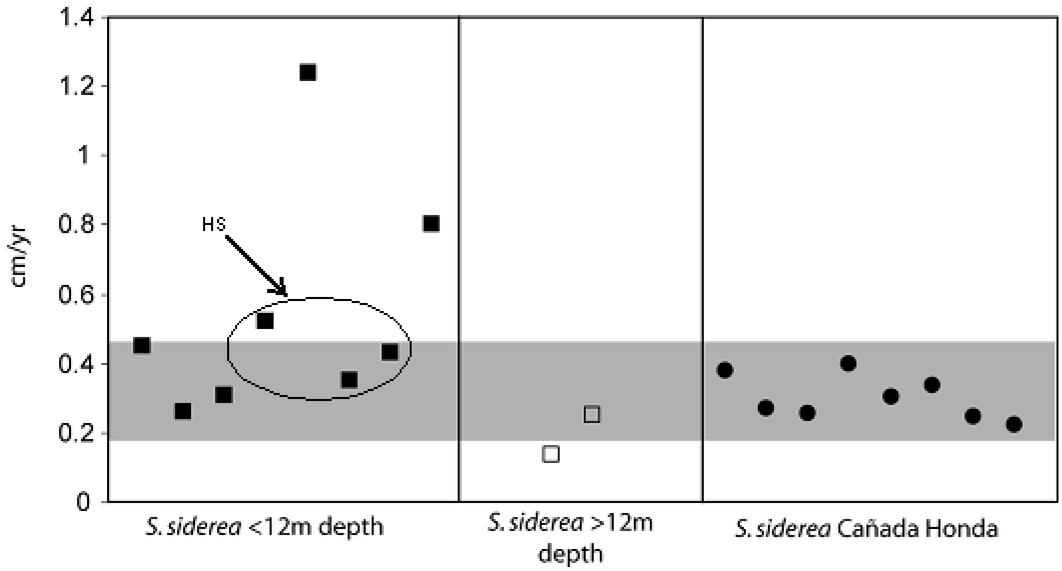

Figure 4.9 Depth range and growth rate data for *Siderastrea siderea* from the Caribbean and Cañada Honda. HS refers to data gathered from high sedimentation sites. Gray rectangle was placed to emphasize the range of values from Cañada Honda.

4.3 Petrographic analyses of corals

Twelve corals from Cañada Honda were chosen for petrographic analyses. Thin-sections were prepared from portions of the corals that contained thin bands of sediment incorporated into the skeleton. In some samples, such bands coincide with reduced coral growth (Figures 4.7 and 4.10). The purpose of the coral petrographic analyses was to describe the presence and nature of the sediment trapped within coral skeletons and also the structure of the coral skeleton. In general, most of the coral thin sections contain sediment incorporated within the skeleton. The amount of sediment varies between 7% and 15% (Table 9). Sediment consists of sub-rounded particles varying in size from approximately 0.3 to 0.7 mm, although particles larger than 1-mm can be found. Most of those sediment particles are confined to the pore spaces within the coral skeletons although some actually cut across the structure. During thin-section preparation and polishing some of the sediment was scrapped-off from the coral leaving only a mold (i.e. void) as evidence of its former presence. For all coral samples, the skeleton appears unaltered for the most part. The presence of bands containing sediment and the reduced coral growth associated with them underscores once again the great influence of terrigenous sedimentation that affected the development of coral reefs within the Enriquillo Basin. In addition, it was noted the presence of cements that developed over the surface of coral skeleton as well as sediment particles. Although a detail study concerning the generation of diagenetic events will be required to make a more definitive conclusion about the mineralogy of such cements, petrographically they appear as calcite bundles (Scholle and Ulmer-Scholle, 2003). If true, the presence of such cements implies that they could be late-stage cements produced by infiltration of meteoric water or groundwater.

4.4 Radiocarbon ages

Calibrated radiocarbon ages obtained from the seven Cañada Honda coral samples ranged from 9,256.0±137 BP to 6,736.5±94.5 BP (Table 10). The oldest was a specimen of *M. faveolata* (9,256.0±137 BP), followed by a specimen of *S. siderea* (8,628.0±165 BP), and located at elevations between -27m and -26m, respectively (Table 10). The youngest was a specimen of *M. faveolata* (6,736.5±94.5 BP), followed by *S. siderea* (7,465.0±83 BP), both at an elevation of -17m. Since no significant vertical motions have occurred in the Cañada Honda site for at least the past 10,000 years (Mann et al., 1984; Mann et al., 2002), radiocarbon ages can therefore be correlated with a well-

Table 9. Petrographic descriptions of thin-sections from corals sampled in Cañada Honda

Sample	Species	Description
M1-10	*M. faveolata*	Approx. 8-10% sediment particles within skeleton, usually confined to skeleton pores. Particles are sub-rounded and vary in size between 0.3 to 0.5 mm. Coral skeleton shows no signs of alteration. A few late calcite cements appear growing over skeleton and sediment surface. Part of the sediment was removed during thin-section preparation leaving only a mold of its previous location.
M1-22	*S. siderea*	Approx. 10-15% sediment particles within skeleton, usually confined to skeleton pores. Particles are sub-rounded and vary in size between 0.3 to 0.5 mm. Coral skeleton shows no signs of alteration. A few late calcite cements appear growing over skeleton and sediment surface. Part of the sediment was removed during thin-section preparation leaving only a mold of its previous location.
M2-1	*S. siderea*	Approx. 7-8% sediment particles within skeleton, usually confined to skeleton pores. Particles are sub-rounded and vary in size between 0.3 to 0.7 mm. Coral skeleton shows no signs of alteration. A few late calcite cements appear growing over skeleton and sediment surface. Part of the sediment was removed during thin-section preparation leaving only a mold of its previous location.
M2-11	*M. faveolata*	Approx. 7-8% sediment particles within skeleton, usually confined to skeleton pores. Particles are sub-rounded and vary in size between 0.3 to 0.5 mm. Coral skeleton shows no signs of alteration. A few late calcite cements appear growing over skeleton and sediment surface. Part of the sediment was removed during thin-section preparation leaving only a mold of its previous location.
M2-21	*M. faveolata*	Approx. 7-8% sediment particles within skeleton, usually confined to skeleton pores. Particles are sub-rounded and vary in size between 0.3 to 0.5 mm. Coral skeleton shows no signs of alteration. A few late calcite cements appear growing over skeleton sediment surface. Part of the sediment was removed during thin-section preparation leaving only a mold of its previous location.
M2-26	*S. siderea*	Approx. 10% sediment particles within skeleton, usually confined to skeleton pores. Particles are sub-rounded and vary in size between 0.3 to 0.5 mm. Coral skeleton shows no signs of alteration. A few late calcite cements appear growing over skeleton and sediment surface. Part of the sediment was removed during thin-section preparation leaving only a mold of its previous location.
Mz-4	*S. siderea*	Approx. 10-15% sediment particles within skeleton, usually confined to skeleton pores. Particles are sub-rounded and vary in size between 0.3 to 0.5 mm. Coral skeleton shows no signs of alteration. A few late calcite cements appear growing over skeleton and sediment surface. Part of the sediment was removed during thin-section preparation leaving only a mold of its previous location.
Mz-12	*S. siderea*	Approx. 7-8% sediment particles within skeleton, usually confined to skeleton pores. Particles are sub-rounded and vary in size between 0.3 to 0.5 mm. Coral skeleton shows no signs of alteration. A few late calcite cements appear growing over skeleton and sediment surface. Part of the sediment was removed during thin-section preparation leaving only a mold of its previous location.
Mz-27	*M. faveolata*	Approx. 10% sediment particles within skeleton, usually confined to skeleton pores. Particles are sub-rounded and vary in size between 0.3 to 0.5 mm. Coral skeleton shows no signs of alteration. A few late calcite cements appear growing over skeleton and sediment surface. Part of the sediment was removed during thin-section preparation leaving only a mold of its previous location.
Mz-29	*M. faveolata*	Approx. 10-15% sediment particles within skeleton, usually confined to pores although some actually cut across skeleton. Particles are sub-rounded and vary in size between 0.3 to 1.0 mm. Coral skeleton shows no signs of alteration. A few late calcite cements appear growing over skeleton and sediment surface. Part of the sediment was removed during thin-section preparation leaving only a mold of its previous location.
M3-18	*M. faveolata*	Approx. 15-17% sediment particles within skeleton, usually confined to pores although some actually cut across skeleton. Particles are sub-rounded and vary in size between 0.3 to 0.5 mm. Coral skeleton shows no signs of alteration. Substantial late calcite cements appear growing over skeleton and sediment surface. Some of the sediment was removed during thin-section preparation leaving only a mold of its previous location.
Pz-01	*M. faveolata*	Approx. 10% sediment particles within skeleton, usually confined to skeleton pores. Particles are sub-rounded and vary in size between 0.3 to 0.5 mm. Coral skeleton shows no signs of alteration. A few late calcite cements appear growing over skeleton and sediment surface. Part of the sediment was removed during thin-section preparation leaving only a mold of its previous location.

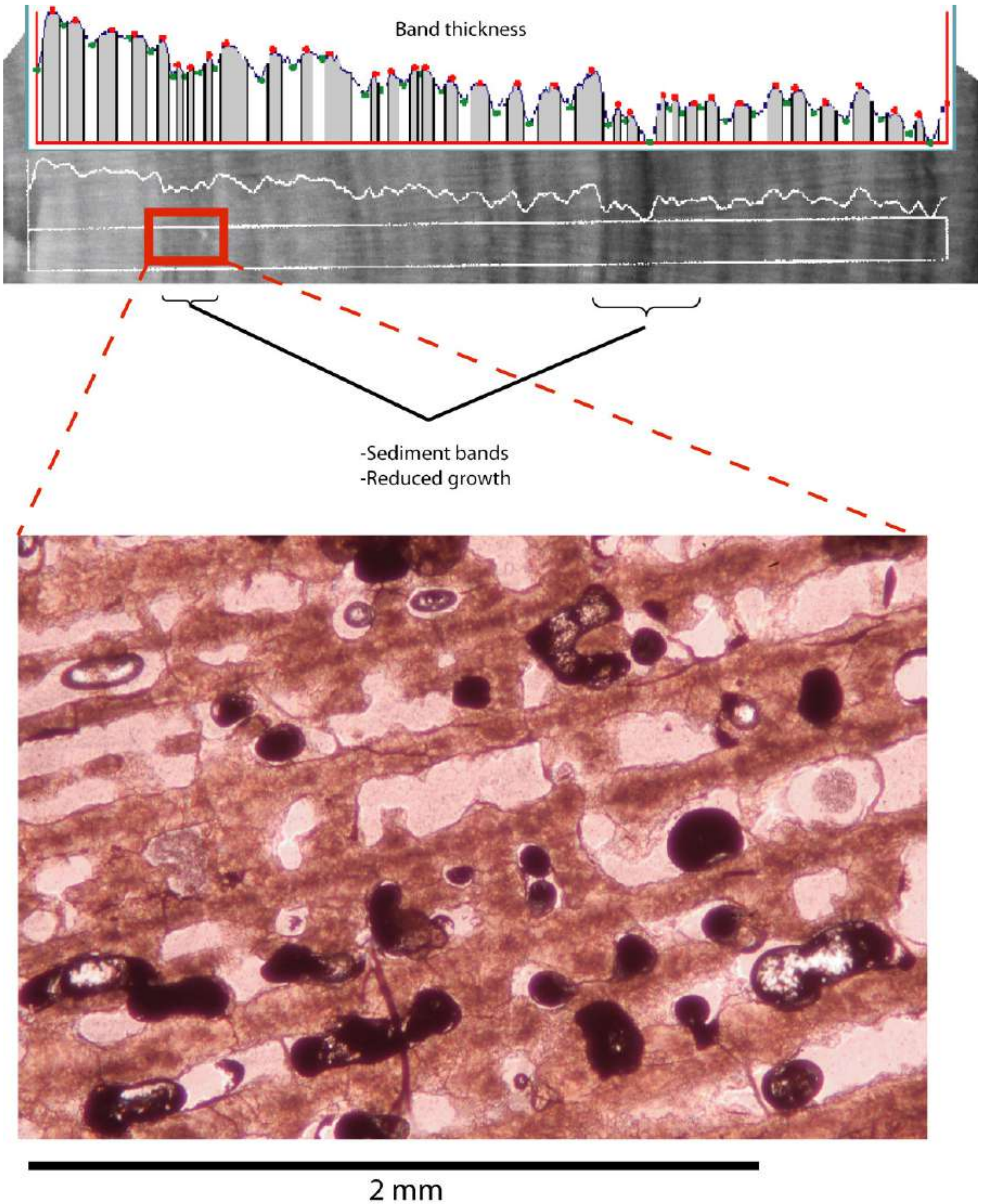

Figure 4.10 Thickness of coral bands against radiograph from sample Pz-01 (*M. faveolata*). Notice reduced growth (thickness) where sediment bands occur. Below is a microphotograph of the bands showing location of sediment (black)

Table 10. Summary of calibrated radiocarbon ages from coral samples in Cañada Honda

Coral Sample	Location from L. Enriquillo	Elevation MSL	$\delta^{13}C$	Initial age (years)	Error (2σ)	Cal. ^{14}C ages (BP)	Error (2σ)	Paleo-depth (±1m)
M. faveolata								
M1-5	169.4 m	-27.0 m	-3.51	8,560	40	9,256.0	137	10.0 m
M2-11	265.6 m	-22.0 m	-3.75	7,390	45	7,882.5	99.5	12.0 m
Mz-10	322.6 m	-17.0 m	-2.13	6,240	30	6,736.5	94.5	10.0 m
Mz-29	382.5 m	-11.0 m	-3.0	7,200	45	7,705.0	106	2.0 m
S. siderea								
M1-17	204.2 m	-26.0 m	-4.53	8,130	45	8,628.0	165	12.0 m
M2-26	275.0 m	-20.0 m	-3.07	7,350	40	7,846.0	97	10.0 m
Mz-12	322.8 m	-17.0 m	-3.47	6,910	40	7,465.0	83	9.0 m

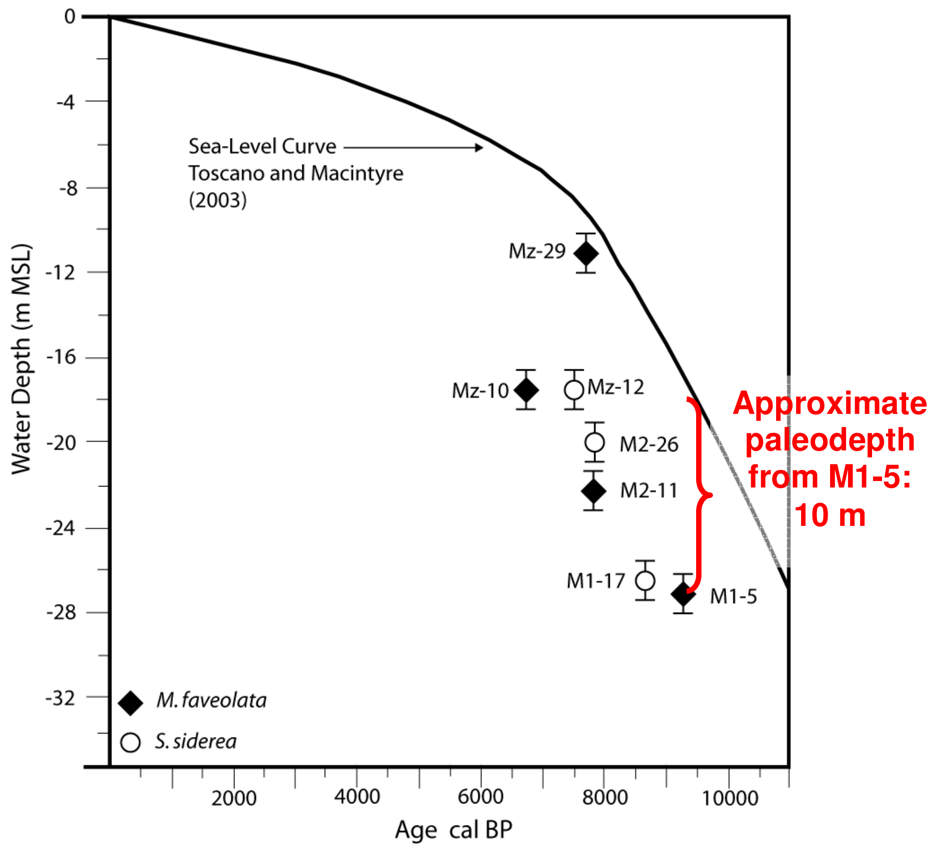

Figure 4.11 Correlation of calibrated radiocarbon ages from Cañada Honda with the corrected Holocene sea-level curve of Toscano and Macintyre (2003). The vertical difference between the elevation of the sample and sea level at the time it was alive (example in red for M1-5) yields the paleodepth of the coral.

established Holocene sea-level curve (Figure 4.11) to establish an approximate paleodepth at which coral specimens grew. Except for coral sample Mz-29, which occurred in a topographic high (Figure 4.1), the remaining corals developed at paleodepths between 9 m to 12 m (Table 10).

4.5 Sediment analyses

4.5.1 Sediment composition

Sediment composition analyses conducted on sediment samples from the Cañada Honda fossil reef are characterized by a high percentage of $CaCO_3$ (Table 11). Carbonate content varied from 84% to 96%. In contrast, the sediment samples from the fluvio-deltaic deposits in Las Clavellinas are characterized by carbonate content varying from 41% to 69% (Table 11). Sediment from Clavellinas still possesses significant amounts of $CaCO_3$ implying that it originated from the Neogene limestones surrounding the Enriquillo Valley and provided and additional source of carbonate to the reef sediment in Cañada Honda and other reef systems within the Enriquillo Basin.

4.5.2. Sediment grain size

Results of grain size analysis indicate that the fluvial sediment from Las Clavellinas (Table 12) consists largely of mud (avg. 61.8% ± 7.2 2σ) whereas most of the Cañada Honda reef sediment (Table 12) is comprised of coarse-grained sediment (avg. 71.4% ± 2.2 2σ).

TABLE 11. Results of sediment composition analyses from Cañada Honda reef sediment and Las Clavellinas

Sediment sample	Elevation MSL (± 1m)	% Organic Matter	% Carbonate	% Non-Carbonate	Site description
LCS-1	~0-5 m	3	69	28	Fluvial sequence (Clavellinas)
LCS-2	~0-5 m	2	50	48	Fluvial sequence (Clavellinas)
LCS-3	~0-5 m	5	41	54	Tidal sediment (Clavellinas)
LCS-4	~0-5 m	8	54	38	Fluvial sequence (Clavellinas)
S-43-1	-35 m	2	89	9	Massive coral subzone
S-43-2	-34 m	4	88	8	Massive coral subzone
S-43-3	-33 m	4	92	4	Platy coral subzone
S-67-1	-33 m	4	92	4	Massive coral subzone
S-67-2	-32 m	0	96	4	Massive coral subzone
S-67-3	-31 m	5	86	9	Massive coral subzone
S-104-1	-30 m	0	93	7	Massive coral subzone
S-104-2	-29 m	3	94	3	Massive coral subzone
S-104-3	-28 m	12	84	4	Platy coral subzone
S-104-4	-27 m	5	88	7	Platy coral subzone
S-136-1	-28 m	3	94	3	Massive coral subzone
S-136-2	-27 m	2	90	8	Massive coral subzone
S-176-1	-25 m	8	90	2	Massive coral subzone
S-176-2	-24 m	3	94	3	Massive coral subzone
S-176-3	-23 m	7	90	3	Platy coral subzone
S-232-1	-21 m	2	94	4	*A. cervicornis* subzone
S-232-2	-20 m	3	96	1	Mixed-coral subzone
S-232-3	-19 m	4	95	1	Mixed-coral subzone
S-400-1	-12 m	2	95	3	*A. cervicornis* subzone

Table 12. Grain size in sediment samples from CH and Las Clavellinas

Sample	>63µ (%)	<63µ (%)
S-30-1	65.5	34.5
S-30-2	69.2	30.8
S-104-1	67.9	32.1
S-104-2	72.6	27.4
S-104-3	63.9	36.1
S-136-1	55.5	44.5
S-136-2	65.0	35.0
S-149-1	66.2	33.8
S-149-2	67.3	32.7
S-176-1	68.8	31.2
S-176-2	63.0	37.0
S-176-3	69.8	30.2
S-202-1	68.4	31.6
S-202-2	72.2	27.8
S-202-3	68.7	31.3
S-221-1	64.4	35.6
S-221-2	72.5	27.5
S-221-3	71.9	28.1
S-232-1	76.9	23.1
S-232-2	71.3	28.7
S-232-3	70.1	29.9
S-244-1	51.6	48.4
S-244-2	94.0	6.0
S-244-3	77.5	22.5
S-252-1	77.7	22.3
S-252-2	73.3	26.7
S-260-1	67.9	32.1
CH-43-1	79.9	20.1
CH-43-2	70.0	30.0
CH-43-3	77.3	22.7
CH-43-4	82.9	17.1
CH-67-1	77.7	22.3
CH-67-2	81.5	18.5
CH-67-3	73.0	27.0
CH-67-4	71.4	28.6
CH-80-1	83.5	16.5
CH-80-2	73.1	26.9
CH-80-3	65.8	34.2
CH-117-1	72.8	27.2
CH-117-2	64.4	35.6
CH-117-3	62.5	37.5
CH-117-4	62.1	37.9
CH-245-1	67.2	32.8
CH-299-1	79.9	20.1
CH-380-1	81.0	19.0
CH-400-1	80.2	19.8
CH-400-2	74.2	25.8
Average C. Honda (±2.2 2σ)	71.4	28.6
LCS-1	45.9	54.1
LCS-2	32.4	67.6
LCS-3	42.7	57.3
LCS-4	31.6	68.4
Average Clavellinas (± 7.2 2σ)	38.2	61.8

4.5.3 XRD analyses

Results show that aragonite, calcite and quartz are the three major mineral phases (Table 13) with the former two being the dominant peaks (Appendix A). Although not identified, most diffractograms show a slight presence of clays which appear between the 4-15 2θ-range (Appendix A). The dominant calcite peak in all Cañada Honda reef sediment samples corresponds to low-Mg calcite (1-4 mol% Mg) (Table A1 in Appendix A) which may imply that the reef sediment in Cañada Honda contains significant amounts of allochtonous low-Mg calcite that originated from the mountains north of Cañada Honda. Some diffractograms show a distinctive high-Mg calcite (12-15 mol% Mg) peak overlapping with the larger and more intense low-Mg calcite peak (Appendix A). Further examination carried out on the separate size fractions of sediment samples from Cañada Honda (i.e. the portion coarser than 63-μ, as well as the mud portion of each sample <63-μ) shows that aragonite, calcite and quartz are still the main mineral phases in the Cañada Honda reef sediment (Table 14). However, due to better resolution in the diffractograms (smaller 2θ range, Appendix A), a distinctive high-Mg calcite peak can now be observed for most of the samples. In addition, most sample diffractograms have peaks related to minerals of the plagioclase group and some samples have dolomite (Appendix A). Close examination of the calcite peaks (Tables A2 and A3 in Appendix A) reveal that the calcite peaks with the highest intensity corresponds to low-Mg calcite whereas the less intense calcite peaks corresponds to high-Mg calcite, similar to previous XRD analyses. The fluvial sediment samples from the Clavellinas site are composed primarily of low-Mg calcite and quartz (Table 14). XRD analyses on the acid-insoluble residue of these same samples confirm the presence of quartz and some plagioclase and vermiculite (Table 14 and Appendix A).

The presence of plagioclase in the sediment samples is problematic becuase there is no immediate source for such minerals close to the Enriquillo Basin and also this mineral alters quite rapidly when weathered. Dust from the Sahara and/or volcanic ash from the Lesser Antilles could bring plagioclase to the environment but this would have had to travel long distances (several hundred kilometers) without being altered and reach the Enriquillo basin, thus this option seems unlikely. Thus, it is possible the plagioclase signals from the diffractograms could have been mixed with the signal from some clays.

Table 13. Summary of XRD results on whole samples of reef sediment from Cañada Honda

Sample	Aragonite	Calcite	Quartz	Other	Comments
S-43-1	X	X	X		
S-43-2	X	X	X		
S-43-3	X	X	X		
S-67-1	X	X	X		Some clays possible
S-67-2	X	X	X		Some clays possible
S-67-3	X	X	X		Some clays possible
S-104-1	X	X	X		Some clays possible
S-104-2	X	X	X		Some clays possible
S-104-3	X	X	X		Some clays possible
S-104-4	X	X	X		Some clays possible
S-136-1	X	X	X		
S-136-2	X	X	X		
S-176-1	X	X	X		
S-176-2	X	X	X		
S-176-3	X	X	X	Halite	
S-232-1	X	X	X	Halite	Some clays possible
S-232-2	X	X	X	Halite	Some clays possible
S-232-3	X	X	X		Some clays possible
S-400-1	X	X	X		Some clays possible

Table 14. Summary of XRD results on sieved reef sediment samples from CH and Las Clavellinas

Sample	Aragonite	Low-Mg calcite	High-Mg calcite	Quartz	Plagioclase?	Other	Comments
Cañada Honda							
CH-43-1 Coarse	X	X	X	X	X		High-Mg calcite peak observable
CH-43-1 Mud	X	X	X	X	X		High-Mg calcite peak observable
CH-43-2 Coarse	X	X	X	X	X		High-Mg calcite peak well-defined
CH-43-2 Mud	X	X	X	X	X		High-Mg calcite peak well-defined
CH-43-3 Coarse	X	X	X	X	X		High-Mg calcite peak well-defined
CH-43-3 Mud	X	X	X	X	X		High-Mg calcite peak well defined
CH-43-4 Coarse	X	X	X	X	X		High-Mg calcite peak well-defined
CH-43-4 Mud	X	X	X	X	X		High-Mg calcite peak well-defined
CH-67-1 Coarse	X	X	X	X	X		High-Mg calcite peak well-defined
CH-67-1Mud	X	X	X	X	X		High-Mg calcite peak observable
CH-67-2 Coarse	X	X	X	X	X		High-Mg calcite peak not well-defined
CH-67-2 Mud	X	X	X	X	X		High-Mg calcite peak observable
CH-67-3 Coarse	X	X	X	X	X		High-Mg calcite peak observable
CH-67-3 Mud	X	X	X	X	X		High-Mg calcite peak observable
CH-67-4 Coarse	X	X	X	X	X		High-Mg calcite peak observable
CH-67-4 Mud	X	X	X	X	X		High-Mg calcite peak well-defined
S-104-1 Coarse	X	X	X	X			High-Mg calcite peak not observable
S-104-1Mud	X	X	X	X	X		High-Mg calcite peak observable
S-104-2 Coarse	X	X	X	X	X		High-Mg calcite peak well-defined
S-104-2 Mud	X	X	X	X	X		High-Mg calcite peak well-defined
S-104-3 Coarse	X	X	X	X	X		High-Mg calcite peak well-defined
S-104-3 Mud	X	X	X	X	X	Dolomite	High-Mg calcite peak well-defined
S-136-1 Coarse	X	X	X	X		Dolomite	High-Mg calcite peak well-defined
S-136-1Mud	X	X	X	X	X		High-Mg calcite peak well-defined
S-136-2 Coarse	X	X	X	X	X		High-Mg calcite peak observable
S-136-2 Mud	X	X	X	X	X		High-Mg calcite peak well-defined
S-176-1 Coarse	X	X	X	X	X		High-Mg calcite peak not observable
S-176-1 Mud	X	X	X	X	X		High-Mg calcite peak not observable
S-176-2 Coarse	X	X	X	X		Dolomite	High-Mg calcite peak observable

Table 14. (Cont).

Sample	Aragonite	Low-Mg calcite	High-Mg calcite	Quartz	Plagioclase?	Other	Comments
S-176-2 Mud	X	X	X	X	X	Dolomite	High-Mg calcite peak observable
S-176-3 Coarse	X	X	X	X			High-Mg calcite peak well-defined
S-176-3 Mud	X	X	X	X	X	Dolomite	High-Mg calcite peak well-defined
S-232-1 Coarse	X	X	X	X		Dolomite	High-Mg calcite peak observable
S-232-1 Mud	X	X	X	X	X		High-Mg calcite peak observable
S-232-2 Coarse	X	X	X	X			High-Mg calcite peak well-defined
S-232-2 Mud	X	X	X	X	X	Dolomite	High-Mg calcite peak well-defined
S-232-3 Coarse	X	X	X	X	X		High-Mg calcite peak well-defined
S-232-3 Mud	X	X	X	X	X	Dolomite	High-Mg calcite peak well-defined
CH-400-1 Coarse	X	X	X	X	X		High-Mg calcite peak not observable
CH-400-1 Mud	X	X	X	X	X		High-Mg calcite peak not observable
CH-400-2 Coarse	X	X	X	X			High-Mg calcite peak well-defined
CH-400-2 Mud	X	X	X	X	X	Dolomite	High-Mg calcite peak well-defined
Clavellinas (Fluvial)							
LCS-1 Coarse		X		X	X		Single low-Mg calcite peak
LCS-1 Mud		X		X	X		Single low-Mg calcite peak
LCS-2 Coarse		X		X	X		Single low-Mg calcite peak
LCS-2 Mud		X		X	X		Single low-Mg calcite peak
LCS-4 Coarse		X		X	X		Single low-Mg calcite peak
LCS-4 Mud		X		X	X		Single low-Mg calcite peak
LCS-1 (acid insoluble)				X	X		
LCS-2 (acid insoluble)				X	X	Vermiculite	
LCS-3 (acid insoluble)				X	X	Vermiculite	
LCS-4 (acid insoluble)				X	X		

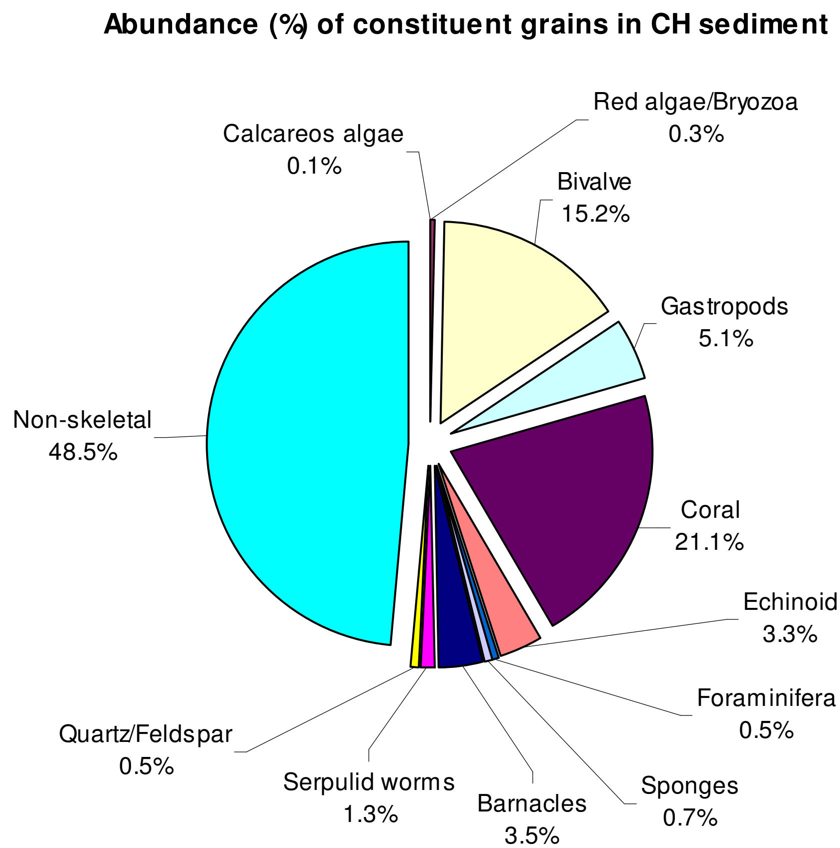

Figure 4.12 Relative average abundance (%) of constituent grains in CH reef sediment

4.5.4 Constituent grain characterization

Twenty thin-sections were made from sediment samples from Cañada Honda and Las Clavellinas. Eighteen reef sediment samples come from Cañada Honda and two fluvial sediment samples come from Las Clavellinas (Table 15). The reef sediment samples from Cañada Honda consists largely of non-skeletal grains (48.5%) in the form of lithoclasts and mud pellets (Figure 4.12 and Table 15) followed by coral fragments (21.1%), bivalve (15.2%), gastropods (5.1%), barnacles (3.5%), echinoderm (3.3%) and serpulids worms (1.3%). Calcareous algae, bryozoans, red algae, foraminifera, sponges, and quartz account for no more than 2% of the grains in Cañada Honda (Figure 4.12).

Fluvial sediment samples from the Clavellinas site (Table 15) are characterized by an abundance of non-skeletal grains (i.e. lithoclasts and mud pellets) between 86-89% with minor ostracods (5-7%), quartz (1%) and gastropods (<1%). Looking in more detail at the distribution of the three most abundant components (i.e. non-skeletal grains, coral and bivalve) throughout the Cañada Honda reef, it can be noticed that the contribution of coral fragments in the reef sediment increases in samples from the shallower part of the Cañada Honda fossil reef (Figure 4.13).

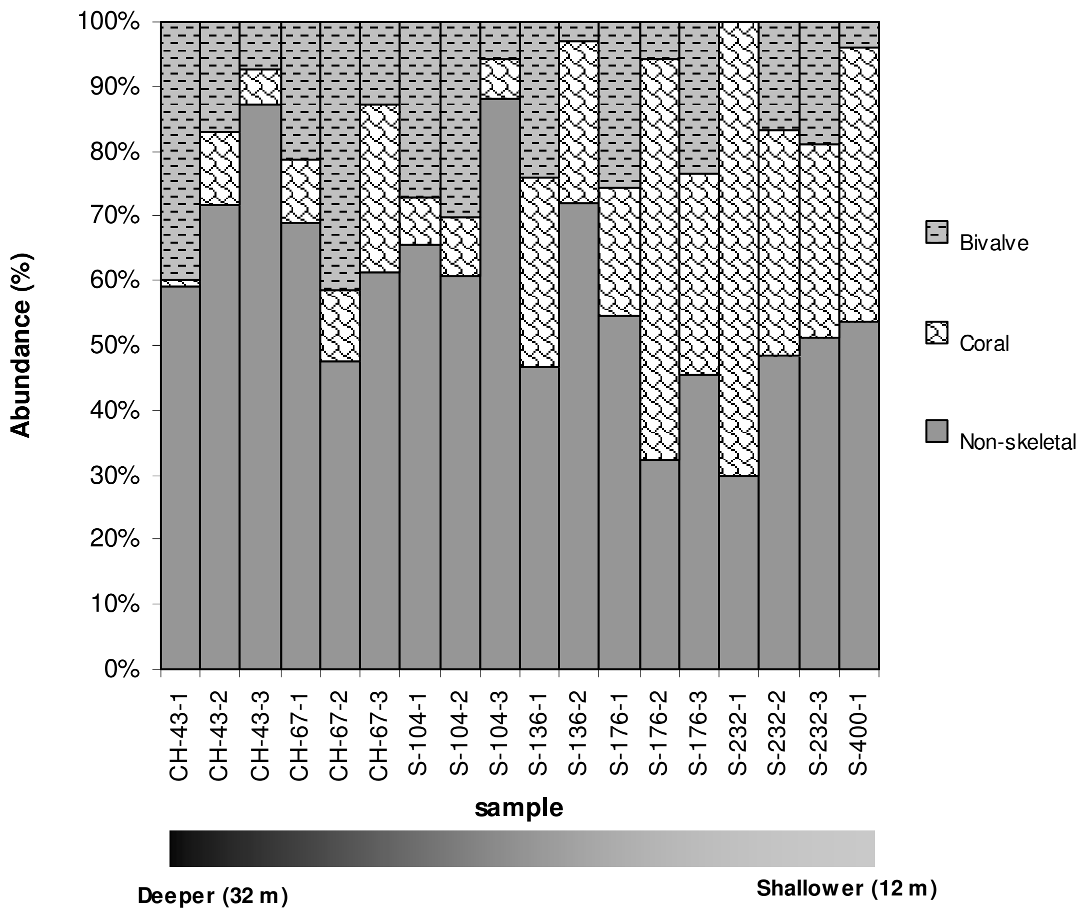

Figure 4.13 Relative abundances of sediment, bivalve and coral fragments in Cañada Honda sediment samples.

Table 15. Summary of constituent grain abundances (%) from reef sediment from Cañada Honda and sediment from Las Clavellinas

Sample	Calcareous algae	Red algae/ Bryozoa	Bivalve	Gastropods	Coral	Echinoid	Foraminifera	Sponges	Barnacles	Serpulid worms	Ostracod	Quartz	Non-skeletal (mud pellets and lithoclasts)
LCS-1*	0.0	0.0	0.0	<1.0	0.0	0.0	0.0	0.0	0.0	0.0	5.0	5.0	89.0
LCS-2*	0.0	0.0	0.0	1.0	0.0	0.0	0.0	0.0	0.0	0.0	7.0	5.0	86.0
CH-43-1	0.0	0.0	35.3	0.3	0.7	9.3	0.3	0.3	0.7	0.3	0	0.3	52.3
CH-43-2	0.0	0.0	15.7	5.3	10.0	1.3	0.3	0.3	1.3	0.3	0.0	0.0	65.3
CH-43-3	0.0	0.7	7.0	0.3	5.0	1.0	1.0	0.3	1.3	0.3	0.0	1.0	82.0
CH-67-1	0.0	0.3	15.3	7.3	7.0	1.7	0.3	0.3	16.7	1.0	0.0	0.7	49.3
CH-67-2	0.0	0.0	38.3	1.0	10.3	0.7	0.3	0.0	4.7	0.3	0.0	0.3	44.0
CH-67-3	0.0	0.0	11.0	3.0	22.3	4.0	0.3	0.7	0.7	4.3	0.0	0.7	53.0
S-104-1	0.0	0.3	19.7	6.3	5.3	5.7	0.0	0.0	14.7	0.0	0.0	0.3	47.7
S-104-2	0.0	0.0	24.3	1.3	7.3	5.7	0.3	1.7	9.3	1.3	0.0	0.0	48.7
S-104-3	0.0	0.7	3.6	24.5	3.6	1.0	1.3	1.3	5.0	4.0	0.0	0.3	54.6
S-136-1	1.3	0.3	21.0	4.0	25.3	3.0	0.7	0.3	2.3	1.0	0.0	0.3	40.3
S-136-2	0.0	0.3	2.7	5.3	22.0	3.3	0.7	1.0	0.7	0.7	0.0	0.3	63.0
S-176-1	0.0	0.0	20.3	13.0	15.7	1.7	1.0	0.7	3.7	0.3	0.0	0.3	43.3
S-176-2	0.0	0.0	5.3	4.0	58.3	1.0	0.0	0.0	0.0	0.7	0.0	0.3	30.3
S-176-3	0.0	0.7	19.3	3.3	25.3	8.3	0.0	1.0	1.3	1.7	0.0	1.7	37.3
S-232-1	0.0	0.0	0.0	0.3	69.0	0.0	0.0	0.7	0.0	0.3	0.0	0.3	29.3
S-232-2	0.0	0.7	14.3	3.3	30.0	5.7	1.3	1.3	0.0	1.0	0.0	0.7	41.7
S-232-3	0.0	1.7	16.0	2.3	25.0	4.0	0.3	1.3	0.0	5.7	0.0	0.7	43.0
S-400-1	0.0	0.0	3.7	7.0	37.7	1.7	0.0	1.0	0.0	0.3	0.0	0.7	48.0

*Fluvial sediment sample from Las Clavellinas site

5.0 Discussion

5.1 The Cañada Honda Fossil Reef Development

The Cañada Honda fossil reef displays characteristics unique to coral reefs influenced by high rates of sedimentation. These are: the large abundances of coral species known to tolerate high sedimentation (e.g. *S. siderea, M.* spp.*, C. natans, S. intersepta*); the tendency for species such as *S. siderea* to form almost monospecific stands (Cortés and Risk, 1985); and the tendency of individual coral colonies to grow as encrusting dome-shaped and platy forms (Van Woesik and Done, 1997). In fact, coral cover data measured along the paleoreef surface in Cañada Honda supports the idea of siltation stress. Only two coral species account for approximately 80% of the "live" coral cover and four coral species account for approximately 97% of the total "live" coral cover (Figure 4.3). Coral colonies along the paleoreef surface are characterized by their large size, being on the order of 20-30 cm with few numbers of juveniles. The high coral cover (40%) is explained by the presence of such large and old colonies in sediment-stressed sites where excess sediment inhibits successful recruitment and colonization of substrate by larvae (Cortés and Risk, 1985). Furthermore, some coral colonies analyzed for coral growth contained bands of sediment incorporated into the skeleton (Figures 4.7 and 4.10). This is especially true for *M. faveolata* colonies. In hand samples, these bands were not so obvious on the *S. siderea* colonies. However, in thin-sections *S. siderea* contained bands with about 10% sediment. This may be because *S. siderea* is very effective at rejecting sediment with larger grain size and has a denser skeleton compared with *Montastraea* spp. (Budd et al., 1993).

The species assemblage of the *A. cervicornis* zone in Cañada Honda is very similar to that in many shallow reef sites throughout the Caribbean, such as reefs in the central lagoon of the Belize Barrier Reef (Aronson et al., 1998 and 2002). Such settings are characterized by limited wave action, but high levels of sedimentation are not necessarily present. On the other hand, the lower coral assemblages in Cañada Honda (*S. siderea* zone) are unique in terms of the high abundances of the massive coral *S. siderea*. The importance of corals of the genus *Siderastrea* in high sedimentation environments has been recognized in the earlier studies of Hubbard and Pocock (1972), Cortés and Risk (1985) and Acevedo et al. (1989). Other coral species associated with environments of high-terrestrial runoff in the Caribbean are *M. cavernosa*, *P. astreoides, Undaria spp.* and *C. natans* (Cortés and Risk, 1985; Acevedo et al., 1989), coral species that are also common in Cañada Honda (Table 2 and Figure 4.2). However, compared with modern reef sites in high-terrestrial runoff (e.g. Cagüita in Costa Rica, Mayagüez Bay and Ponce, Puerto Rico), *S. siderea* is the most important coral species at Cañada Honda to the point that it can form almost monospecific stands in some areas (Table 2), whereas in the modern reef sites its importance, at least in terms of coral cover, is minor (Figure 4.6). In fact, when coral species abundances between Cañada Honda and modern reef sites in SW Puerto Rico are compared (Figure 4.6) differences in community structure are evident. These differences are essentially the result of the overwhelming abundance of *Siderastrea spp.* in Cañada Honda and the dominant role of coral species of the *M. annularis* complex and *M. cavernosa* in the modern reef sites, even those characterized by high-terrestrial runoff like Mayagüez and Ponce (Figure 4.6). Although more data in terms of community structure from the greater Caribbean will be required to make a more definitive conclusion, it seems that the abundances of *Siderastrea spp.* in Cañada Honda are unique even for a site with high-terrestrial runoff. It is very interesting, however, that coral cover data from the paleoreef surface in Cañada Honda shows *M. faveolata* as the dominant species (Figure 4.4) as expected for many modern reefs. The coral assemblage from the paleoreef surface could represent an unusual community that is not necessarily representative of the whole community structure in Cañada Honda.

A possible explanation for the large abundances of *S. siderea* is that there were unique conditions in Cañada Honda that favored this coral species over others in terms of growth and survival. The answer to this may lie in the sedimentary processes that occurred in the entire Enriquillo Basin and its vicinity. According to Budd et al. (1993), *S. siderea* not only possesses one of the highest sediment rejection rates but also is more tolerant to salinity fluctuations (Muthiga and Szmant, 1987). Considering the physiography and oceanography of the former Enriquillo Bay, it is likely that high salinity fluctuations occurred, in addition to high-terrestrial runoff. This may well explain the high abundances of the coral species *S. siderea* in the Cañada Honda fossil reef. Isotopic data in fossil corals from the Enriquillo Basin suggest that during the Mid-Holocene, salinity fluctuated as much as 15 ppt (Greer and Swart, 2006) due to a combination of increased precipitation due to more than typical northward migration of the Intertropical Convergence Zone (ITCZ) and the particular geomorphology of the Enriquillo Basin where salinity effects are amplified.

Figure 5.1 Model for the formation of ragged margins in coral colonies and the development of the so-called “stack of pancakes” morphology in CH due to the occurrence of multiple high-sedimentation events (From Hubbard et al. 2005).

The predominant coral morphologies in Cañada Honda are hemispheres and cones with ragged margins (Table 5). Ragged margins in reef-building organisms develop as a result of high sedimentation events that cause nearly complete burial of the colony (James and Bourque, 1992). Although the coral initially started growing as a hemisphere, the colony is almost drowned during a high sedimentation event. The exposed part of the colony continues to grow again as a cone or hemisphere until the next sedimentation event comes. High sedimentation rates influence the colonial organism to focus growth upright as sedimentation rates increase resulting in the so-called “stack of pancakes” (Davis et al., 2008) morphology (Figure 5.1). In fact, data from Davis et al. (2008) and Hubbard et al. (2008) show that *M. faveolata* colonies tend to develop a columnar morphology over the long-term. Díaz and Ramírez (2005) determined sedimentation rates from a single *M. faveolata* colony (sample M2-11) from Cañada Honda and found that sedimentation events occurred at intervals between 4 to 14 years. The sediment horizons (Figure 4.7) found within the coral samples tend to occur in the narrower portions of the colony (i.e. between "pancakes"), supporting the idea that periodic high sedimentation events are the explanation for the formation of the ragged margins in the coral colonies. The areas within the coral affected by such sediment accumulation are also characterized by reduced linear extension (Figure 4.10). The ragged margin occurring over intervals between 4-14 years highlights an additional feature of the terrestrial runoff in Cañada Honda. This occurred sporadically, allowing time for reef corals to keep-up with sedimentation in a rising sea-level scenario.

Given the evidence for high sedimentation, low coral growth rates would be expected in the Cañada Honda fossil reef. At least for *M. faveolata*, this may be the case. Table 8 shows annual growth rates of modern *M. annularis* and *M. faveolata* from around the Caribbean and these are typically higher than those of fossil *M. faveolata* from Cañada Honda. In contrast, growth rates of fossil *S. siderea* from Cañada Honda are similar to most growth rate data from the Caribbean. However, if the data from Table 8 are clustered within different depth ranges and then graphically plotted against the coral growth rate values obtained from Cañada Honda, it can also be observed that fossil *M. faveolata* from Cañada Honda fall within the range of modern coral growth near or below 12 m (Figure 4.8). This implies that the low coral growth rates of *M. faveolata* in Cañada Honda could also be explained as the response of these corals to reduced light penetration at depths near 12 m as a result of high turbidity. This statement cannot be made unequivocally for *S. siderea* (Figure 4.9). It is possible that due to the different feeding mechanism and adaptability of *S. siderea* to stress conditions as pointed out by Budd et al. (1993), coral growth rates in this species are less affected by either sedimentation or depths greater than 12 m.

Calibrated radiocarbon ages from this study came from corals located today at elevations between -27m to -11m and ranged between 9,200 to 6,736 BP (Table 10). Using the corrected sea-level curve of Toscano and MacIntyre (2003) and given the fact that no significant vertical motions have occurred in the Cañada Honda site for at least the past 10,000 years (Mann et al., 1984; Mann et al., 2002), these dates imply that most corals from Cañada Honda sampled in this study lived at water depths between approximately 10m to 12m (Figure 4.11). Coral growth rate values of *M. faveolata* from Cañada Honda are consistent with growth at such depths (Figure 4.8). It is evident that corals in Cañada Honda were able to grow at the threshold of coral development in potentially turbid waters. Some modern Caribbean coral reefs described as being under severe siltation stress do not have coral development beyond depths of 12 m (Acevedo et al., 1989; Fabricius, 2005).

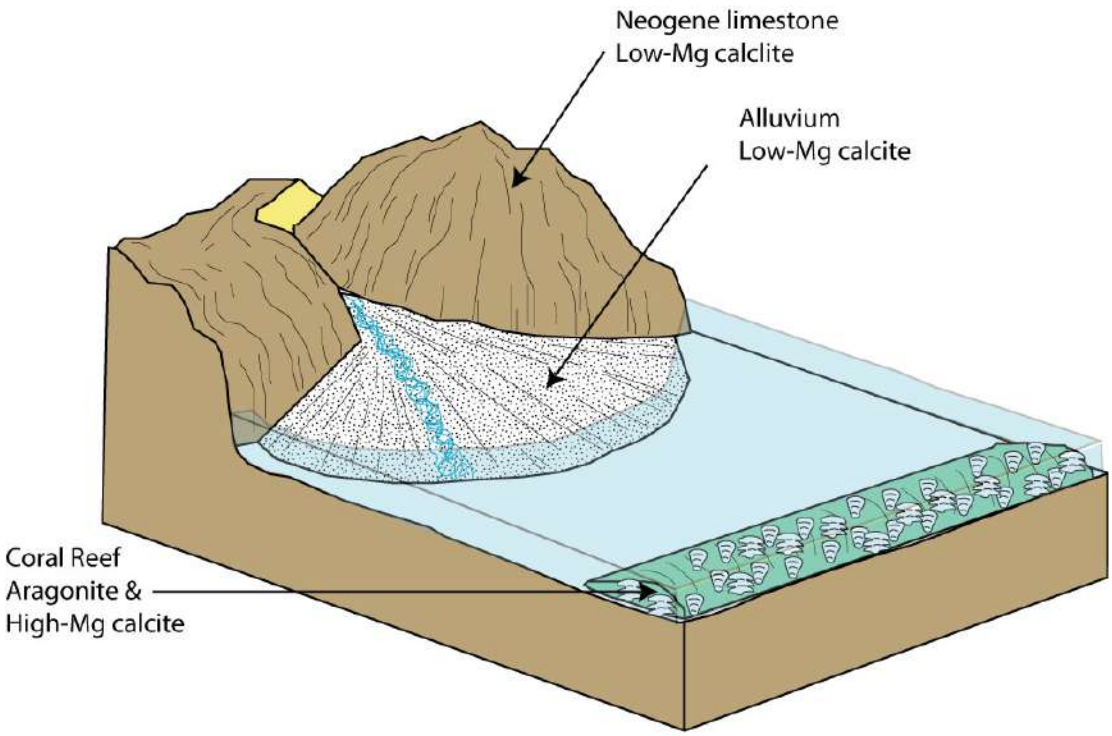

Figure 5.2 Sedimentary processes within the paleo-Enriquillo Bay illustrating a general model for the mineralogy of sediment based on provenance.

The reef sediment collected from the Cañada Honda fossil reef is characterized by a high percentage of $CaCO_3$. These proportions are comparable to reef sediment in sites far from terrigenous sediment influence, such as the reef tract off La Parguera, southwestern Puerto Rico (Morelock et al., 1994). However, the low concentrations of non-carbonate, insoluble material should not be interpreted as indicating a lack of terrigenous sediment influx to the Cañada Honda fossil reef. The mountains north and south of the Enriquillo Lake consist of Neogene and Pleistocene carbonate rocks (Mann et al., 1984) that are the source rocks for much of the sediment coming into the Enriquillo Basin. As evidenced by the sediment composition and mineralogy of fluvio-deltaic sequences near Las Clavellinas (Tables 11 & 14), these contain significant amounts of allochtonous (extrabasinal) carbonate that was introduced to the reef environment. In fact, the carbonate fraction in these samples is made entirely of low-Mg calcite or old, extrabasinal carbonate (Table 14) as expected from the carbonate originated from the Neogene limestones (see Figure 5.2). Therefore, it is not unreasonable to expect that the reef sediment in Cañada Honda should consists of more than 90% carbonate material even though is characterized by high-terrestrial runoff. As an example, sediment from reefs within the Mayagüez Bay in western Puerto Rico, which are characterized by high-terrestrial runoff, can contain above 70% siliciclastic material (Morelock et al., 1983). XRD analyses on Cañada Honda reef sediment show that low-Mg calcite, high-Mg calcite and aragonite are the main carbonate mineral phases (Tables 14-15). Although diagenesis could have removed the magnesium of the high-Mg calcite (becoming low-Mg calcite), the fact that high-Mg calcite and aragonite are still abundant in the sediments implies that alteration has been minimal. Petrography of Cañada Honda reef sediment shows that non-skeletal grains, i.e. lithoclasts and mud pellets, comprise about 48.5% of the grain fraction (Table 15). This non-skeletal material is similar to the sediment described for the Las Clavellinas sediment samples which by definition are allochtonous (e.g. the alluvial material in Figure 5.2). The similarity in character of the non-skeletal material within Cañada Honda sediment and the fluvial sediment from Las Clavellinas could imply similar origin (i.e. allochtonous) for both. However, it is important to point out that lithoclasts and mud-pellets can also form by reef processes (Flügel, 2004), thus more data in terms of the geochemistry of the sediment would be required to make a more definitive conclusion.

The constituent grain analyses conducted on the sediment samples can provide essential information about the environmental conditions that prevailed in the Cañada

Honda reef 10,000 to 5,000 years ago. The amounts of non-skeletal grains are not only considerable, but also dominant in most of the Cañada Honda reef sediment samples (Table 15). They are followed in abundance by coral and bivalve fragments (Table 15). Normally, reef sediment is dominated by skeletal grains (Ginsburg, 1956; Swinchatt, 1965; Pandolfi et al., 1999; Lidz and Hallock, 2000), which is not the case in Cañada Honda. In addition, the data show the negligible importance of calcareous algae (e.g. *Halimeda spp.*) and encrusters such as red coralline algae and bryozoans (Table 15). These type of grains constitute a substantial fraction regularly in coral reef sediment (Ginsburg, 1956; Pandolfi et al., 1999; Lidz and Hallock, 2000), even for reefs with high terrestrial runoff. One possible explanation is that the large sedimentation that existed in Cañada Honda inhibited (i.e. smothered) the settlement and successful growth of calcareous green algae and coralline red algae (Fabricius, 2005). In terms of the greater abundance of corals fragments in the *A. cervicornis* zone and mixed-coral subzone (Figure 4.13), these could be explained by an increase in bioerosion (Lidz and Hallock, 2000). However, it could also be the result of the greater abundance of fast-growing branching coral forms in these zones (Figures 4.1 and 4.2). Likewise, this portion of the Cañada Honda reef occurred in an area of relative higher energy that was more susceptible to storms that would inflict more coral colony fragmentation.

Another interesting attribute of the Cañada Honda reef sediment is the significant amount (3.5% avg.) of barnacle fragments (Figure 4.12). In individual samples, it can reach up to 16% (Table 15). These can be seen commonly attached to coral colonies in the Cañada Honda outcrop. Although barnacles can certainly be found in reef environments, they usually do not represent a major sediment contributor (Ginsburg, 1956; Perry, 1998; Pandolfi et al., 1999; Lidz and Hallock, 2000). In Discovery Bay, Jamaica, barnacles did not account for more than 0.1% of the total macroborer community (Perry, 1998). Barnacles are more common in cold water environments or in environments of high nutrients (Flügel, 2004). Nevertheless, increasing nutrient influx in reef environments can cause an increase in the number of suspension feeders, especially macroborers, which in great abundance can reduce reef accretion significantly (Hallock and Schlager, 1986). Thus, it is possible that the high abundance of barnacles in Cañada Honda could indicate high nutrient levels, which suggests that there may have been high nutrient levels in the Cañada Honda fossil reef and the entire paleo-Enriquillo Bay as well. Data from Estep et al. (2008) indicates that bioerosion in corals from the fossil reefs of the Enriquillo Valley range between 20-60% and is dominated by bivalves (*Lithophaga spp.*) whereas in the modern reefs of St. Croix, USVI, bioerosion ranges between 10-20% and is dominated by sponges (*Cliona spp.*). The modern reefs are located in an oligotrophic, wave-exposed setting in St. Croix (Estep et al., 2008). Similarly, Perry (1998) found that *Cliona* spp. is the dominant macroborer in reefs of Discovery Bay, Jamaica. The greater bioerosion and the shift in macroboring fauna observed in the fossil reefs of the Enriquillo Valley is consistent with the interpretation of higher nutrients (Estep et al., 2008) and may well explain the high abundances of barnacles in Cañada Honda. The fossil reefs occurred in a more protected, high sedimentation environment thus the interpretation that sedimentation was accompanied by high nutrients is plausible from this point of view. An important implication of high nutrients in Cañada Honda, besides a greater abundance of suspension feeders, is that phytoplankton productivity may also have been under such environmental conditions (Fabricius, 2005). There are many consequences produced by high phytoplankton abundances. Two of these are the production of particulate organic matter and turbidity (Fabricius, 2005). Data from reef sediment in Cañada Honda, however, shows little evidence for high particulate organic matter (Table 11) and turbidity, if it occurred, was minimal and episodically based on the evidence of coral development at depths above 12m in Cañada Honda (Table 10). Thus, the conclusion is that if there were high nutrient conditions in Cañada Honda, these were not chronic and were not a factor limiting coral reef development, at least in shallow water.

The high concentration of $CaCO_3$ from both incoming terrigenous sediment and reef-produced sediment was probably an advantage for the development of this Early to Mid-Holocene coral reef. According to Te (1997), fine-grained siliciclastic sediment reduces light penetration and coral photosynthesis two to three times more than equal amounts of fine-grained carbonate sediment. This is due to the light-colored, highly scattering optical properties of carbonate silt compared to the dark-colored, light-absorbing and weak scattering in the former (Te, 1997). It is possible, therefore, that due to the high carbonate content of incoming terrigenous sediment, light penetrated slightly deeper and better than expected for a reef under similar conditions but with mostly siliciclastic silt. Another possibility is that even though sedimentation was high, it occurred sporadically allowing time for the reef corals to respond and grow back, in such a way that they were able to keep-up with sedimentation and sea-level rise. In relation to this, although turbidity was definitely present, it was probably not a controlling factor in the development of coral reefs at Cañada Honda, in contrast to the well-known marginal reefs of the GBR (Smithers and Larcombe, 2003; Perry et al., 2008). The allochtonous sediment that reached Cañada Honda did not come from distant sources due to the proximity of the Sierra de Neiba, and was rich in sand and coarser grains (Table 12). This, and the fact that little siliciclastic clay is present in Cañada Honda sediment (Tables 11-14) implies that most of the sediment in Cañada Honda settled rapidly or did not stay suspended for long time periods, allowing coral reef development at depths of at least 12 m. As mentioned above, the propensity of corals to grow as encrusting domes and plates that eventually developed into "stack of pancakes" morphology supports the argument of rapid and episodic sediment settlement.

5.2 Lessons from Cañada Honda in terms of applicability to modern reef studies

As mentioned earlier, even with the excellent preservation and spatial exposure found in Cañada Honda, there are limitations that could be problematic when making direct comparisons with modern reefs. The community that is preserved is only a portion of the whole community that can be found in a living modern reef. For example, there are bioeroders (e.g. parrotfish) that can easily be quantified in a modern reef, whereas in the fossil reef we have to settle for scars of damaged coral surfaces as evidence of their former presence. Another example is the presence of fleshy macroalgae in modern reefs that, if abundant, could reduce significantly the coral cover. Since fleshy macroalgae cannot be preserved in fossil reefs, overestimation of coral cover could result. This is a potential source of error for the "living"coral estimates made from Cañada Honda.

The reef sediment found in Cañada Honda (and Clavellinas as well) is unconsolidated. This means that it could easily be washed-out during storms causing also overestimation of the coral cover measurements in Cañada Honda. Sediment removal during storms also affects the measurements from the vertical transects, where coral counts could be larger due to a lack of reef sediment in some quadrats (Figure 3.1). Such sources of error become particularly important when community structure comparisons between Cañada Honda and modern reef sites are made. At least with the data from the subhorizontal chain-transects in Cañada Honda, the community structure bear similarities with modern reefs in terms of the higher abundance of *Montastraea* spp. This brings to the table another aspect of the community structure measurements from Cañada Honda.

It was noted before the differences between the coral abundance data from vertical transects and the coral abundance data from the modern reefs, but also from the fossil subhorizontal chain-transect data. One possible explanation given earlier was that data from the chain-transects in Cañada Honda represents only a unique event "frozen" in time and not necessarily representative of the whole coral community. In Figure 4.4, for example, if the total coral cover is considered ("dead" and "live"), the abundance of *Siderastrea* spp. increases substantially compared with other species. Furthermore, abundance of *Siderastrea* spp. in "dead" assemblages is superior to the other coral species (Figure 4.4), similar to the abundances shown on vertical transects from the Siderastrea zone (Table 2). This difference in species composition might reflect the temporal variations in data acquisition (instantaneous vs. time averaged). Other possibility comes from the effect of the different methods employed for obtaining the data (vertical cross-sectional transects versus subhorizontal surface transects). In the vertical transects there could be several events and generations of corals even for a single quadrat. Especially large and old colonies could overwhelm the smaller and juvenile coral colonies. The latter could be underestimated in the vertical transects, especially if they are smaller than 10 cm. The coral data gathered by Morelock et al. (2001) from SW Puerto Rico come from photoquadrats where even the smallest coral colonies account for the total coral cover and abundance within the quadrat.

In terms of the sediment data, there are disadvantages in Cañada Honda that result in certain gaps in the interpretation of sedimentary processes. Although very useful information was gathered, this was limited and inaccurate compared with the high quality sediment data that can be obtained from a modern reef. For instance, in a modern reef major concerns about diagenesis and changes in sediment character are not an issue. In a modern reef we can actually sample sediment from its actual sources and also collect sediment samples from the water column and determine sedimentation rates. One major problem in Cañada Honda was that all sources of sediment (i.e. intrabasinal and extrabasinal) were made of $CaCO_3$, thus it was necessary to study the sediment in more detail (XRD, petrography) to determine its provenance. This problem was further complicated by the large presence of non-skeletal mud pelloids which can be produced from both extrabasinal and intrabasinal sources.

Extrapolating the conditions for reef development in Cañada Honda with the conditions in modern reefs could be a major complication considering the unique oceanographic conditions (e.g. highly variable salinity, lack of siliciclastic terrigenous sediment) that are difficult to find in modern analogues in settings where high terrestrial runoff is present. Perhaps the most significant implication about the Cañada Honda fossil coral reef is that, indeed, there are coral reef systems that can develop within natural conditions of high-terrestrial runoff. Here, we present an Early to Mid-Holocene fossil reef that developed prior to any human settlement in Hispaniola, and there is substantial evidence to document that high-terrestrial runoff was present and that corals were able to thrive in such conditions. Furthermore, there is evidence that the coral communities in Cañada Honda and elsewhere in the Enriquillo Basin were highly resilient. In Cañada Honda, for example, there are sediment horizons (Figure 2.7) that represent one or several events of rapid burial of the reef. One of these sediment horizons consists of reworked bivalve, gastropod and coral fragments (mostly *Madracis* sp.) and can be traced tens of meters throughout the outcrop (Figure 2.7). Corals below this horizon are often toppled in one direction indicating that such sedimentation events were of high energy and rapid. Coral communities above this horizon were reestablished with very little taxonomical change. Radiocarbon data presented in this study reveals over 2,500 years of continuous reef accretion under conditions of high-terrestrial runoff, coral development at depths near 12m and rising sea-level (Figure 4.11). Moreover, Greer et al. (2009) presents data showing that *A. cervicornis* in the Enriquillo Valley flourished during a 4,000 yr period, and, high-resolution radiocarbon dating reveals continuous growth for at least 2,000 yrs. According to Greer et al. (2009), the fossil corals of the Enriquillo Valley faced a period of nearly present day temperatures, if not higher, known as the

Holocene Thermal Maximum (ca. 6 ka; Sandweiss et al., 1996), variable salinity (Greer and Swart, 2006), hurricanes (Guerard et al., 2004), and rapid sea-level rise with remarkable resilience. Thus, even for the highly impacted fossil reefs of the Enriquillo Valley, it can be seen that reef corals can adapt and are resilient to numerous disturbances.

6.0 Summary and conclusions

The Early to Mid-Holocene Cañada Honda fossil reef in the Dominican Republic shows signs of development in an environment of high sedimentation, as indicated by the relatively high abundance of sediment-tolerant coral species, the tendency of these to form almost monospecific stands, and the propensity of individual colonies to grow as encrusting, dome-shaped, platy-like forms resulting in the development of ragged-margins or the so-called “stack of pancakes” morphology. Sediment incorporated into coral skeletons supports the introduction of silt during coral growth. In comparison with modern coral reefs in high-terrestrial runoff, the Cañada Honda fossil reef shows surprisingly high abundances of the massive coral *Siderastrea siderea*. This finding is explained by high-terrestrial runoff in Cañada Honda but also by salinity fluctuations, which this particular coral species can tolerate.

For a reef that had been developed in a site with high runoff and steep hillsides, the reef sediment in Cañada Honda is characterized by remarkable amounts of $CaCO_3$, much of it dominated by allochtonous (i.e. extrabasinal) sources as revealed by XRD analyses and petrography of the sediment. Furthermore the sediment shows negligible contributions by calcareous algae, bryozoans and coralline red algae, which indicates that sedimentation rates were high enough to inhibit successful substrate recruitment and colonization by these organisms (Fabricius, 2005). The notable presence of barnacle fragments in Cañada Honda reef sediment could indicate that high nutrients were present in the paleo-Enriquillo Bay, however high nutrients were not a limiting factor in the development of the fossil reef.

Coral growth rates measured for fossil *Montastraea faveolata* in Cañada Honda are relatively low compared with growth rates of modern corals at similar depths throughout the Caribbean. These low growth rates resulted from low light penetration caused from a combination of turbidity and growth near 12m depth. Nonetheless, if these conditions are correct, coral development occurred at depths not expected for a reef under siltation stress. The high carbonate content of the incoming terrigenous sediment probably allowed greater light penetration than similar amounts of siliciclastic sediment, and, thus, allowed corals to grow at greater depths than typically expected under these conditions. Other possibilities are that even though sedimentation was high, it occurred sporadically allowing time for the reef corals to respond and grow back, in such a way that they were able to "keep-up" with sedimentation in a rising sea-level scenario. Turbidity, although evident, did not present an issue. The findings presented in this study confirms, once again, that coral reefs can develop under certain conditions of natural disturbance with high resiliency, something that has not been observed for the past 30 years in most of the Caribbean, particularly due to the combined effects of natural and anthropogenic pressures.

7.0 Literature cited

Abrantes, F., I. Gil, C. Lopes and M. Castro. 2005. Quantitative diatom analyses-a faster cleaning procedure. *Deep-Sea Research I* 52:189-198.

Acevedo, R., J. Morelock, and R.A. Olivieri. 1989. Modification of coral reef zonation by terrigenous sediment stress. *Palaios* 4: 92-100.

Aronson, R.B., W.F. Precht and I.G Macintyre. 1998. Extrinsic control of species replacement on a Holocene Reef in Belize: the role of coral disease. *Coral Reefs* 17: 223-230.

Aronson, R.B., I.G. Macintyre, W.F. Precht, T.J.T. Murdoch, and C.M. Wapnick. 2002. The expanding scale of species turnover events on coral reefs in Belize. *Ecological Monographs* 72: 233-249.

Ballantine D.L., R.S. Appledoorn, P. Yoshioka, E. Weil, R. Armstrong, J.R. García, E. Otero, F. Pagán, C. Sherman, E.A. Hernández-Delgado, A. Bruckner and C. Lilyestrom. 2008. Biology and ecology of Puerto Rican coral reefs. *In:* B.M. Riegl and R.E. Dodge (eds.), *Coral Reefs of the USA,* Springer Science + Business Media B.V. p. 375-406.

Barnard, L.A., I.G. Macintyre and J.W. Pierce. 1974. Possible environmental index in tropical reef corals. *Nature* 252: 219-220.

Bischoff, W.D., M.A. Bertram, F.T. Mackenzie and F.C. Bishop. 1993. Diagenetic stabilization pathways of magnesian calcites. *Carbonates and Evaporites* 8: 82-89.

Broecker, W.S. and E.A. Olson. 1961. Lamont radiocarbon measurements VIII. *Radiocarbon* 3:176-204.

Budd, A.F. 2000. Diversity and extinction in the Cenozoic history of Caribbean reefs. *Coral Reefs* 19: 25-35.

Budd, A.F., K.O. Mann and H.M. Guzmán. 1993. Environmental interpretation using insoluble residues within reef coral skeletons: problems, pitfalls, and preliminary results. *Coral Reefs* 12: 31-42.

Carpenter, K.E., M. Abrar, G. Aeby, R.B. Aronson, S. Banks, A. Bruckner, A. Chiriboga, J. Cortés, J.C. Delbeek, L. DeVantier, G.J. Edgar, A.J. Edwards, D. Fenner, H.M. Guzmán, B.W. Hoeksema, G. Hodgson, O. Johan, W.Y. Licuanan, S.R. Livingstone, E.R. Lovell, J.A. Moore, D.O. Obura, D. Ochavillo, B.A. Polidoro, W.F. Precht, M.C. Quibilan, C. Reboton, Z.T. Richards, A.D. Rogers, J. Sanciangco, A. Sheppard, C. Sheppard, J. Smith, S. Stuart, E. Turak, J.E.N. Veron, C. Wallace, E. Weil and E. Wood. 2008. One-third of reef-building corals face elevated extinction risk from climate change and local impacts. *Science* 321: 560-563.

Cortés, J. and M.J Risk. 1985: A reef under siltation stress: Cahuita, Costa Rica. *Bulletin of Marine Science* 36: 339-356.

Cruz-Piñón, G., J. P. Carricart-Ganivet and J. Espinoza-Avalos. 2003. Monthly skeletal extension rates of the hermatypic corals *Montastraea annularis* and *Montastraea faveolata*: biological and environmental controls. *Marine Biology* 143: 491-500.

Davis, A., D. Hubbard and A. Stein. 2008. Coral morphology as an indication of sedimentation rates in two exposed Holocene Reefs: Western Dominican Republic. *11th International Coral Reef Symposium Abstracts Book*, Ft. Lauderdale, Florida, USA. p. 265.

Díaz, V.D. and W. Ramírez. 2005. The effects of terrigenous sedimentation on the growth rate and morphology of the Holocene fossil corals of Cañada Honda in Enriquillo Valley, Southwestern Dominican Republic. *Undergraduate Research Thesis,* Dept. of Geology, University of Puerto Rico at Mayagüez. 30 pp.

Dokken, Q.R., I.R. MacDonald, J.W. Tunnell Jr., T. Wade, K. Withers, S.J. Dilworth, T.W. Bates, C.R. Beaver, and C.M. Rigaud. 2003. Long-term monitoring at the East and West Flower Garden Banks National Marine Sanctuary, 1998-2001. *U.S. Department of the Interior, Minerals Management Service*, Gulf of Mexico OCS Region.

Draper G., P. Mann and J.F. Lewis JF. 1994. Hispaniola. *In:* S.K. Donovan and T.A. Jackson (eds.) *Caribbean Geology*. The University of the West Indies Publishers' Association, Kingston. pp 129-150.

Edinger, E. N., J. Jompa, G. V. Limmon, W. Widjatmoko and M. J. Risk. 1998. Reef degradation and biodiversity in Indonesia: effects of land-based pollution, destructive overfishing practices, and changes through time. *Marine Pollution Bulletin* 36: 617-630.

Edinger, E.N., G.V. Limmon, J. Jompa, W. Widjatmoko, J.M. Heikoop, and M.J. Risk. 2000. Normal coral growth rates on dying reefs: are coral growth rates good indicators of reef health? *Marine Pollution Bulletin* 5: 404-425.

Estep, A., T. Erickson and D.K. Hubbard. 2008. A comparison of rates and styles of bioerosion with varying sedimentation: Holocene reefs in the Western Dominican Republic versus modern reefs off St. Croix, USVI. *11th International Coral Reef Symposium Abstracts Book*, Ft. Lauderdale, Florida, USA. p. 261.

Fabricius, K.E. 2005. Effects of terrestrial runoff on the ecology of corals and coral reefs: review and synthesis. *Marine Pollution Bulletin* 50: 125-146.

Fabry, V. J., B.A. Seibel, R.A. Feely and J.C. Orr. 2008. Impacts of ocean acidification on marine fauna and ecosystem processes. *ICES Journal of Marine Science* 65: 414-432.

Fairbanks, R.G. and R.E. Dodge. 1979. Annual periodicity of the $^{18}O/^{16}O$ and $^{13}C/^{12}C$ ratios in the coral *Montastraea annularis*. *Geochimica et Cosmochimica Acta* 43:1009-1020.

Flügel, E. 2004. *Microfacies of carbonate rocks: analysis, interpretation and application* Springer-Verlag, Germany, 976 pp.

Geister, J. 1977. The influence of wave exposure on the ecological zonation of Caribbean coral reefs. *Proceedings of the 3rd International Coral Reef Symposium* 1: 23–29.

Ginsburg, R.N. 1956. Environmental relationships of grain size and constituent particles in some South Florida carbonate sediments. *Am. Assoc. Petroleum Geologists Mem. 47*, p. 1-130.

Gischler, E., and W. Oschmann. 2005. Historical climate variation in Belize (Central America) as recorded in scleractinian coral skeletons. *Palaios* 20(2): 159-174.

Gladfelter, E.H., R.K. Monahan, and W.B. Gladfelter. 1978. Growth rates of five reef-building corals in the Northeastern Caribbean. *Bulletin of Marine Science* 28(4): 728-734.

Greer, L. 2001. Seasonal to centennial, Holocene and modern climate variability in the Dominican Republic. *Ph.D. Thesis*. University of Miami, Coral Gables, Florida, USA. 228 pp.

Greer, L., J.E. Jackson, H.A. Curran, T. Guilderson and L. Teneva. 2009. How vulnerable is *Acropora cervicornis* to environmental change: Lessons from the Early to Middle Holocene. *Geology* 37: 263-266.

Greer, L. and P.K. Swart. 2006. Decadal cyclicity of regional mid-Holocene precipitation as driven by tropical Atlantic sea surface temperatures: Evidence from Dominican coral proxies: *Paleoceanography* 21: 21, PA2020, doi: 10.1029/2005PA001166.

Guerard, G.M., L. Greer and H.A. Curran. 2004. Environmental indicator proxies from a mid-Holocene coral reef, Enriquillo Valley, Dominican Republic. *In* R.D. Lewis and B.C. Panuska (eds.) *Proceedings of the 11th Symposium on the Geology of the Bahamas and Other Carbonate Regions*: Gerace Research Center, San Salvador, p. 35-48.

Hallock, P. and W. Schlager. 1986. Nutrient excess and the demise of coral reefs and carbonate platforms. *Palaios* 1: 389-398.

Hubbard, D.K. and D. Scaturo. 1985. Growth rates of seven Scleractinian corals from Cane Bay and Salt River, St. Croix, USVI. *Bulletin of Marine Science* 36(2): 325-338.

Hubbard, D.K., W. Ramírez, A. Davis, G. Lawson, J. Oram, K. Parsons-Hubbard, D. Cuevas and M. del Coro. 2005. Holocene coral-reef development in Cañada Honda, SW Dominican Republic. *Transactions of the 17th Caribbean Geological Conference*, San Juan, Puerto Rico, July 17-21 2005, p. 35.

Hubbard, D., W. Ramírez, D. Cuevas, T. Erickson, and A. Estep. 2008. Holocene Reef Accretion Along the North Side of Bahia Enriquillo (Western Dominican Republic): Unique Insights Into Patterns of Reef Development in Response to Sea-Level Rise. *Proceedings of the 11th international Coral Reef Symposium, Fort Lauderdale, Florida, USA, July 7-11 2008,* pp. 43-47.

Hubbard, J.A.E.B. and Y.P. Pocock. 1972. Sediment rejection by recent scleractinian corals: A key to paleo-environmental reconstruction. *Geologische Rundschau* 61: 598-626.

Hughen, K.A., M.G.L. Baillie, E. Bard, A. Bayliss, J.W. Beck, P.G. Blackwell, C.E. Buck, G.S. Burr, K.B. Cutler, P.E. Damon, R.L. Edwards, R.G. Fairbanks, M. Friedrich, T.P. Guilderson, C. Herring, B. Kromer, F.G. McCormac, S.W. Manning, C.B. Ramsey, P.J. Reimer, R.W. Reimer, S. Remmele, J.R. Southon, M. Stuiver, S. Talamo, F.W. Taylor, J. van der Plicht, and C.E. Weyhenmeyer. 2004. Marine04 Marine radiocarbon age calibration, 26 - 0 ka BP. *Radiocarbon* 46:1059-1086.

Hughes, T. P. 1994. Catastrophes, phase shifts and large-scale degradation of a Caribbean coral reef. *Science* 265: 1547-1551.

Hughes, T.P. and J.H. Connell. 1999. Multiple stresses on coral reefs. *Limnology and Oceanograph*y 44(3):932–940.

Jackson, J.B.C. 1997. Reefs since Columbus. Coral Reefs 16 Suppl.: S23-S32.

James, N.P. and P.A. Bourque. 1992. Reefs and Mounds. *In*: R.G. Walker and N.P. James (eds.) Facies Models: Response to Sea Level Change. *Geological Association of Canada*, 454 pp.

Kleypas, J.A., R.W. Buddemeier and J.P. Gattuso. 2001. The future of coral reefs in an age of global change. *Int. J. Earth Sciences (Geol. Rundsch.)* 90: 426-437.

Knowlton, N., E. Weil, L. A. Weigt, and H. M. Guzman. 1992. Sibling species in *Montastraea annularis*, coral bleaching, and the coral climate record. *Science* 255: 330-333.

Kohler, K.E. 2003. Coral X-radiography Densitometry System. *Nova Southeastern University Oceanographic Center/ National Coral Reef Institute.*

Lescinsky, H.L. 2004. Bioerosion in the Caribbean: using coral bleaching as a natural experiment. *In* R.D. Lewis and B.C. Panuska (eds.) *Proceedings of the 11th Symposium on the Geology of the Bahamas and other Carbonate Regions*: Gerace Research Center, San Salvador, Bahamas, p. 25-34.

Lidz, B.H. and P. Hallock. 2000. Sedimentary petrology of a declining reef ecosystem, Florida Reef Tract (U.S.A.). *J. Coastal Research* 16(3): 675-697.

Loya Y. 1978. Plotless and transect methods. In: *Monographs on Oceanic Methodology. Coral Reefs: Research Methods*. D.R. Stoddart and R.E. Johannes (eds.). UNESCO Press, 5: 197-218.

Mann, P., F. W. Taylor, K. Burke, and R. Kulstad. 1984. Subaerially exposed Holocene coral reef, Enriquillo Valley, Dominican Republic. *Geological Society of America Bulletin* 95: 1084-1092.

Mann, P., E. Calais, J. C. Ruegg, C. DeMets, T. Dixon, P. Jansma, and G. Mattioli. 2002. Oblique collision in the northeastern Caribbean from GPS measurements and geological observations. *Tectonics* 21(6): 1057, doi: 10.1029/2001TC001304.

Morelock, J., E. Winget, and C. Goenaga. 1994. Marine geology of the Parguera-Guánica quadrangles, Puerto Rico. *United States Geological Survey Miscellaneous Map Series*, Washington, D.C.

Morelock, J., K. Grove and M.L. Hernandez. 1983. Oceanography and patterns of shelf sediments, Mayaguez, Puerto Rico. *J. Sedimentary Petrology* 53:371-381.

Morelock, J., W. Ramírez, A. Bruckner and M. Carlo. 2001. Status of coral reefs, southwest Puerto Rico, *Caribbean Journal of Science Special Publication No.4*, 57 pp.

Moses, C.S. and P.K. Swart. 2006. Stable isotope and growth records in corals from the island of Tobago: Not simply a record from the Orinoco. *Proceedings of the 10th International Coral Reef Symposium* 580-587.

Muthiga, N.A. and A.M. Szmant. 1987. The effects of salinity stress on the rates of aerobic respiration and photosynthesis in the hermatypic coral *Siderastrea siderea*. *Biol. Bull.* 173: 539– 551.

Pandolfi, J.M. 2002. Coral community dynamics at multiple scales. *Coral Reefs* 21:13-23.

Pandolfi, J.M., G. Llewellyn and J.B.C. Jackson. 1999. Pleistocene reef environments, constituent grains, and coral community structure: Curaçao, Netherlands Antilles. *Coral Reefs* 18: 107-122.

Pandolfi, J.M. and J.B.C. Jackson. 2001. Community structure of Pleistocene coral reefs of Curaçao, Netherlands Antilles. *Ecological Monographs* 71: 49-67.

Pandolfi, J.M. and J.B.C. Jackson. 2006. Ecological persistence interrupted in Caribbean coral reefs. *Ecology Letters* 9(7): 818-826.

Perry C.T. 1998. Macroborers within coral framework at Discovery Bay, north Jamaica: species distribution and abundance, and effects on coral preservation. *Coral Reefs* 17: 277-287.

Perry, C.T., S.G. Smithers, S.E. Palmer, P. Larcombe and K.G. Johnson. 2008. 1200 year paleoecological record of coral community development from the terrigenous inner shelf of the Great Barrier Reef. *Geology* 36(9): 691-694.

Rapp, P., W.R. Ramírez, J.A. Rivera, M. Carlo and R. Luciano. 2007. Measurement of organic loading under an open-ocean aquaculture cage, using sediment traps on the bottom. *J. Appl. Ichthyol.* 23: 661-667.

Sandweiss, D.H., J.B. Richardson III and H.B. Rollins. 1996. Geoarchaeological evidence from Peru for a 5000 years B.P. onset of El Niño. *Science* 273: 1531-1533.

Scholle, P.A. and D.S. Ulmer-Scholle. 2003. Color Guide to Petrography of Carbonate Rocks. *Memoir 77 of the American Association of Petroleum Geologists*, 474 pp.

Scoffin, T. P. 1986. Banding of coral skeletons from Pulau Seribu as revealed by X-ray and U/V light values. *In*: B. E. Brown (ed.) Human-Induced Damage to Coral Reefs. *UNESCO reports in Marine Science* 40:126-134.

Smithers, S.G. and P. Larcombe. 2003. Late Holocene initiation and growth of a nearshore turbid-zone coral reef: Paluma Schoals, central Great Barrier Reef, Australia. *Coral Reefs* 22: 499-505.

Stemann, T.A. and K.G. Johnson. 1992. Coral assemblages, biofacies and ecological zones in the Mid-Holocene reef deposits of the Enriquillo Valley, Dominican Republic. *Lethaia* 25: 231-241.

Stuiver, M. and P.J. Reimer. 1993. Extended ^{14}C data base and revised CALIB 3.0 ^{14}C age calibration program. *Radiocarbon* 35:215-230.

Swinchatt, J.P. 1965. Significance of constituent composition, texture, and skeletal breakdown in some Recent carbonate sediments. *J. Sedimentary Petrology* 35(1): 71-90.

Taylor, F.W., P. Mann, S. Valastro Jr. and K. Burke. 1985. Stratigraphy and radiocarbon chronology of a subaerially exposed Holocene coral reef, Dominican Republic. *Journal of Geology* 3: 311-332.

Te, F.T. 1997. Turbidity and its effect on corals: a model using the extinction coefficient (K) of photosynthetic active radiance (PAR). *Proceedings of the Eighth International Coral Reef Symposium* 2:1899-1904.

Torres, J. and J. Morelock. 2002. Effect of terrigenous sediment influx on coral cover and linear extension rates of three Caribbean massive coral species. *Caribbean Journal of Science,* 38(3-4): 222-229.

Toscano, M.A., and I. G. Macintyre. 2003. Corrected western Atlantic sea-level curve for the last 11,000 years based on calibrated ^{14}C dates from *Acropora palmata* framework and intertidal mangrove peat. *Coral Reefs* 22: 257-270.

Van Woesik, R. and T.J. Done. 1997. Coral communities and reef growth in the southern Great Barrier Reef. *Coral Reefs* 16:103-115.

Appendix A

X-Ray Powder Diffraction Data

Table A1. Determination of molar % of Mg in main calcite peak from whole sample XRD analyses

Sample	2θ analytical Aragonite (Deg.)	Offset in 2θ (Deg.)	2θ analytical Calcite (Deg.)	Corrected 2θ Calcite (Deg.)	D spacing Calcite (corrected)	mole% Mg
S-43-1	26.219612	0.006988	29.452444	29.445456	3.03099	1.38
S-43-2	26.31163	0.099006	29.547988	29.448982	3.03063	1.50
S-43-3	26.205141	-0.007483	29.446094	29.453577	3.03017	1.66
S-67-1	26.221495	0.008871	29.468037	29.459166	3.02961	1.85
S-67-2	26.186081	-0.026543	29.422576	29.449119	3.03062	1.50
S-67-3	26.193492	-0.019132	29.442717	29.461849	3.02934	1.94
S-104-1	26.160081	-0.052543	29.420005	29.472548	3.02826	2.31
S-104-2	26.193022	-0.019602	29.464269	29.483871	3.02713	2.70
S-104-3	26.157493	-0.055131	29.380424	29.435555	3.03198	1.03
S-104-4	26.131024	-0.0816	29.376076	29.457676	3.02976	1.80
S-136-1	26.213494	0.00087	29.476592	29.475722	3.02794	2.42
S-136-2	26.217377	0.004753	29.452539	29.447786	3.03075	1.46
S-176-1	26.225142	0.012518	29.470632	29.458114	3.02971	1.81
S-176-2	26.232908	0.020284	29.499888	29.479604	3.02755	2.55
S-176-3	26.215847	0.003223	29.513752	29.510529	3.02445	3.62
S-232-1	26.265619	0.052995	29.579311	29.526316	3.02287	4.16
S-232-2	26.205611	-0.007013	29.454127	29.46114	3.02941	1.92
S-232-3	26.262089	0.049465	29.515944	29.466479	3.02887	2.10
S-400-1	26.214671	0.002047	29.47709	29.475043	3.02801	2.40

Table A2. Determination of molar % of Mg in main calcite peak from sieved samples from CH

Sample	2θ analytical Aragonite (Deg.)	Offset in 2θ (Deg.)	2θ analytical Calcite (Deg.)	Corrected 2θ Calcite (Deg.)	D spacing Calcite (corrected)	mole% Mg
CH-43-1 G	26.19210881	-0.02051519	29.4383476	29.45886279	3.02964	1.84
CH-43-1 M	26.24943048	0.036806483	29.49550754	29.45870106	3.02965	1.83
CH-43-2 G	26.15713364	-0.055490361	29.39228625	29.44777661	3.03075	1.46
CH-43-2 M	26.24699113	0.034367128	29.49381437	29.45944725	3.02958	1.86
CH-43-3 G	26.27211477	0.059490772	29.52212606	29.46263529	3.02926	1.97
CH-43-3 M	26.19610527	-0.016518735	29.42595117	29.4424699	3.03129	1.27
CH-43-4 G	26.32701967	0.114395666	29.56219513	29.44779946	3.03075	1.46
CH-43-4 M	26.12778671	-0.084837287	29.37439639	29.45923368	3.02960	1.85
CH-67-1G	26.18819191	-0.024432089	29.44837163	29.47280372	3.02824	2.32
CH-67-1M	26.14073487	-0.071889128	29.42595117	29.49784029	3.02572	3.18
CH-67-2 G	26.2998938	0.087269804	29.56419647	29.47692666	3.02782	2.46
CH-67-2 M	26.17089337	-0.041730632	29.43249516	29.4742258	3.02809	2.37
CH-67-3 G	26.2250575	0.012433501	29.47251719	29.46008369	3.02952	1.88
CH-67-3 M	26.17464856	-0.037975443	29.4184193	29.45639474	3.02989	1.75
CH-67-4 G	26.13683346	-0.075790538	29.39525354	29.47104408	3.02841	2.26
CH-67-4 M	26.18513755	-0.02748645	29.43894289	29.46642934	3.02888	2.10
S-104-1G	26.257145	0.044521004	29.54279636	29.49827536	3.02568	3.20
S-104-1M	26.20684694	-0.005777063	29.47221885	29.47799591	3.02772	2.50
S-104-2 G	26.31989663	0.10727263	29.58101854	29.47374591	3.02814	2.35
S-104-2 M	26.22513605	0.01251205	29.48634686	29.47383481	3.02813	2.35
S-104-3 G	26.16416804	-0.048455961	29.42010372	29.46855968	3.02866	2.17
S-104-3 M	26.23315055	0.020526553	29.48515242	29.46462586	3.02906	2.04
S-136-1G	26.26313084	0.050506845	29.53640241	29.48589557	3.02692	2.77
S-136-1M	26.22427204	0.011648037	29.47838574	29.4667377	3.02885	2.11
S-136-2 G	26.31831426	0.105690261	29.57190418	29.46621392	3.02890	2.09
S-136-2 M	26.14994686	-0.062677137	29.39990353	29.46258067	3.02926	1.97
S-176-1 G	26.20378818	-0.008835816	29.45492573	29.46376154	3.02915	2.01
S-176-1 M	26.21885362	0.006229623	29.45701174	29.45078211	3.03045	1.56
S-176-2 G	26.21579204	0.003168041	29.49680245	29.49363441	3.02615	3.04

Table A2. (Cont.)

Sample	**2θ analytical Aragonite (Deg.)**	**Offset in 2θ (Deg.)**	**2θ analytical Calcite (Deg.)**	**Corrected 2θ Calcite (Deg.)**	**D spacing Calcite (corrected)**	**mole% Mg**
S-176-2 M	26.14292018	-0.069703824	29.4021796	29.47188343	3.02833	2.29
S-176-3 G	26.11500726	-0.09761674	29.39782569	29.49544243	3.02596	3.10
S-176-3 M	26.19673227	-0.015891728	29.4569124	29.47280412	3.02824	2.32
S-232-1 G	26.23173587	0.01911187	29.51943209	29.50032022	3.02547	3.27
S-232-1 M	26.15799319	-0.054630806	29.42595117	29.48058197	3.02746	2.59
S-232-2 G	26.29112754	0.078503541	29.5630957	29.48459216	3.02705	2.72
S-232-2 M	26.21477167	0.002147674	29.46466301	29.46251533	3.02927	1.96
S-232-3 G	26.21108332	-0.001540676	29.49331642	29.4948571	3.02602	3.08
S-232-3 M	26.31894719	0.106323185	29.59114114	29.48481795	3.02703	2.73
CH-400-1 G	26.31056343	0.097939429	29.59114114	29.49320171	3.02619	3.02
CH-400-1 M	26.11064643	-0.101977568	29.4336853	29.53566287	3.02194	4.48
CH-400-2 G	26.15088404	-0.061739958	29.4336853	29.49542526	3.02597	3.10
CH-400-2 M	26.2097495	-0.002874503	29.50497298	29.50784748	3.02472	3.52

Table A3. Determination of molar % of Mg in secondary calcite peak from sieved samples from CH

Sample	2θ analytical Aragonite (Deg.)	Offset in 2θ (Deg.)	2θ analytical Calcite (Deg.)	Corrected 2θ Calcite (Deg.)	D spacing Calcite (corrected)	mole% Mg
CH-43-1 G	26.19210881	-0.02051519	29.80595728	29.82647247	2.99313	14.36
CH-43-1 M	26.24943048	0.036806483	29.86600244	29.82919595	2.99286	14.45
CH-43-2 G	26.15713364	-0.055490361	29.76014533	29.8156357	2.99419	13.99
CH-43-2 M	26.24699113	0.034367128	29.84589219	29.81152506	2.99460	13.85
CH-43-3 G	26.27211477	0.059490772	29.85711788	29.79762711	2.99596	13.38
CH-43-3 M	26.19610527	-0.016518735	29.78359217	29.80011091	2.99572	13.47
CH-43-4 G	26.32701967	0.114395666	29.95534873	29.84095307	2.99171	14.84
CH-43-4 M	26.12778671	-0.084837287	29.75781285	29.84265013	2.99154	14.90
CH-67-1G	26.18819191	-0.024432089	29.80127813	29.82571022	2.99320	14.33
CH-67-1M	26.14073487	-0.071889128	29.76592745	29.83781657	2.99202	14.74
CH-67-2 G	26.2998938	0.087269804	29.96614368	29.87887388	2.98800	16.11
CH-67-2 M	26.17089337	-0.041730632	29.82601308	29.86774371	2.98909	15.74
CH-67-3 G	26.2250575	0.012433501	29.86600244	29.85356893	2.99047	15.27
CH-67-3 M	26.17464856	-0.037975443	29.78592875	29.8239042	2.99338	14.27
CH-67-4 G	26.13683346	-0.075790538	29.78592875	29.86171929	2.98968	15.54
CH-67-4 M	26.18513755	-0.02748645	29.78592875	29.8134152	2.99441	13.92
S-104-1G	26.257145	0.044521004	Not found	-	-	-
S-104-1M	26.20684694	-0.005777063	29.86600244	29.8717795	2.98869	15.88
S-104-2 G	26.31989663	0.10727263	29.92608779	29.81881516	2.99388	14.10
S-104-2 M	26.22513605	0.01251205	29.8471164	29.83460435	2.99233	14.63
S-104-3 G	26.16416804	-0.048455961	29.76592745	29.81438341	2.99432	13.95
S-104-3 M	26.23315055	0.020526553	29.83967072	29.81914416	2.99385	14.11
S-136-1G	26.26313084	0.050506845	29.84130232	29.79079548	2.99663	13.15
S-136-1M	26.22427204	0.011648037	29.79965095	29.78800291	2.99691	13.06
S-136-2 G	26.31831426	0.105690261	29.94610218	29.84041192	2.99176	14.82
S-136-2 M	26.14994686	-0.062677137	29.76592745	29.82860458	2.99292	14.43
S-176-1 G	26.20378818	-0.008835816	Not found	-	-	-
S-176-1 M	26.21885362	0.006229623	Not found	-	-	-

Table A3. (Cont.)

Sample	2θ analytical Aragonite (Deg.)	Offset in 2θ (Deg.)	2θ analytical Calcite (Deg.)	Corrected 2θ Calcite (Deg.)	D spacing Calcite (corrected)	mole% Mg
S-176-2 G	26.21579204	0.003168041	29.82601308	29.82284504	2.99349	14.23
S-176-2 M	26.14292018	-0.069703824	29.76592745	29.83563127	2.99223	14.66
S-176-3 G	26.11500726	-0.09761674	29.75365585	29.85127259	2.99070	15.19
S-176-3 M	26.19673227	-0.015891728	29.79792226	29.81381399	2.99437	13.93
S-232-1 G	26.23173587	0.01911187	29.88603784	29.86692597	2.98917	15.71
S-232-1 M	26.15799319	-0.054630806	29.80595728	29.86058809	2.98979	15.50
S-232-2 G	26.29112754	0.078503541	29.90097985	29.82247631	2.99352	14.22
S-232-2 M	26.21477167	0.002147674	29.82601308	29.82386541	2.99339	14.27
S-232-3 G	26.21108332	-0.001540676	29.84905493	29.85059561	2.99077	15.17
S-232-3 M	26.31894719	0.106323185	29.94651302	29.84018983	2.99179	14.82
CH-400-1 G	26.31056343	0.097939429	Not found	-	-	-
CH-400-1 M	26.11064643	-0.101977568	Not found	-	-	-
CH-400-2 G	26.15088404	-0.061739958	29.80148154	29.8632215	2.98953	15.59
CH-400-2 M	26.2097495	-0.002874503	29.81959633	29.82247083	2.99352	14.22

M1-5

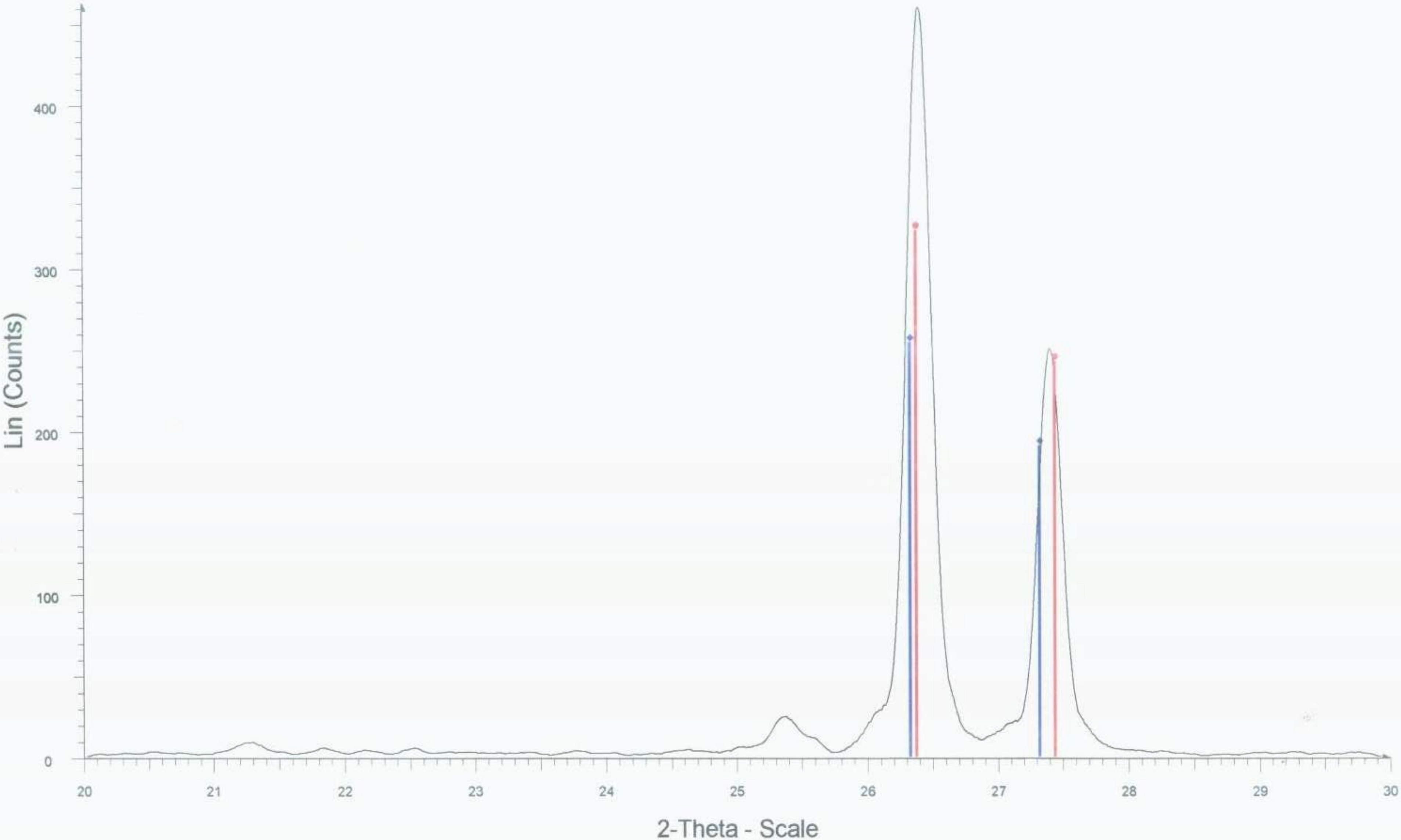

M1-5 - File: David Cuevas-M1-5.RAW - Type: 2Th/Th locked - Start: 20.000 ° - End: 30.000 ° - Step: 0.010 ° - Step time: 2. s - Temp.: 25 °C (Room) - Time Started: 28 s - 2-Theta: 20.000 ° - Theta: 10.00
Operations: Smooth 0.150 | Background 1.000,1.000 | Import
03-1067 (D) - Aragonite - gamma-CaCO3 - Y: 68.75 % - d x by: 1. - WL: 1.54056 - Orthorhombic - a 4.94000 - b 7.94000 - c 5.72000 - alpha 90.000 - beta 90.000 - gamma 90.000 - Primitive - Pnma (62)
03-1067 (D) - Aragonite - gamma-CaCO3 - Y: 87.50 % - d x by: 0.9958 - WL: 1.54056 - Orthorhombic - a 4.94000 - b 7.94000 - c 5.72000 - alpha 90.000 - beta 90.000 - gamma 90.000 - Primitive - Pnma

M1-17

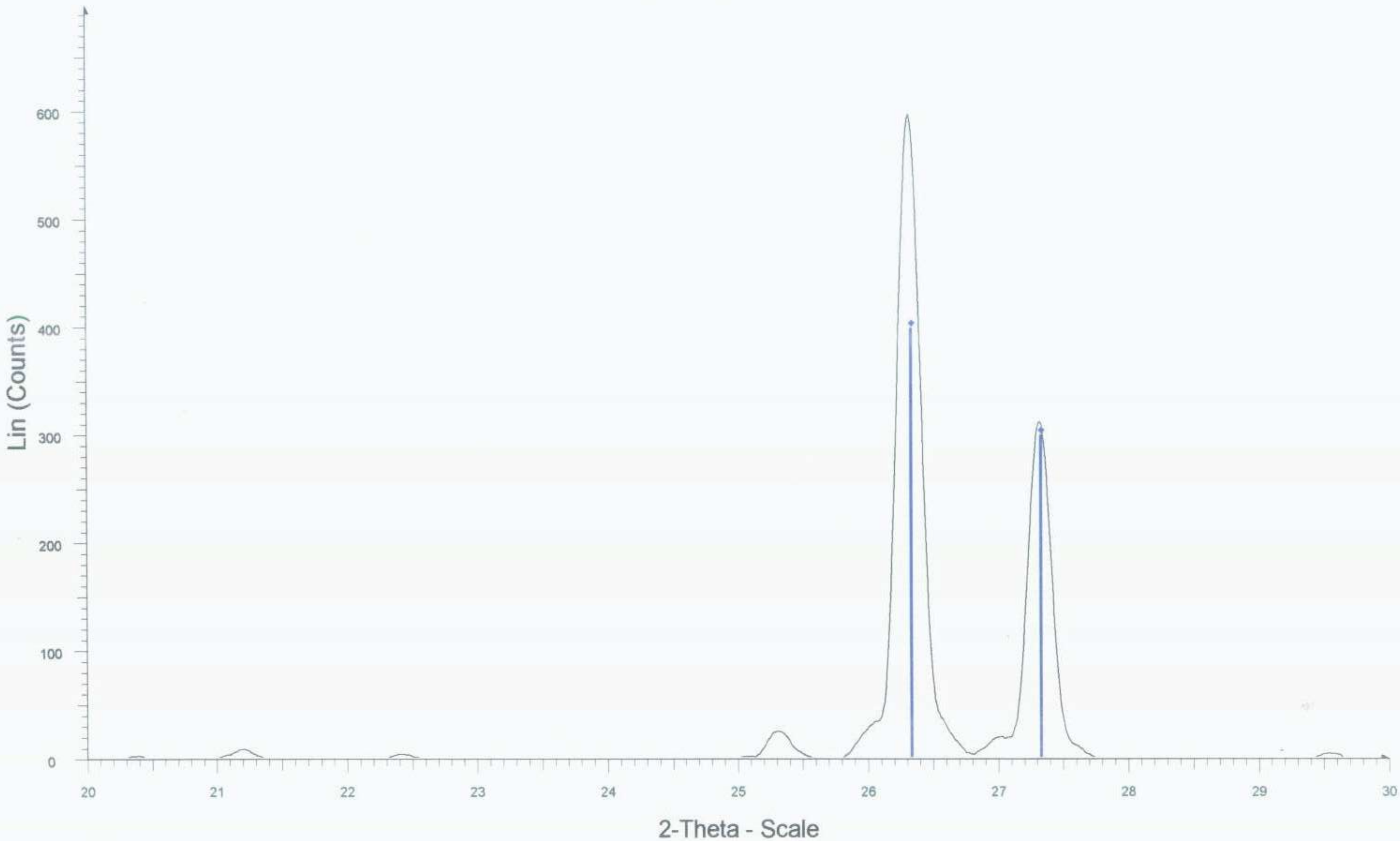

M1-17 - File: David Cuevas-M1-17.RAW - Type: 2Th/Th locked - Start: 20.000 ° - End: 30.000 ° - Step: 0.010 ° - Step time: 2. s - Temp.: 25 °C (Room) - Time Started: 16 s - 2-Theta: 20.000 ° - Theta: 10.
Operations: Background 1.000,1.000 | Smooth 0.150 | Import
03-1067 (D) - Aragonite - gamma-CaCO3 - Y: 83.33 % - d x by: 1. - WL: 1.54056 - Orthorhombic - a 4.94000 - b 7.94000 - c 5.72000 - alpha 90.000 - beta 90.000 - gamma 90.000 - Primitive - Pnma (62)

M2-11

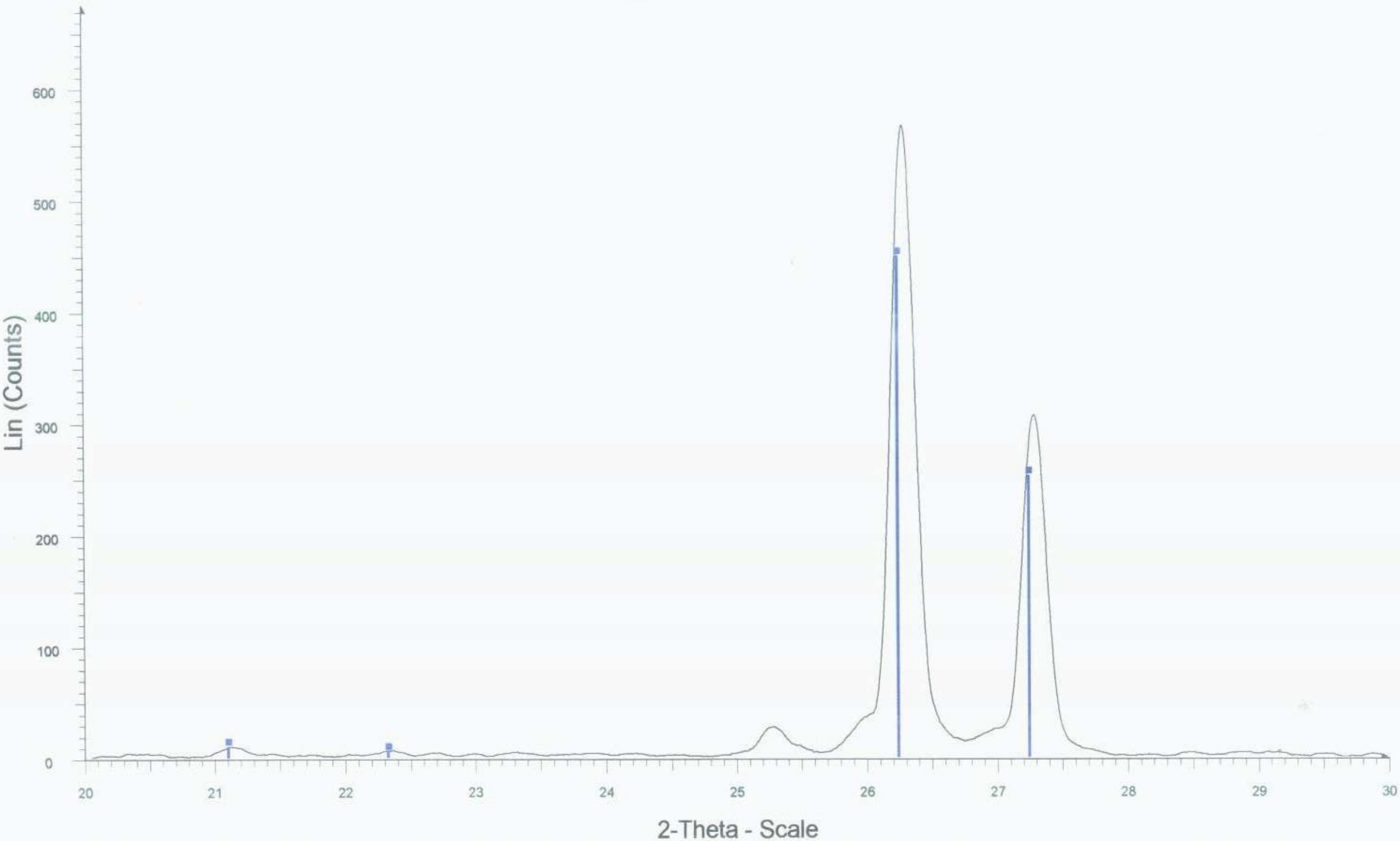

M2-11 - File: David Cuevas-M2-11.RAW - Type: 2Th/Th locked - Start: 20.000 ° - End: 30.000 ° - Step: 0.010 ° - Step time: 2. s - Temp.: 25 °C (Room) - Time Started: 16 s - 2-Theta: 20.000 ° - Theta: 10.

Operations: Smooth 0.150 | Background 1.000,1.000 | Import

76-0606 (A) - Aragonite - Ca(CO3) - Y: 79.17 % - d x by: 1. - WL: 1.54056 - Orthorhombic - a 4.95980 - b 7.96410 - c 5.73790 - alpha 90.000 - beta 90.000 - gamma 90.000 - Primitive - Pmcn (62) - 4 - 22

M2-26

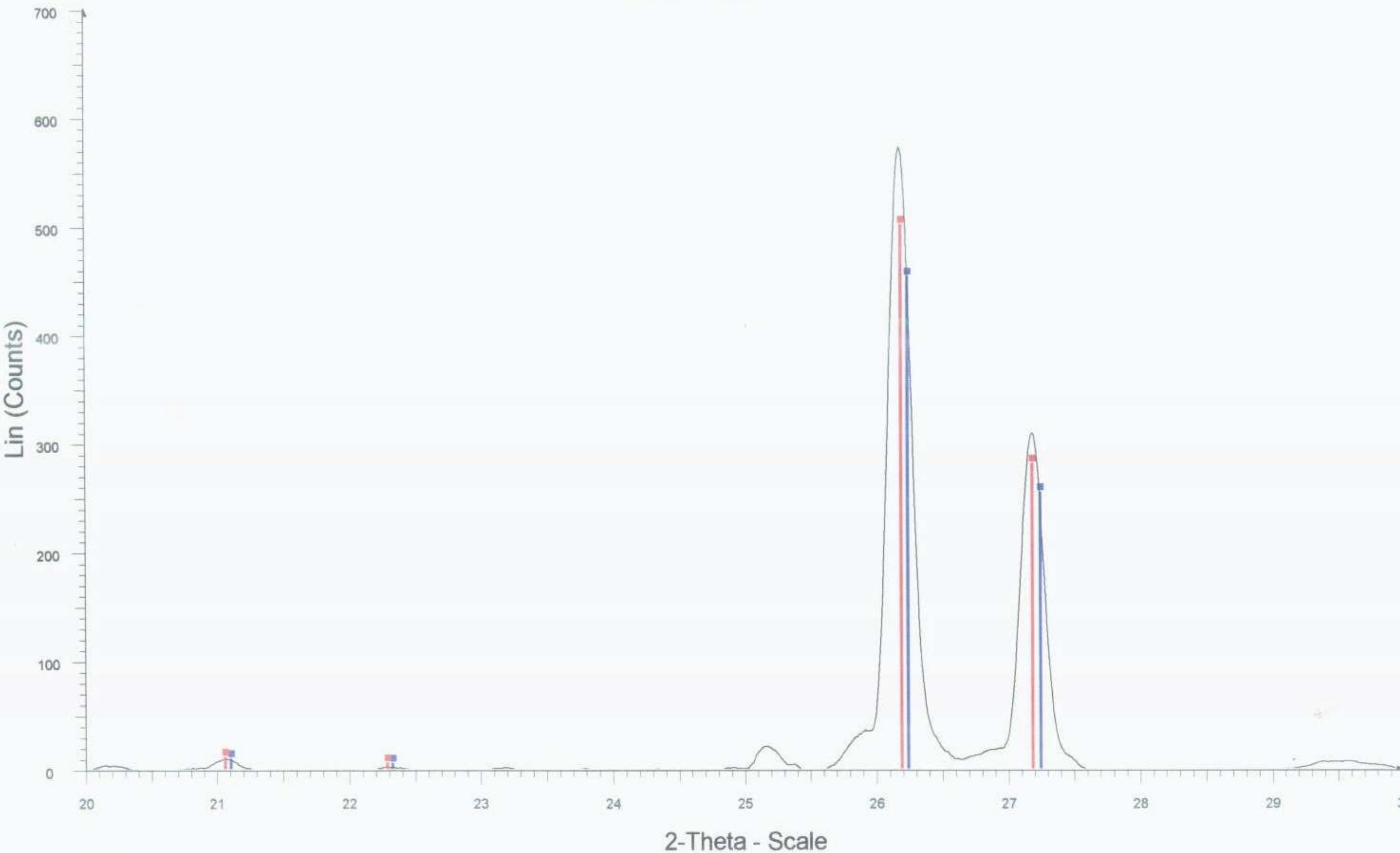

M2-26 - File: David Cuevas-M2-26.RAW - Type: 2Th/Th locked - Start: 20.000 ° - End: 30.000 ° - Step: 0.010 ° - Step time: 2. s - Temp.: 25 °C (Room) - Time Started: 16 s - 2-Theta: 20.000 ° - Theta: 10.
Operations: Background 1.000,1.000 | Smooth 0.150 | Import

76-0606 (A) - Aragonite - Ca(CO3) - Y: 79.17 % - d x by: 1. - WL: 1.54056 - Orthorhombic - a 4.95980 - b 7.96410 - c 5.73790 - alpha 90.000 - beta 90.000 - gamma 90.000 - Primitive - Pmcn (62) - 4 - 22

76-0606 (A) - Aragonite - Ca(CO3) - Y: 87.50 % - d x by: 1.0021 - WL: 1.54056 - Orthorhombic - a 4.95980 - b 7.96410 - c 5.73790 - alpha 90.000 - beta 90.000 - gamma 90.000 - Primitive - Pmcn (62) -

MZ-10

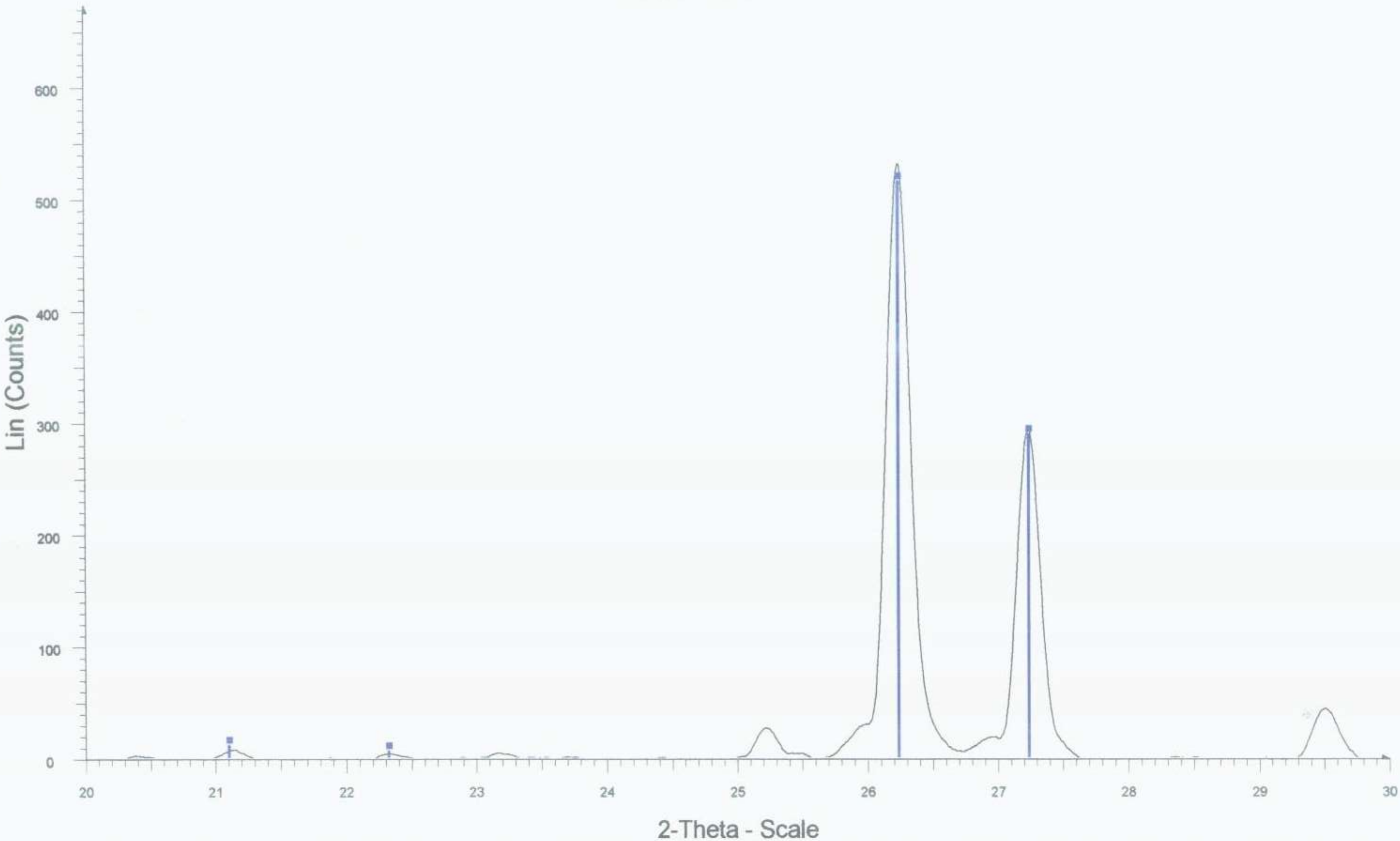

MZ-10 - File: David Cuevas-MZ-10.RAW - Type: 2Th/Th locked - Start: 20.000 ° - End: 30.000 ° - Step: 0.010 ° - Step time: 2. s - Temp.: 25 °C (Room) - Time Started: 16 s - 2-Theta: 20.000 ° - Theta: 10.
Operations: Background 1.000,1.000 | Smooth 0.150 | Import

76-0606 (A) - Aragonite - Ca(CO3) - Y: 97.04 % - d x by: 1. - WL: 1.54056 - Orthorhombic - a 4.95980 - b 7.96410 - c 5.73790 - alpha 90.000 - beta 90.000 - gamma 90.000 - Primitive - Pmcn (62) - 4 - 22

MZ-12

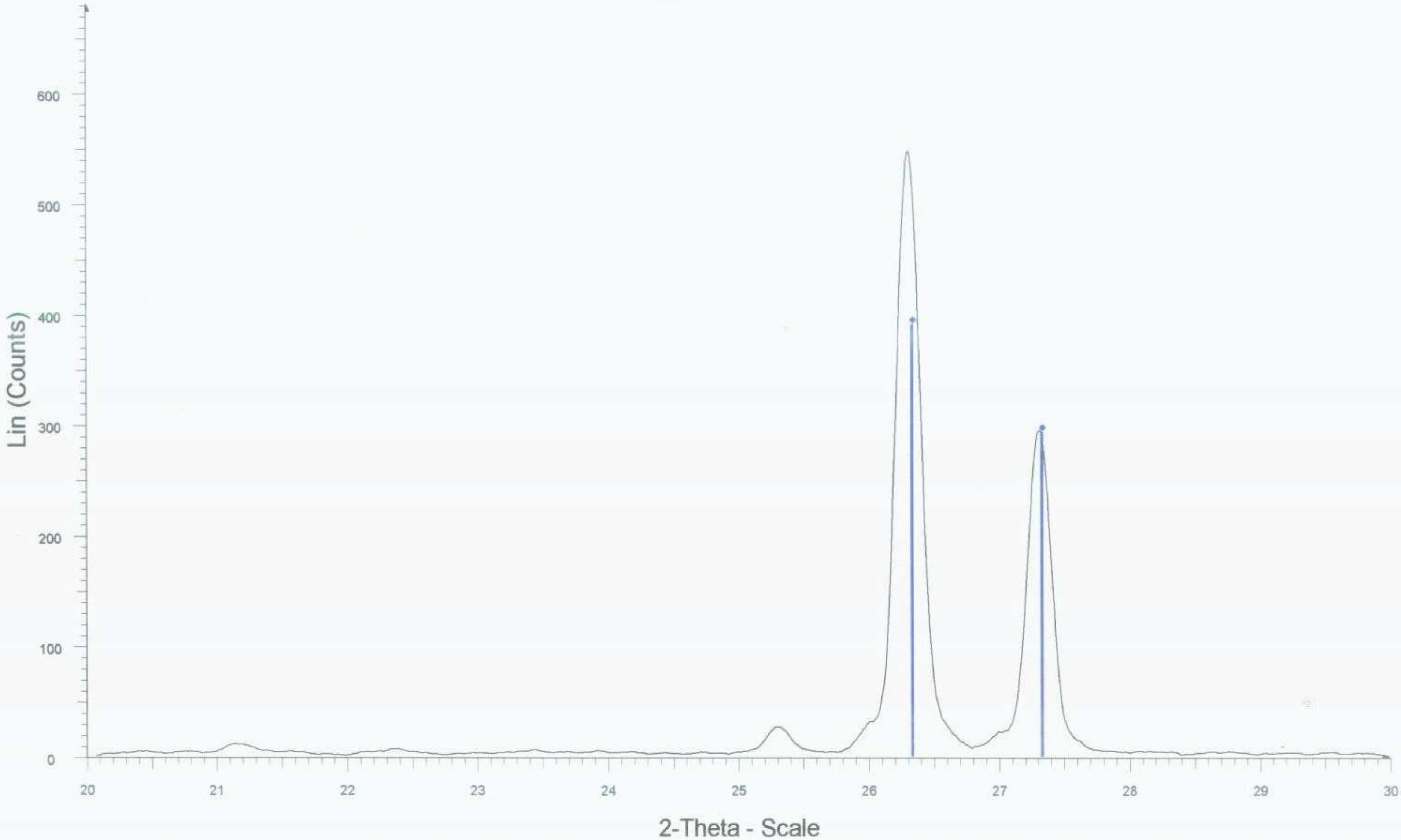

MZ-12 - File: David Cuevas-MZ-12.RAW - Type: 2Th/Th locked - Start: 20.000 ° - End: 30.000 ° - Step: 0.010 ° - Step time: 2. s - Temp.: 25 °C (Room) - Time Started: 16 s - 2-Theta: 20.000 ° - Theta: 10.
Operations: Smooth 0.150 | Background 1.000,1.000 | Import
03-1067 (D) - Aragonite - gamma-CaCO3 - Y: 88.98 % - d x by: 1. - WL: 1.54056 - Orthorhombic - a 4.94000 - b 7.94000 - c 5.72000 - alpha 90.000 - beta 90.000 - gamma 90.000 - Primitive - Pnma (62)

MZ-29

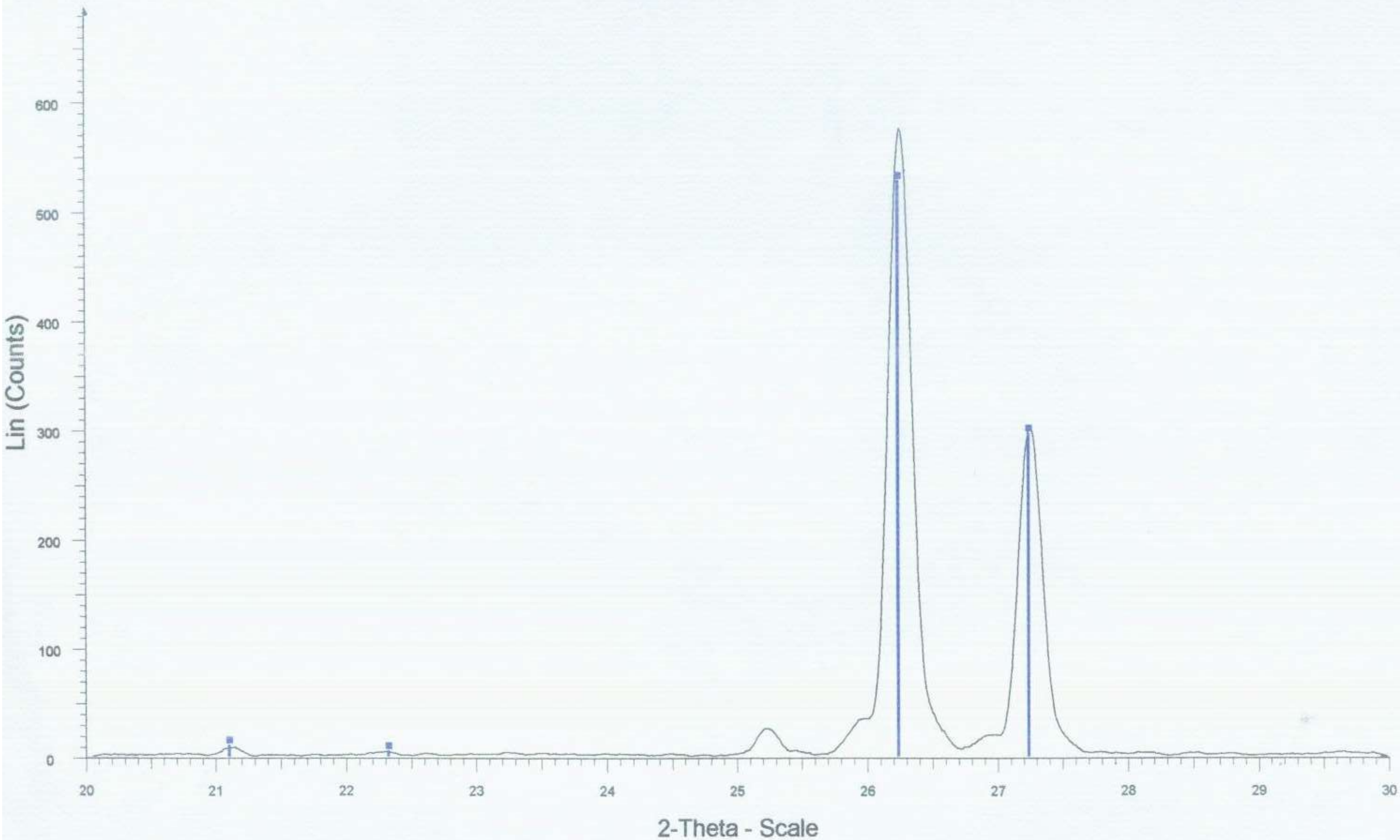

MZ-29 - File: David Cuevas-MZ-29.RAW - Type: 2Th/Th locked - Start: 20.000 ° - End: 30.000 ° - Step: 0.010 ° - Step time: 2. s - Temp.: 25 °C (Room) - Time Started: 16 s - 2-Theta: 20.000 ° - Theta: 10.
Operations: Smooth 0.150 | Background 1.000,1.000 | Import
76-0606 (A) - Aragonite - Ca(CO3) - Y: 91.67 % - d x by: 1. - WL: 1.54056 - Orthorhombic - a 4.95980 - b 7.96410 - c 5.73790 - alpha 90.000 - beta 90.000 - gamma 90.000 - Primitive - Pmcn (62) - 4 - 22

Sample: S-232-3-G

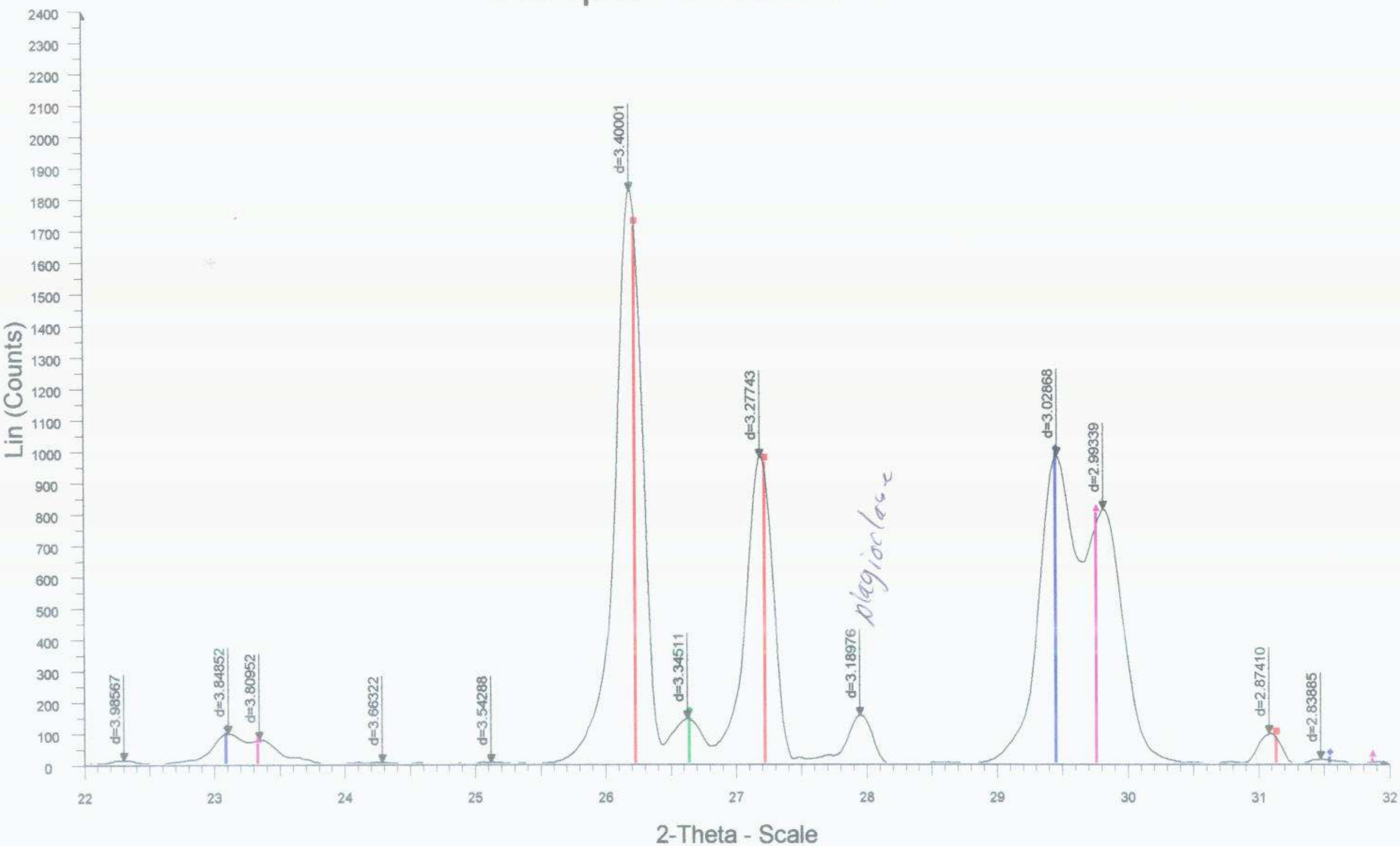

Sample: S-232-3-G - File: Clark-Sherman-26-5-09-S-232-3-G.RAW - Type: 2Th/Th locked - Start: 22.000 ° - End: 32.000 ° - Step: 0.020 ° - Step time: 1. s - Temp.: 25 °C (Room) - Time Started: 16 s - 2-T

Operations: Background 1.000,1.000 | Background 1.000,1.000 | Smooth 0.150 | Import

24-0025 (D) - Aragonite - $CaCO_3$ - Y: 93.75 % - d x by: 1. - WL: 1.54056 - Orthorhombic - a 5.74000 - b 4.96100 - c 2.92900 - alpha 90.000 - beta 90.000 - gamma 90.000 - Primitive - Pnma (62) - 4 - 83.

72-1652 (A) - Calcite - $CaCO_3$ - Y: 54.19 % - d x by: 1. - WL: 1.54056 - Hexagonal (Rh) - a 4.99000 - b 4.99000 - c 17.00200 - alpha 90.000 - beta 90.000 - gamma 120.000 - Primitive - R-3c (167) - 6 - 3

86-1560 (C) - Quartz low - SiO_2 - Y: 8.33 % - d x by: 1. - WL: 1.54056 - Hexagonal - a 4.91600 - b 4.91600 - c 5.40540 - alpha 90.000 - beta 90.000 - gamma 120.000 - Primitive - P3221 (154) - 3 - 113.1

86-2336 (C) - Calcite magnesian - $(Mg_{.129}Ca_{.871})(CO_3)$ - Y: 43.75 % - d x by: 1. - WL: 1.54056 - Hexagonal (Rh) - a 4.93820 - b 4.93820 - c 16.83200 - alpha 90.000 - beta 90.000 - gamma 120.000 - F

Sample: CH-43-1-G

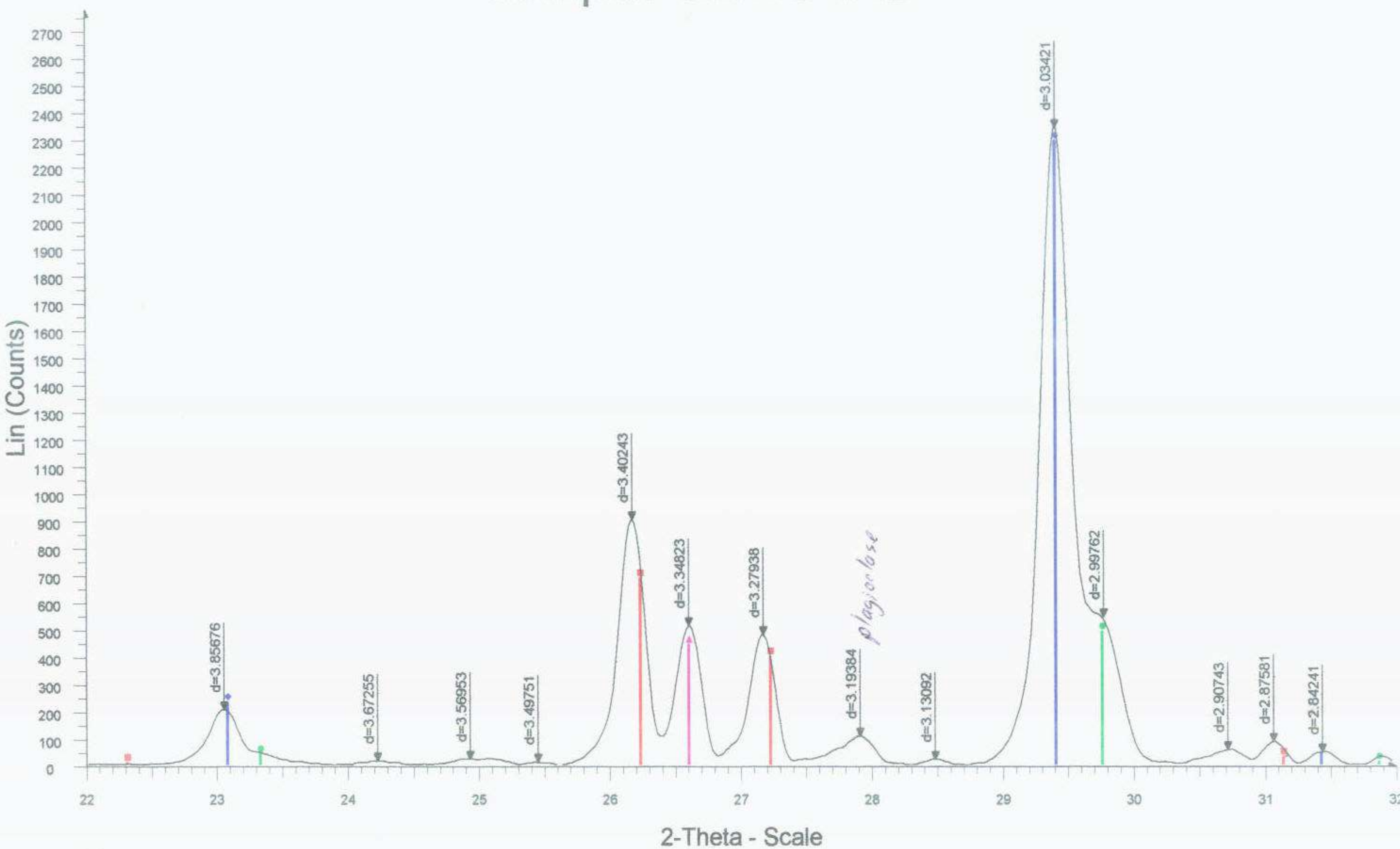

Sample: CH-43-1-G - File: Clark-Sherman-26-5-09-CH-43-1-G.RAW - Type: 2Th/Th locked - Start: 22.000 ° - End: 32.000 ° - Step: 0.020 ° - Step time: 1. s - Temp.: 25 °C (Room) - Time Started: 16 s - 2-
Operations: Background 1.000,1.000 | Background 1.000,1.000 | Smooth 0.150 | Import
71-2396 (A) - Aragonite - $CaCO_3$ - Y: 29.17 % - d x by: 1. - WL: 1.54056 - Orthorhombic - a 4.96160 - b 7.97050 - c 5.73940 - alpha 90.000 - beta 90.000 - gamma 90.000 - Primitive - Pmcn (62) - 4 - 226
86-2336 (C) - Calcite magnesian - $(Mg_{.129}Ca_{.871})(CO_3)$ - Y: 20.83 % - d x by: 1. - WL: 1.54056 - Hexagonal (Rh) - a 4.93820 - b 4.93820 - c 16.83200 - alpha 90.000 - beta 90.000 - gamma 120.000 - F
86-2334 (A) - Calcite - $Ca(CO_3)$ - Y: 97.92 % - d x by: 1. - WL: 1.54056 - Hexagonal (Rh) - a 4.98800 - b 4.98800 - c 17.06100 - alpha 90.000 - beta 90.000 - gamma 120.000 - Primitive - R-3c (167) - 6 -
83-0539 (A) - Quartz - SiO_2 - Y: 18.75 % - d x by: 1. - WL: 1.54056 - Hexagonal - a 4.92100 - b 4.92100 - c 5.41630 - alpha 90.000 - beta 90.000 - gamma 120.000 - Primitive - P3121 (152) - 3 - 113.590

Sample: CH-43-1; Fined grained (Mud)

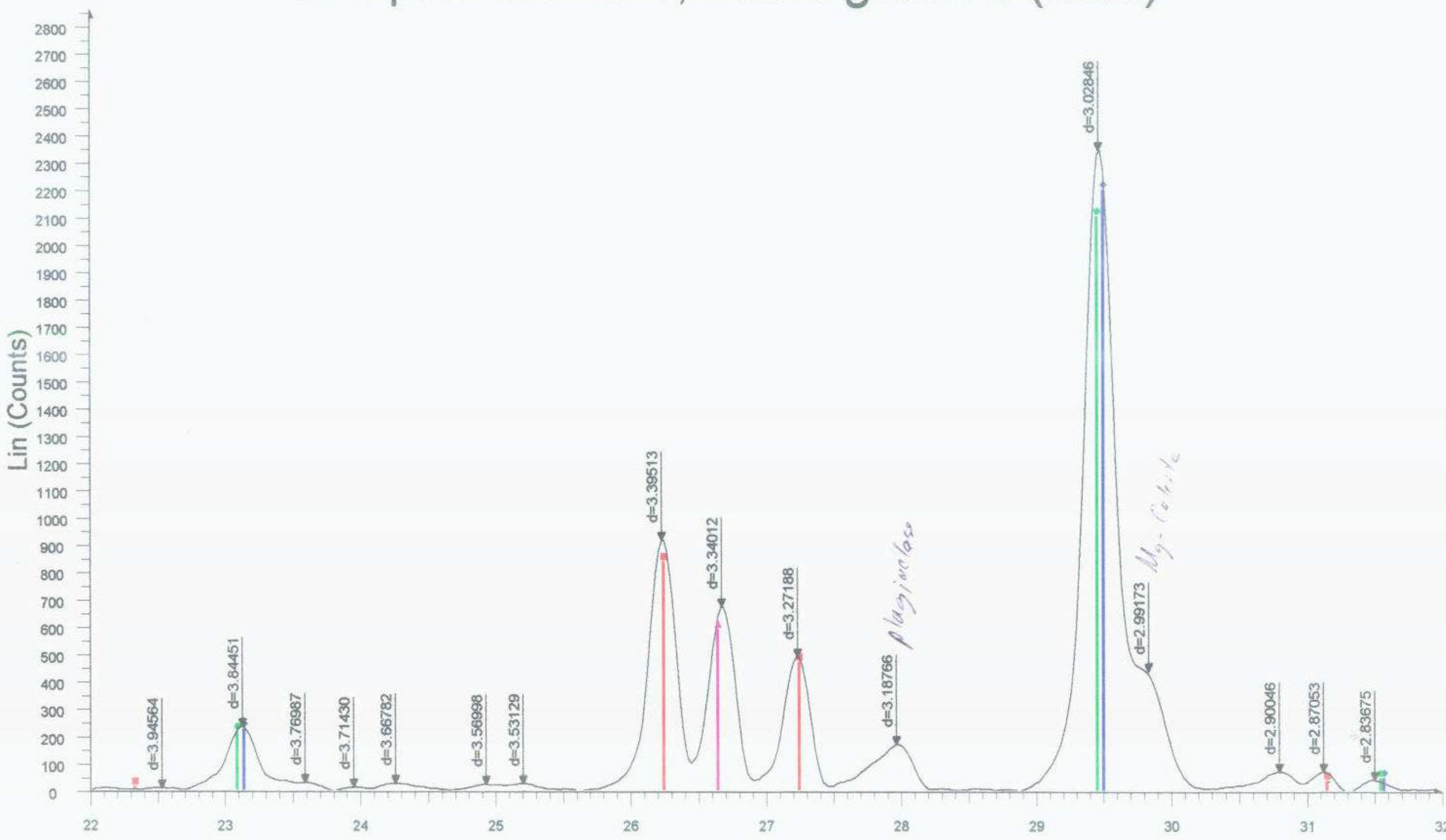

Sample: CH-43-1; Fined grained (Mud) - File: Clark-Sherman-26-5-09-CH-43-1.RAW - Type: 2Th/Th locked - Start: 22.000 ° - End: 32.000 ° - Step: 0.020 ° - Step time: 1. s - Temp.: 25 °C (Room) - Time
Operations: Background 1.000,1.000 | Background 1.000,1.000 | Smooth 0.150 | Import
76-0606 (A) - Aragonite - Ca(CO3) - Y: 35.42 % - d x by: 1. - WL: 1.54056 - Orthorhombic - a 4.95980 - b 7.96410 - c 5.73790 - alpha 90.000 - beta 90.000 - gamma 90.000 - Primitive - Pmcn (62) - 4 - 22
89-1304 (C) - Magnesium calcite, syn - (Mg0.03Ca0.97)(CO3) - Y: 93.75 % - d x by: 1. - WL: 1.54056 - Hexagonal (Rh) - a 4.97800 - b 4.97800 - c 16.98800 - alpha 90.000 - beta 90.000 - gamma 120.0(
72-1652 (A) - Calcite - CaCO3 - Y: 89.58 % - d x by: 1. - WL: 1.54056 - Hexagonal (Rh) - a 4.99000 - b 4.99000 - c 17.00200 - alpha 90.000 - beta 90.000 - gamma 120.000 - Primitive - R-3c (167) - 6 - 3
83-2465 (A) - Quartz, syn - SiO2 - Y: 25.00 % - d x by: 1. - WL: 1.54056 - Hexagonal - a 4.91480 - b 4.91480 - c 5.40620 - alpha 90.000 - beta 90.000 - gamma 120.000 - Primitive - P3121 (152) - 3 - 113

Sample: CH-43-2-G

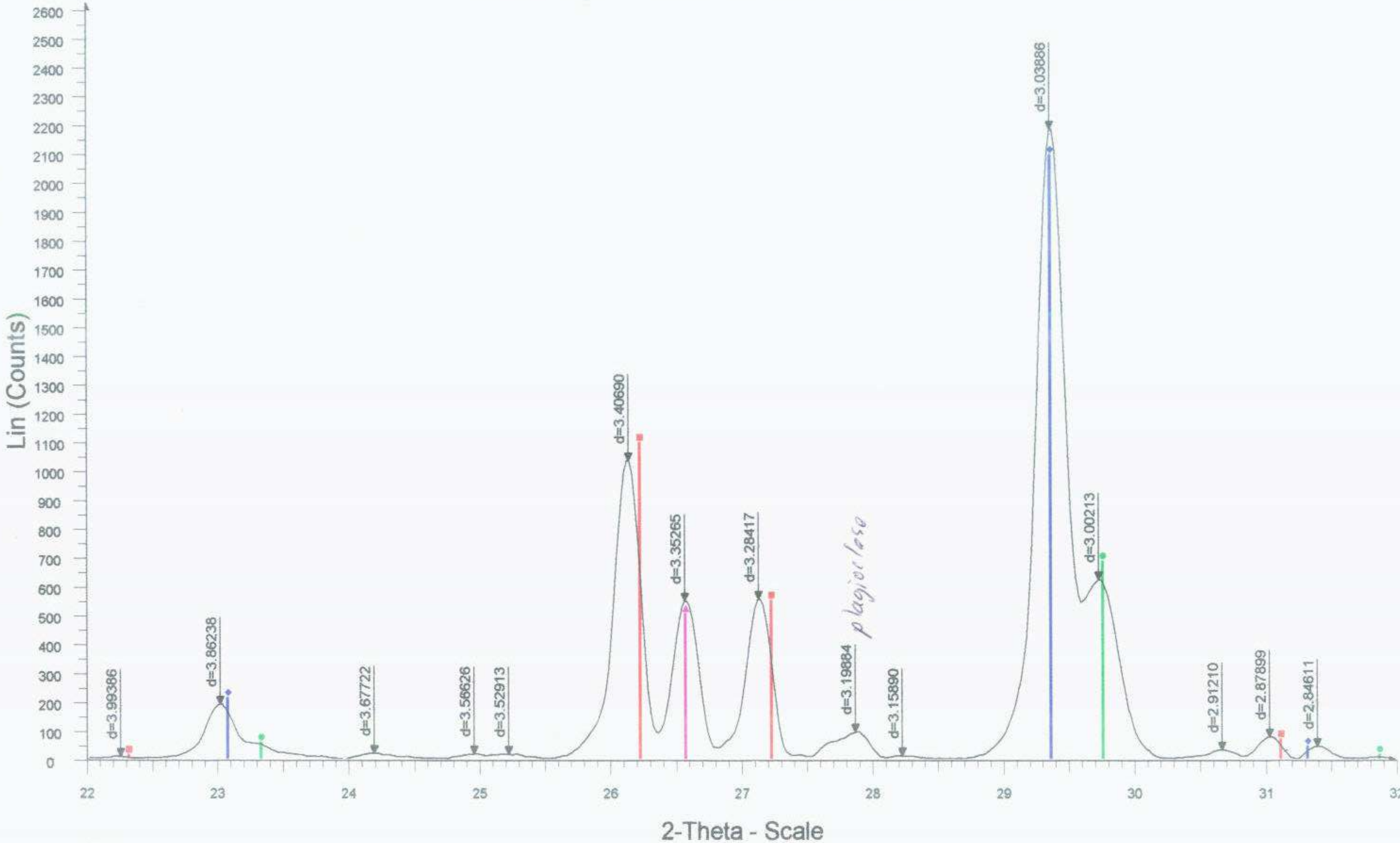

Sample: CH-43-2-G - File: Clark-Sherman-26-5-09-CH-43-2-G.RAW - Type: 2Th/Th locked - Start: 22.000 ° - End: 32.000 ° - Step: 0.020 ° - Step time: 1. s - Temp.: 25 °C (Room) - Time Started: 16 s - 2-
Operations: Background 1.000,1.000 | Background 1.000,1.000 | Smooth 0.150 | Import

41-1475 (*) - Aragonite - $CaCO_3$ - Y: 50.00 % - d x by: 1. - WL: 1.54056 - Orthorhombic - a 4.96230 - b 7.96800 - c 5.74390 - alpha 90.000 - beta 90.000 - gamma 90.000 - Primitive - Pmcn (62) - 4 - 227.

86-2339 (C) - Calcite - $Ca(CO_3)$ - Y: 95.83 % - d x by: 1. - WL: 1.54056 - Hexagonal (Rh) - a 4.98400 - b 4.98400 - c 17.12100 - alpha 90.000 - beta 90.000 - gamma 120.000 - Primitive - R-3c (167) - 6 -

86-2336 (C) - Calcite magnesian - $(Mg.129Ca.871)(CO_3)$ - Y: 31.25 % - d x by: 1. - WL: 1.54056 - Hexagonal (Rh) - a 4.93820 - b 4.93820 - c 16.83200 - alpha 90.000 - beta 90.000 - gamma 120.000 - F

85-1780 (A) - Quartz - SiO_2 - Y: 22.92 % - d x by: 1. - WL: 1.54056 - Hexagonal - a 4.89000 - b 4.89000 - c 5.49000 - alpha 90.000 - beta 90.000 - gamma 120.000 - Primitive - P3221 (154) - 3 - 113.690

Sample: CH-43-2; < 4-phi

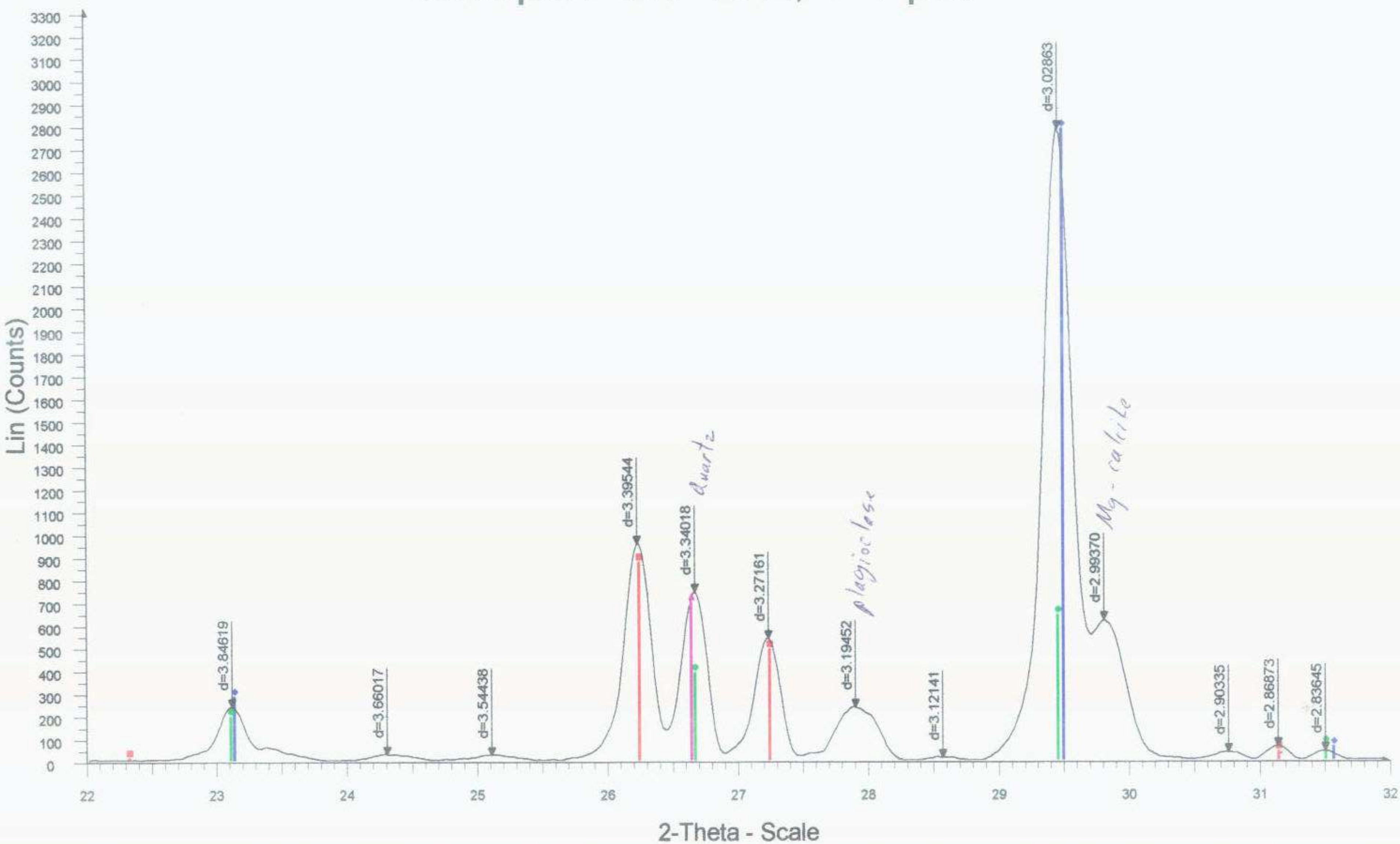

Sample: CH-43-2; < 4-phi - File: Clark-Sherman-26-5-09-CH-43-2.RAW - Type: 2Th/Th locked - Start: 22.000 ° - End: 32.000 ° - Step: 0.020 ° - Step time: 1. s - Temp.: 25 °C (Room) - Time Started: 16 s

Operations: Background 1.000,1.000 | Background 1.000,1.000 | Smooth 0.150 | Import

76-0606 (A) - Aragonite - Ca(CO3) - Y: 31.25 % - d x by: 1. - WL: 1.54056 - Orthorhombic - a 4.95980 - b 7.96410 - c 5.73790 - alpha 90.000 - beta 90.000 - gamma 90.000 - Primitive - Pmcn (62) - 4 - 22

89-1304 (C) - Magnesium calcite, syn - (Mg0.03Ca0.97)(CO3) - Y: 100.00 % - d x by: 1. - WL: 1.54056 - Hexagonal (Rh) - a 4.97800 - b 4.97800 - c 16.98800 - alpha 90.000 - beta 90.000 - gamma 120.(

03-0596 (D) - Calcite - beta-CaCO3 - Y: 22.92 % - d x by: 1. - WL: 1.54056 - Hexagonal (Rh) - a 4.98300 - b 4.98300 - c 17.02000 - alpha 90.000 - beta 90.000 - gamma 120.000 - Primitive - R-3c (167) -

83-2465 (A) - Quartz, syn - SiO2 - Y: 25.00 % - d x by: 1. - WL: 1.54056 - Hexagonal - a 4.91480 - b 4.91480 - c 5.40620 - alpha 90.000 - beta 90.000 - gamma 120.000 - Primitive - P3121 (152) - 3 - 113

Sample: CH-43-3-G

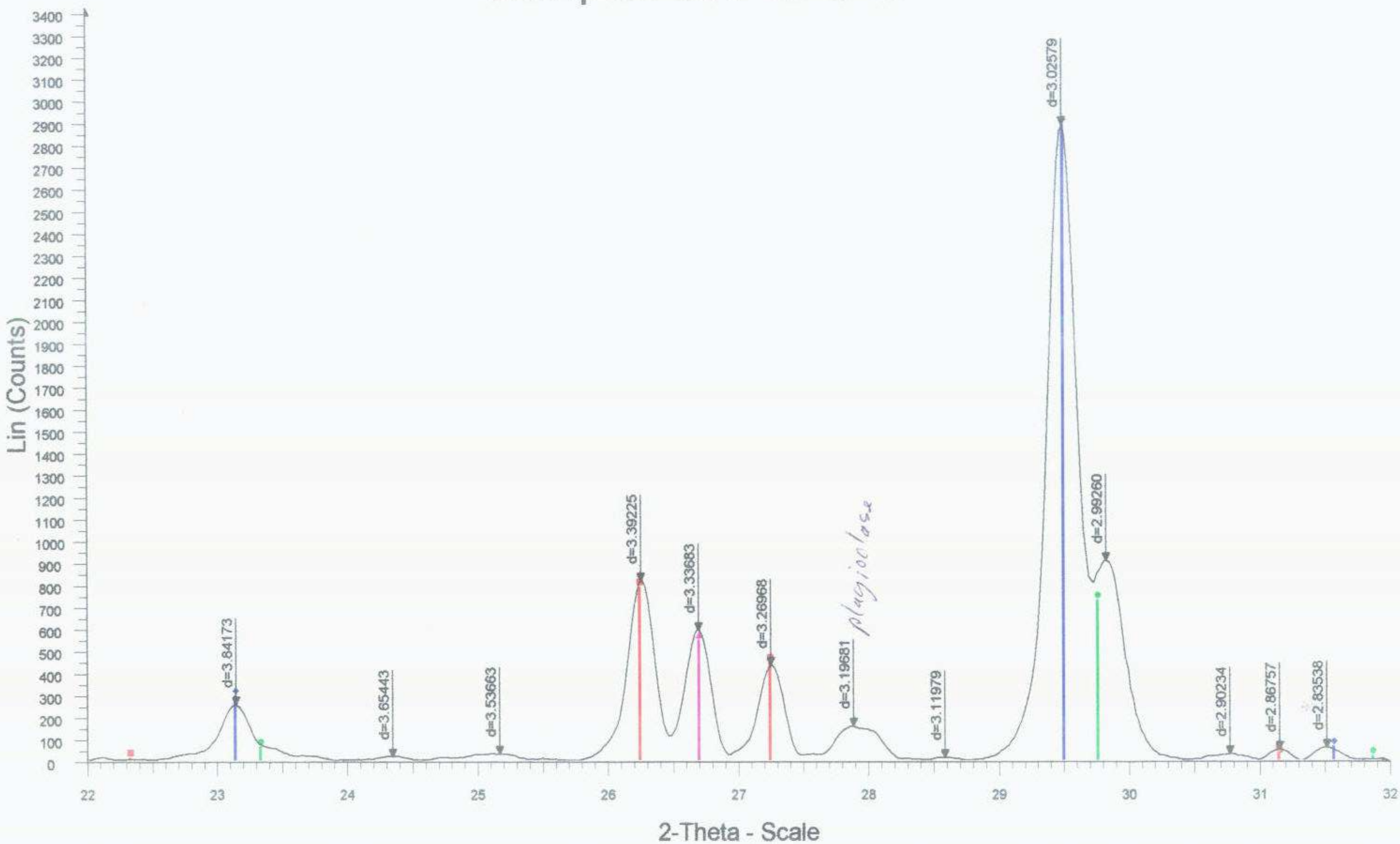

Sample: CH-43-3-G - File: Clark-Sherman-26-5-09-CH-43-3-G.RAW - Type: 2Th/Th locked - Start: 22.000 ° - End: 32.000 ° - Step: 0.020 ° - Step time: 1. s - Temp.: 25 °C (Room) - Time Started: 16 s - 2-

Operations: Background 1.000,1.000 | Background 1.000,1.000 | Smooth 0.150 | Import

76-0606 (A) - Aragonite - Ca(CO3) - Y: 27.08 % - d x by: 1. - WL: 1.54056 - Orthorhombic - a 4.95980 - b 7.96410 - c 5.73790 - alpha 90.000 - beta 90.000 - gamma 90.000 - Primitive - Pmcn (62) - 4 - 22

89-1304 (C) - Magnesium calcite, syn - (Mg0.03Ca0.97)(CO3) - Y: 100.00 % - d x by: 1. - WL: 1.54056 - Hexagonal (Rh) - a 4.97800 - b 4.97800 - c 16.98800 - alpha 90.000 - beta 90.000 - gamma 120.(

86-2336 (C) - Calcite magnesian - (Mg.129Ca.871)(CO3) - Y: 25.00 % - d x by: 1. - WL: 1.54056 - Hexagonal (Rh) - a 4.93820 - b 4.93820 - c 16.83200 - alpha 90.000 - beta 90.000 - gamma 120.000 - F

86-1629 (A) - Quartz low - SiO2 - Y: 18.75 % - d x by: 1. - WL: 1.54056 - Hexagonal - a 4.90300 - b 4.90300 - c 5.39990 - alpha 90.000 - beta 90.000 - gamma 120.000 - Primitive - P3121 (152) - 3 - 112.

Sample: CH-43-3; < 4-phi

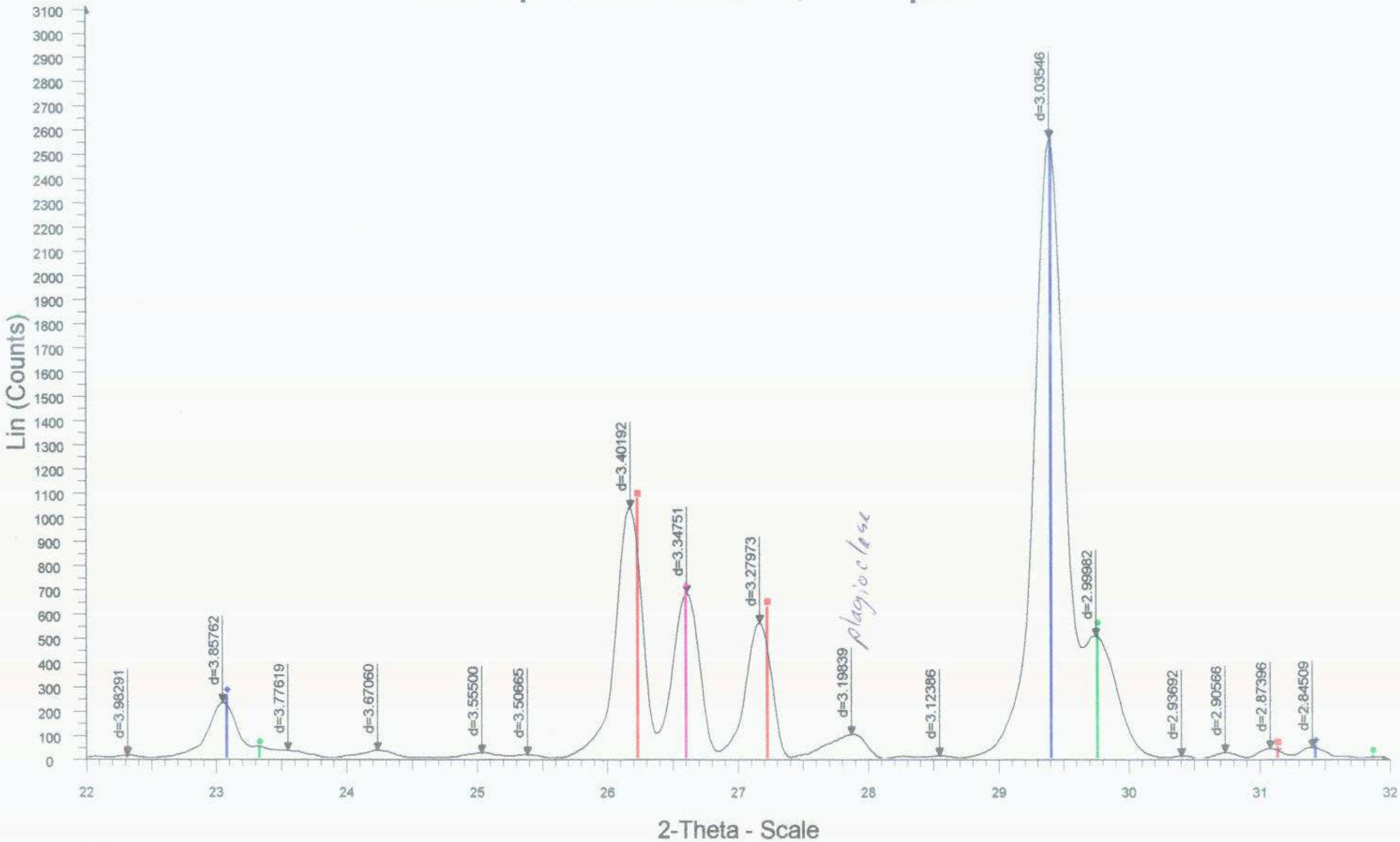

Sample: CH-43-3; < 4-phi - File: Clark-Sherman-26-5-09-CH-43-3.RAW - Type: 2Th/Th locked - Start: 22.000 ° - End: 32.000 ° - Step: 0.020 ° - Step time: 1. s - Temp.: 25 °C (Room) - Time Started: 16 s

Operations: Background 1.000,1.000 | Background 1.000,1.000 | Smooth 0.150 | Import

71-2396 (A) - Aragonite - CaCO3 - Y: 41.67 % - d x by: 1. - WL: 1.54056 - Orthorhombic - a 4.96160 - b 7.97050 - c 5.73940 - alpha 90.000 - beta 90.000 - gamma 90.000 - Primitive - Pmcn (62) - 4 - 226

86-2336 (C) - Calcite magnesian - (Mg.129Ca.871)(CO3) - Y: 20.83 % - d x by: 1. - WL: 1.54056 - Hexagonal (Rh) - a 4.93820 - b 4.93820 - c 16.83200 - alpha 90.000 - beta 90.000 - gamma 120.000 - F

86-2334 (A) - Calcite - Ca(CO3) - Y: 100.00 % - d x by: 1. - WL: 1.54056 - Hexagonal (Rh) - a 4.98800 - b 4.98800 - c 17.06100 - alpha 90.000 - beta 90.000 - gamma 120.000 - Primitive - R-3c (167) - 6

89-1961 (C) - Quartz low, dauphinee-twinned - SiO2 - Y: 27.08 % - d x by: 1. - WL: 1.54056 - Hexagonal - a 4.92100 - b 4.92100 - c 5.41600 - alpha 90.000 - beta 90.000 - gamma 120.000 - Primitive - P

Sample: CH-43-4-G

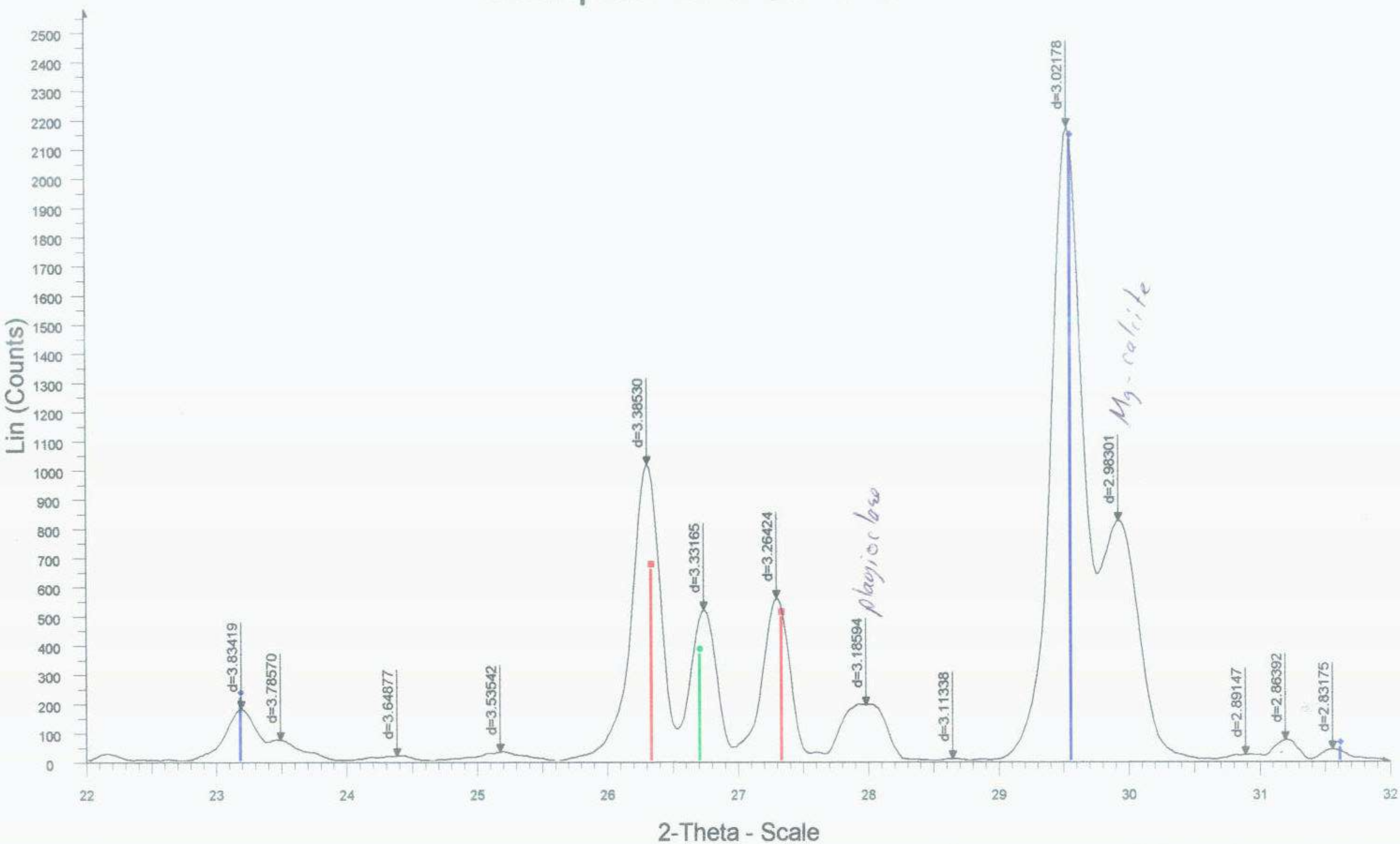

Sample: CH-43-4-G - File: Clark-Sherman-26-5-09-CH-43-4-G.RAW - Type: 2Th/Th locked - Start: 22.000 ° - End: 32.000 ° - Step: 0.020 ° - Step time: 1. s - Temp.: 25 °C (Room) - Time Started: 16 s - 2-
Operations: Background 1.000,1.000 | Background 1.000,1.000 | Smooth 0.150 | Import

03-1067 (D) - Aragonite - gamma-$CaCO_3$ - Y: 37.50 % - d x by: 1. - WL: 1.54056 - Orthorhombic - a 4.94000 - b 7.94000 - c 5.72000 - alpha 90.000 - beta 90.000 - gamma 90.000 - Primitive - Pnma (62)

86-2335 (C) - Calcite magnesian - $(Mg_{.064}Ca_{.936})(CO_3)$ - Y: 97.92 % - d x by: 1. - WL: 1.54056 - Hexagonal (Rh) - a 4.96730 - b 4.96730 - c 16.96310 - alpha 90.000 - beta 90.000 - gamma 120.000 - F

85-0865 (A) - Quartz - alpha-SiO_2 - Y: 16.67 % - d x by: 1. - WL: 1.54056 - Hexagonal - a 4.90000 - b 4.90000 - c 5.40000 - alpha 90.000 - beta 90.000 - gamma 120.000 - Primitive - P3121 (152) - 3 - 11

Sample: CH-43-4; < 4-phi

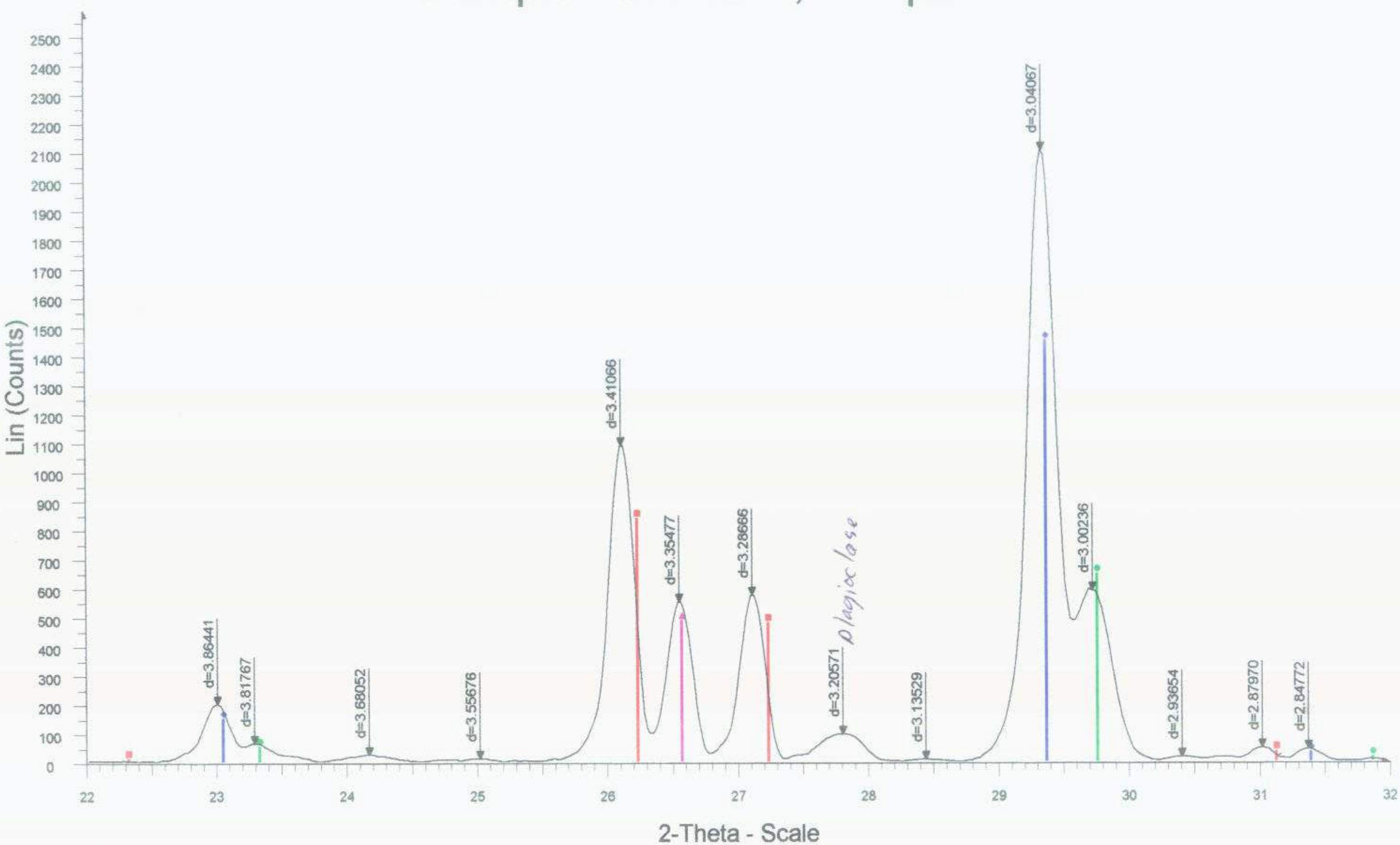

Sample: CH-43-4; < 4-phi - File: Clark-Sherman-26-5-09-CH-43-4.RAW - Type: 2Th/Th locked - Start: 22.000 ° - End: 32.000 ° - Step: 0.020 ° - Step time: 1. s - Temp.: 25 °C (Room) - Time Started: 16 s
Operations: Background 1.000,1.000 | Background 1.000,1.000 | Smooth 0.150 | Import

75-2230 (C) - Aragonite - Ca(CO3) - Y: 39.58 % - d x by: 1. - WL: 1.54056 - Orthorhombic - a 4.96100 - b 7.96700 - c 5.74100 - alpha 90.000 - beta 90.000 - gamma 90.000 - Primitive - Pmcn (62) - 4 - 2

86-2336 (C) - Calcite magnesian - (Mg.129Ca.871)(CO3) - Y: 30.55 % - d x by: 1. - WL: 1.54056 - Hexagonal (Rh) - a 4.93820 - b 4.93820 - c 16.83200 - alpha 90.000 - beta 90.000 - gamma 120.000 - F

72-1937 (C) - Calcite - CaCO3 - Y: 68.75 % - d x by: 1. - WL: 1.54056 - Hexagonal (Rh) - a 4.99400 - b 4.99400 - c 17.08100 - alpha 90.000 - beta 90.000 - gamma 120.000 - Primitive - R-3c (167) - 6 - 3

85-1780 (A) - Quartz - SiO2 - Y: 22.92 % - d x by: 1. - WL: 1.54056 - Hexagonal - a 4.89000 - b 4.89000 - c 5.49000 - alpha 90.000 - beta 90.000 - gamma 120.000 - Primitive - P3221 (154) - 3 - 113.690

Sample: CH-67-1-G

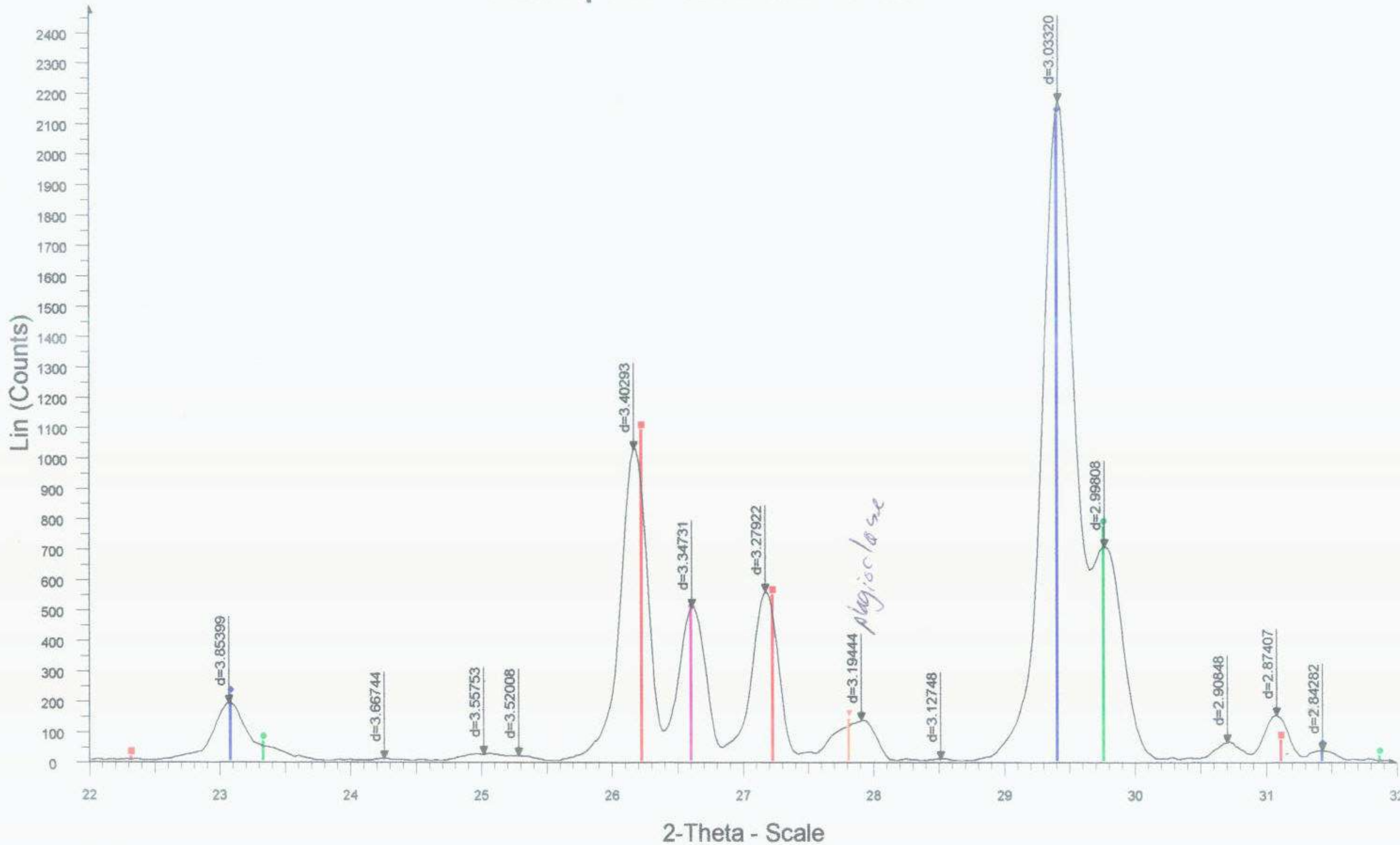

Sample: CH-67-1-G - File: Clark-Sherman-26-5-09-CH-67-1-G.RAW - Type: 2Th/Th locked - Start: 22.000 ° - End: 32.000 ° - Step: 0.020 ° - Step time: 1. s - Temp.: 25 °C (Room) - Time Started: 16 s - 2-

Operations: Background 1.000,1.000 | Background 1.000,1.000 | Smooth 0.150 | Import

41-1475 (*) - Aragonite - CaCO3 - Y: 50.00 % - d x by: 1. - WL: 1.54056 - Orthorhombic - a 4.96230 - b 7.96800 - c 5.74390 - alpha 90.000 - beta 90.000 - gamma 90.000 - Primitive - Pmcn (62) - 4 - 227.

86-2336 (C) - Calcite magnesian - (Mg.129Ca.871)(CO3) - Y: 35.42 % - d x by: 1. - WL: 1.54056 - Hexagonal (Rh) - a 4.93820 - b 4.93820 - c 16.83200 - alpha 90.000 - beta 90.000 - gamma 120.000 - F

86-2334 (A) - Calcite - Ca(CO3) - Y: 97.92 % - d x by: 1. - WL: 1.54056 - Hexagonal (Rh) - a 4.98800 - b 4.98800 - c 17.06100 - alpha 90.000 - beta 90.000 - gamma 120.000 - Primitive - R-3c (167) - 6 -

89-1961 (C) - Quartz low, dauphinee-twinned - SiO2 - Y: 22.92 % - d x by: 1. - WL: 1.54056 - Hexagonal - a 4.92100 - b 4.92100 - c 5.41600 - alpha 90.000 - beta 90.000 - gamma 120.000 - Primitive - P

83-0541 (A) - Quartz - SiO2 - Y: 6.25 % - d x by: 1. - WL: 1.54056 - Hexagonal - a 4.67640 - b 4.67640 - c 5.24750 - alpha 90.000 - beta 90.000 - gamma 120.000 - Primitive - P3121 (152) - 3 - 99.3817 -

Sample: CH-67-1; < 4-phi

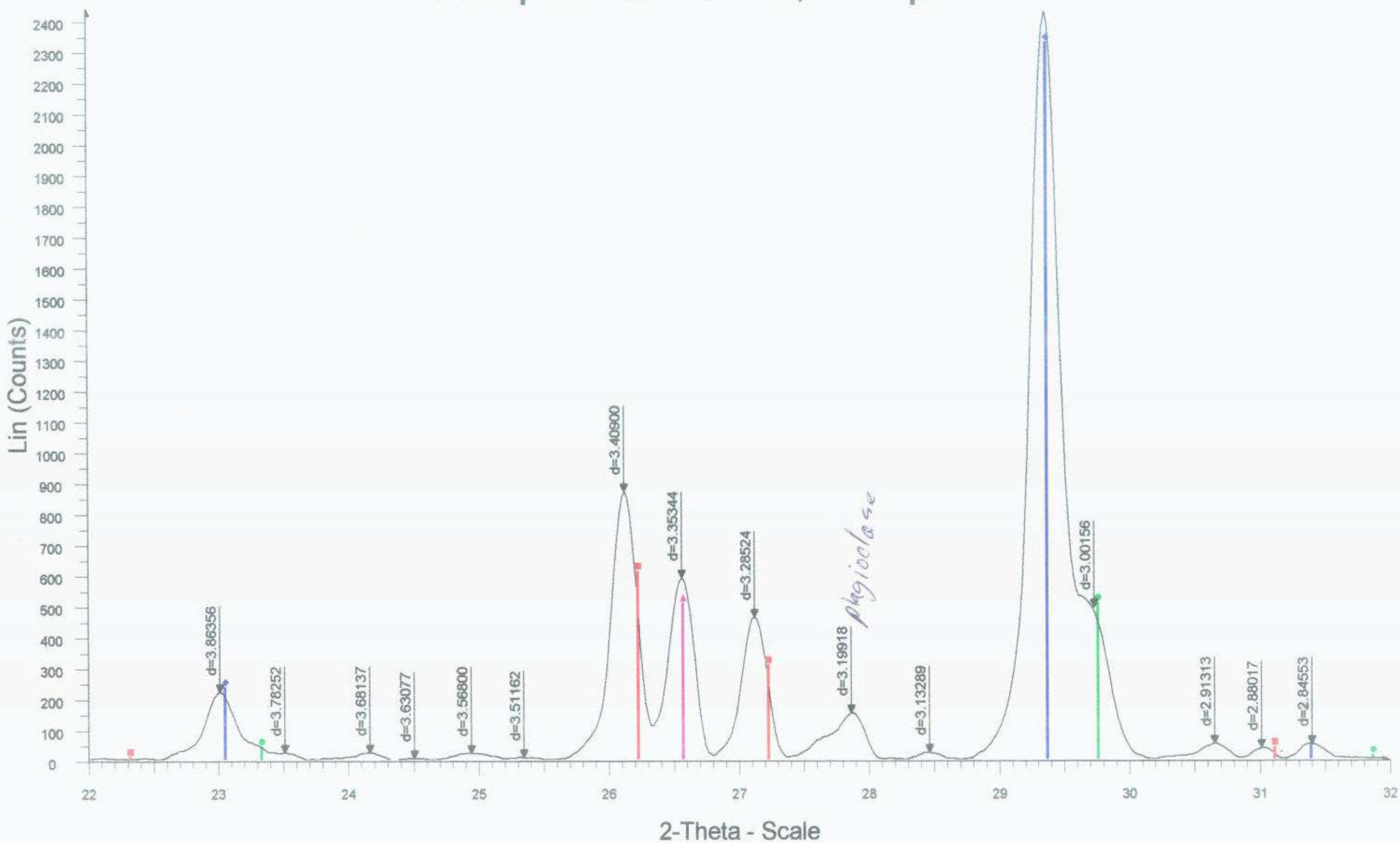

Sample: CH-67-1; < 4-phi - File: Clark-Sherman-26-5-09-CH-67-1.RAW - Type: 2Th/Th locked - Start: 22.000 ° - End: 32.000 ° - Step: 0.020 ° - Step time: 1. s - Temp.: 25 °C (Room) - Time Started: 16 s

Operations: Background 1.000,1.000 | Background 1.000,1.000 | Smooth 0.150 | Import

41-1475 (*) - Aragonite - CaCO3 - Y: 25.00 % - d x by: 1. - WL: 1.54056 - Orthorhombic - a 4.96230 - b 7.96800 - c 5.74390 - alpha 90.000 - beta 90.000 - gamma 90.000 - Primitive - Pmcn (62) - 4 - 227.

86-2336 (C) - Calcite magnesian - (Mg.129Ca.871)(CO3) - Y: 20.83 % - d x by: 1. - WL: 1.54056 - Hexagonal (Rh) - a 4.93820 - b 4.93820 - c 16.83200 - alpha 90.000 - beta 90.000 - gamma 120.000 - F

72-1937 (C) - Calcite - CaCO3 - Y: 95.83 % - d x by: 1. - WL: 1.54056 - Hexagonal (Rh) - a 4.99400 - b 4.99400 - c 17.08100 - alpha 90.000 - beta 90.000 - gamma 120.000 - Primitive - R-3c (167) - 6 - 3

85-1780 (A) - Quartz - SiO2 - Y: 20.83 % - d x by: 1. - WL: 1.54056 - Hexagonal - a 4.89000 - b 4.89000 - c 5.49000 - alpha 90.000 - beta 90.000 - gamma 120.000 - Primitive - P3221 (154) - 3 - 113.690

Sample: CH-67-2-G

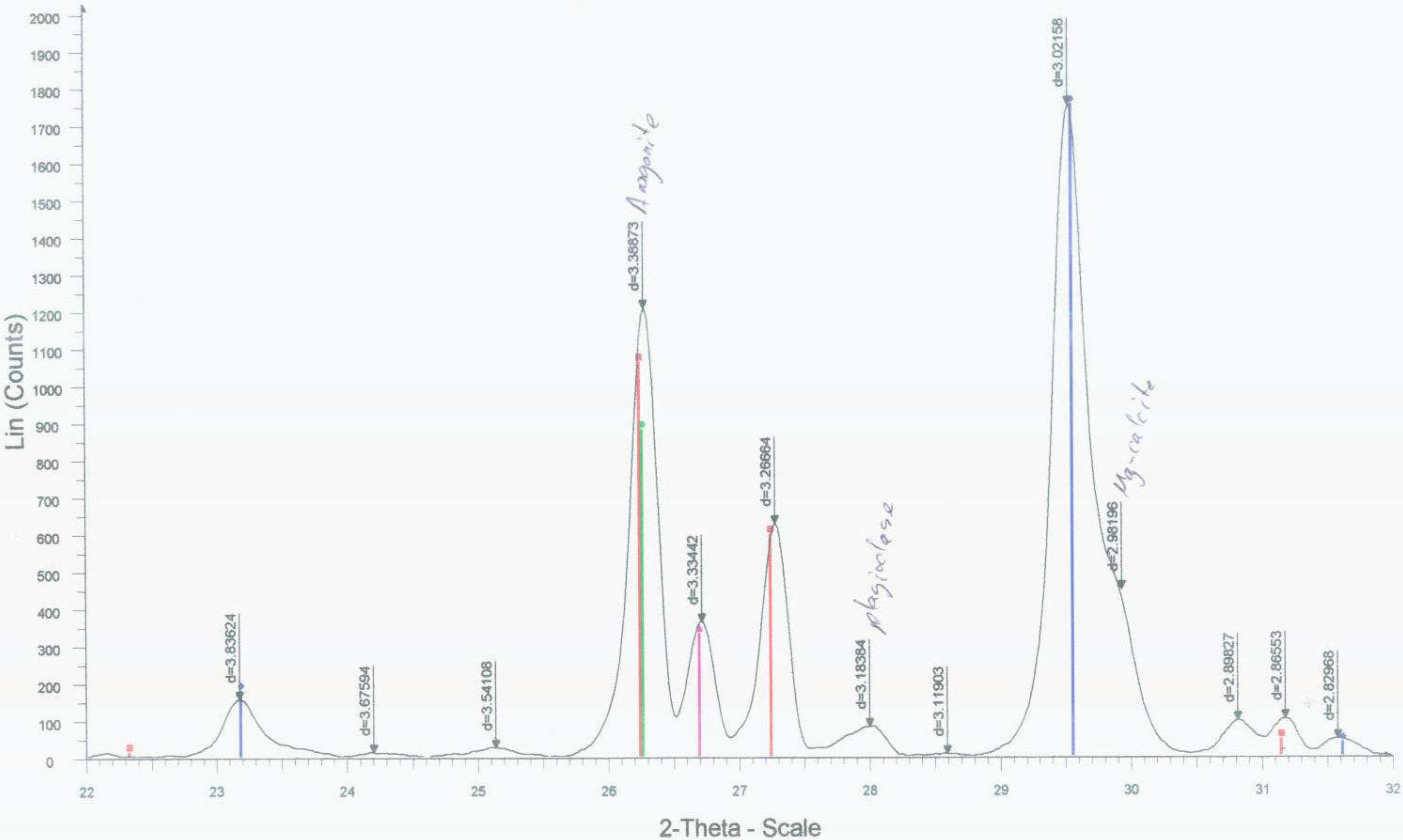

Sample: CH-67-2-G - File: Clark-Sherman-26-5-09-CH-67-2-G.RAW - Type: 2Th/Th locked - Start: 22.000 ° - End: 32.000 ° - Step: 0.020 ° - Step time: 1. s - Temp.: 25 °C (Room) - Time Started: 16 s - 2-
Operations: Background 1.000,1.000 | Background 1.000,1.000 | Smooth 0.150 | Import

76-0606 (A) - Aragonite - Ca(CO3) - Y: 60.42 % - d x by: 1. - WL: 1.54056 - Orthorhombic - a 4.95980 - b 7.96410 - c 5.73790 - alpha 90.000 - beta 90.000 - gamma 90.000 - Primitive - Pmcn (62) - 4 - 22

86-2335 (C) - Calcite magnesian - (Mg.064Ca.936)(CO3) - Y: 100.00 % - d x by: 1. - WL: 1.54056 - Hexagonal (Rh) - a 4.96730 - b 4.96730 - c 16.96310 - alpha 90.000 - beta 90.000 - gamma 120.000 -

87-0703 (C) - Quartz high, syn - SiO2 - Y: 50.00 % - d x by: 1. - WL: 1.54056 - Hexagonal - a 4.99770 - b 4.99770 - c 5.46010 - alpha 90.000 - beta 90.000 - gamma 120.000 - Primitive - P6222 (180) - 3

86-1629 (A) - Quartz low - SiO2 - Y: 18.75 % - d x by: 1. - WL: 1.54056 - Hexagonal - a 4.90300 - b 4.90300 - c 5.39990 - alpha 90.000 - beta 90.000 - gamma 120.000 - Primitive - P3121 (152) - 3 - 112.

Sample: CH-67-2; < 4-phi

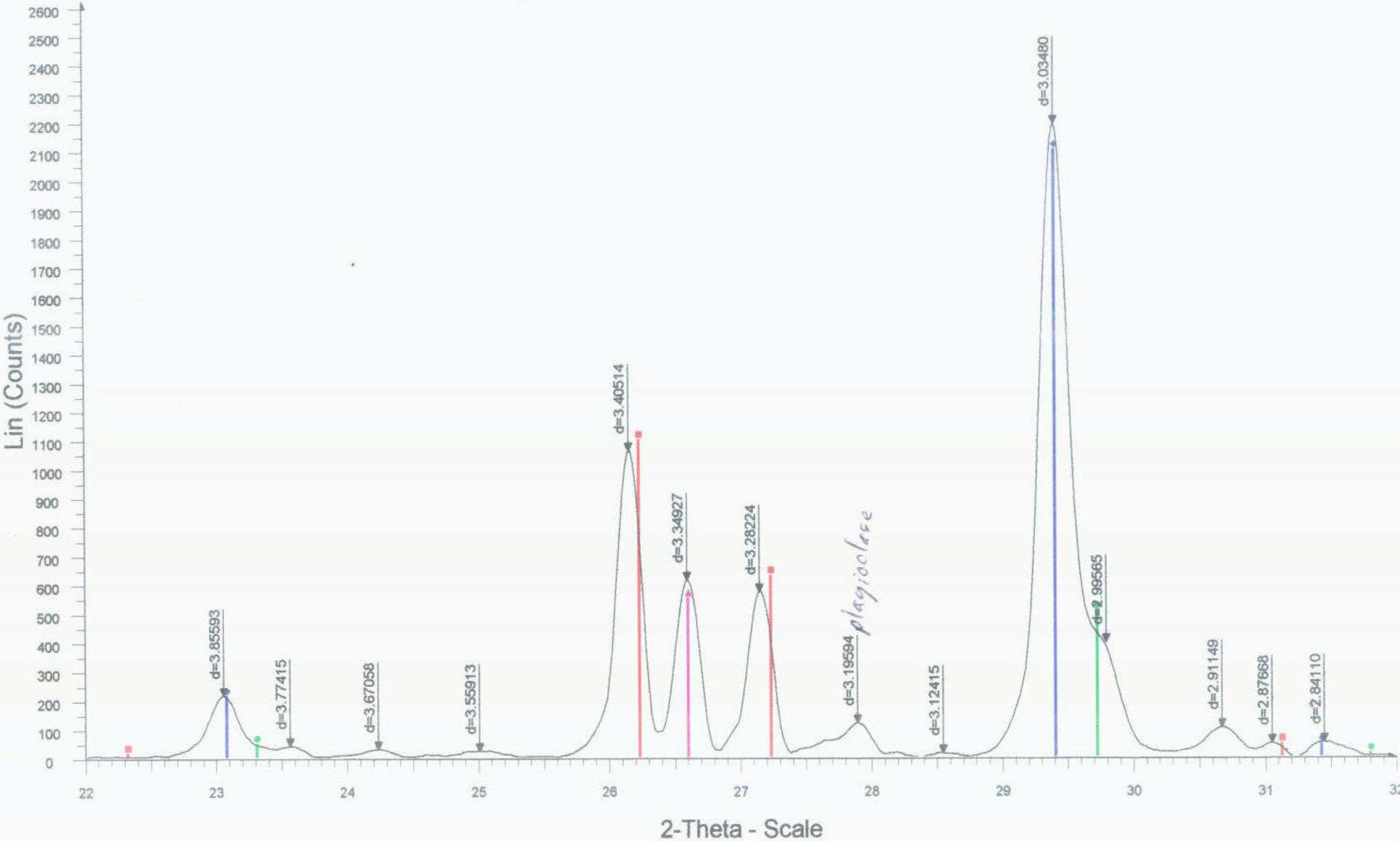

Sample: CH-67-2; < 4-phi - File: Clark-Sherman-26-5-09-CH-67-2.RAW - Type: 2Th/Th locked - Start: 22.000 ° - End: 32.000 ° - Step: 0.020 ° - Step time: 1. s - Temp.: 25 °C (Room) - Time Started: 16 s

Operations: Background 1.000,1.000 | Background 1.000,1.000 | Smooth 0.150 | Import

75-2230 (C) - Aragonite - Ca(CO3) - Y: 50.00 % - d x by: 1. - WL: 1.54056 - Orthorhombic - a 4.96100 - b 7.96700 - c 5.74100 - alpha 90.000 - beta 90.000 - gamma 90.000 - Primitive - Pmcn (62) - 4 - 2

86-2334 (A) - Calcite - Ca(CO3) - Y: 95.83 % - d x by: 1. - WL: 1.54056 - Hexagonal (Rh) - a 4.98800 - b 4.98800 - c 17.06100 - alpha 90.000 - beta 90.000 - gamma 120.000 - Primitive - R-3c (167) - 6 -

71-1663 (C) - Calcite, magnesian - Mg0.1Ca0.9CO3 - Y: 22.92 % - d x by: 1. - WL: 1.54056 - Hexagonal (Rh) - a 4.94100 - b 4.94100 - c 16.86400 - alpha 90.000 - beta 90.000 - gamma 120.000 - Primit

89-1961 (C) - Quartz low, dauphinee-twinned - SiO2 - Y: 25.00 % - d x by: 1. - WL: 1.54056 - Hexagonal - a 4.92100 - b 4.92100 - c 5.41600 - alpha 90.000 - beta 90.000 - gamma 120.000 - Primitive - P

Sample: CH-67-3-G

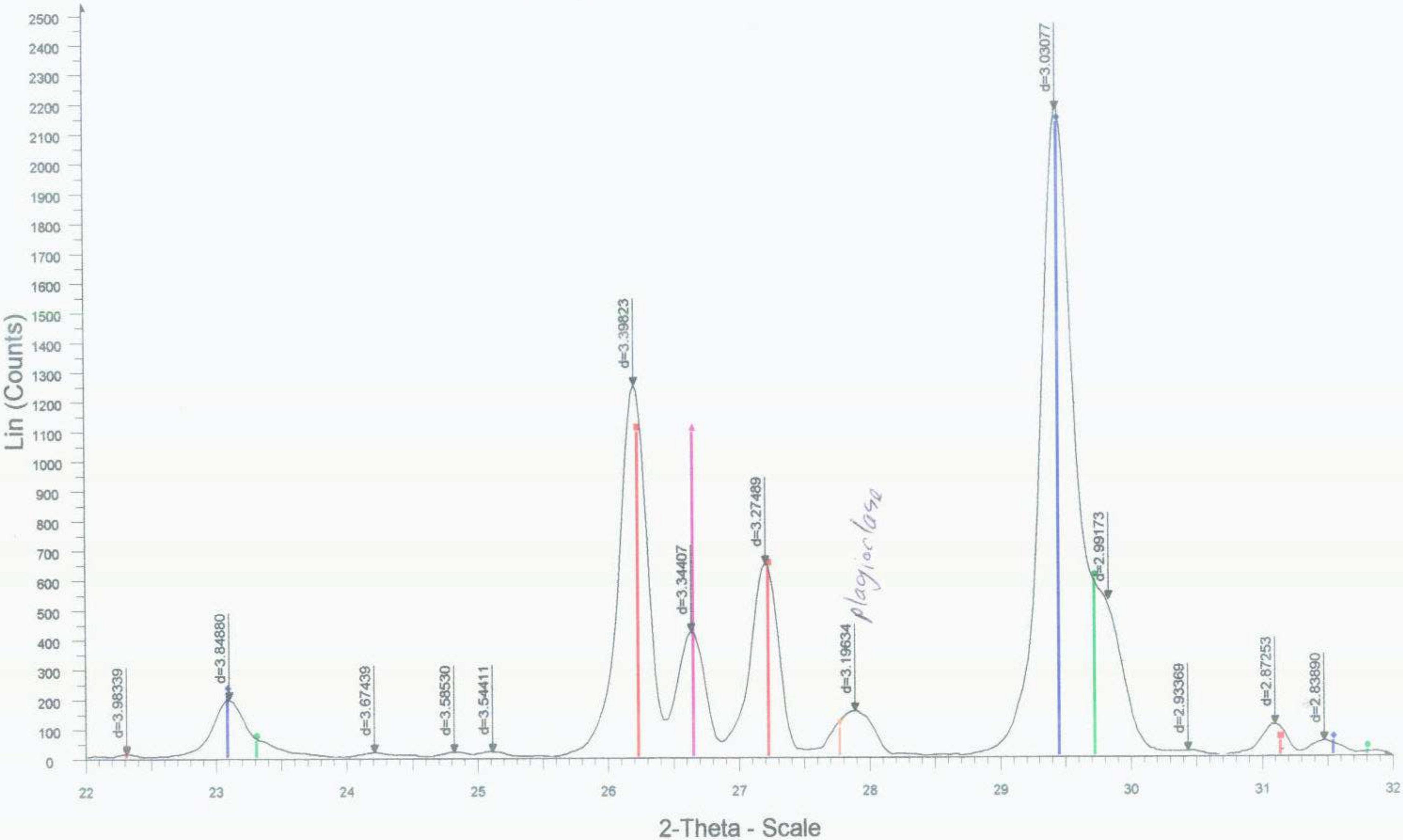

Sample: CH-67-3-G - File: Clark-Sherman-26-5-09-CH-67-3-G.RAW - Type: 2Th/Th locked - Start: 22.000 ° - End: 32.000 ° - Step: 0.020 ° - Step time: 1. s - Temp.: 25 °C (Room) - Time Started: 16 s - 2-
Operations: Background 1.000,1.000 | Background 1.000,1.000 | Smooth 0.150 | Import

71-2396 (A) - Aragonite - $CaCO_3$ - Y: 50.00 % - d x by: 1. - WL: 1.54056 - Orthorhombic - a 4.96160 - b 7.97050 - c 5.73940 - alpha 90.000 - beta 90.000 - gamma 90.000 - Primitive - Pmcn (62) - 4 - 226

72-1652 (A) - Calcite - $CaCO_3$ - Y: 97.92 % - d x by: 1. - WL: 1.54056 - Hexagonal (Rh) - a 4.99000 - b 4.99000 - c 17.00200 - alpha 90.000 - beta 90.000 - gamma 120.000 - Primitive - R-3c (167) - 6 - 3

71-1663 (C) - Calcite, magnesian - $Mg_{0.1}Ca_{0.9}CO_3$ - Y: 27.08 % - d x by: 1. - WL: 1.54056 - Hexagonal (Rh) - a 4.94100 - b 4.94100 - c 16.86400 - alpha 90.000 - beta 90.000 - gamma 120.000 - Primit

87-2096 (A) - Quartz - SiO_2 - Y: 50.00 % - d x by: 1. - WL: 1.54056 - Hexagonal - a 4.91270 - b 4.91270 - c 5.40450 - alpha 90.000 - beta 90.000 - gamma 120.000 - Primitive - P3221 (154) - 3 - 112.961

85-0462 (A) - Quartz low - SiO_2 - Y: 4.17 % - d x by: 1. - WL: 1.54056 - Hexagonal - a 4.68400 - b 4.68400 - c 5.25200 - alpha 90.000 - beta 90.000 - gamma 120.000 - Primitive - P3221 (154) - 3 - 99.79

Sample: CH-67-3; < 4-phi

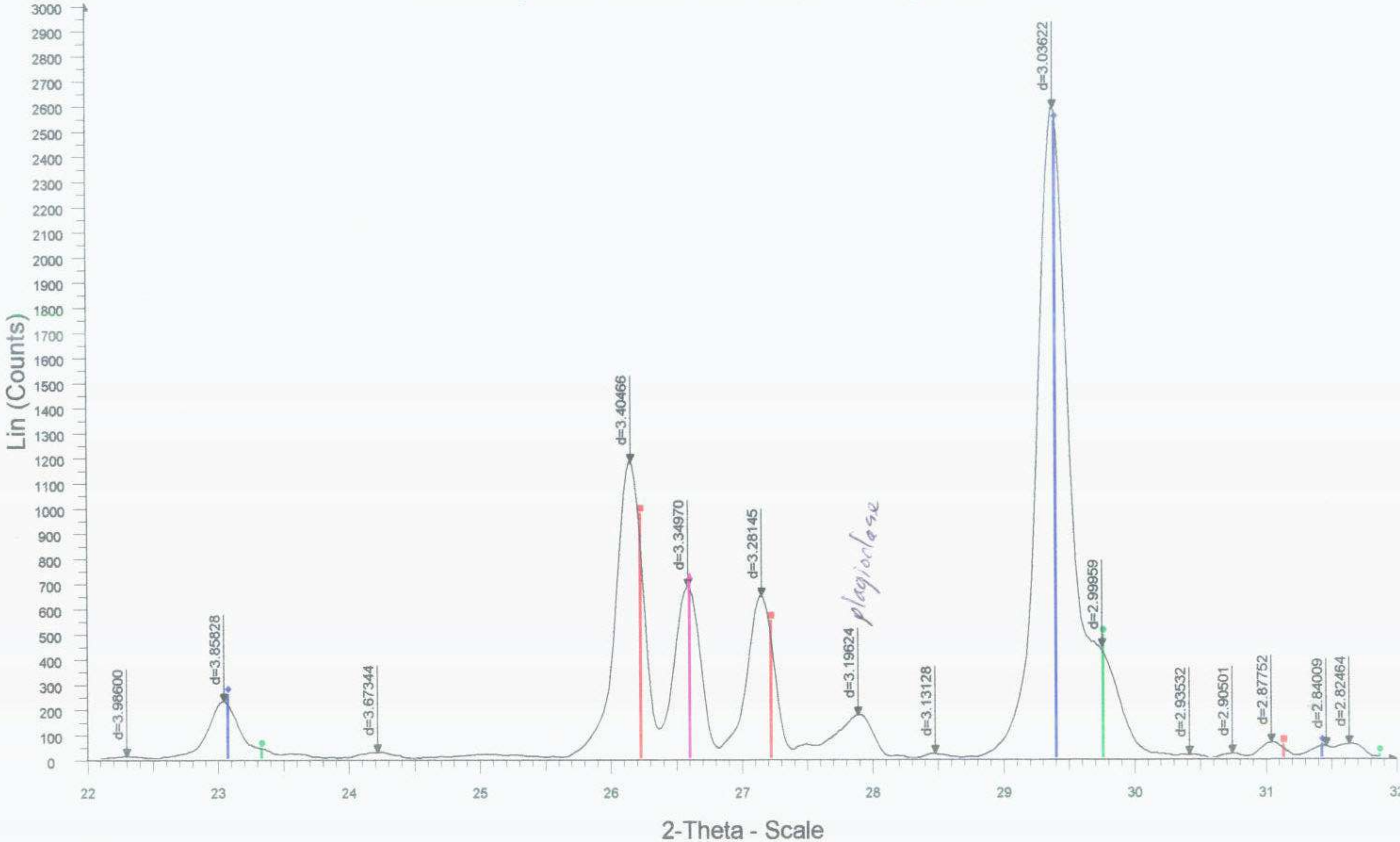

Sample: CH-67-3; < 4-phi - File: Clark-Sherman-26-5-09-CH-67-3.RAW - Type: 2Th/Th locked - Start: 22.000 ° - End: 32.000 ° - Step: 0.020 ° - Step time: 1. s - Temp.: 25 °C (Room) - Time Started: 16 s

Operations: Smooth 0.150 | Background 1.000,1.000 | Import

24-0025 (D) - Aragonite - $CaCO_3$ - Y: 37.50 % - d x by: 1. - WL: 1.54056 - Orthorhombic - a 5.74000 - b 4.96100 - c 2.92900 - alpha 90.000 - beta 90.000 - gamma 90.000 - Primitive - Pnma (62) - 4 - 83.

86-2336 (C) - Calcite magnesian - $(Mg_{.129}Ca_{.871})(CO_3)$ - Y: 18.75 % - d x by: 1. - WL: 1.54056 - Hexagonal (Rh) - a 4.93820 - b 4.93820 - c 16.83200 - alpha 90.000 - beta 90.000 - gamma 120.000 - F

83-1762 (A) - Calcite - $Ca(CO_3)$ - Y: 97.92 % - d x by: 1. - WL: 1.54056 - Hexagonal (Rh) - a 4.98960 - b 4.98960 - c 17.06100 - alpha 90.000 - beta 90.000 - gamma 120.000 - Primitive - R-3c (167) - 6 -

89-1961 (C) - Quartz low, dauphinee-twinned - SiO_2 - Y: 27.08 % - d x by: 1. - WL: 1.54056 - Hexagonal - a 4.92100 - b 4.92100 - c 5.41600 - alpha 90.000 - beta 90.000 - gamma 120.000 - Primitive - P

Sample: CH-67-4-G

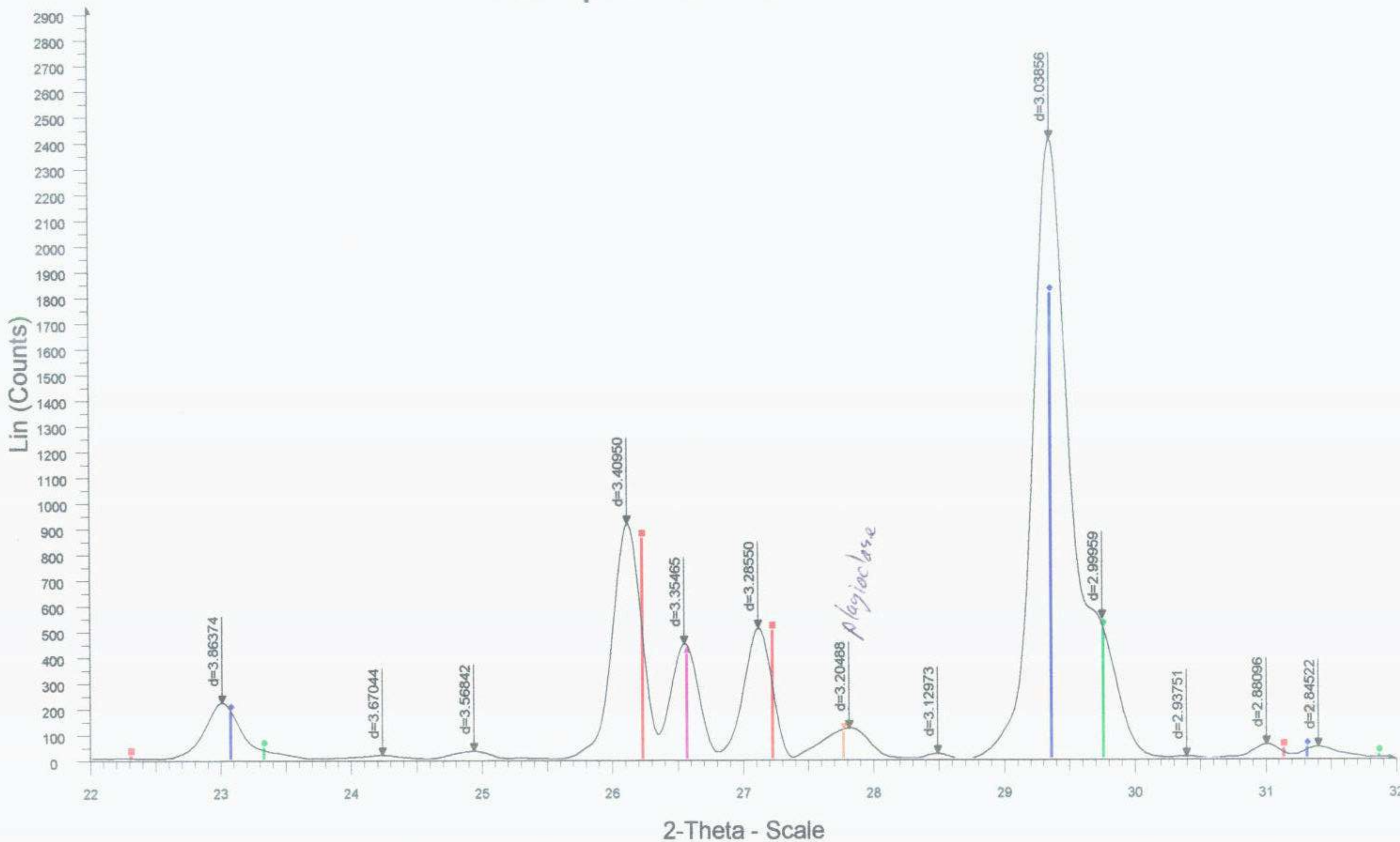

Sample: CH-67-4-G - File: Clark-Sherman-26-5-09-CH-67-4-G.RAW - Type: 2Th/Th locked - Start: 22.000 ° - End: 32.000 ° - Step: 0.020 ° - Step time: 1. s - Temp.: 25 °C (Room) - Time Started: 16 s - 2-

Operations: Background 1.000,1.000 | Background 1.000,1.000 | Smooth 0.150 | Smooth 0.150 | Import

71-2396 (A) - Aragonite - $CaCO_3$ - Y: 35.42 % - d x by: 1. - WL: 1.54056 - Orthorhombic - a 4.96160 - b 7.97050 - c 5.73940 - alpha 90.000 - beta 90.000 - gamma 90.000 - Primitive - Pmcn (62) - 4 - 226

86-2339 (C) - Calcite - $Ca(CO_3)$ - Y: 75.00 % - d x by: 1. - WL: 1.54056 - Hexagonal (Rh) - a 4.98400 - b 4.98400 - c 17.12100 - alpha 90.000 - beta 90.000 - gamma 120.000 - Primitive - R-3c (167) - 6 -

86-2336 (C) - Calcite magnesian - $(Mg.129Ca.871)(CO_3)$ - Y: 20.83 % - d x by: 1. - WL: 1.54056 - Hexagonal (Rh) - a 4.93820 - b 4.93820 - c 16.83200 - alpha 90.000 - beta 90.000 - gamma 120.000 - F

85-1780 (A) - Quartz - SiO_2 - Y: 16.67 % - d x by: 1. - WL: 1.54056 - Hexagonal - a 4.89000 - b 4.89000 - c 5.49000 - alpha 90.000 - beta 90.000 - gamma 120.000 - Primitive - P3221 (154) - 3 - 113.690

85-0462 (A) - Quartz low - SiO_2 - Y: 4.17 % - d x by: 1. - WL: 1.54056 - Hexagonal - a 4.68400 - b 4.68400 - c 5.25200 - alpha 90.000 - beta 90.000 - gamma 120.000 - Primitive - P3221 (154) - 3 - 99.79

Sample: CH-67-4; < 4-phi

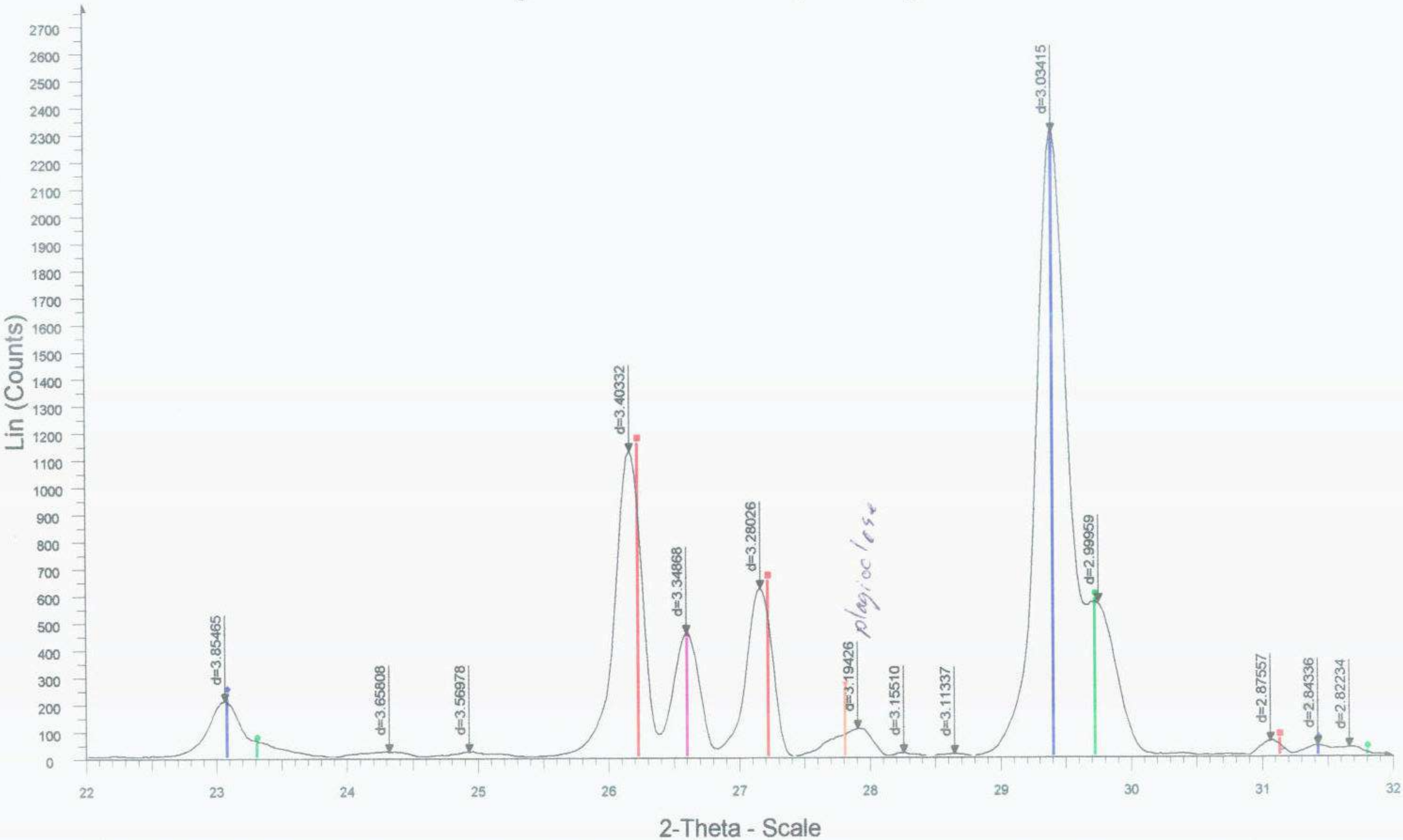

Sample: CH-67-4; < 4-phi - File: Clark-Sherman-26-5-09-CH-67-4.RAW - Type: 2Th/Th locked - Start: 22.000 ° - End: 32.000 ° - Step: 0.020 ° - Step time: 1. s - Temp.: 25 °C (Room) - Time Started: 16 s
Operations: Background 1.000,1.000 | Background 1.000,1.000 | Smooth 0.150 | Import
24-0025 (D) - Aragonite - CaCO3 - Y: 50.00 % - d x by: 1. - WL: 1.54056 - Orthorhombic - a 5.74000 - b 4.96100 - c 2.92900 - alpha 90.000 - beta 90.000 - gamma 90.000 - Primitive - Pnma (62) - 4 - 83.
86-2334 (A) - Calcite - Ca(CO3) - Y: 100.00 % - d x by: 1. - WL: 1.54056 - Hexagonal (Rh) - a 4.98800 - b 4.98800 - c 17.06100 - alpha 90.000 - beta 90.000 - gamma 120.000 - Primitive - R-3c (167) - 6
71-1663 (C) - Calcite, magnesian - Mg0.1Ca0.9CO3 - Y: 25.00 % - d x by: 1. - WL: 1.54056 - Hexagonal (Rh) - a 4.94100 - b 4.94100 - c 16.86400 - alpha 90.000 - beta 90.000 - gamma 120.000 - Primit
89-1961 (C) - Quartz low, dauphinee-twinned - SiO2 - Y: 18.75 % - d x by: 1. - WL: 1.54056 - Hexagonal - a 4.92100 - b 4.92100 - c 5.41600 - alpha 90.000 - beta 90.000 - gamma 120.000 - Primitive - P
83-0541 (A) - Quartz - SiO2 - Y: 10.42 % - d x by: 1. - WL: 1.54056 - Hexagonal - a 4.67640 - b 4.67640 - c 5.24750 - alpha 90.000 - beta 90.000 - gamma 120.000 - Primitive - P3121 (152) - 3 - 99.3817

Sample: CH-400-1-G

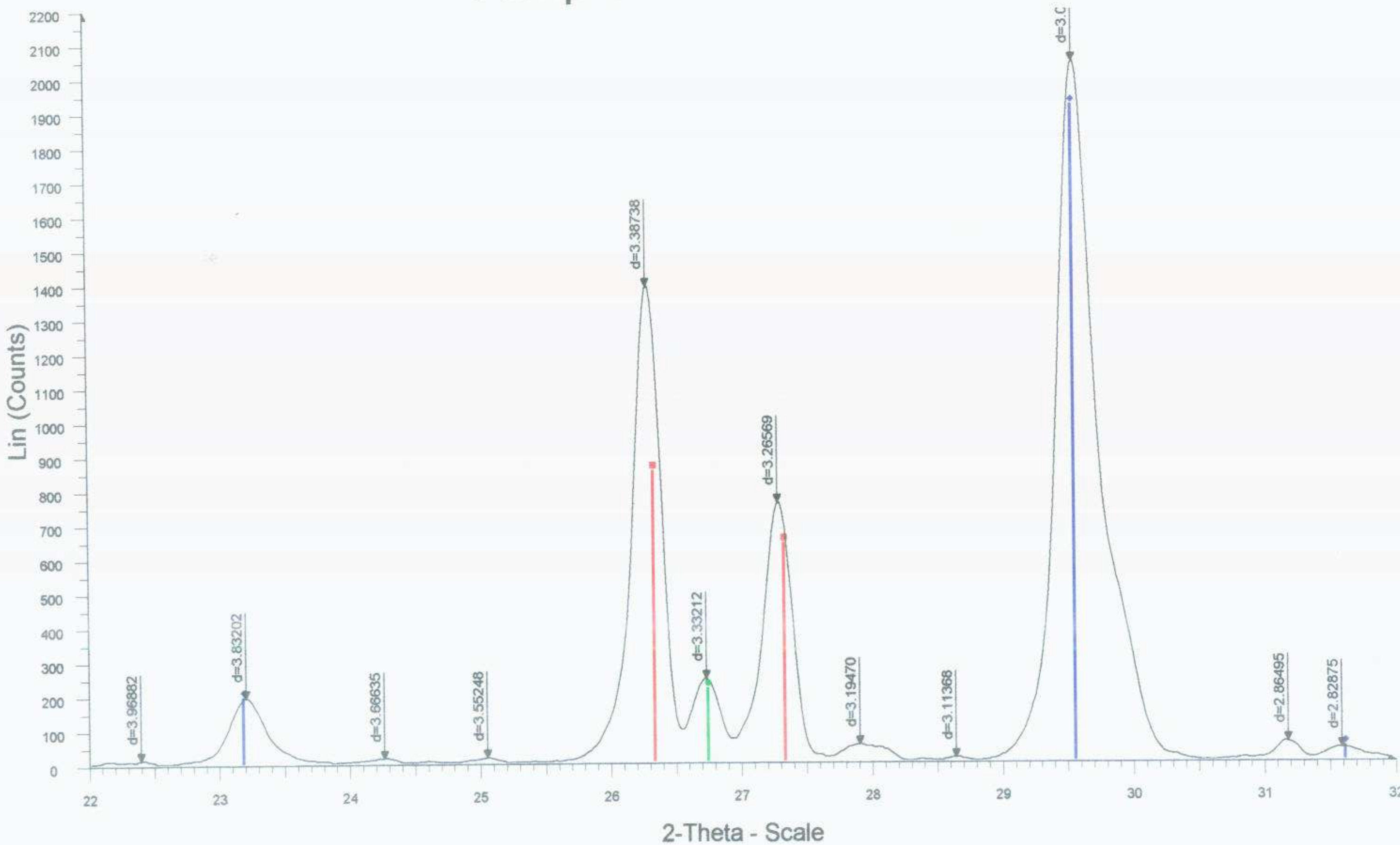

Sample: CH-400-1-G - File: Clark-Sherman-26-5-09-CH-400-1-G.RAW - Type: 2Th/Th locked - Start: 22.000 ° - End: 32.000 ° - Step: 0.020 ° - Step time: 1. s - Temp.: 25 °C (Room) - Time Started: 28 s -
Operations: Background 1.000,1.000 | Background 1.000,1.000 | Smooth 0.150 | Import
03-1067 (D) - Aragonite - gamma-CaCO3 - Y: 52.08 % - d x by: 1. - WL: 1.54056 - Orthorhombic - a 4.94000 - b 7.94000 - c 5.72000 - alpha 90.000 - beta 90.000 - gamma 90.000 - Primitive - Pnma (62)
86-2335 (C) - Calcite magnesian - (Mg.064Ca.936)(CO3) - Y: 93.75 % - d x by: 1. - WL: 1.54056 - Hexagonal (Rh) - a 4.96730 - b 4.96730 - c 16.96310 - alpha 90.000 - beta 90.000 - gamma 120.000 - F
82-0511 (A) - Quartz - SiO2 - Y: 10.42 % - d x by: 1. - WL: 1.54056 - Hexagonal - a 4.86500 - b 4.86500 - c 5.44300 - alpha 90.000 - beta 90.000 - gamma 120.000 - Primitive - P3121 (152) - 3 - 111.567

Sample: CH-400-1; < 4-phi

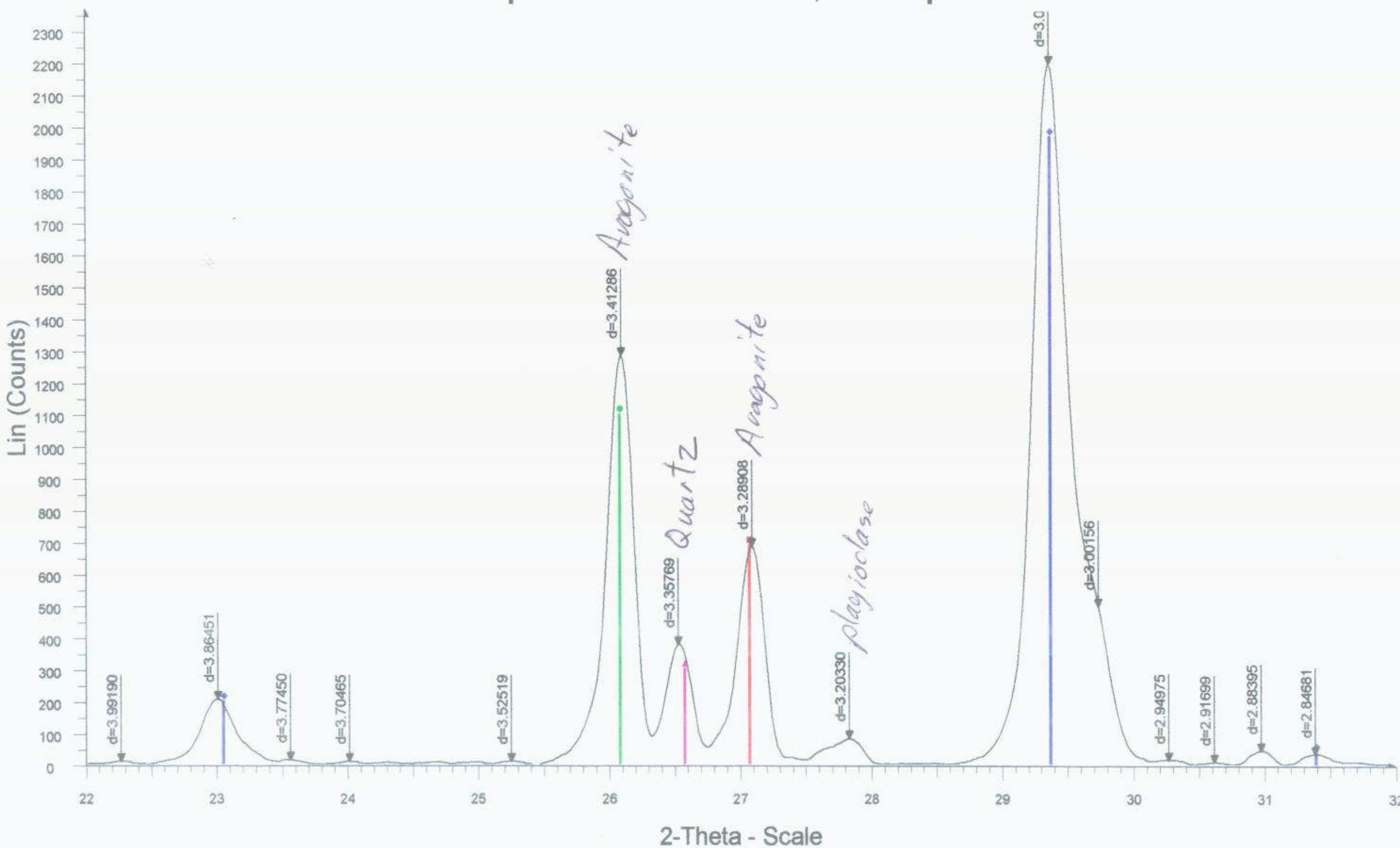

Sample: CH-400-1; < 4-phi - File: Clark-Sherman-26-5-09-CH-400-1.RAW - Type: 2Th/Th locked - Start: 22.000 ° - End: 32.000 ° - Step: 0.020 ° - Step time: 1. s - Temp.: 25 °C (Room) - Time Started: 1€

Operations: Background 1.000,1.000 | Background 1.000,1.000 | Smooth 0.150 | Import

78-1259 (C) - Quartz alpha, syn - SiO_2 - Y: 31.25 % - d x by: 1. - WL: 1.54056 - Hexagonal - a 4.83180 - b 4.83180 - c 5.33370 - alpha 90.000 - beta 90.000 - gamma 120.000 - Primitive - P3121 (152) - :

72-1937 (C) - Calcite - $CaCO_3$ - Y: 89.58 % - d x by: 1. - WL: 1.54056 - Hexagonal (Rh) - a 4.99400 - b 4.99400 - c 17.08100 - alpha 90.000 - beta 90.000 - gamma 120.000 - Primitive - R-3c (167) - 6 - 3

07-0346 (D) - Quartz - beta-SiO_2 - Y: 50.00 % - d x by: 1. - WL: 1.54056 - Hexagonal - a 5.11000 - b 5.11000 - c 5.37000 - alpha 90.000 - beta 90.000 - gamma 120.000 - 121.436 -

81-0065 (C) - Quartz - SiO_2 - Y: 13.67 % - d x by: 1. - WL: 1.54056 - Hexagonal - a 4.88610 - b 4.88610 - c 5.49440 - alpha 90.000 - beta 90.000 - gamma 120.000 - Primitive - P3121 (152) - 3 - 113.599

Sample: CH-400-2-G

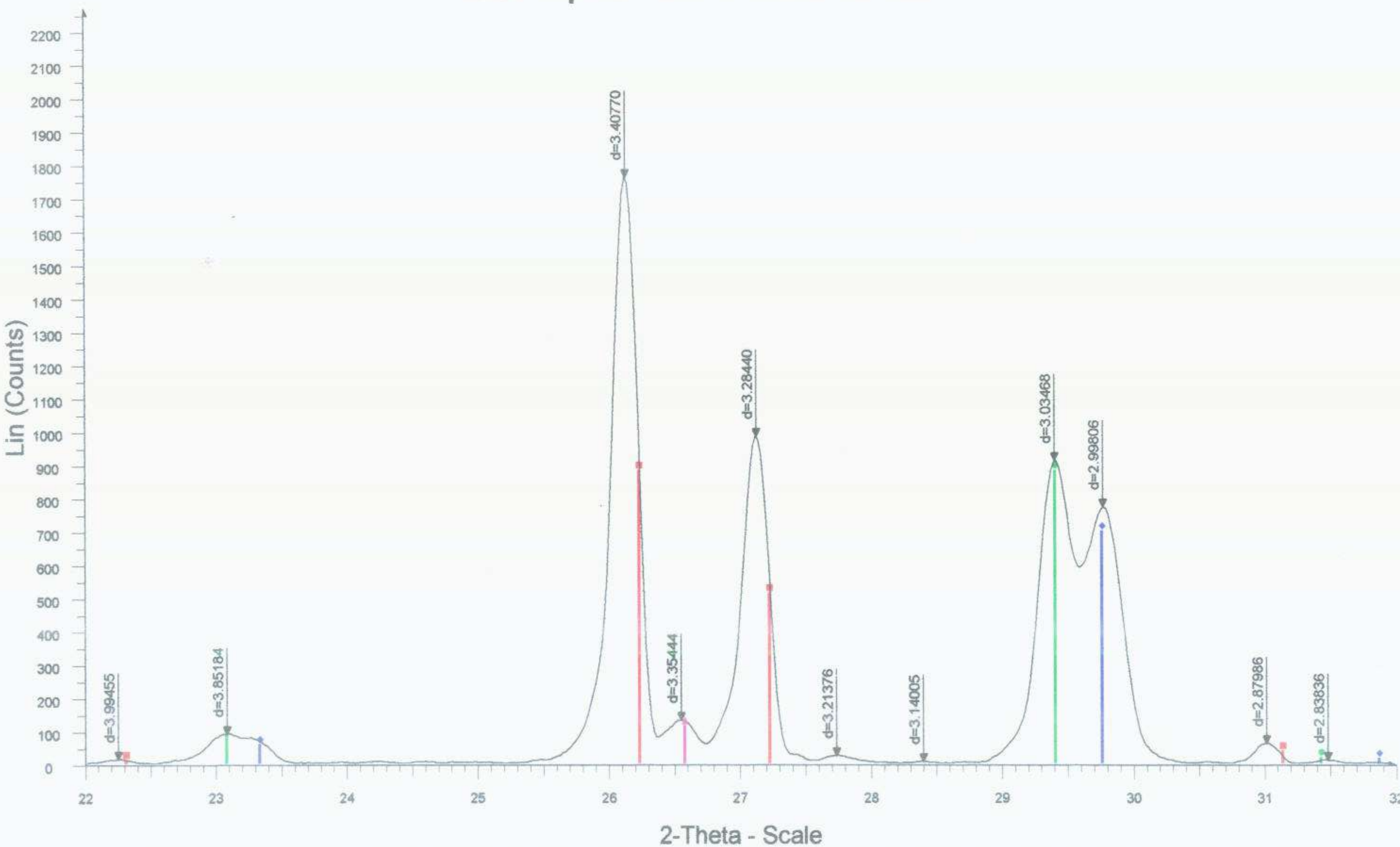

Sample: CH-400-2-G - File: Clark-Sherman-26-5-09-CH-400-2-G.RAW - Type: 2Th/Th locked - Start: 22.000 ° - End: 32.000 ° - Step: 0.020 ° - Step time: 1. s - Temp.: 25 °C (Room) - Time Started: 16 s -
Operations: Background 1.000,1.000 | Background 1.000,1.000 | Smooth 0.150 | Import
71-2396 (A) - Aragonite - CaCO3 - Y: 50.00 % - d x by: 1. - WL: 1.54056 - Orthorhombic - a 4.96160 - b 7.97050 - c 5.73940 - alpha 90.000 - beta 90.000 - gamma 90.000 - Primitive - Pmcn (62) - 4 - 226
86-2336 (C) - Calcite magnesian-- (Mg.129Ca.871)(CO3) - Y: 39.58 % - d x by: 1. - WL: 1.54056 - Hexagonal (Rh) - a 4.93820 - b 4.93820 - c 16.83200 - alpha 90.000 - beta 90.000 - gamma 120.000 - F
86-2334 (A) - Calcite - Ca(CO3) - Y: 50.00 % - d x by: 1. - WL: 1.54056 - Hexagonal (Rh) - a 4.98800 - b 4.98800 - c 17.06100 - alpha 90.000 - beta 90.000 - gamma 120.000 - Primitive - R-3c (167) - 6 -
81-0065 (C) - Quartz - SiO2 - Y: 6.25 % - d x by: 1. - WL: 1.54056 - Hexagonal - a 4.88610 - b 4.88610 - c 5.49440 - alpha 90.000 - beta 90.000 - gamma 120.000 - Primitive - P3121 (152) - 3 - 113.599 -

Sample: CH-400-2; < 4-phi

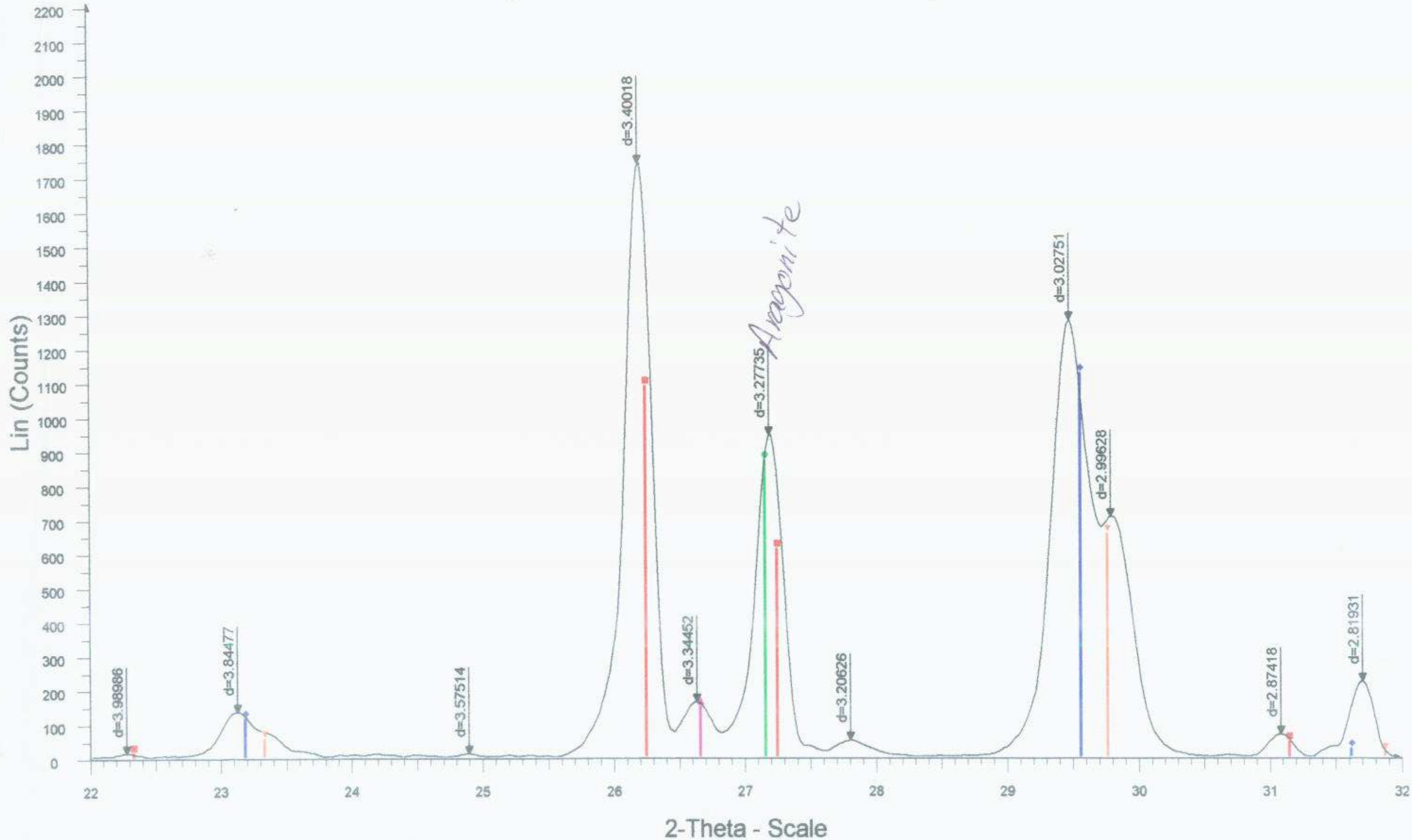

Sample: CH-400-2; < 4-phi - File: Clark-Sherman-26-5-09-CH-400-2.RAW - Type: 2Th/Th locked - Start: 22.000 ° - End: 32.000 ° - Step: 0.020 ° - Step time: 1. s - Temp.: 25 °C (Room) - Time Started: 16

Operations: Background 1.000,1.000 | Background 1.000,1.000 | Smooth 0.150 | Import

76-0606 (A) - Aragonite - Ca(CO3) - Y: 62.50 % - d x by: 1. - WL: 1.54056 - Orthorhombic - a 4.95980 - b 7.96410 - c 5.73790 - alpha 90.000 - beta 90.000 - gamma 90.000 - Primitive - Pmcn (62) - 4 - 22

86-2335 (C) - Calcite magnesian - (Mg.064Ca.936)(CO3) - Y: 64.58 % - d x by: 1. - WL: 1.54056 - Hexagonal (Rh) - a 4.96730 - b 4.96730 - c 16.96310 - alpha 90.000 - beta 90.000 - gamma 120.000 - F

79-1911 (A) - Quartz - SiO2 - Y: 50.00 % - d x by: 1. - WL: 1.54056 - Hexagonal - a 4.81200 - b 4.81200 - c 5.32700 - alpha 90.000 - beta 90.000 - gamma 120.000 - Primitive - P3121 (152) - 3 - 106.823

78-2315 (C) - Quartz - SiO2 - Y: 8.33 % - d x by: 1. - WL: 1.54056 - Hexagonal - a 4.91239 - b 4.91239 - c 5.40385 - alpha 90.000 - beta 90.000 - gamma 120.000 - Primitive - P3221 (154) - 3 - 112.933 -

86-2336 (C) - Calcite magnesian - (Mg.129Ca.871)(CO3) - Y: 37.50 % - d x by: 1. - WL: 1.54056 - Hexagonal (Rh) - a 4.93820 - b 4.93820 - c 16.83200 - alpha 90.000 - beta 90.000 - gamma 120.000 - F

Sample: LCS-1; < 4-phi

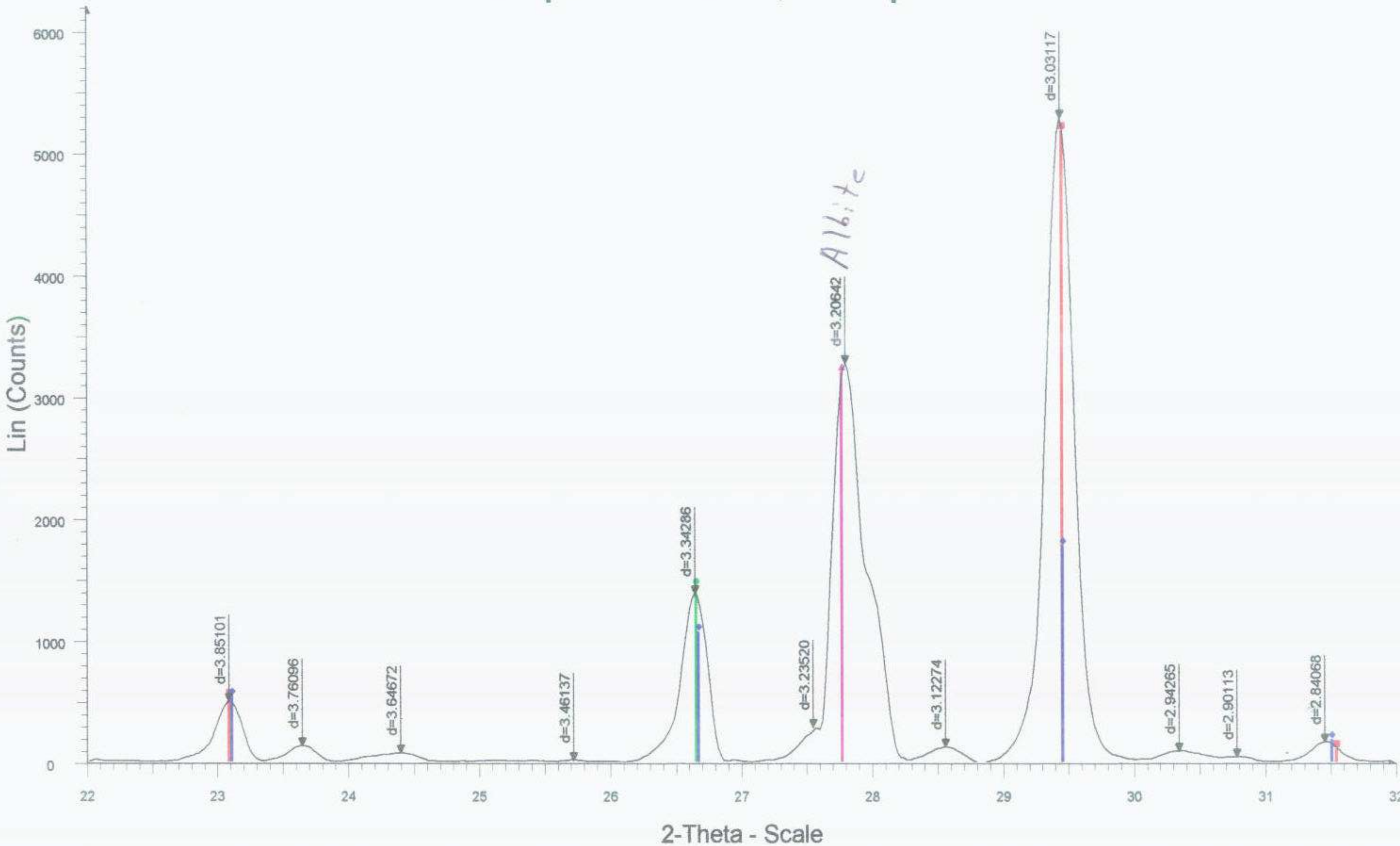

Sample: LCS-1; < 4-phi - File: Clark-Sherman-26-5-09-LCS-1.RAW - Type: 2Th/Th locked - Start: 22.000 ° - End: 32.000 ° - Step: 0.020 ° - Step time: 1. s - Temp.: 25 °C (Room) - Time Started: 16 s - 2-1
Operations: Background 1.000,1.000 | Background 1.000,1.000 | Smooth 0.150 | Import
72-1652 (A) - Calcite - $CaCO_3$ - Y: 97.92 % - d x by: 1. - WL: 1.54056 - Hexagonal (Rh) - a 4.99000 - b 4.99000 - c 17.00200 - alpha 90.000 - beta 90.000 - gamma 120.000 - Primitive - R-3c (167) - 6 - 3
03-0596 (D) - Calcite - beta-$CaCO_3$ - Y: 33.33 % - d x by: 1. - WL: 1.54056 - Hexagonal (Rh) - a 4.98300 - b 4.98300 - c 17.02000 - alpha 90.000 - beta 90.000 - gamma 120.000 - Primitive - R-3c (167) -
87-2096 (A) - Quartz - SiO_2 - Y: 27.08 % - d x by: 1. - WL: 1.54056 - Hexagonal - a 4.91270 - b 4.91270 - c 5.40450 - alpha 90.000 - beta 90.000 - gamma 120.000 - Primitive - P3221 (154) - 3 - 112.961
85-0462 (A) - Quartz low - SiO_2 - Y: 60.42 % - d x by: 1. - WL: 1.54056 - Hexagonal - a 4.68400 - b 4.68400 - c 5.25200 - alpha 90.000 - beta 90.000 - gamma 120.000 - Primitive - P3221 (154) - 3 - 99.7

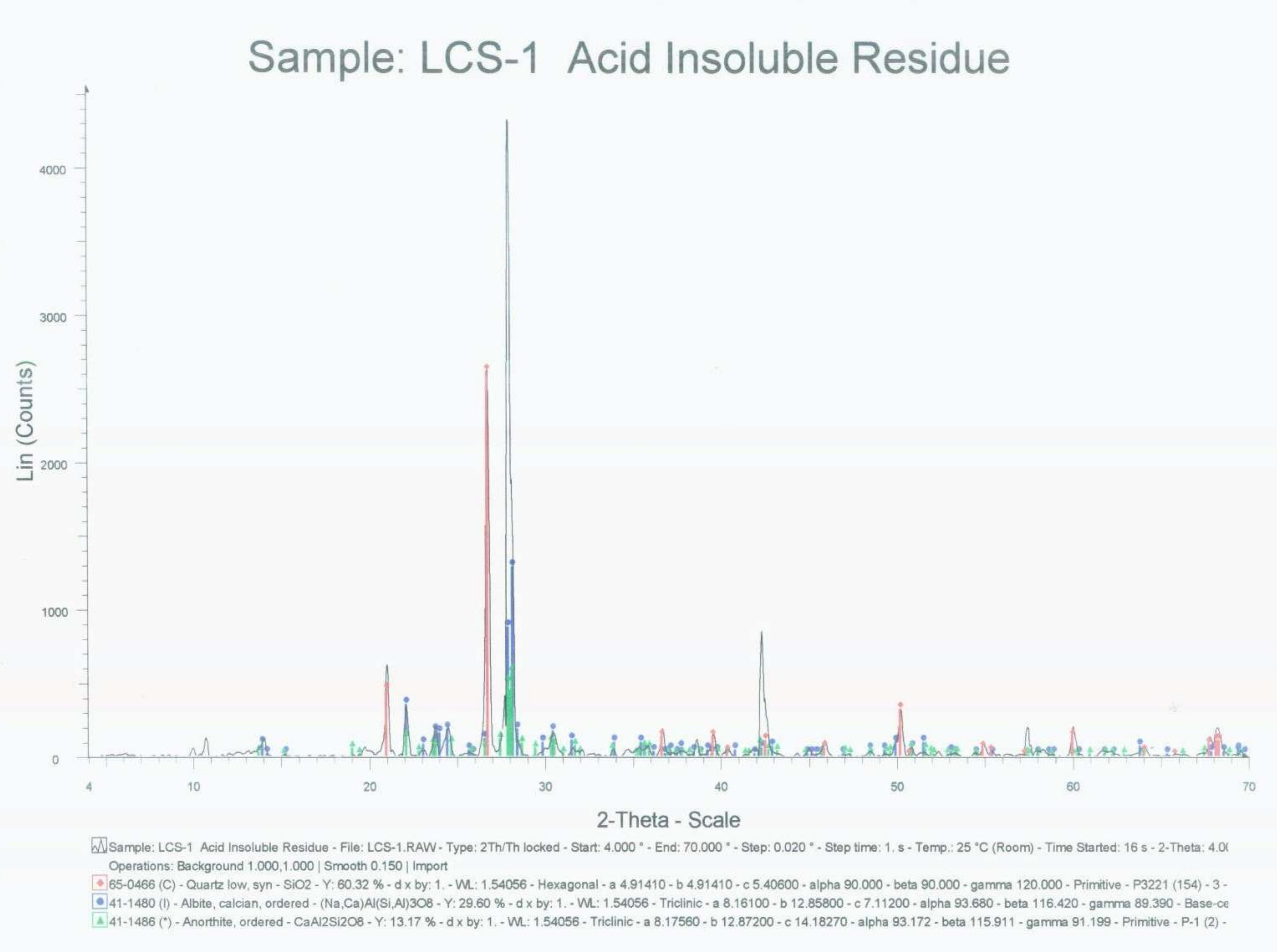
Sample: LCS-1 Acid Insoluble Residue
Lin (Counts)
4000
3000
2000
1000
0
4
10
20
30
40
50
60
70
2-Theta - Scale
Sample: LCS-1 Acid Insoluble Residue - File: LCS-1.RAW - Type: 2Th/Th locked - Start: 4.000 ° - End: 70.000 ° - Step: 0.020 ° - Step time: 1. s - Temp.: 25 °C (Room) - Time Started: 16 s - 2-Theta: 4.0
Operations: Background 1.000,1.000 | Smooth 0.150 | Import
65-0466 (C) - Quartz low, syn - SiO2 - Y: 60.32 % - d x by: 1. - WL: 1.54056 - Hexagonal - a 4.91410 - b 4.91410 - c 5.40600 - alpha 90.000 - beta 90.000 - gamma 120.000 - Primitive - P3221 (154) - 3 -
41-1480 (I) - Albite, calcian, ordered - (Na,Ca)Al(Si,Al)3O8 - Y: 29.60 % - d x by: 1. - WL: 1.54056 - Triclinic - a 8.16100 - b 12.85800 - c 7.11200 - alpha 93.680 - beta 116.420 - gamma 89.390 - Base-ce
41-1486 (*) - Anorthite, ordered - CaAl2Si2O8 - Y: 13.17 % - d x by: 1. - WL: 1.54056 - Triclinic - a 8.17560 - b 12.87200 - c 14.18270 - alpha 93.172 - beta 115.911 - gamma 91.199 - Primitive - P-1 (2) -

Sample: LCS-1-G

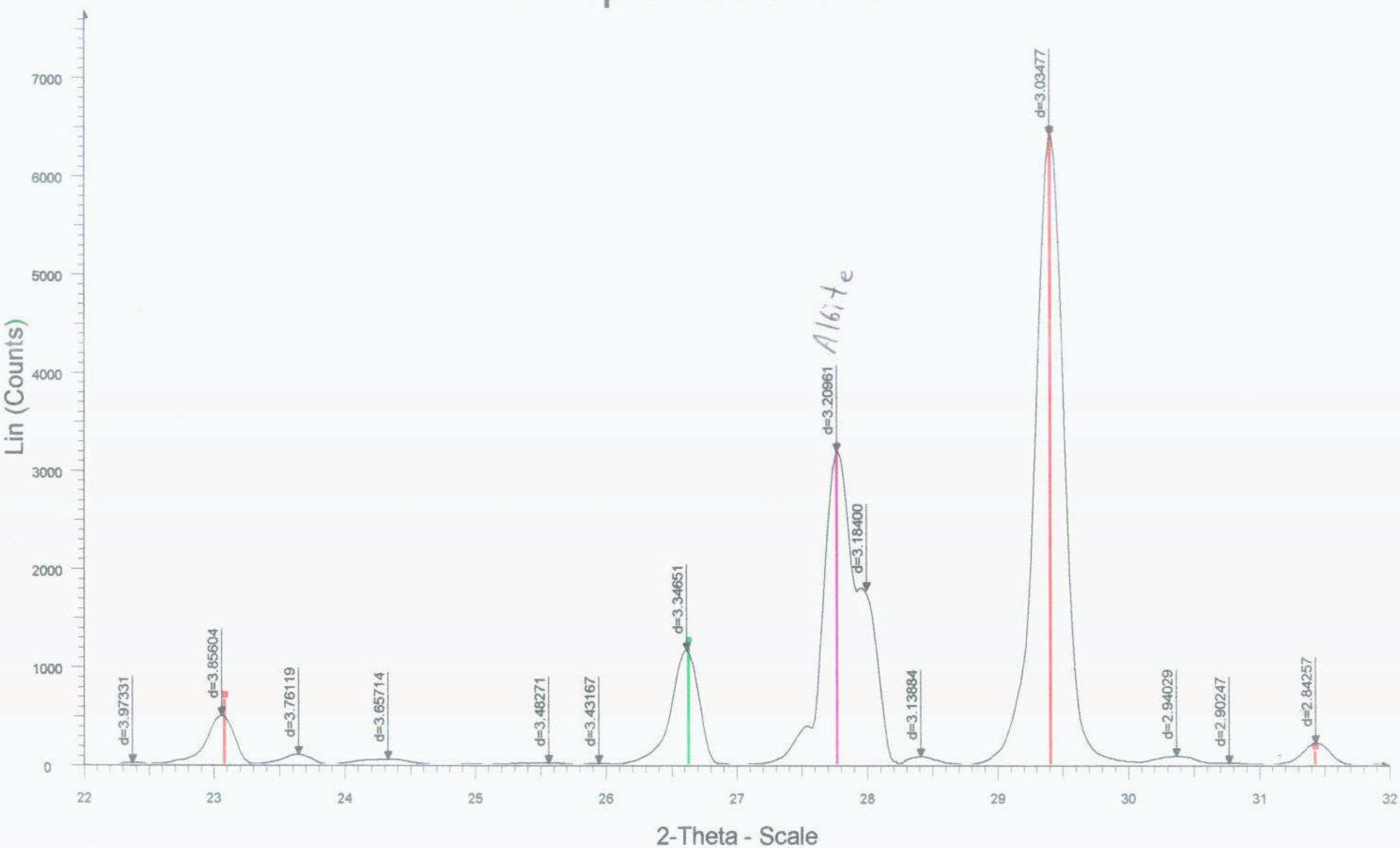

Sample: LCS-1-G - File: Clark-Sherman-26-5-09-LCS-1-G.RAW - Type: 2Th/Th locked - Start: 22.000 ° - End: 32.000 ° - Step: 0.020 ° - Step time: 1. s - Temp.: 25 °C (Room) - Time Started: 16 s - 2-The

Operations: Background 1.000,1.000 | Smooth 0.150 | Import

86-2334 (A) - Calcite - $Ca(CO_3)$ - Y: 100.00 % - d x by: 1. - WL: 1.54056 - Hexagonal (Rh) - a 4.98800 - b 4.98800 - c 17.06100 - alpha 90.000 - beta 90.000 - gamma 120.000 - Primitive - R-3c (167) - 6

88-2487 (C) - Quartz low - SiO_2 - Y: 18.75 % - d x by: 1. - WL: 1.54056 - Hexagonal - a 4.93000 - b 4.93000 - c 5.38500 - alpha 90.000 - beta 90.000 - gamma 120.000 - Primitive - P3221 (154) - 3 - 113.

85-0462 (A) - Quartz low - SiO_2 - Y: 50.00 % - d x by: 1. - WL: 1.54056 - Hexagonal - a 4.68400 - b 4.68400 - c 5.25200 - alpha 90.000 - beta 90.000 - gamma 120.000 - Primitive - P3221 (154) - 3 - 99.7

Sample: LCS-2; < 4-phi

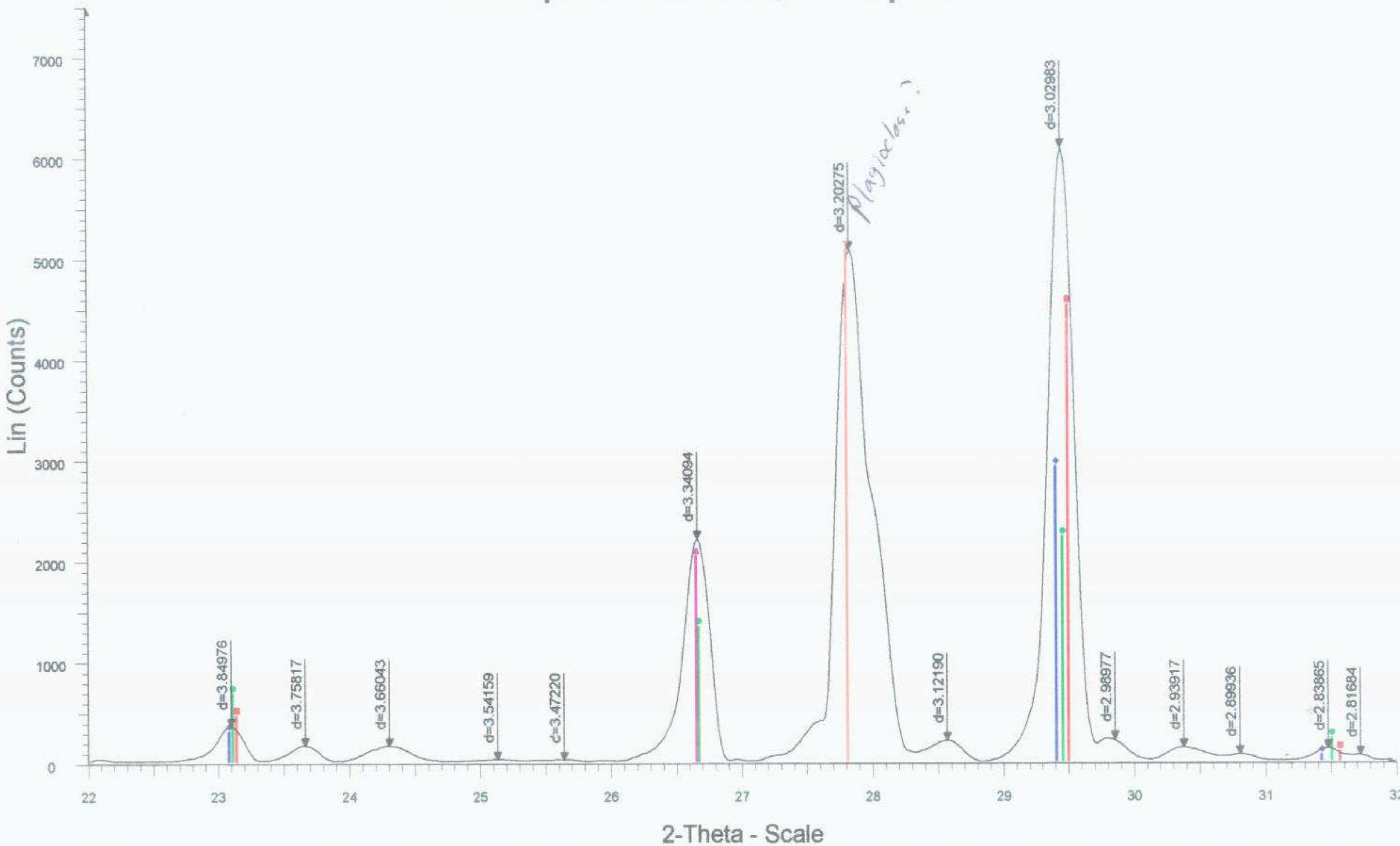

Sample: LCS-2; < 4-phi - File: Clark-Sherman-26-5-09-LCS-2.RAW - Type: 2Th/Th locked - Start: 22.000 ° - End: 32.000 ° - Step: 0.020 ° - Step time: 1. s - Temp.: 25 °C (Room) - Time Started: 16 s - 2-1
Operations: Background 1.000,1.000 | Background 1.000,1.000 | Background 1.000,1.000 | Smooth 0.150 | Import
89-1304 (C) - Magnesium calcite, syn - (Mg0.03Ca0.97)(CO3) - Y: 74.22 % - d x by: 1. - WL: 1.54056 - Hexagonal (Rh) - a 4.97800 - b 4.97800 - c 16.98800 - alpha 90.000 - beta 90.000 - gamma 120.0(
86-2334 (A) - Calcite - Ca(CO3) - Y: 47.92 % - d x by: 1. - WL: 1.54056 - Hexagonal (Rh) - a 4.98800 - b 4.98800 - c 17.06100 - alpha 90.000 - beta 90.000 - gamma 120.000 - Primitive - R-3c (167) - 6 -
03-0596 (D) - Calcite - beta-CaCO3 - Y: 36.46 % - d x by: 1. - WL: 1.54056 - Hexagonal (Rh) - a 4.98300 - b 4.98300 - c 17.02000 - alpha 90.000 - beta 90.000 - gamma 120.000 - Primitive - R-3c (167) -
85-0504 (A) - Quartz - SiO2 - Y: 33.33 % - d x by: 1. - WL: 1.54056 - Hexagonal - a 4.91280 - b 4.91280 - c 5.40420 - alpha 90.000 - beta 90.000 - gamma 120.000 - Primitive - P3221 (154) - 3 - 112.959
83-0541 (A) - Quartz - SiO2 - Y: 83.33 % - d x by: 1. - WL: 1.54056 - Hexagonal - a 4.67640 - b 4.67640 - c 5.24750 - alpha 90.000 - beta 90.000 - gamma 120.000 - Primitive - P3121 (152) - 3 - 99.3817

Sample: LCS-2 Acid Insoluble Residue

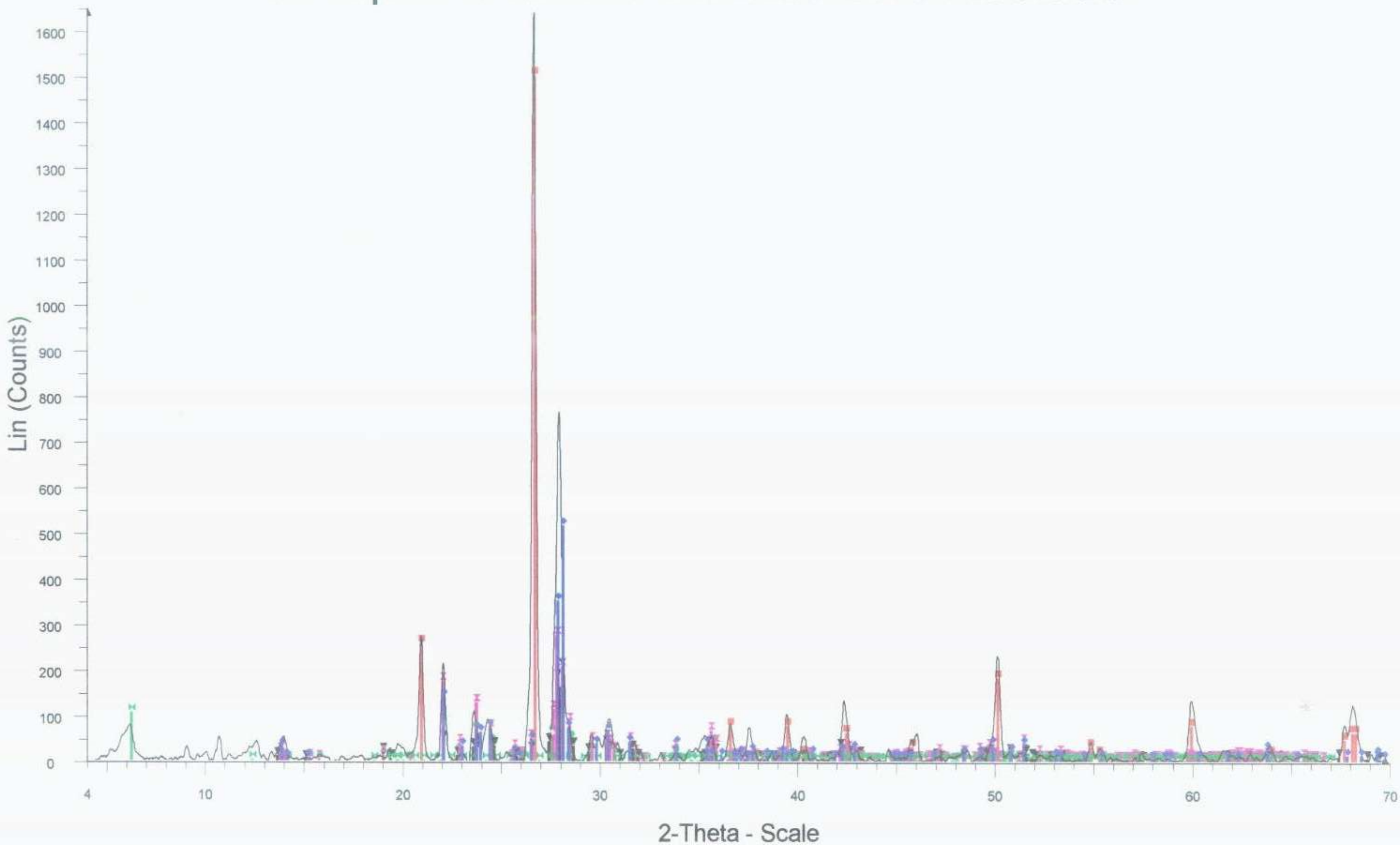

Sample: LCS-2 Acid Insoluble Residue - File: LCS-2.RAW - Type: 2Th/Th locked - Start: 4.000 ° - End: 70.000 ° - Step: 0.020 ° - Step time: 1. s - Temp.: 25 °C (Room) - Time Started: 16 s - 2-Theta: 4.0(

Operations: Smooth 0.150 | Background 1.000,1.000 | Import

65-0466 (C) - Quartz low, syn - SiO2 - Y: 91.40 % - d x by: 1. - WL: 1.54056 - Hexagonal - a 4.91410 - b 4.91410 - c 5.40600 - alpha 90.000 - beta 90.000 - gamma 120.000 - Primitive - P3221 (154) - 3 -

41-1480 (I) - Albite, calcian, ordered - (Na,Ca)Al(Si,Al)3O8 - Y: 31.25 % - d x by: 1. - WL: 1.54056 - Triclinic - a 8.16100 - b 12.85800 - c 7.11200 - alpha 93.680 - beta 116.420 - gamma 89.390 - Base-ce

83-1368 (C) - Labradorite - Ca0.65Na0.32(Al1.62Si2.38O8) - Y: 8.33 % - d x by: 1. - WL: 1.54056 - Triclinic - a 8.17360 - b 12.87360 - c 7.10220 - alpha 93.462 - beta 116.054 - gamma 90.475 - Base-ce

41-1486 (*) - Anorthite, ordered - CaAl2Si2O8 - Y: 12.50 % - d x by: 1. - WL: 1.54056 - Triclinic - a 8.17560 - b 12.87200 - c 14.18270 - alpha 93.172 - beta 115.911 - gamma 91.199 - Primitive - P-1 (2) -

79-1149 (C) - Andesine - Na.499Ca.491(Al1.488Si2.506O8) - Y: 16.67 % - d x by: 1. - WL: 1.54056 - Triclinic - a 8.17900 - b 12.88000 - c 7.11200 - alpha 93.440 - beta 116.210 - gamma 90.230 - Base-

74-1732 (C) - Vermiculite 2 ITM RG - Mg3Si4O10(OH)2 - Y: 6.25 % - d x by: 1. - WL: 1.54056 - Monoclinic - a 5.33000 - b 9.18000 - c 28.84999 - alpha 90.000 - beta 93.250 - gamma 90.000 - Base-cent

Sample: LCS-2-G

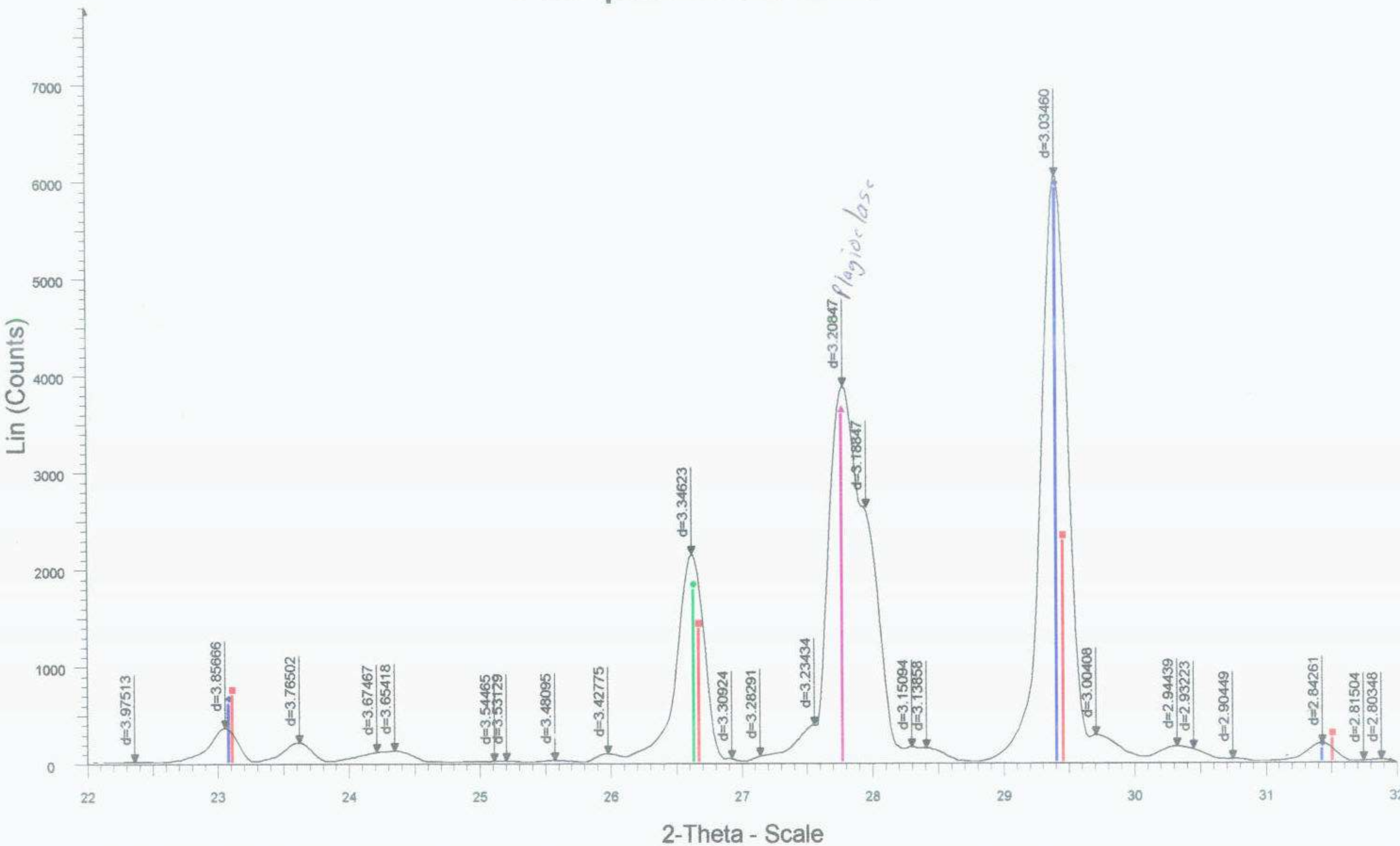

Sample: LCS-2-G - File: Clark-Sherman-26-5-09-LCS-2-G.RAW - Type: 2Th/Th locked - Start: 22.000 ° - End: 32.000 ° - Step: 0.020 ° - Step time: 1. s - Temp.: 25 °C (Room) - Time Started: 16 s - 2-Thet

Operations: Background 1.000,1.000 | Smooth 0.150 | Import

86-2334 (A) - Calcite - Ca(CO3) - Y: 97.92 % - d x by: 1. - WL: 1.54056 - Hexagonal (Rh) - a 4.98800 - b 4.98800 - c 17.06100 - alpha 90.000 - beta 90.000 - gamma 120.000 - Primitive - R-3c (167) - 6 -

03-0596 (D) - Calcite - beta-CaCO3 - Y: 37.50 % - d x by: 1. - WL: 1.54056 - Hexagonal (Rh) - a 4.98300 - b 4.98300 - c 17.02000 - alpha 90.000 - beta 90.000 - gamma 120.000 - Primitive - R-3c (167) -

88-2487 (C) - Quartz low - SiO2 - Y: 29.17 % - d x by: 1. - WL: 1.54056 - Hexagonal - a 4.93000 - b 4.93000 - c 5.38500 - alpha 90.000 - beta 90.000 - gamma 120.000 - Primitive - P3221 (154) - 3 - 113.

85-0462 (A) - Quartz low - SiO2 - Y: 59.20 % - d x by: 1. - WL: 1.54056 - Hexagonal - a 4.68400 - b 4.68400 - c 5.25200 - alpha 90.000 - beta 90.000 - gamma 120.000 - Primitive - P3221 (154) - 3 - 99.7

Sample: LCS-3; < 4-phi

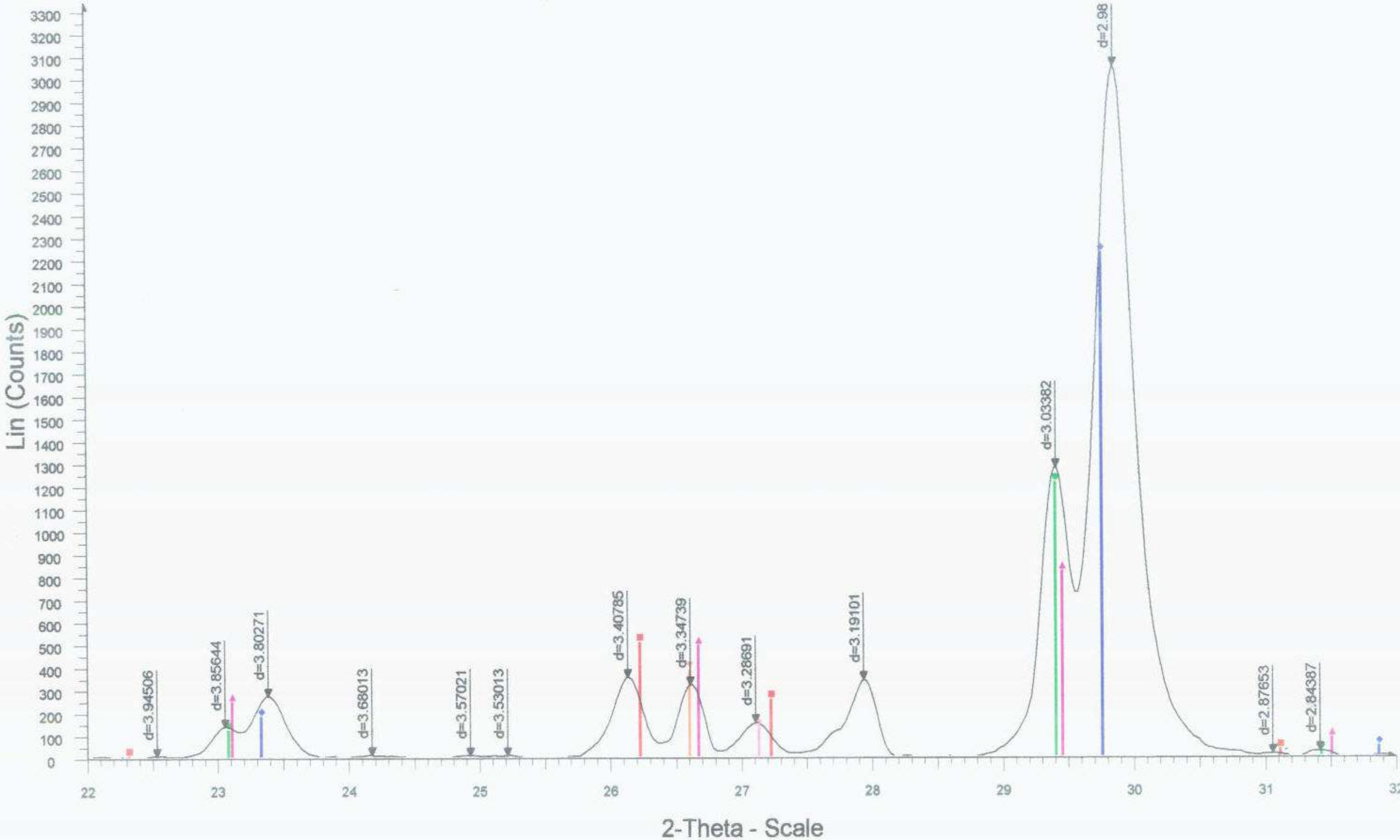

Sample: LCS-3; < 4-phi - File: Clark-Sherman-26-5-09-LCS-3.RAW - Type: 2Th/Th locked - Start: 22.000 ° - End: 32.000 ° - Step: 0.020 ° - Step time: 1. s - Temp.: 25 °C (Room) - Time Started: 16 s - 2-1

Operations: Background 1.000,1.000 | Background 1.000,1.000 | Smooth 0.150 | Import

41-1475 (*) - Aragonite - $CaCO_3$ - Y: 16.50 % - d x by: 1. - WL: 1.54056 - Orthorhombic - a 4.96230 - b 7.96800 - c 5.74390 - alpha 90.000 - beta 90.000 - gamma 90.000 - Primitive - Pmcn (62) - 4 - 227.

86-2336 (C) - Calcite magnesian - $(Mg.129Ca.871)(CO_3)$ - Y: 72.92 % - d x by: 1. - WL: 1.54056 - Hexagonal (Rh) - a 4.93820 - b 4.93820 - c 16.83200 - alpha 90.000 - beta 90.000 - gamma 120.000 - F

86-2334 (A) - Calcite - $Ca(CO_3)$ - Y: 39.58 % - d x by: 1. - WL: 1.54056 - Hexagonal (Rh) - a 4.98800 - b 4.98800 - c 17.06100 - alpha 90.000 - beta 90.000 - gamma 120.000 - Primitive - R-3c (167) - 6 -

03-0596 (D) - Calcite - beta-$CaCO_3$ - Y: 26.74 % - d x by: 1. - WL: 1.54056 - Hexagonal (Rh) - a 4.98300 - b 4.98300 - c 17.02000 - alpha 90.000 - beta 90.000 - gamma 120.000 - Primitive - R-3c (167) -

89-1961 (C) - Quartz low, dauphinee-twinned - SiO_2 - Y: 12.50 % - d x by: 1. - WL: 1.54056 - Hexagonal - a 4.92100 - b 4.92100 - c 5.41600 - alpha 90.000 - beta 90.000 - gamma 120.000 - Primitive - P

83-2472 (A) - Quartz, syn - SiO_2 - Y: 4.17 % - d x by: 1. - WL: 1.54056 - Hexagonal - a 4.81700 - b 4.81700 - c 5.32800 - alpha 90.000 - beta 90.000 - gamma 120.000 - Primitive - P3121 (152) - 3 - 107.(

Sample: LCS-3 Acid Insoluble Residue

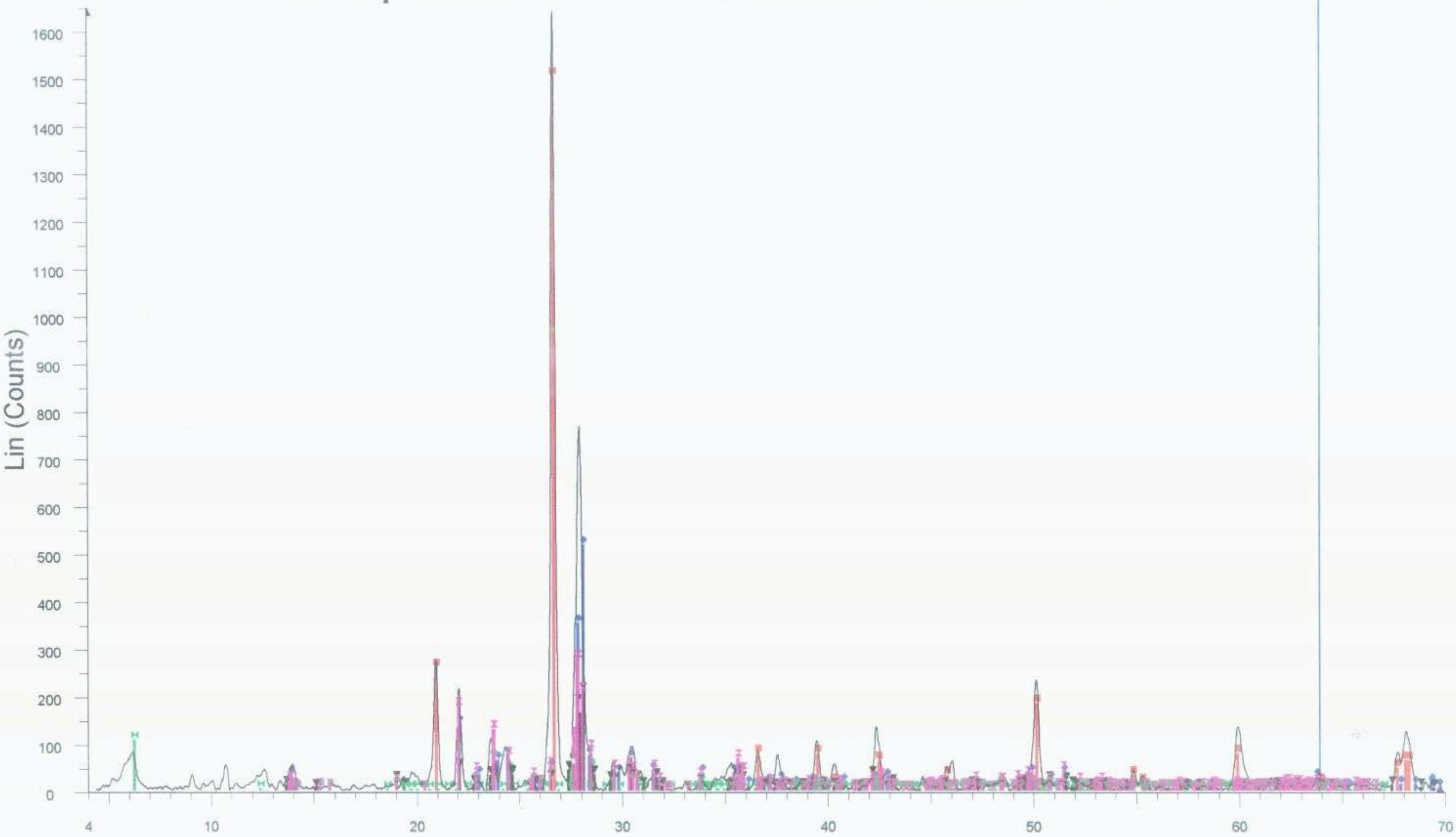

Sample: LCS-2 Acid Insoluble Residue - File: LCS-2.RAW - Type: 2Th/Th locked - Start: 4.000 ° - End: 70.000 ° - Step: 0.020 ° - Step time: 1. s - Temp.: 25 °C (Room) - Time Started: 16 s - 2-Theta: 4.0(

Operations: Smooth 0.150 | Background 1.000,1.000 | Import

65-0466 (C) - Quartz low, syn - SiO2 - Y: 249.41 % - d x by: 1. - WL: 1.54056 - Hexagonal - a 4.91410 - b 4.91410 - c 5.40600 - alpha 90.000 - beta 90.000 - gamma 120.000 - Primitive - P3221 (154) - 3

41-1480 (I) - Albite, calcian, ordered - (Na,Ca)Al(Si,Al)3O8 - Y: 85.27 % - d x by: 1. - WL: 1.54056 - Triclinic - a 8.16100 - b 12.85800 - c 7.11200 - alpha 93.680 - beta 116.420 - gamma 89.390 - Base-ce

83-1368 (C) - Labradorite - Ca0.65Na0.32(Al1.62Si2.38O8) - Y: 22.73 % - d x by: 1. - WL: 1.54056 - Triclinic - a 8.17360 - b 12.87360 - c 7.10220 - alpha 93.462 - beta 116.054 - gamma 90.475 - Base-c

41-1486 (*) - Anorthite, ordered - CaAl2Si2O8 - Y: 34.11 % - d x by: 1. - WL: 1.54056 - Triclinic - a 8.17560 - b 12.87200 - c 14.18270 - alpha 93.172 - beta 115.911 - gamma 91.199 - Primitive - P-1 (2) -

79-1149 (C) - Andesine - Na.499Ca.491(Al1.488Si2.506O8) - Y: 45.49 % - d x by: 1. - WL: 1.54056 - Triclinic - a 8.17900 - b 12.88000 - c 7.11200 - alpha 93.440 - beta 116.210 - gamma 90.230 - Base-

74-1732 (C) - Vermiculite 2 ITM RG - Mg3Si4O10(OH)2 - Y: 17.05 % - d x by: 1. - WL: 1.54056 - Monoclinic - a 5.33000 - b 9.18000 - c 28.84999 - alpha 90.000 - beta 93.250 - gamma 90.000 - Base-cer

Sample: LCS-3-G

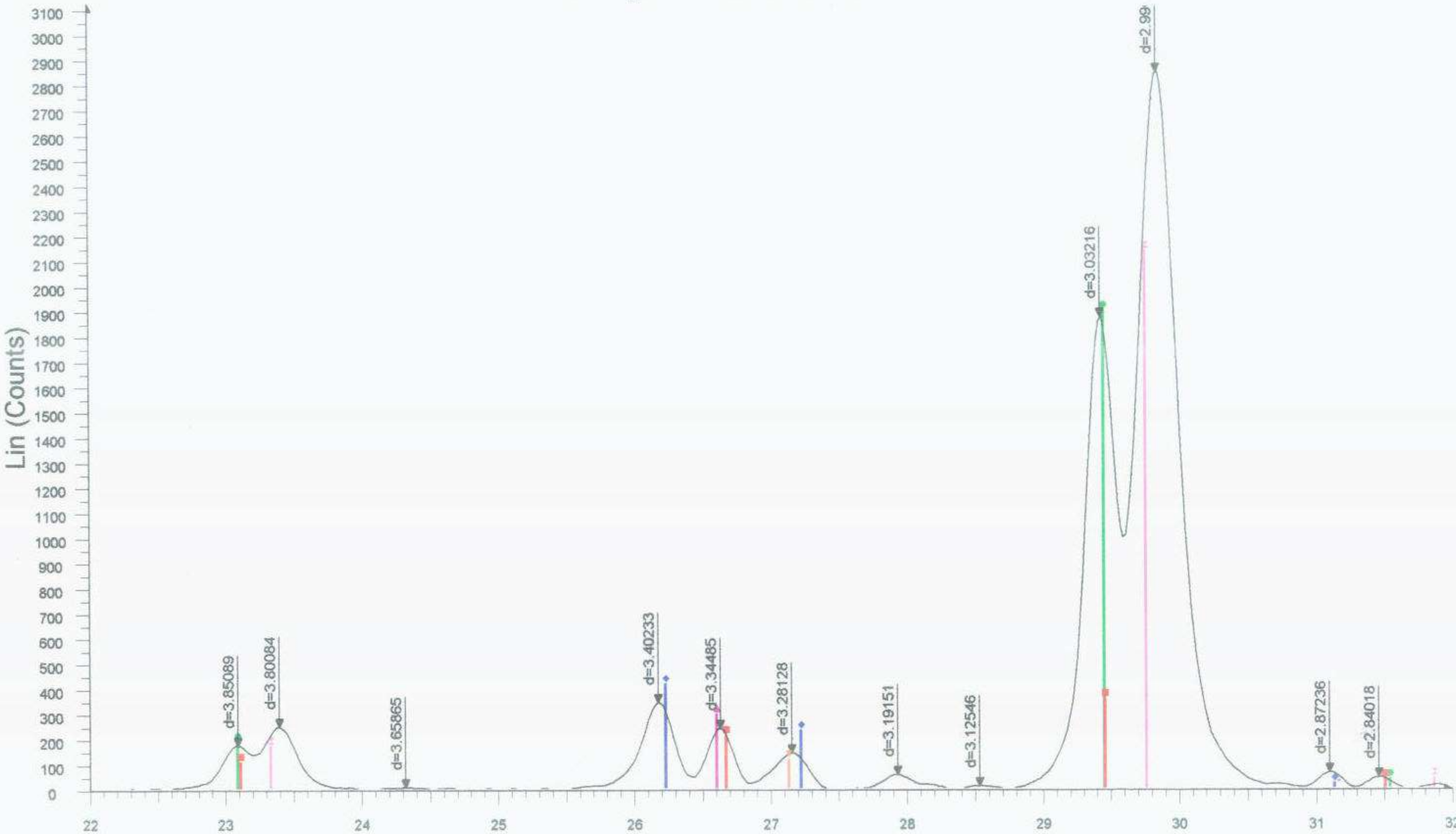

Sample: LCS-3-G - File: Clark-Sherman-26-5-09-LCS-3-G.RAW - Type: 2Th/Th locked - Start: 22.000 ° - End: 32.000 ° - Step: 0.020 ° - Step time: 1. s - Temp.: 25 °C (Room) - Time Started: 16 s - 2-The

Operations: Background 1.000,1.000 | Background 1.000,1.000 | Smooth 0.150 | Import

24-0025 (D) - Aragonite - CaCO3 - Y: 14.58 % - d x by: 1. - WL: 1.54056 - Orthorhombic - a 5.74000 - b 4.96100 - c 2.92900 - alpha 90.000 - beta 90.000 - gamma 90.000 - Primitive - Pnma (62) - 4 - 83.

72-1652 (A) - Calcite - CaCO3 - Y: 66.67 % - d x by: 1. - WL: 1.54056 - Hexagonal (Rh) - a 4.99000 - b 4.99000 - c 17.00200 - alpha 90.000 - beta 90.000 - gamma 120.000 - Primitive - R-3c (167) - 6 - 3

03-0596 (D) - Calcite - beta-CaCO3 - Y: 12.50 % - d x by: 1. - WL: 1.54056 - Hexagonal (Rh) - a 4.98300 - b 4.98300 - c 17.02000 - alpha 90.000 - beta 90.000 - gamma 120.000 - Primitive - R-3c (167) -

89-1961 (C) - Quartz low, dauphinee-twinned - SiO2 - Y: 10.42 % - d x by: 1. - WL: 1.54056 - Hexagonal - a 4.92100 - b 4.92100 - c 5.41600 - alpha 90.000 - beta 90.000 - gamma 120.000 - Primitive - P

83-2472 (A) - Quartz, syn - SiO2 - Y: 4.17 % - d x by: 1. - WL: 1.54056 - Hexagonal - a 4.81700 - b 4.81700 - c 5.32800 - alpha 90.000 - beta 90.000 - gamma 120.000 - Primitive - P3121 (152) - 3 - 107.(

86-2336 (C) - Calcite magnesian - (Mg.129Ca.871)(CO3) - Y: 75.00 % - d x by: 1. - WL: 1.54056 - Hexagonal (Rh) - a 4.93820 - b 4.93820 - c 16.83200 - alpha 90.000 - beta 90.000 - gamma 120.000 - F

Sample: LCS-4; < 4-phi

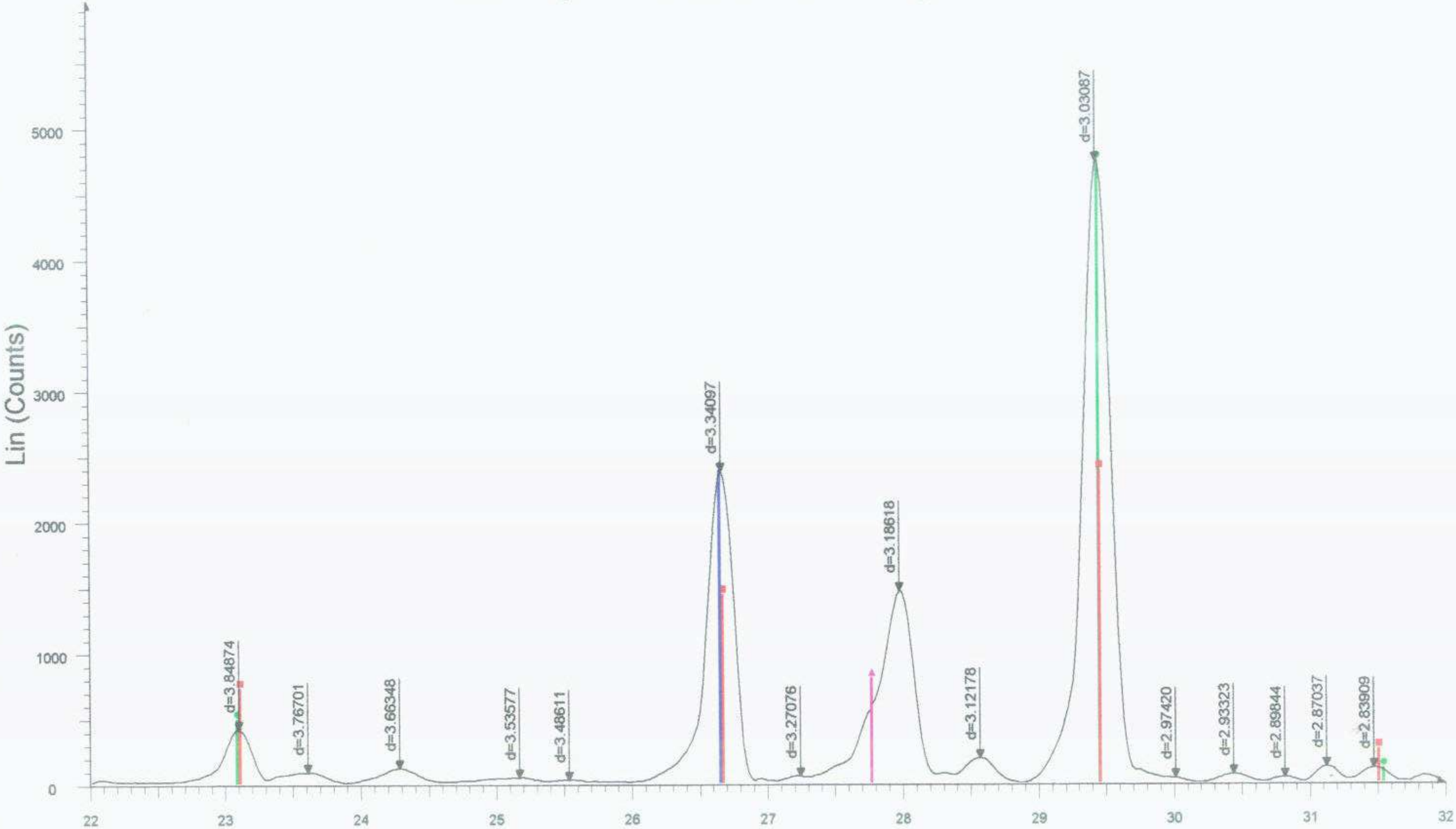

2-Theta - Scale

Sample: LCS-4; < 4-phi - File: Clark-Sherman-26-5-09-LCS-4.RAW - Type: 2Th/Th locked - Start: 22.000 ° - End: 32.000 ° - Step: 0.020 ° - Step time: 1. s - Temp.: 25 °C (Room) - Time Started: 16 s - 2-1

Operations: Background 1.000,1.000 | Background 1.000,1.000 | Smooth 0.150 | Import

72-1652 (A) - Calcite - $CaCO_3$ - Y: 100.00 % - d x by: 1. - WL: 1.54056 - Hexagonal (Rh) - a 4.99000 - b 4.99000 - c 17.00200 - alpha 90.000 - beta 90.000 - gamma 120.000 - Primitive - R-3c (167) - 6 -

03-0596 (D) - Calcite - beta-$CaCO_3$ - Y: 50.00 % - d x by: 1. - WL: 1.54056 - Hexagonal (Rh) - a 4.98300 - b 4.98300 - c 17.02000 - alpha 90.000 - beta 90.000 - gamma 120.000 - Primitive - R-3c (167) -

87-2096 (A) - Quartz - SiO_2 - Y: 50.00 % - d x by: 1. - WL: 1.54056 - Hexagonal - a 4.91270 - b 4.91270 - c 5.40450 - alpha 90.000 - beta 90.000 - gamma 120.000 - Primitive - P3221 (154) - 3 - 112.961

85-0462 (A) - Quartz low - SiO_2 - Y: 16.67 % - d x by: 1. - WL: 1.54056 - Hexagonal - a 4.68400 - b 4.68400 - c 5.25200 - alpha 90.000 - beta 90.000 - gamma 120.000 - Primitive - P3221 (154) - 3 - 99.7

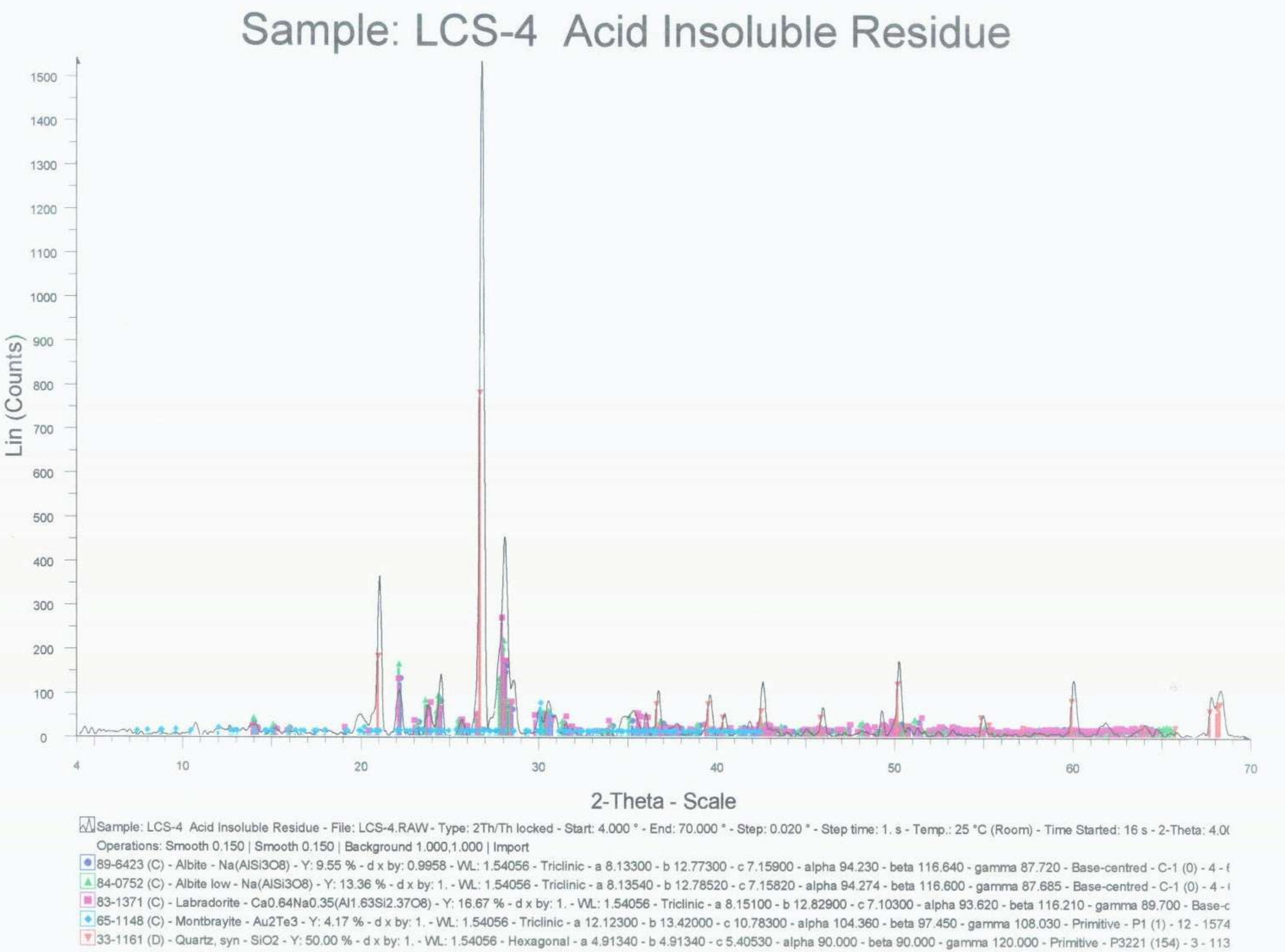
Sample: LCS-4 Acid Insoluble Residue
Lin (Counts)
1500
1400
1300
1200
1100
1000
900
800
700
600
500
400
300
200
100
0
4
10
20
30
40
50
60
70
2-Theta - Scale
Sample: LCS-4 Acid Insoluble Residue - File: LCS-4.RAW - Type: 2Th/Th locked - Start: 4.000 ° - End: 70.000 ° - Step: 0.020 ° - Step time: 1. s - Temp.: 25 °C (Room) - Time Started: 16 s - 2-Theta: 4.0(
Operations: Smooth 0.150 | Smooth 0.150 | Background 1.000,1.000 | Import
89-6423 (C) - Albite - Na(AlSi3O8) - Y: 9.55 % - d x by: 0.9958 - WL: 1.54056 - Triclinic - a 8.13300 - b 12.77300 - c 7.15900 - alpha 94.230 - beta 116.640 - gamma 87.720 - Base-centred - C-1 (0) - 4 -
84-0752 (C) - Albite low - Na(AlSi3O8) - Y: 13.36 % - d x by: 1. - WL: 1.54056 - Triclinic - a 8.13540 - b 12.78520 - c 7.15820 - alpha 94.274 - beta 116.600 - gamma 87.685 - Base-centred - C-1 (0) - 4 -
83-1371 (C) - Labradorite - Ca0.64Na0.35(Al1.63Si2.37O8) - Y: 16.67 % - d x by: 1. - WL: 1.54056 - Triclinic - a 8.15100 - b 12.82900 - c 7.10300 - alpha 93.620 - beta 116.210 - gamma 89.700 - Base-c
65-1148 (C) - Montbrayite - Au2Te3 - Y: 4.17 % - d x by: 1. - WL: 1.54056 - Triclinic - a 12.12300 - b 13.42000 - c 10.78300 - alpha 104.360 - beta 97.450 - gamma 108.030 - Primitive - P1 (1) - 12 - 1574
33-1161 (D) - Quartz, syn - SiO2 - Y: 50.00 % - d x by: 1. - WL: 1.54056 - Hexagonal - a 4.91340 - b 4.91340 - c 5.40530 - alpha 90.000 - beta 90.000 - gamma 120.000 - Primitive - P3221 (154) - 3 - 113

Sample: LCS-4-G

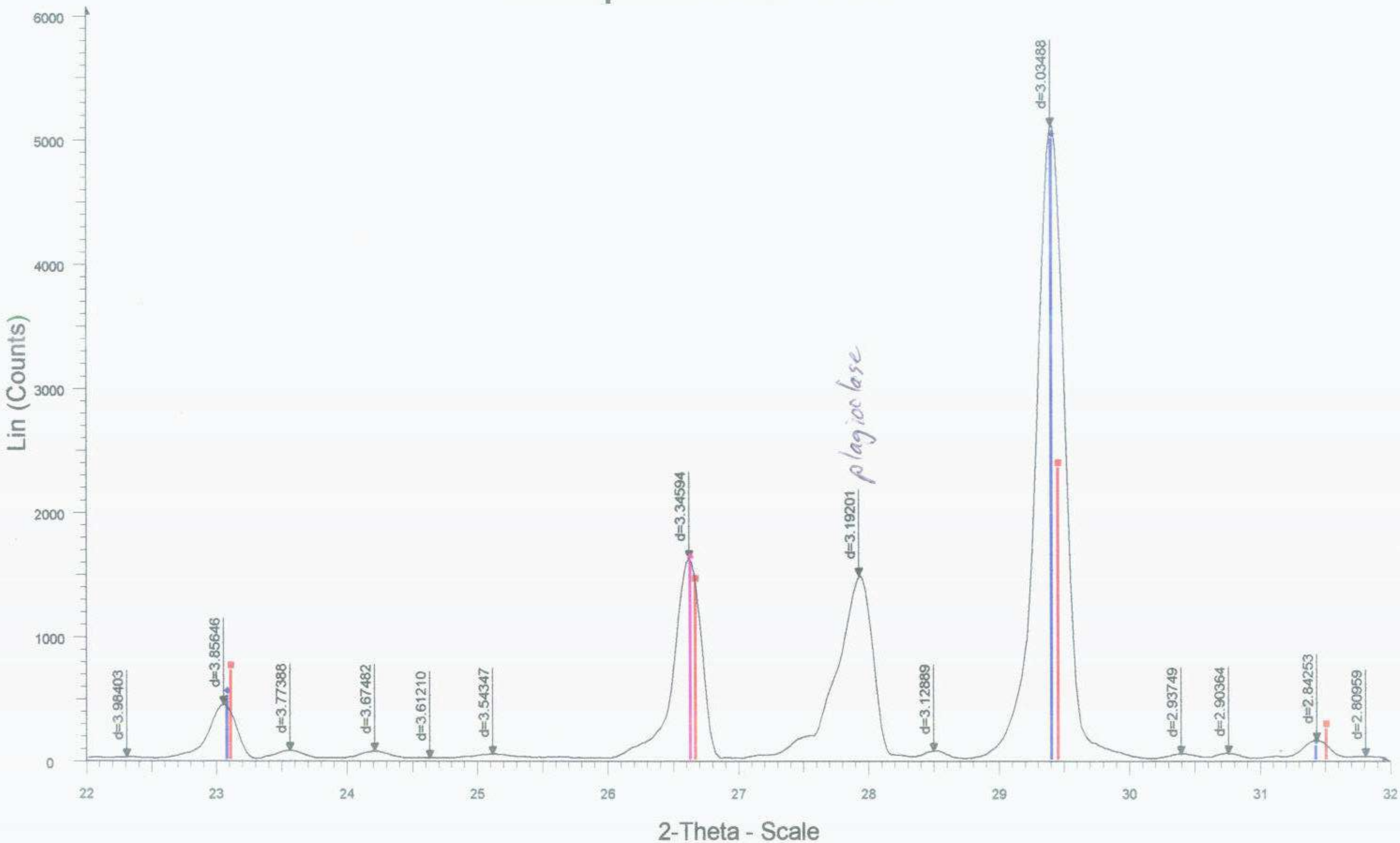

Sample: LCS-4-G - File: Clark-Sherman-26-5-09-LCS-4-G.RAW - Type: 2Th/Th locked - Start: 22.000 ° - End: 32.000 ° - Step: 0.020 ° - Step time: 1. s - Temp.: 25 °C (Room) - Time Started: 16 s - 2-The
Operations: Background 1.000,1.000 | Background 1.000,1.000 | Smooth 0.150 | Import
86-2334 (A) - Calcite - Ca(CO3) - Y: 97.92 % - d x by: 1. - WL: 1.54056 - Hexagonal (Rh) - a 4.98800 - b 4.98800 - c 17.06100 - alpha 90.000 - beta 90.000 - gamma 120.000 - Primitive - R-3c (167) - 6 -
03-0596 (D) - Calcite - beta-CaCO3 - Y: 45.83 % - d x by: 1. - WL: 1.54056 - Hexagonal (Rh) - a 4.98300 - b 4.98300 - c 17.02000 - alpha 90.000 - beta 90.000 - gamma 120.000 - Primitive - R-3c (167) -
88-2487 (C) - Quartz low - SiO2 - Y: 31.25 % - d x by: 1. - WL: 1.54056 - Hexagonal - a 4.93000 - b 4.93000 - c 5.38500 - alpha 90.000 - beta 90.000 - gamma 120.000 - Primitive - P3221 (154) - 3 - 113.

Sample: S-104-1-G

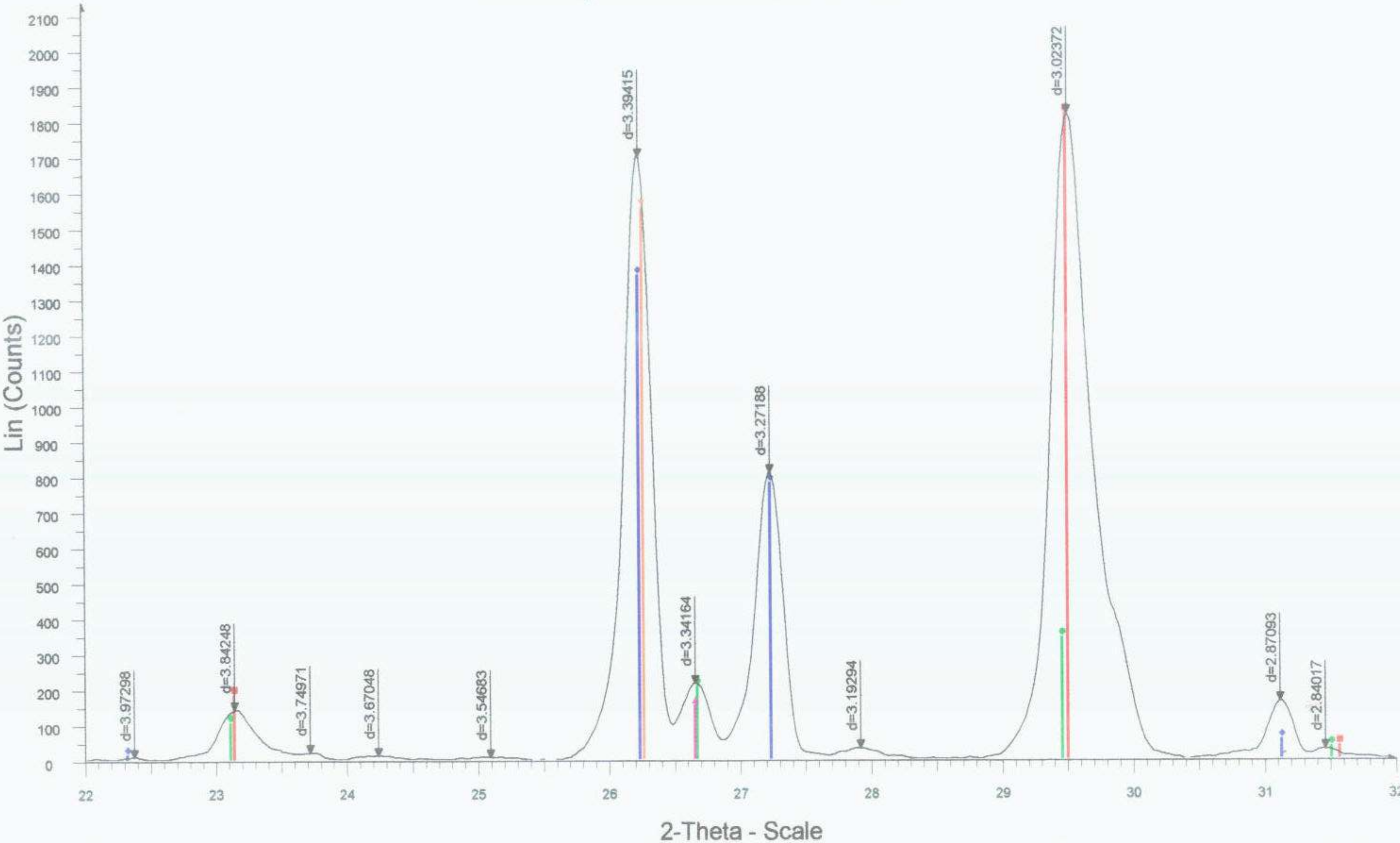

Sample: S-104-1-G - File: Clark-Sherman-26-5-09-S-104-1-G.RAW - Type: 2Th/Th locked - Start: 22.000 ° - End: 32.000 ° - Step: 0.020 ° - Step time: 1. s - Temp.: 25 °C (Room) - Time Started: 16 s - 2-T

Operations: Background 1.000,1.000 | Background 1.000,1.000 | Smooth 0.150 | Import

75-2230 (C) - Aragonite - Ca(CO3) - Y: 75.00 % - d x by: 1. - WL: 1.54056 - Orthorhombic - a 4.96100 - b 7.96700 - c 5.74100 - alpha 90.000 - beta 90.000 - gamma 90.000 - Primitive - Pmcn (62) - 4 - 22

89-1304 (C) - Magnesium calcite, syn - (Mg0.03Ca0.97)(CO3) - Y: 100.00 % - d x by: 1. - WL: 1.54056 - Hexagonal (Rh) - a 4.97800 - b 4.97800 - c 16.98800 - alpha 90.000 - beta 90.000 - gamma 120.(

03-0596 (D) - Calcite - beta-CaCO3 - Y: 18.75 % - d x by: 1. - WL: 1.54056 - Hexagonal (Rh) - a 4.98300 - b 4.98300 - c 17.02000 - alpha 90.000 - beta 90.000 - gamma 120.000 - Primitive - R-3c (167) -

87-2096 (A) - Quartz - SiO2 - Y: 8.33 % - d x by: 1. - WL: 1.54056 - Hexagonal - a 4.91270 - b 4.91270 - c 5.40450 - alpha 90.000 - beta 90.000 - gamma 120.000 - Primitive - P3221 (154) - 3 - 112.961 -

~~87-0703 (C) - Quartz high~~, syn - SiO2 - Y: 85.42 % - d x by: 1. - WL: 1.54056 - Hexagonal - a 4.99770 - b 4.99770 - c 5.46010 - alpha 90.000 - beta 90.000 - gamma 120.000 - Primitive - P6222 (180) - 3

Sample: S-104-1; < 4-phi

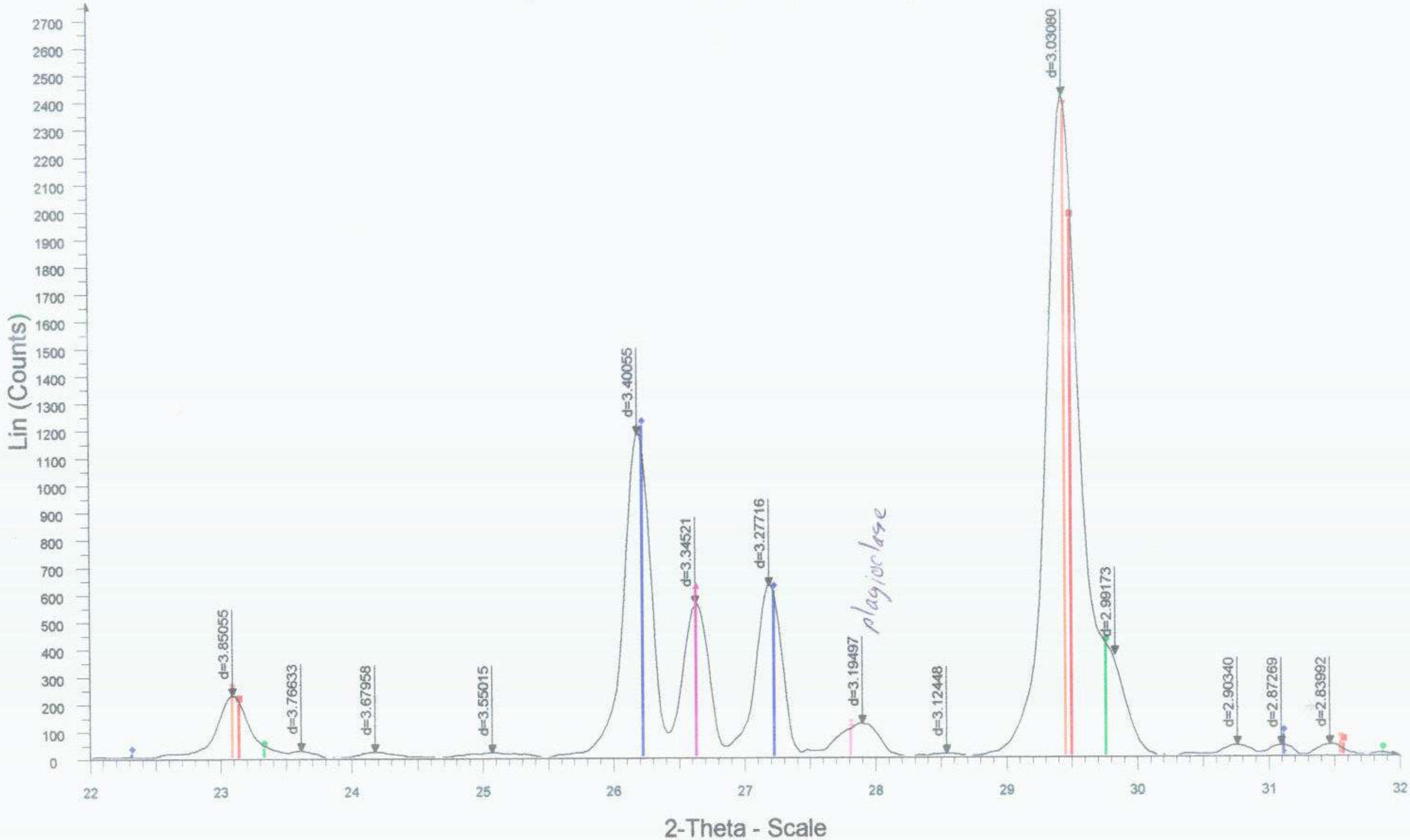

Sample: S-104-1; < 4-phi - File: Clark-Sherman-26-5-09-S-104-1.RAW - Type: 2Th/Th locked - Start: 22.000 ° - End: 32.000 ° - Step: 0.020 ° - Step time: 1. s - Temp.: 25 °C (Room) - Time Started: 16 s -
Operations: Background 1.000,1.000 | Background 1.000,1.000 | Smooth 0.150 | Import

41-1475 (*) - Aragonite - $CaCO_3$ - Y: 50.00 % - d x by: 1. - WL: 1.54056 - Orthorhombic - a 4.96230 - b 7.96800 - c 5.74390 - alpha 90.000 - beta 90.000 - gamma 90.000 - Primitive - Pmcn (62) - 4 - 227.

89-1304 (C) - Magnesium calcite, syn - $(Mg_{0.03}Ca_{0.97})(CO_3)$ - Y: 81.25 % - d x by: 1. - WL: 1.54056 - Hexagonal (Rh) - a 4.97800 - b 4.97800 - c 16.98800 - alpha 90.000 - beta 90.000 - gamma 120.0(

86-2336 (C) - Calcite magnesian - $(Mg_{.129}Ca_{.871})(CO_3)$ - Y: 16.67 % - d x by: 1. - WL: 1.54056 - Hexagonal (Rh) - a 4.93820 - b 4.93820 - c 16.83200 - alpha 90.000 - beta 90.000 - gamma 120.000 - F

72-1652 (A) - Calcite - $CaCO_3$ - Y: 97.92 % - d x by: 1. - WL: 1.54056 - Hexagonal (Rh) - a 4.99000 - b 4.99000 - c 17.00200 - alpha 90.000 - beta 90.000 - gamma 120.000 - Primitive - R-3c (167) - 6 - 3

88-2487 (C) - Quartz low - SiO_2 - Y: 25.00 % - d x by: 1. - WL: 1.54056 - Hexagonal - a 4.93000 - b 4.93000 - c 5.38500 - alpha 90.000 - beta 90.000 - gamma 120.000 - Primitive - P3221 (154) - 3 - 113.

83-0541 (A) - Quartz - SiO_2 - Y: 4.17 % - d x by: 1. - WL: 1.54056 - Hexagonal - a 4.67640 - b 4.67640 - c 5.24750 - alpha 90.000 - beta 90.000 - gamma 120.000 - Primitive - P3121 (152) - 3 - 99.3617 -

Sample: S-104-2-G

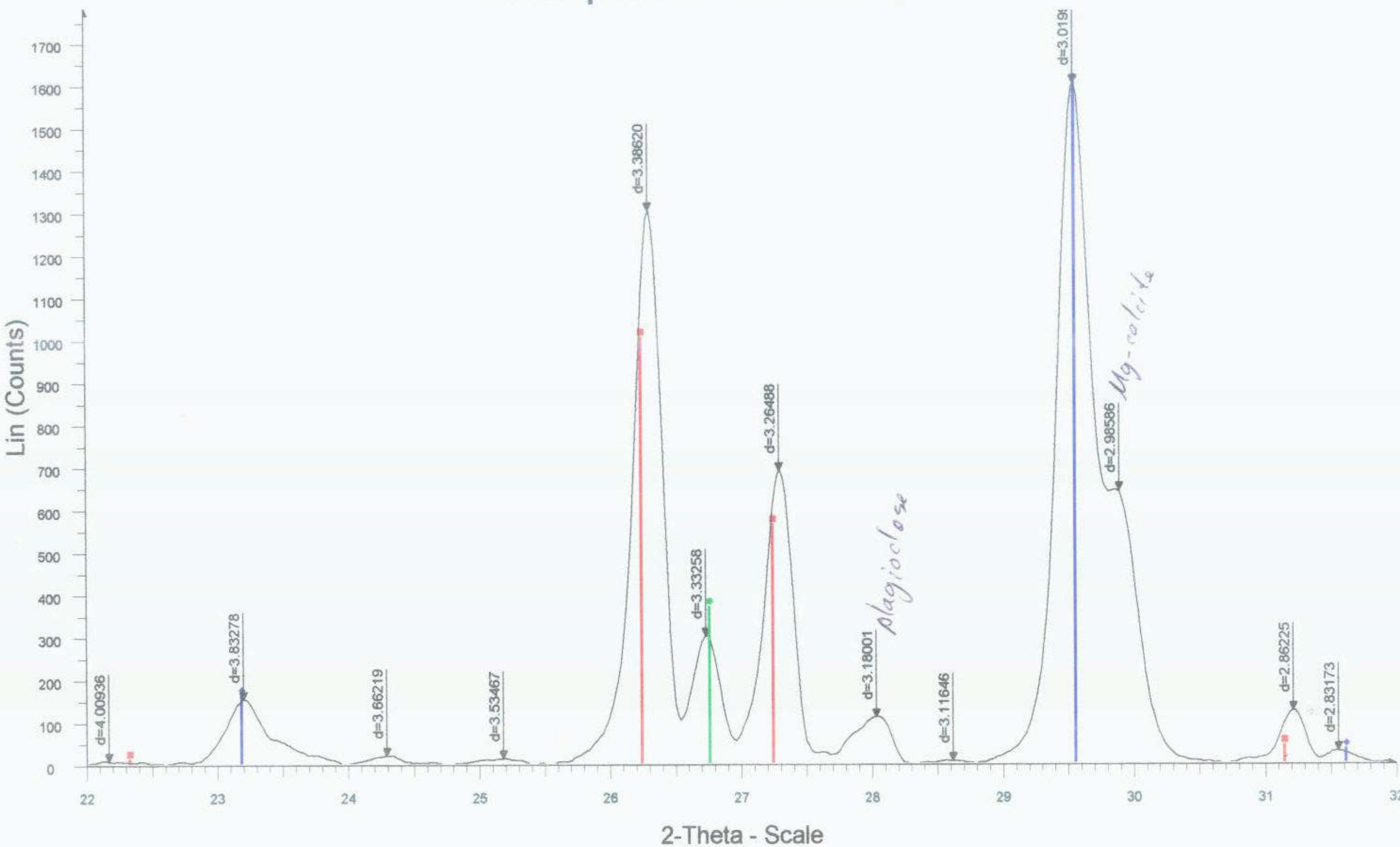

Sample: S-104-2-G - File: Clark-Sherman-26-5-09-S-104-2-G.RAW - Type: 2Th/Th locked - Start: 22.000 ° - End: 32.000 ° - Step: 0.020 ° - Step time: 1. s - Temp.: 25 °C (Room) - Time Started: 16 s - 2-1

Operations: Background 1.000,1.000 | Background 1.000,1.000 | Smooth 0.150 | Import

76-0606 (A) - Aragonite - Ca(CO3) - Y: 62.50 % - d x by: 1. - WL: 1.54056 - Orthorhombic - a 4.95980 - b 7.96410 - c 5.73790 - alpha 90.000 - beta 90.000 - gamma 90.000 - Primitive - Pmcn (62) - 4 - 22

86-2335 (C) - Calcite magnesian - (Mg.064Ca.936)(CO3) - Y: 100.00 % - d x by: 1. - WL: 1.54056 - Hexagonal (Rh) - a 4.96730 - b 4.96730 - c 16.96310 - alpha 90.000 - beta 90.000 - gamma 120.000 -

83-2466 (A) - Quartz, syn - SiO2 - Y: 22.92 % - d x by: 1. - WL: 1.54056 - Hexagonal - a 4.89120 - b 4.89120 - c 5.38800 - alpha 90.000 - beta 90.000 - gamma 120.000 - Primitive - P3121 (152) - 3 - 111

Sample: S-104-2; < 4-phi

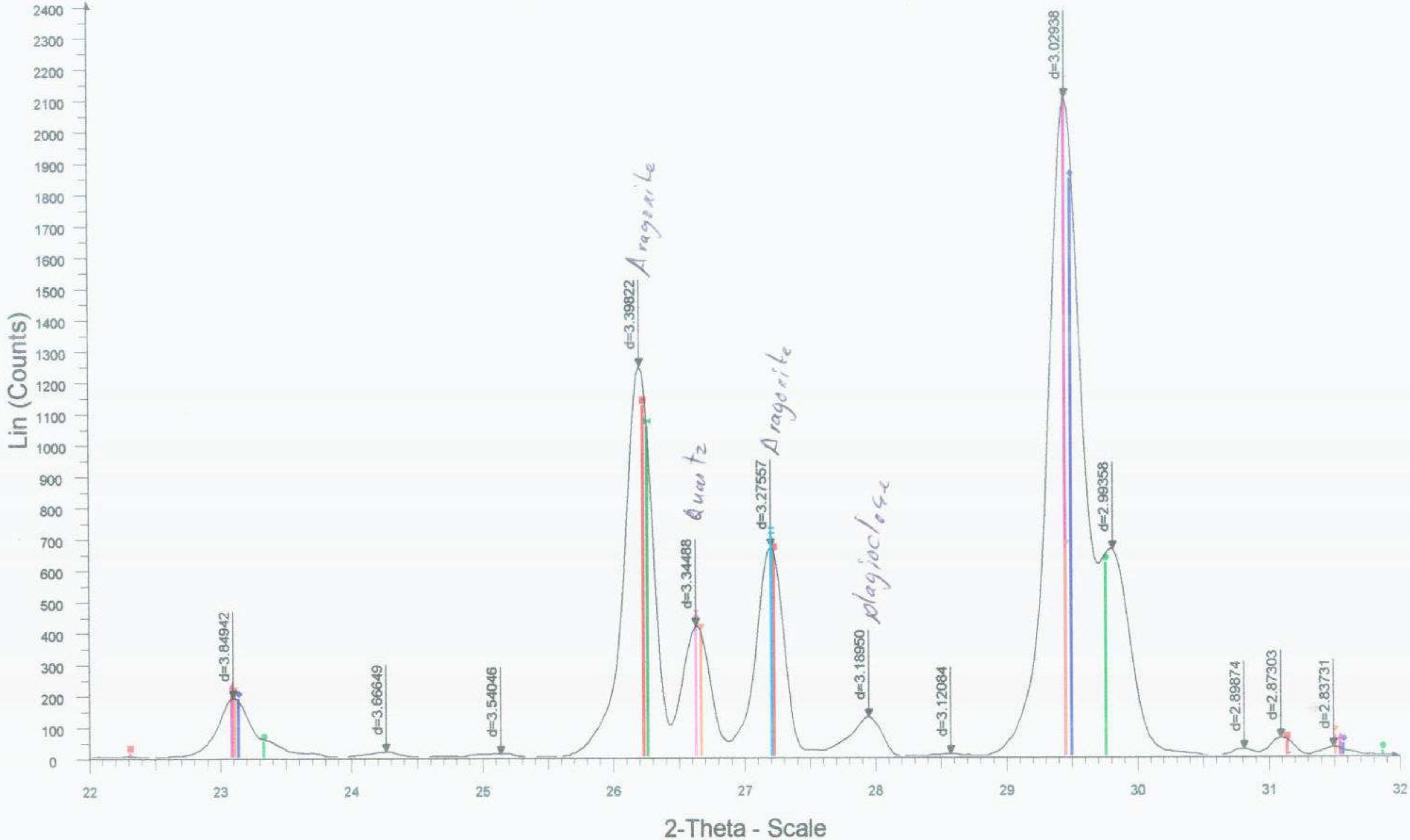

Sample: S-104-2; < 4-phi - File: Clark-Sherman-26-5-09-S-104-2.RAW - Type: 2Th/Th locked - St
Operations: Background 1.000,1.000 | Background 1.000,1.000 | Smooth 0.150 | Import
71-2396 (A) - Aragonite - $CaCO_3$ - Y: 53.12 % - d x by: 1. - WL: 1.54056 - Orthorhombic - a 4.961
89-1304 (C) - Magnesium calcite, syn - $(Mg_{0.03}Ca_{0.97})(CO_3)$ - Y: 87.50 % - d x by: 1. - WL: 1.54
86-2336 (C) - Calcite magnesian - $(Mg_{.129}Ca_{.871})(CO_3)$ - Y: 29.17 % - d x by: 1. - WL: 1.54056 -
72-1652 (A) - Calcite - $CaCO_3$ - Y: 100.00 % - d x by: 1. - WL: 1.54056 - Hexagonal (Rh) - a 4.99(
03-0596 (D) - Calcite - beta-$CaCO_3$ - Y: 31.25 % - d x by: 1. - WL: 1.54056 - Hexagonal (Rh) - a 4
88-2487 (C) - Quartz low - SiO_2 - Y: 20.83 % - d x by: 1. - WL: 1.54056 - Hexagonal - a 4.93000 -
87-0703 (C) - Quartz high, syn - SiO_2 - Y: 50.00 % - d x by: 1. - WL: 1.54056 - Hexagonal - a 4.99
83-2473 (A) - Quartz, syn - SiO_2 - Y: 33.33 % - d x by: 1. - WL: 1.54056 - Hexagonal - a 4.80160 -

Sample: S-104-3-G

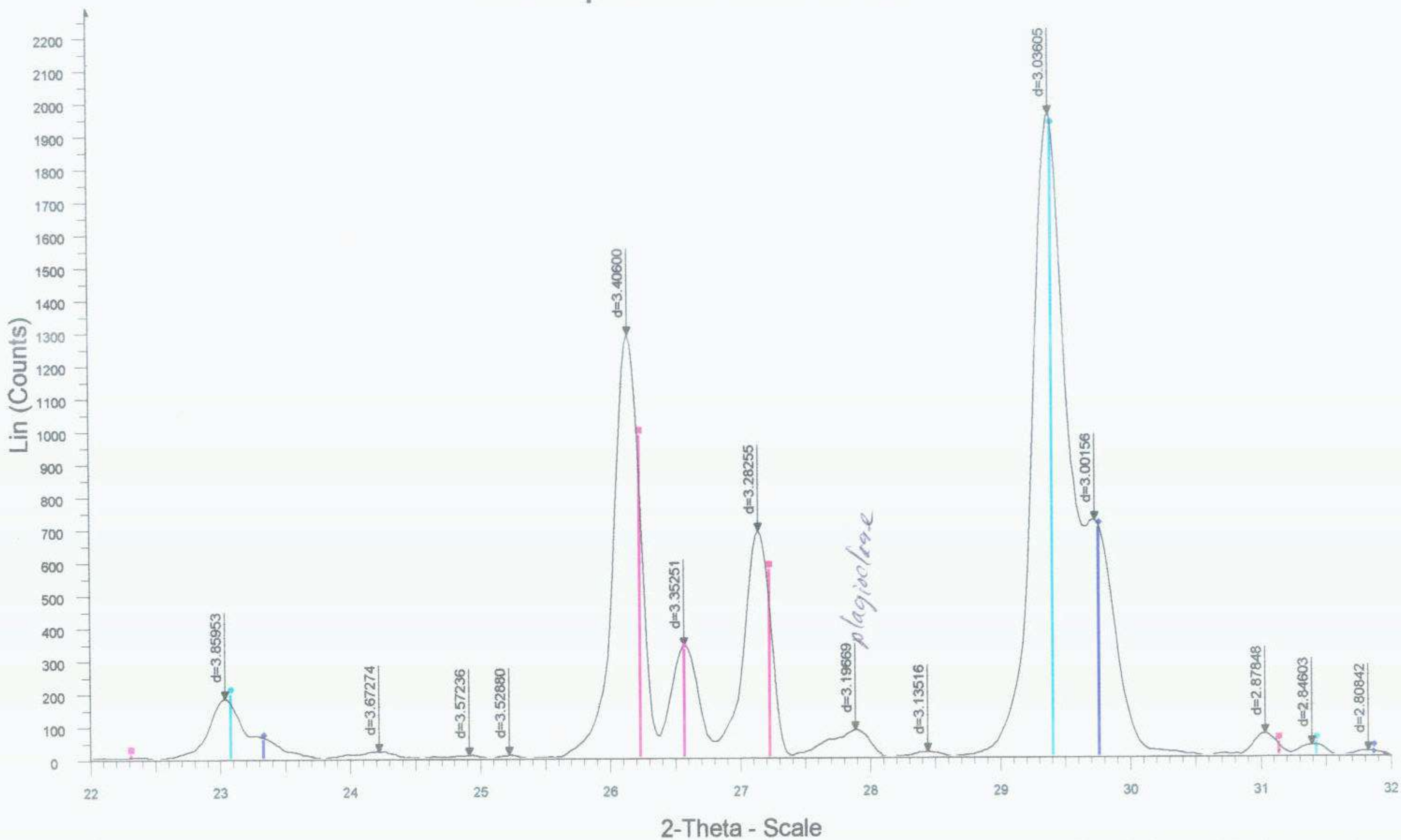

Sample: S-104-3-G - File: Clark-Sherman-26-5-09-S-104-3-G.RAW - Type: 2Th/Th locked - Start: 22.000 ° - End: 32.000 ° - Step: 0.020 ° - Step time: 1. s - Temp.: 25 °C (Room) - Time Started: 16 s - 2-T

Operations: Background 1.000,1.000 | Background 1.000,1.000 | Smooth 0.150 | Import

71-2396 (A) - Aragonite - CaCO3 - Y: 50.00 % - d x by: 1. - WL: 1.54056 - Orthorhombic - a 4.96160 - b 7.97050 - c 5.73940 - alpha 90.000 - beta 90.000 - gamma 90.000 - Primitive - Pmcn (62) - 4 - 226

86-2336 (C) - Calcite magnesian - (Mg.129Ca.871)(CO3) - Y: 35.42 % - d x by: 1. - WL: 1.54056 - Hexagonal (Rh) - a 4.93820 - b 4.93820 - c 16.83200 - alpha 90.000 - beta 90.000 - gamma 120.000 - F

86-2334 (A) - Calcite - Ca(CO3) - Y: 97.92 % - d x by: 1. - WL: 1.54056 - Hexagonal (Rh) - a 4.98800 - b 4.98800 - c 17.06100 - alpha 90.000 - beta 90.000 - gamma 120.000 - Primitive - R-3c (167) - 6 -

85-1780 (A) - Quartz - SiO2 - Y: 16.67 % - d x by: 1. - WL: 1.54056 - Hexagonal - a 4.89000 - b 4.89000 - c 5.49000 - alpha 90.000 - beta 90.000 - gamma 120.000 - Primitive - P3221 (154) - 3 - 113.690

Sample: S-104-3; < 4-phi

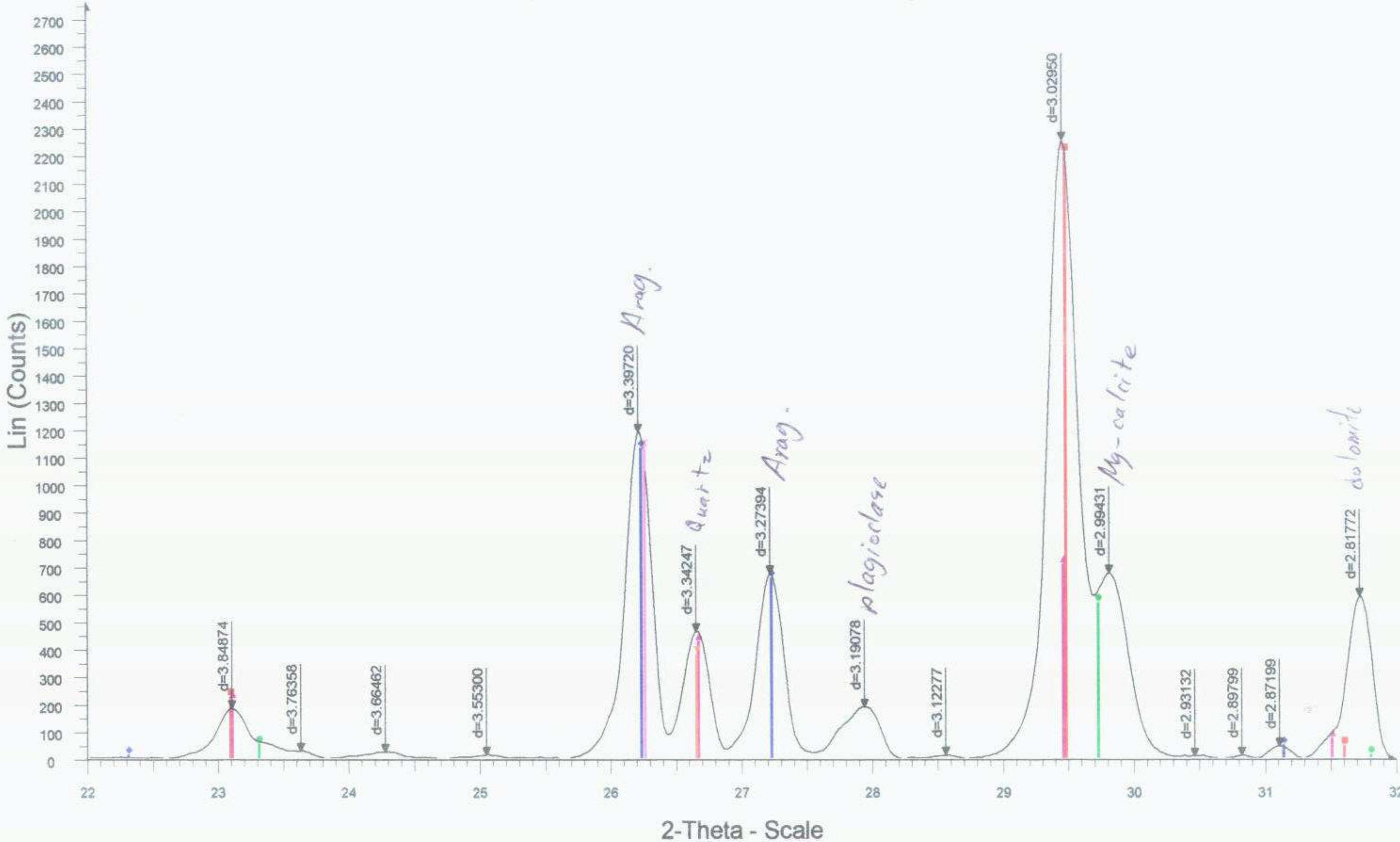

Sample: S-104-3; < 4-phi - File: Clark-Sherman-26-5-09-S-104-3.RAW - Type: 2Th/Th locked - Start: 22.000 ° - End: 32.000 ° - Step: 0.020 ° - Step time: 1. s - Temp.: 25 °C (Room) - Time Started: 16 s - Operations: Background 1.000,1.000 | Background 1.000,1.000 | Smooth 0.150 | Import

- 71-2396 (A) - Aragonite - $CaCO_3$ - Y: 50.00 % - d x by: 1. - WL: 1.54056 - Orthorhombic - a 4.96160 - b 7.97050 - c 5.73940 - alpha 90.000 - beta 90.000 - gamma 90.000 - Primitive - Pmcn (62) - 4 - 226
- 72-1651 (A) - Calcite - $CaCO_3$ - Y: 97.92 % - d x by: 1. - WL: 1.54056 - Hexagonal (Rh) - a 4.99100 - b 4.99100 - c 16.97200 - alpha 90.000 - beta 90.000 - gamma 120.000 - Primitive - R-3c (167) - 6 - 3
- 71-1663 (C) - Calcite, magnesian - $Mg_{0.1}Ca_{0.9}CO_3$ - Y: 25.00 % - d x by: 1. - WL: 1.54056 - Hexagonal (Rh) - a 4.94100 - b 4.94100 - c 16.86400 - alpha 90.000 - beta 90.000 - gamma 120.000 - Primit
- 03-0596 (D) - Calcite - beta-$CaCO_3$ - Y: 31.25 % - d x by: 1. - WL: 1.54056 - Hexagonal (Rh) - a 4.98300 - b 4.98300 - c 17.02000 - alpha 90.000 - beta 90.000 - gamma 120.000 - Primitive - R-3c (167) -
- 87-2096 (A) - Quartz - SiO_2 - Y: 16.67 % - d x by: 1. - WL: 1.54056 - Hexagonal - a 4.91270 - b 4.91270 - c 5.40450 - alpha 90.000 - beta 90.000 - gamma 120.000 - Primitive - P3221 (154) - 3 - 112.961
- 87-0703 (C) - Quartz high, syn - SiO_2 - Y: 50.00 % - d x by: 1. - WL: 1.54056 - Hexagonal - a 4.99770 - b 4.99770 - c 5.46010 - alpha 90.000 - beta 90.000 - gamma 120.000 - Primitive - P6222 (180) - 3

Sample: S-136-1-G

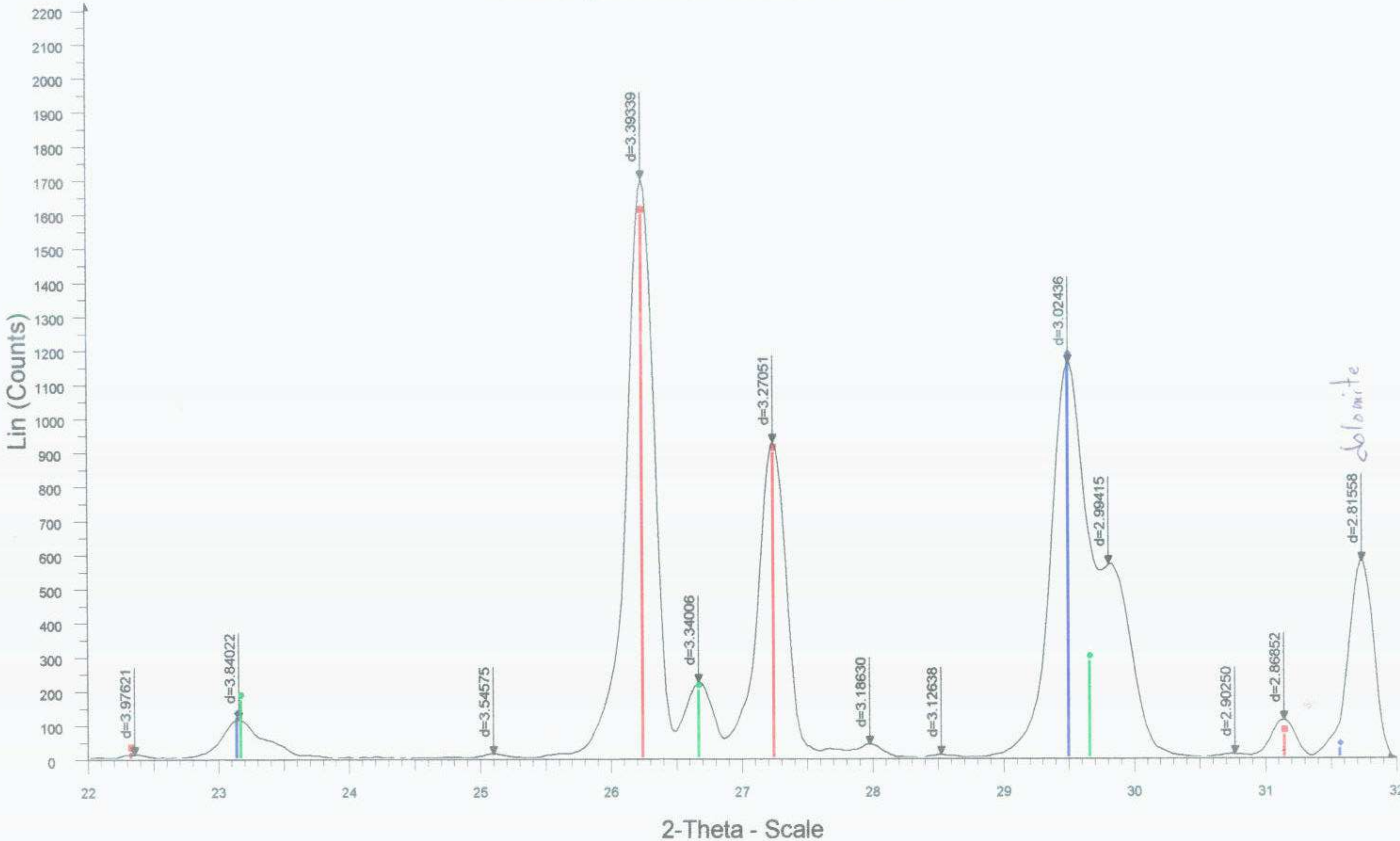

Sample: S-136-1-G - File: Clark-Sherman-26-5-09-S-136-1-G.RAW - Type: 2Th/Th locked - Start: 22.000 ° - End: 32.000 ° - Step: 0.020 ° - Step time: 1. s - Temp.: 25 °C (Room) - Time Started: 16 s - 2-1

Operations: Background 1.000,1.000 | Background 1.000,1.000 | Smooth 0.150 | Import

76-0606 (A) - Aragonite - Ca(CO3) - Y: 93.75 % - d x by: 1. - WL: 1.54056 - Orthorhombic - a 4.95980 - b 7.96410 - c 5.73790 - alpha 90.000 - beta 90.000 - gamma 90.000 - Primitive - Pmcn (62) - 4 - 22

89-1304 (C) - Magnesium calcite, syn - (Mg0.03Ca0.97)(CO3) - Y: 68.75 % - d x by: 1. - WL: 1.54056 - Hexagonal (Rh) - a 4.97800 - b 4.97800 - c 16.98800 - alpha 90.000 - beta 90.000 - gamma 120.0

03-0612 (D) - Calcite - CaCO3 - Y: 16.50 % - d x by: 1. - WL: 1.54056 - Hexagonal (Rh) - a 4.49830 - b 4.49830 - c 17.02000 - alpha 90.000 - beta 90.000 - gamma 120.000 - Primitive - R-3c (167) - 2 - 2

Sample: S-136-1; < 4-phi

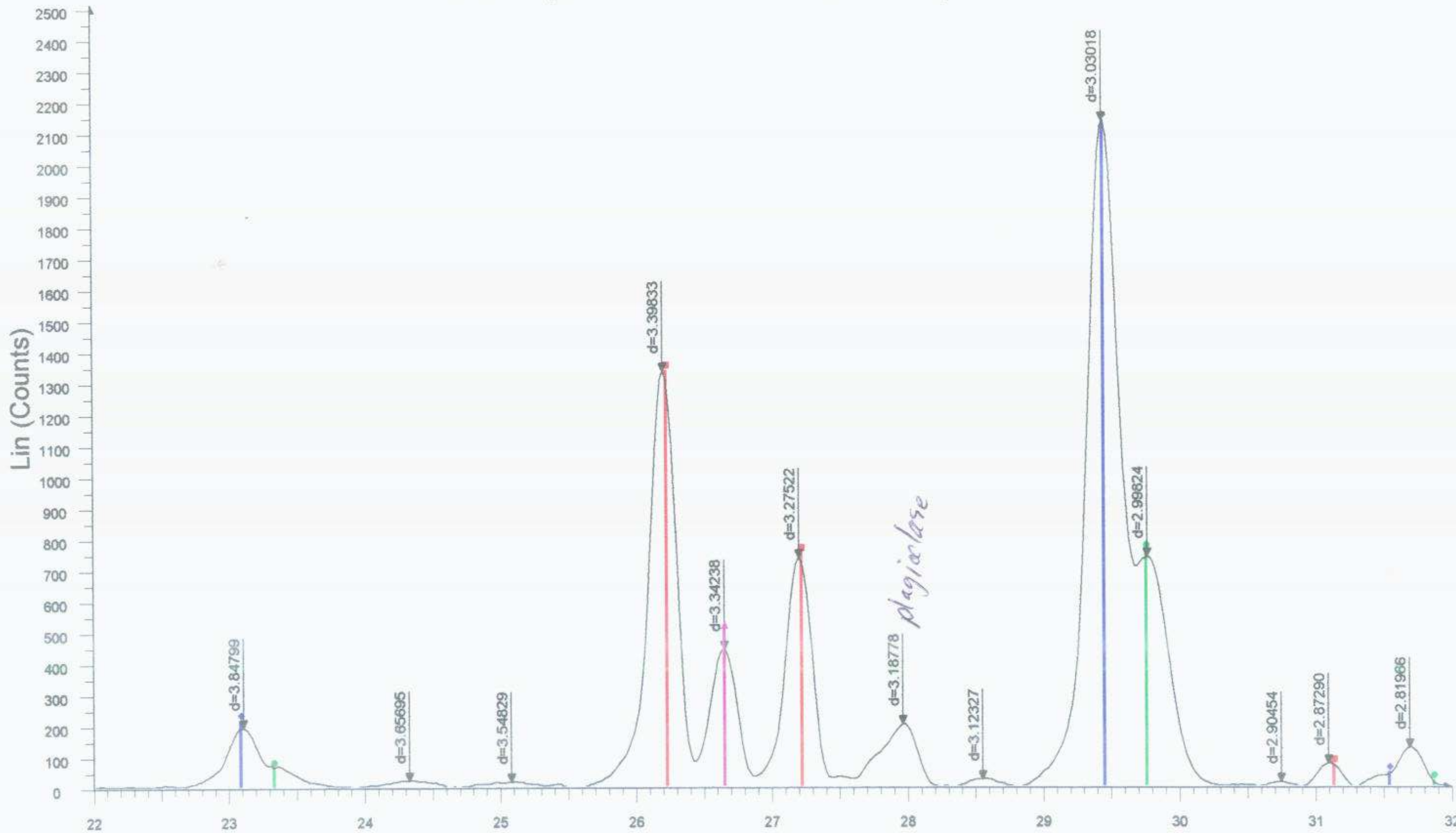

Sample: S-136-1; < 4-phi - File: Clark-Sherman-26-5-09-S-136-1.RAW - Type: 2Th/Th locked - Start: 22.000 ° - End: 32.000 ° - Step: 0.020 ° - Step time: 1. s - Temp.: 25 °C (Room) - Time Started: 16 s -
Operations: Background 1.000,1.000 | Background 1.000,1.000 | Smooth 0.150 | Import

24-0025 (D) - Aragonite - CaCO3 - Y: 62.50 % - d x by: 1. - WL: 1.54056 - Orthorhombic - a 5.74000 - b 4.96100 - c 2.92900 - alpha 90.000 - beta 90.000 - gamma 90.000 - Primitive - Pnma (62) - 4 - 83.

86-2336 (C) - Calcite magnesian - (Mg.129Ca.871)(CO3) - Y: 35.42 % - d x by: 1. - WL: 1.54056 - Hexagonal (Rh) - a 4.93820 - b 4.93820 - c 16.83200 - alpha 90.000 - beta 90.000 - gamma 120.000 - F

72-1652 (A) - Calcite - CaCO3 - Y: 100.00 % - d x by: 1. - WL: 1.54056 - Hexagonal (Rh) - a 4.99000 - b 4.99000 - c 17.00200 - alpha 90.000 - beta 90.000 - gamma 120.000 - Primitive - R-3c (167) - 6 -

87-2096 (A) - Quartz - SiO2 - Y: 23.44 % - d x by: 1. - WL: 1.54056 - Hexagonal - a 4.91270 - b 4.91270 - c 5.40450 - alpha 90.000 - beta 90.000 - gamma 120.000 - Primitive - P3221 (154) - 3 - 112.961

Sample: S-136-2-G

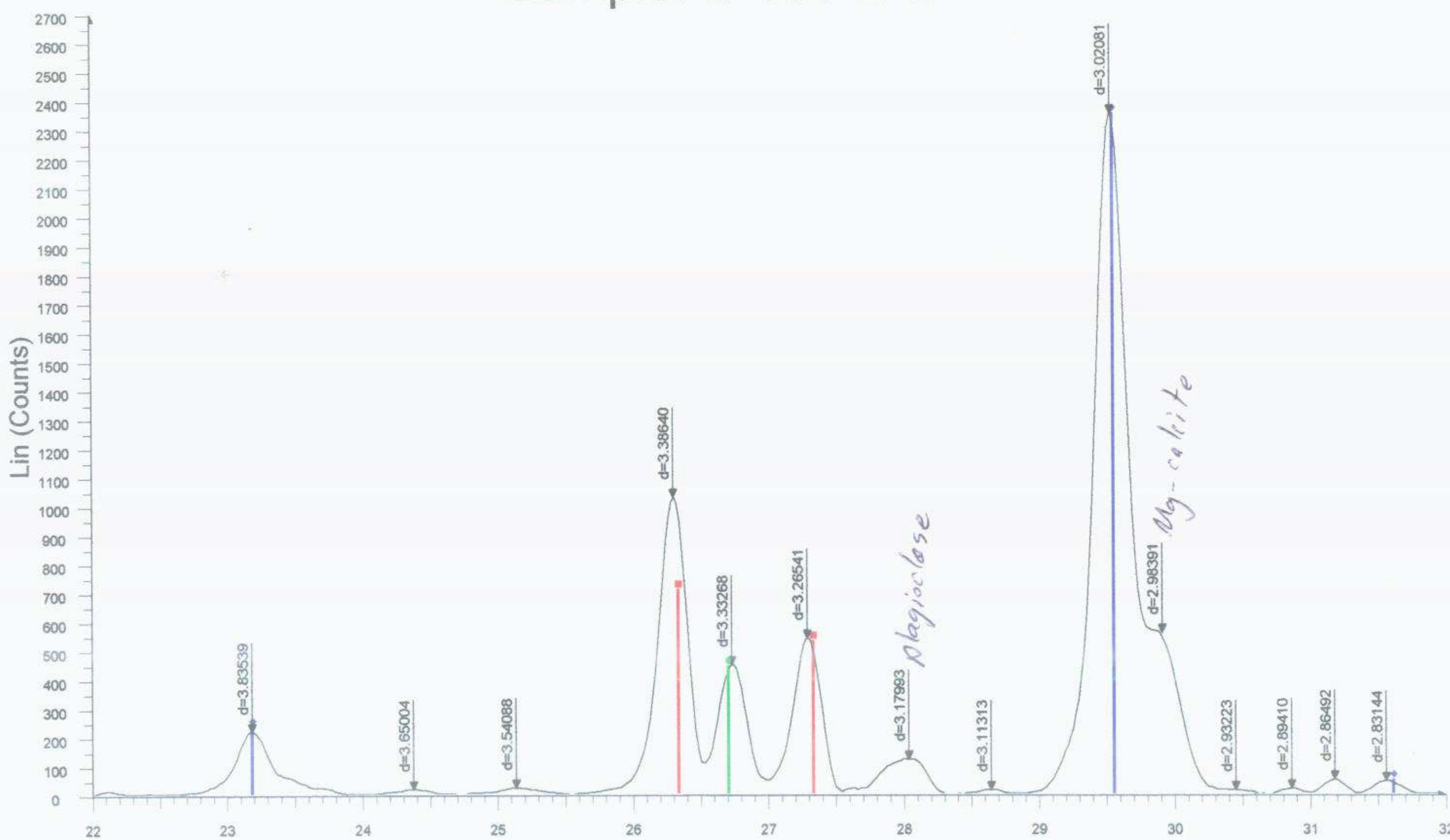

Sample: S-136-2-G - File: Clark-Sherman-26-5-09-S-136-2-G.RAW - Type: 2Th/Th locked - Start: 22.000 ° - End: 32.000 ° - Step: 0.020 ° - Step time: 1. s - Temp.: 25 °C (Room) - Time Started: 16 s - 2-1
Operations: Background 1.000,1.000 | Background 1.000,1.000 | Smooth 0.150 | Import
03-1067 (D) - Aragonite - gamma-$CaCO_3$ - Y: 37.50 % - d x by: 1. - WL: 1.54056 - Orthorhombic - a 4.94000 - b 7.94000 - c 5.72000 - alpha 90.000 - beta 90.000 - gamma 90.000 - Primitive - Pnma (62)
86-2335 (C) - Calcite magnesian - $(Mg_{.064}Ca_{.936})(CO_3)$ - Y: 100.00 % - d x by: 1. - WL: 1.54056 - Hexagonal (Rh) - a 4.96730 - b 4.96730 - c 16.96310 - alpha 90.000 - beta 90.000 - gamma 120.000 -
85-0865 (A) - Quartz - alpha-SiO_2 - Y: 18.75 % - d x by: 1. - WL: 1.54056 - Hexagonal - a 4.90000 - b 4.90000 - c 5.40000 - alpha 90.000 - beta 90.000 - gamma 120.000 - Primitive - P3121 (152) - 3 - 11

Sample: S-136-2; < 4-phi

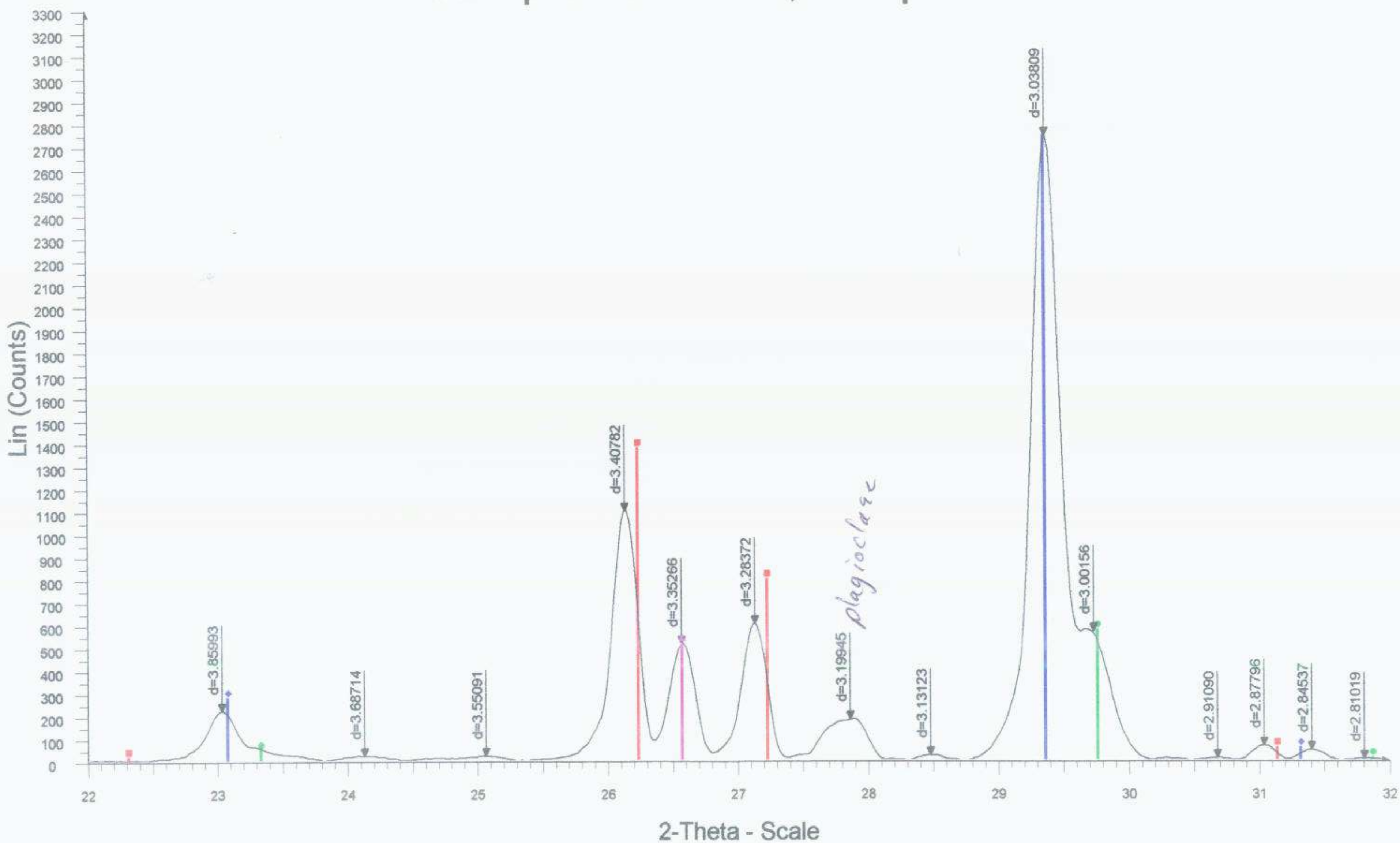

Sample: S-136-2; < 4-phi - File: Clark-Sherman-26-5-09-S-136-2.RAW - Type: 2Th/Th locked - Start: 22.000 ° - End: 32.000 ° - Step: 0.020 ° - Step time: 1. s - Temp.: 25 °C (Room) - Time Started: 16 s -
Operations: Background 1.000,1.000 | Background 1.000,1.000 | Smooth 0.150 | Import

71-2396 (A) - Aragonite - $CaCO_3$ - Y: 50.00 % - d x by: 1. - WL: 1.54056 - Orthorhombic - a 4.96160 - b 7.97050 - c 5.73940 - alpha 90.000 - beta 90.000 - gamma 90.000 - Primitive - Pmcn (62) - 4 - 226

86-2339 (C) - Calcite - $Ca(CO_3)$ - Y: 100.00 % - d x by: 1. - WL: 1.54056 - Hexagonal (Rh) - a 4.98400 - b 4.98400 - c 17.12100 - alpha 90.000 - beta 90.000 - gamma 120.000 - Primitive - R-3c (167) - 6

86-2336 (C) - Calcite magnesian - $(Mg.129Ca.871)(CO_3)$ - Y: 20.83 % - d x by: 1. - WL: 1.54056 - Hexagonal (Rh) - a 4.93820 - b 4.93820 - c 16.83200 - alpha 90.000 - beta 90.000 - gamma 120.000 - F

85-1780 (A) - Quartz - SiO_2 - Y: 18.75 % - d x by: 1. - WL: 1.54056 - Hexagonal - a 4.89000 - b 4.89000 - c 5.49000 - alpha 90.000 - beta 90.000 - gamma 120.000 - Primitive - P3221 (154) - 3 - 113.690

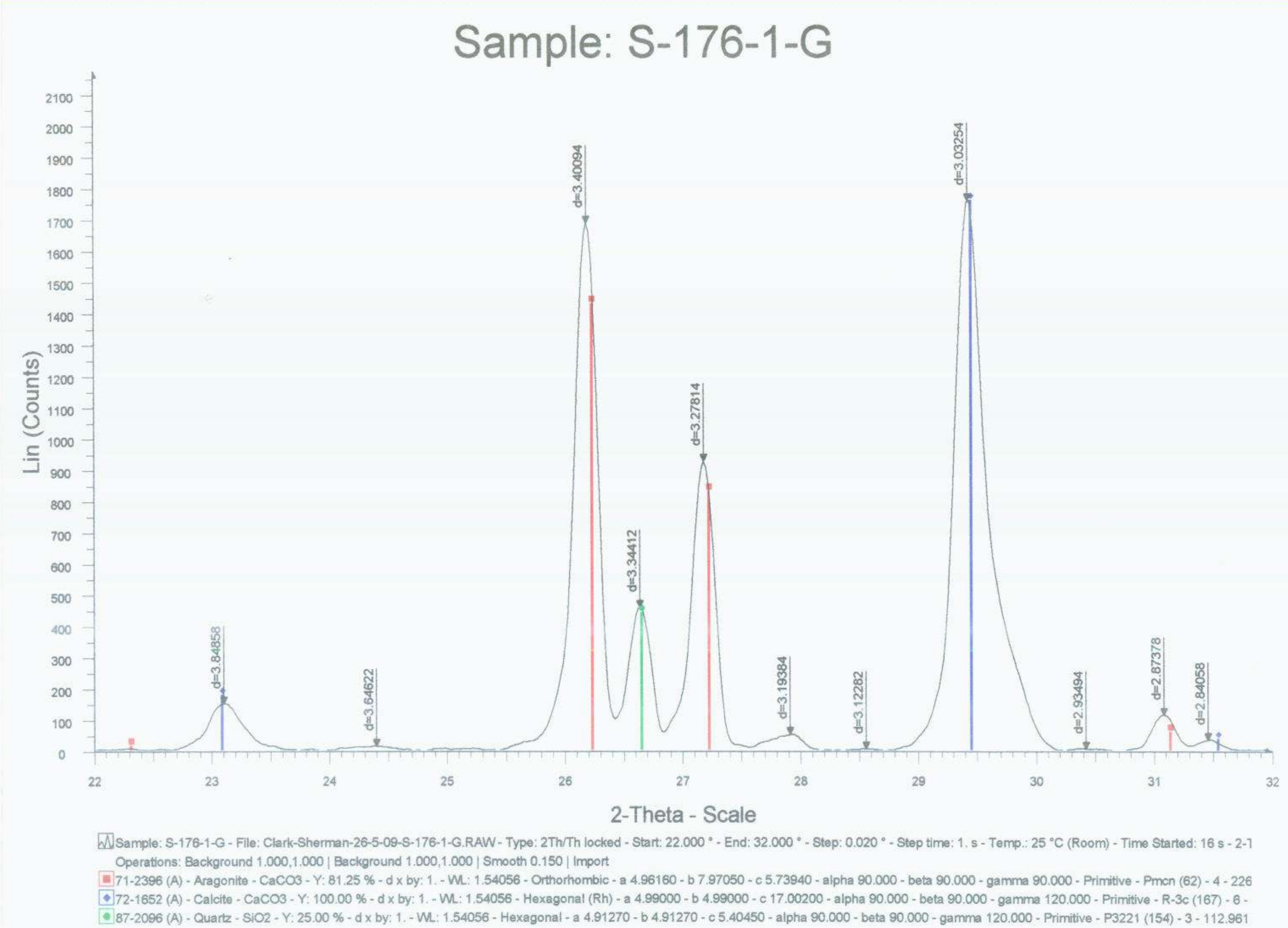
Sample: S-176-1-G
Lin (Counts)
2-Theta - Scale
d=3.84858
d=3.64622
d=3.40094
d=3.34412
d=3.27814
d=3.19384
d=3.12282
d=3.03254
d=2.93494
d=2.87378
d=2.84058
Sample: S-176-1-G - File: Clark-Sherman-26-5-09-S-176-1-G.RAW - Type: 2Th/Th locked - Start: 22.000 ° - End: 32.000 ° - Step: 0.020 ° - Step time: 1. s - Temp.: 25 °C (Room) - Time Started: 16 s - 2-1
Operations: Background 1.000,1.000 | Background 1.000,1.000 | Smooth 0.150 | Import
71-2396 (A) - Aragonite - CaCO3 - Y: 81.25 % - d x by: 1. - WL: 1.54056 - Orthorhombic - a 4.96160 - b 7.97050 - c 5.73940 - alpha 90.000 - beta 90.000 - gamma 90.000 - Primitive - Pmcn (62) - 4 - 226
72-1652 (A) - Calcite - CaCO3 - Y: 100.00 % - d x by: 1. - WL: 1.54056 - Hexagonal (Rh) - a 4.99000 - b 4.99000 - c 17.00200 - alpha 90.000 - beta 90.000 - gamma 120.000 - Primitive - R-3c (167) - 6 -
87-2096 (A) - Quartz - SiO2 - Y: 25.00 % - d x by: 1. - WL: 1.54056 - Hexagonal - a 4.91270 - b 4.91270 - c 5.40450 - alpha 90.000 - beta 90.000 - gamma 120.000 - Primitive - P3221 (154) - 3 - 112.961

Sample: S-176-1; < 4-phi

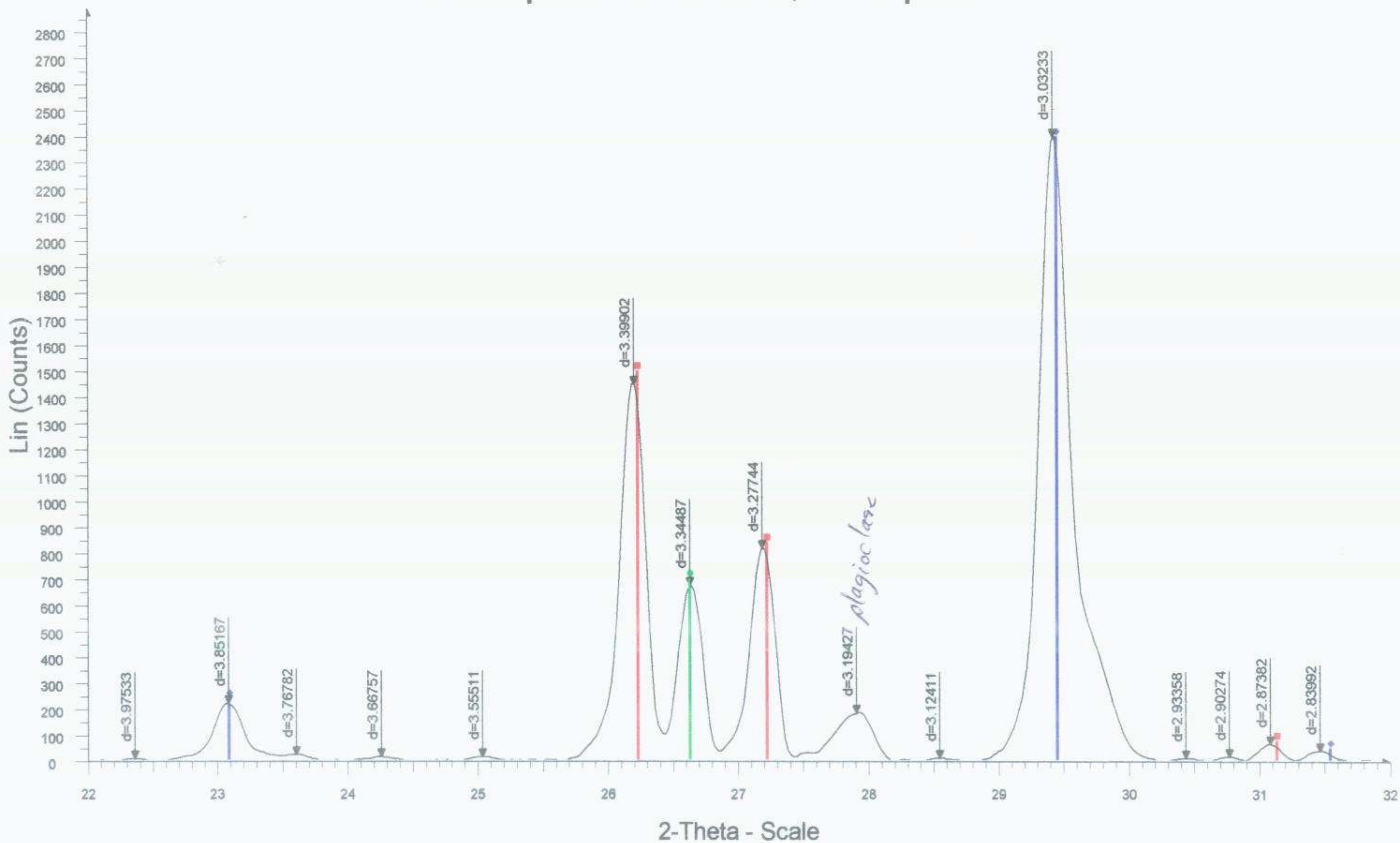

Sample: S-176-1; < 4-phi - File: Clark-Sherman-26-5-09-S-176-1.RAW - Type: 2Th/Th locked - Start: 22.000 ° - End: 32.000 ° - Step: 0.020 ° - Step time: 1. s - Temp.: 25 °C (Room) - Time Started: 16 s -
Operations: Background 1.000,1.000 | Background 1.000,1.000 | Smooth 0.150 | Import

24-0025 (D) - Aragonite - $CaCO_3$ - Y: 62.50 % - d x by: 1. - WL: 1.54056 - Orthorhombic - a 5.74000 - b 4.96100 - c 2.92900 - alpha 90.000 - beta 90.000 - gamma 90.000 - Primitive - Pnma (62) - 4 - 83.

72-1652 (A) - Calcite - $CaCO_3$ - Y: 100.00 % - d x by: 1. - WL: 1.54056 - Hexagonal (Rh) - a 4.99000 - b 4.99000 - c 17.00200 - alpha 90.000 - beta 90.000 - gamma 120.000 - Primitive - R-3c (167) - 6 -

88-2487 (C) - Quartz low - SiO_2 - Y: 29.17 % - d x by: 1. - WL: 1.54056 - Hexagonal - a 4.93000 - b 4.93000 - c 5.38500 - alpha 90.000 - beta 90.000 - gamma 120.000 - Primitive - P3221 (154) - 3 - 113.

Sample: S-176-2-G

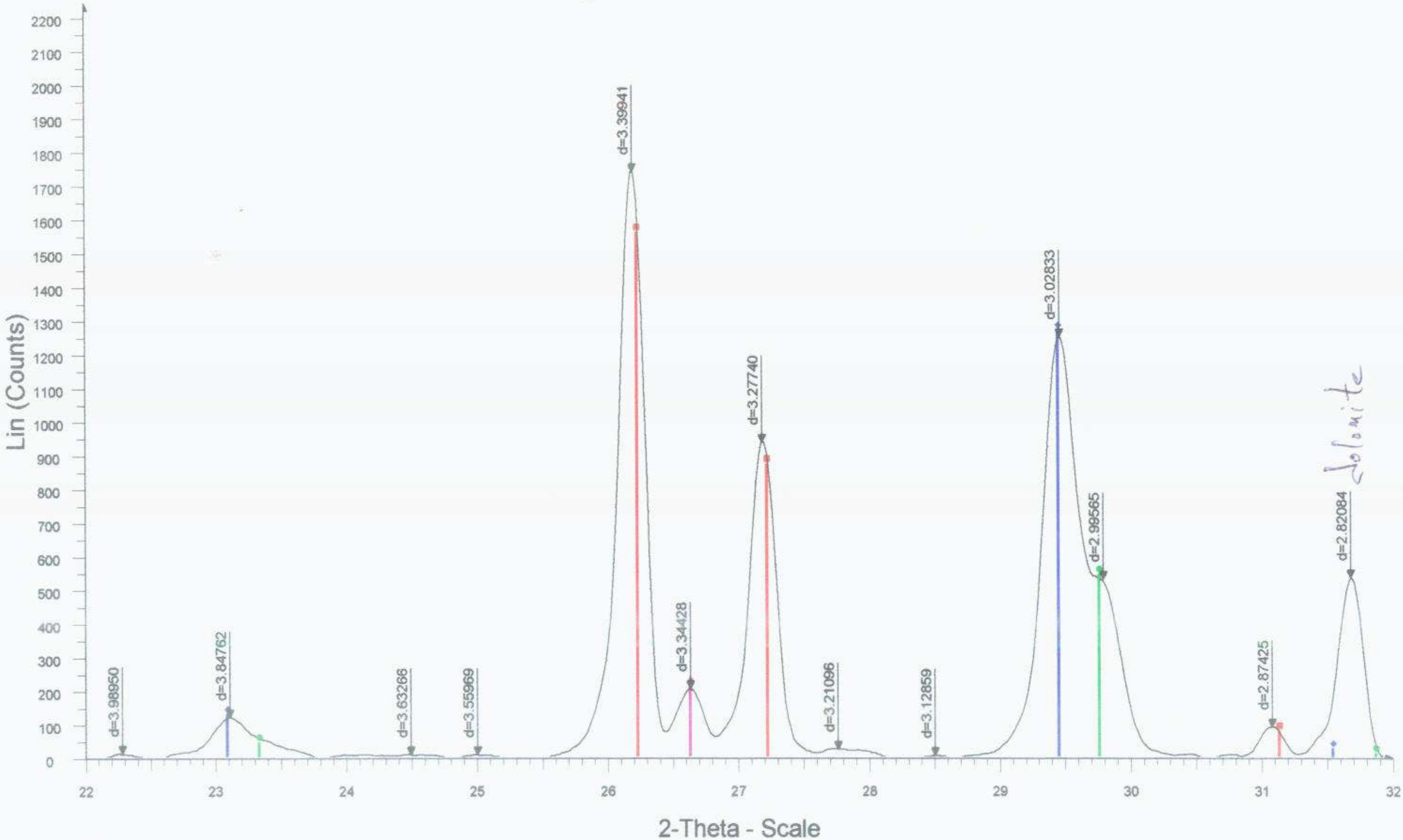

Sample: S-176-2-G - File: Clark-Sherman-26-5-09-S-176-2-G.RAW - Type: 2Th/Th locked - Start: 22.000 ° - End: 32.000 ° - Step: 0.020 ° - Step time: 1. s - Temp.: 25 °C (Room) - Time Started: 19 s - 2-1

Operations: Background 1.000,1.000 | Background 1.000,1.000 | Smooth 0.150 | Import

24-0025 (D) - Aragonite - CaCO3 - Y: 89.58 % - d x by: 1. - WL: 1.54056 - Orthorhombic - a 5.74000 - b 4.96100 - c 2.92900 - alpha 90.000 - beta 90.000 - gamma 90.000 - Primitive - Pnma (62) - 4 - 83.

86-2336 (C) - Calcite magnesian - (Mg.129Ca.871)(CO3) - Y: 31.25 % - d x by: 1. - WL: 1.54056 - Hexagonal (Rh) - a 4.93820 - b 4.93820 - c 16.83200 - alpha 90.000 - beta 90.000 - gamma 120.000 - F

72-1652 (A) - Calcite - CaCO3 - Y: 72.92 % - d x by: 1. - WL: 1.54056 - Hexagonal (Rh) - a 4.99000 - b 4.99000 - c 17.00200 - alpha 90.000 - beta 90.000 - gamma 120.000 - Primitive - R-3c (167) - 6 - 3

88-2487 (C) - Quartz low - SiO2 - Y: 12.50 % - d x by: 1. - WL: 1.54056 - Hexagonal - a 4.93000 - b 4.93000 - c 5.38500 - alpha 90.000 - beta 90.000 - gamma 120.000 - Primitive - P3221 (154) - 3 - 113.

Sample: S-176-2; < 4-phi

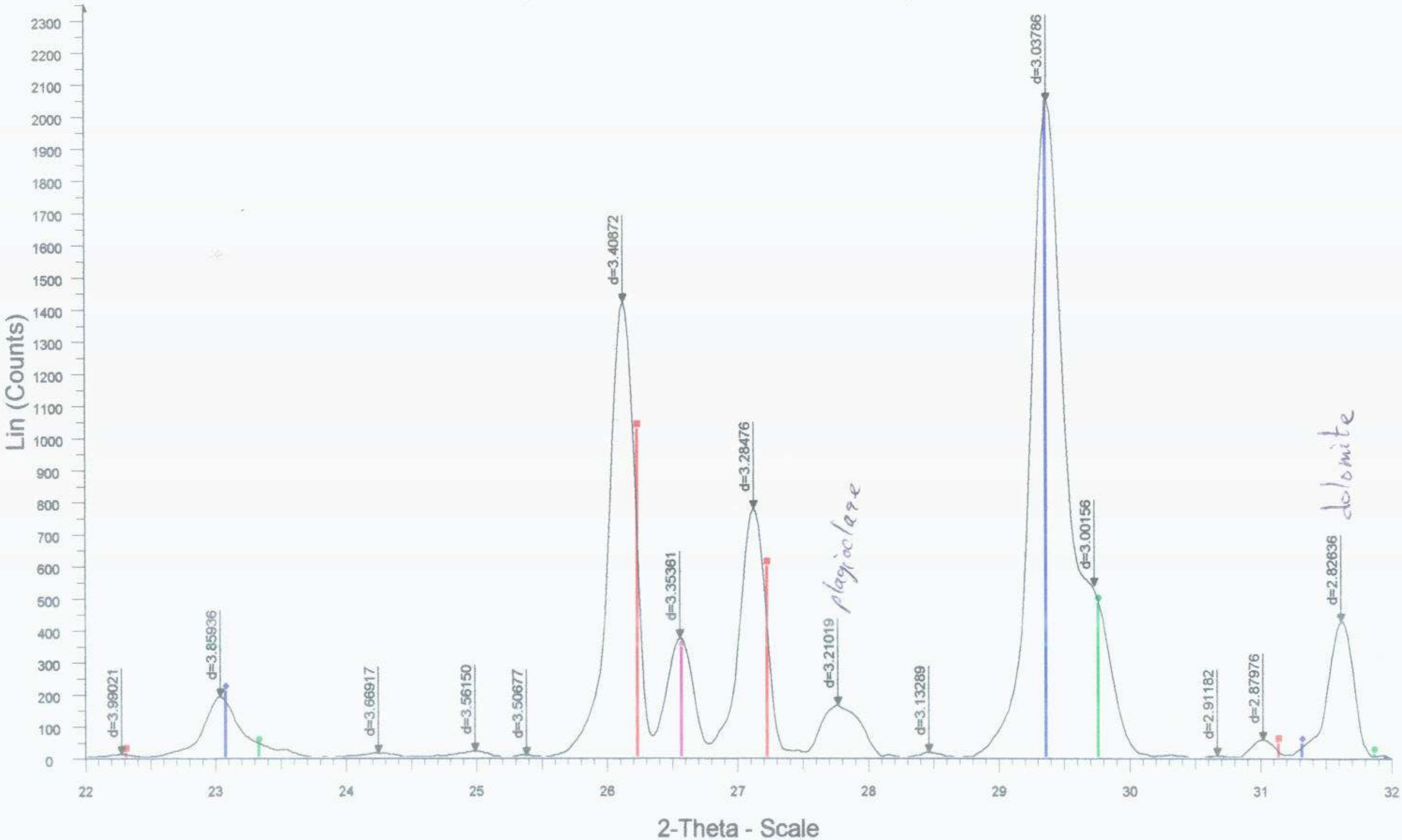

Sample: S-176-2; < 4-phi - File: Clark-Sherman-26-5-09-S-176-2.RAW - Type: 2Th/Th locked - Start: 22.000 ° - End: 32.000 ° - Step: 0.020 ° - Step time: 1. s - Temp.: 25 °C (Room) - Time Started: 16 s - Operations: Background 1.000,1.000 | Background 1.000,1.000 | Smooth 0.150 | Import

71-2396 (A) - Aragonite - CaCO3 - Y: 50.00 % - d x by: 1. - WL: 1.54056 - Orthorhombic - a 4.96160 - b 7.97050 - c 5.73940 - alpha 90.000 - beta 90.000 - gamma 90.000 - Primitive - Pmcn (62) - 4 - 226

86-2339 (C) - Calcite - Ca(CO3) - Y: 100.00 % - d x by: 1. - WL: 1.54056 - Hexagonal (Rh) - a 4.98400 - b 4.98400 - c 17.12100 - alpha 90.000 - beta 90.000 - gamma 120.000 - Primitive - R-3c (167) - 6

86-2336 (C) - Calcite magnesian - (Mg.129Ca.871)(CO3) - Y: 23.44 % - d x by: 1. - WL: 1.54056 - Hexagonal (Rh) - a 4.93820 - b 4.93820 - c 16.83200 - alpha 90.000 - beta 90.000 - gamma 120.000 - F

85-1780 (A) - Quartz - SiO2 - Y: 16.67 % - d x by: 1. - WL: 1.54056 - Hexagonal - a 4.89000 - b 4.89000 - c 5.49000 - alpha 90.000 - beta 90.000 - gamma 120.000 - Primitive - P3221 (154) - 3 - 113.690

Sample: S-176-3-G

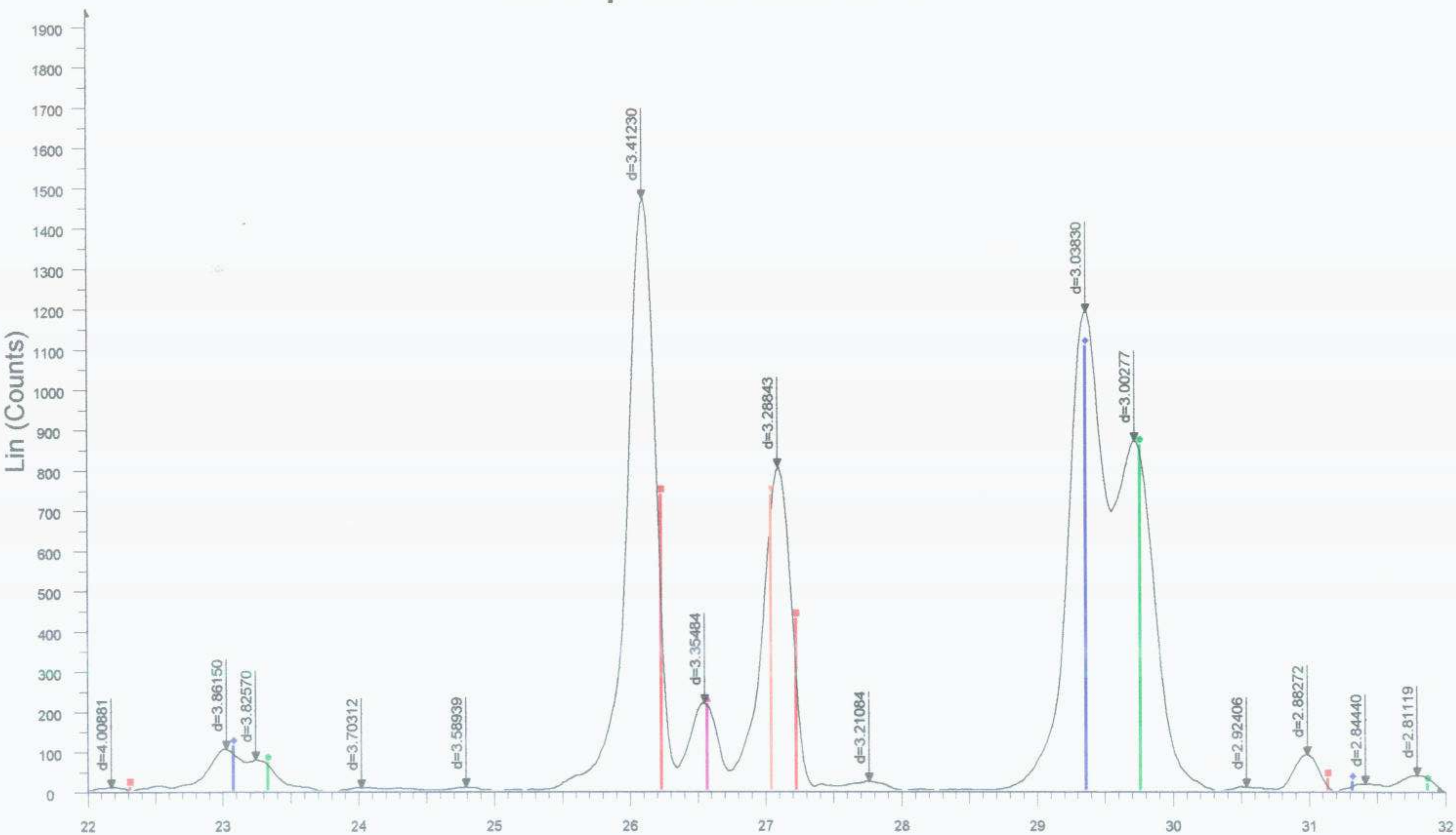

Sample: S-176-3-G - File: Clark-Sherman-26-5-09-S-176-3-G.RAW - Type: 2Th/Th locked - Start: 22.000 ° - End: 32.000 ° - Step: 0.020 ° - Step time: 1. s - Temp.: 25 °C (Room) - Time Started: 16 s - 2-1
Operations: Background 1.000,1.000 | Background 1.000,1.000 | Smooth 0.150 | Import
71-2396 (A) - Aragonite - CaCO3 - Y: 50.00 % - d x by: 1. - WL: 1.54056 - Orthorhombic - a 4.96160 - b 7.97050 - c 5.73940 - alpha 90.000 - beta 90.000 - gamma 90.000 - Primitive - Pmcn (62) - 4 - 226
86-2339 (C) - Calcite - Ca(CO3) - Y: 75.00 % - d x by: 1. - WL: 1.54056 - Hexagonal (Rh) - a 4.98400 - b 4.98400 - c 17.12100 - alpha 90.000 - beta 90.000 - gamma 120.000 - Primitive - R-3c (167) - 6 -
86-2336 (C) - Calcite magnesian - (Mg.129Ca.871)(CO3) - Y: 58.33 % - d x by: 1. - WL: 1.54056 - Hexagonal (Rh) - a 4.93820 - b 4.93820 - c 16.83200 - alpha 90.000 - beta 90.000 - gamma 120.000 - F
85-1780 (A) - Quartz - SiO2 - Y: 14.58 % - d x by: 1. - WL: 1.54056 - Hexagonal - a 4.89000 - b 4.89000 - c 5.49000 - alpha 90.000 - beta 90.000 - gamma 120.000 - Primitive - P3221 (154) - 3 - 113.690
85-0458 (A) - Quartz low - alpha-SiO2 - Y: 50.00 % - d x by: 1. - WL: 1.54056 - Hexagonal - a 4.83200 - b 4.83200 - c 5.34700 - alpha 90.000 - beta 90.000 - gamma 120.000 - Primitive - P3221 (154) - 3

Sample: S-176-3; < 4-phi

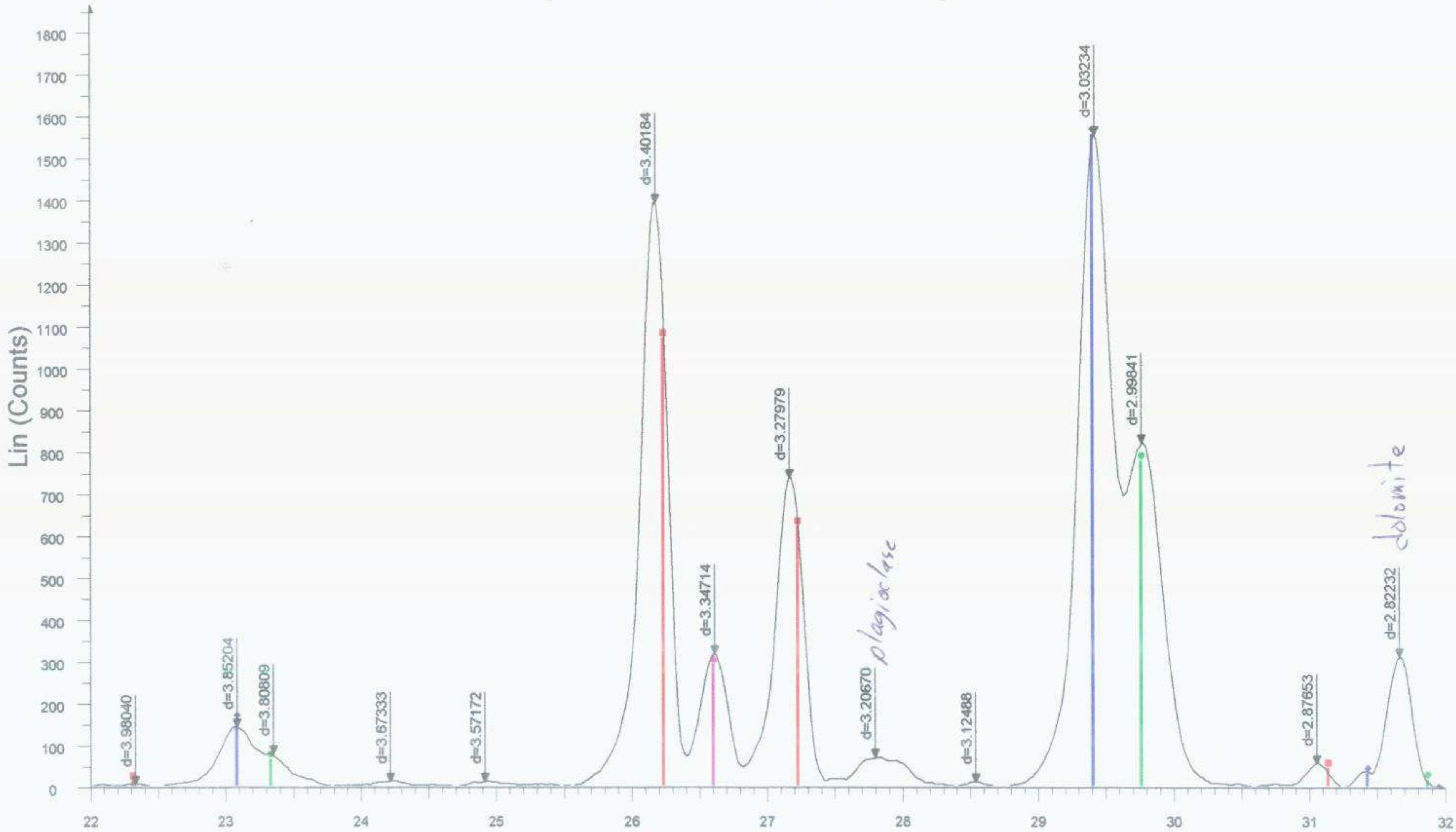

Sample: S-176-3; < 4-phi - File: Clark-Sherman-26-5-09-S-176-3.RAW - Type: 2Th/Th locked - Start: 22.000 ° - End: 32.000 ° - Step: 0.020 ° - Step time: 1. s - Temp.: 25 °C (Room) - Time Started: 16 s -
Operations: Background 1.000,1.000 | Background 1.000,1.000 | Smooth 0.150 | Import

71-2396 (A) - Aragonite - $CaCO_3$ - Y: 68.75 % - d x by: 1. - WL: 1.54056 - Orthorhombic - a 4.96160 - b 7.97050 - c 5.73940 - alpha 90.000 - beta 90.000 - gamma 90.000 - Primitive - Pmcn (62) - 4 - 226

86-2336 (C) - Calcite magnesian - $(Mg_{.129}Ca_{.871})(CO_3)$ - Y: 50.00 % - d x by: 1. - WL: 1.54056 - Hexagonal (Rh) - a 4.93820 - b 4.93820 - c 16.83200 - alpha 90.000 - beta 90.000 - gamma 120.000 - F

86-2334 (A) - Calcite - $Ca(CO_3)$ - Y: 100.00 % - d x by: 1. - WL: 1.54056 - Hexagonal (Rh) - a 4.98800 - b 4.98800 - c 17.06100 - alpha 90.000 - beta 90.000 - gamma 120.000 - Primitive - R-3c (167) - 6

89-1961 (C) - Quartz low, dauphinee-twinned - SiO_2 - Y: 18.75 % - d x by: 1. - WL: 1.54056 - Hexagonal - a 4.92100 - b 4.92100 - c 5.41600 - alpha 90.000 - beta 90.000 - gamma 120.000 - Primitive - P

Sample: S-232-1-G

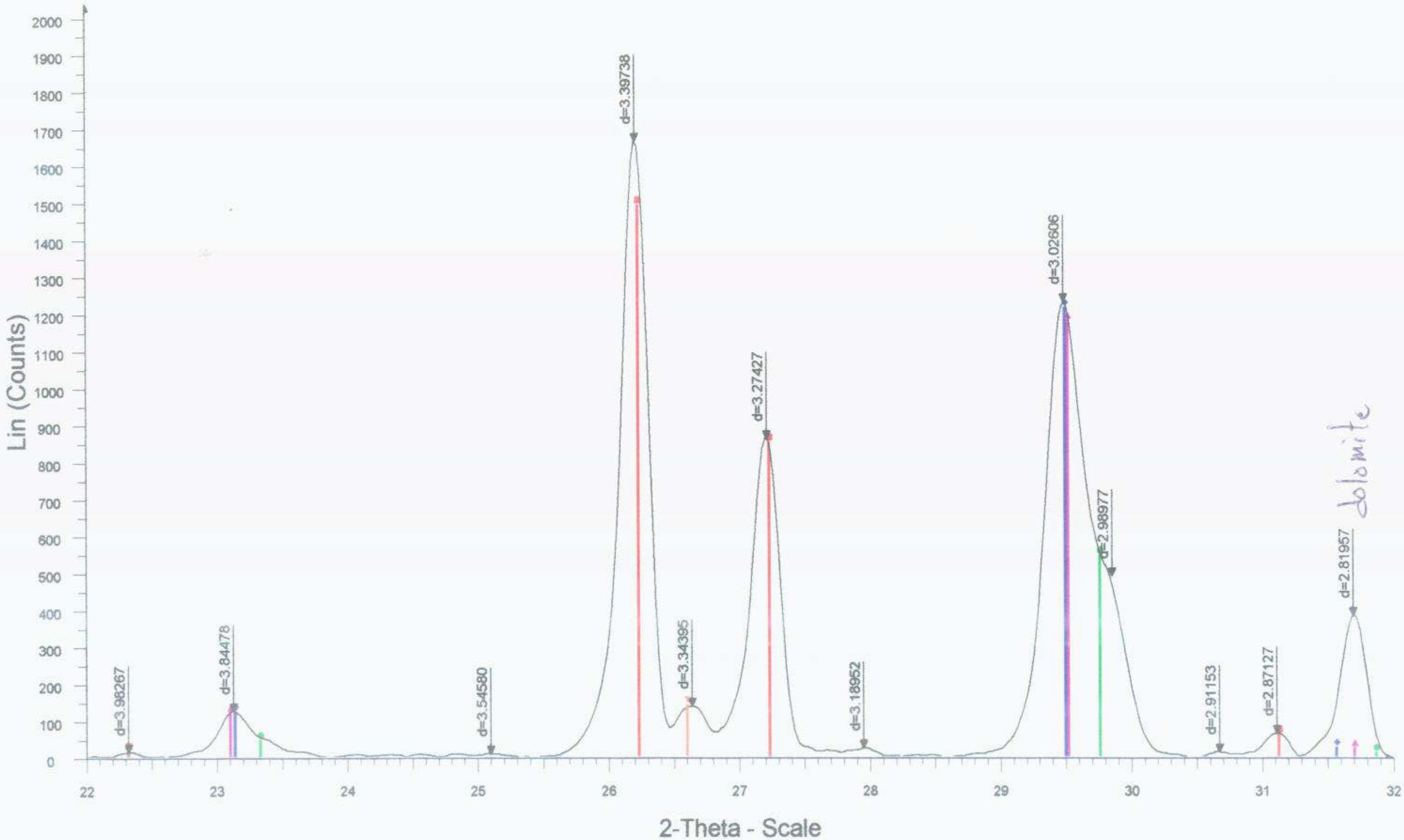

Sample: S-232-1-G - File: Clark-Sherman-26-5-09-S-232-1-G.RAW - Type: 2Th/Th locked - Start: 22.000 ° - End: 32.000 ° - Step: 0.020 ° - Step time: 1. s - Temp.: 25 °C (Room) - Time Started: 16 s - 2-1

Operations: Background 1.000,1.000 | Background 1.000,1.000 | Smooth 0.150 | Import

75-2230 (C) - Aragonite - Ca(CO3) - Y: 89.58 % - d x by: 1. - WL: 1.54056 - Orthorhombic - a 4.96100 - b 7.96700 - c 5.74100 - alpha 90.000 - beta 90.000 - gamma 90.000 - Primitive - Pmcn (62) - 4 - 22

89-1304 (C) - Magnesium calcite, syn - (Mg0.03Ca0.97)(CO3) - Y: 72.92 % - d x by: 1. - WL: 1.54056 - Hexagonal (Rh) - a 4.97800 - b 4.97800 - c 16.98800 - alpha 90.000 - beta 90.000 - gamma 120.0

86-2336 (C) - Calcite magnesian - (Mg.129Ca.871)(CO3) - Y: 32.72 % - d x by: 1. - WL: 1.54056 - Hexagonal (Rh) - a 4.93820 - b 4.93820 - c 16.83200 - alpha 90.000 - beta 90.000 - gamma 120.000 - F

72-1650 (C) - Calcite - CaCO3 - Y: 70.83 % - d x by: 1. - WL: 1.54056 - Hexagonal (Rh) - a 4.99300 - b 4.99300 - c 16.91700 - alpha 90.000 - beta 90.000 - gamma 120.000 - Primitive - R-3c (167) - 6 - 3

89-1961 (C) - Quartz low, dauphinee-twinned - SiO2 - Y: 8.33 % - d x by: 1. - WL: 1.54056 - Hexagonal - a 4.92100 - b 4.92100 - c 5.41600 - alpha 90.000 - beta 90.000 - gamma 120.000 - Primitive - P6

Sample: S-232-1; < 4-phi

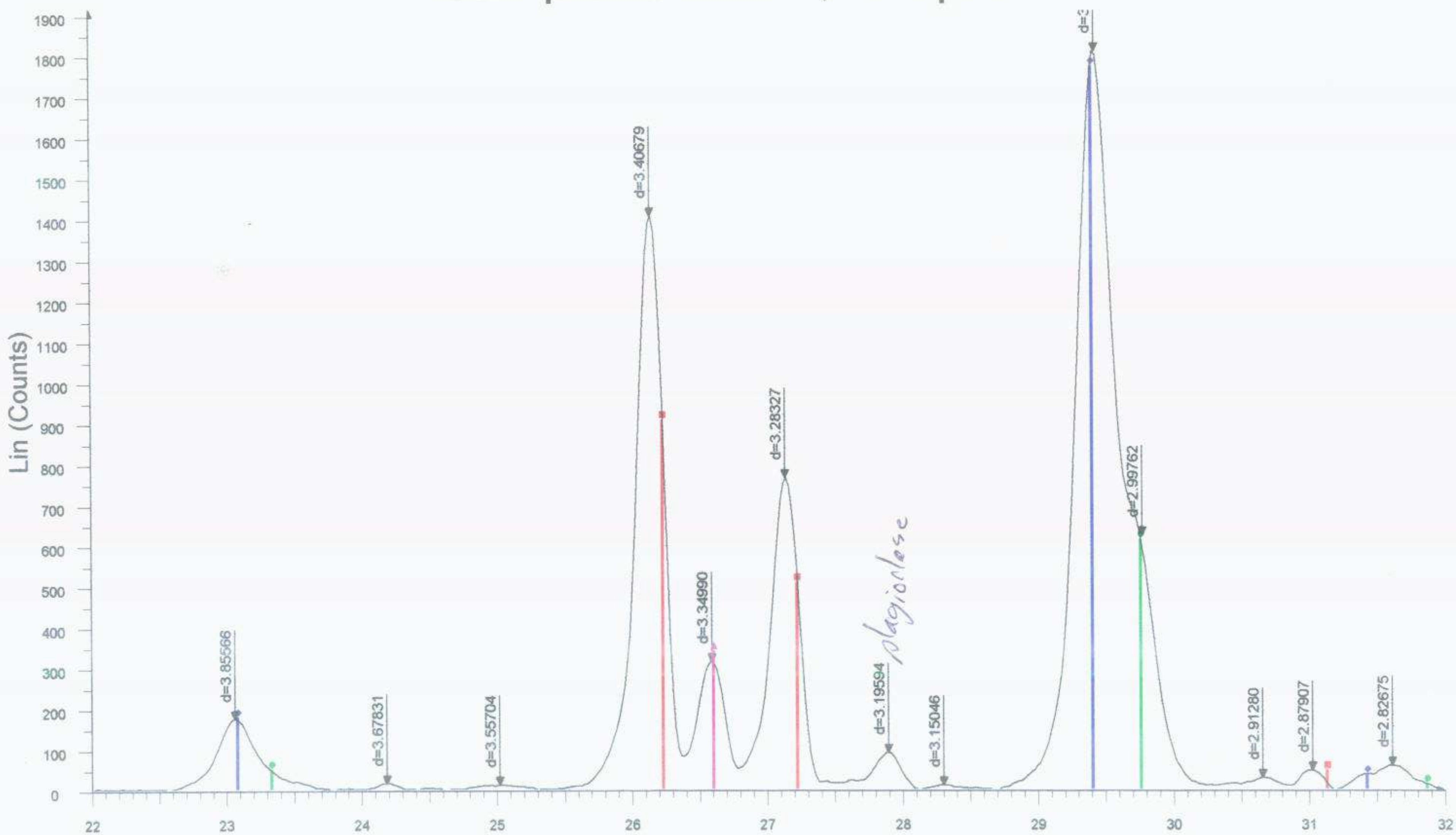

Sample: S-232-1; < 4-phi - File: Clark-Sherman-26-5-09-S-232-1.RAW - Type: 2Th/Th locked - Start: 22.000 ° - End: 32.000 ° - Step: 0.020 ° - Step time: 1. s - Temp.: 25 °C (Room) - Time Started: 16 s -
Operations: Background 1.000,1.000 | Background 1.000,1.000 | Smooth 0.150 | Import

24-0025 (D) - Aragonite - $CaCO_3$ - Y: 50.00 % - d x by: 1. - WL: 1.54056 - Orthorhombic - a 5.74000 - b 4.96100 - c 2.92900 - alpha 90.000 - beta 90.000 - gamma 90.000 - Primitive - Pnma (62) - 4 - 83.

86-2336 (C) - Calcite magnesian - (Mg.129Ca.871)(CO3) - Y: 33.85 % - d x by: 1. - WL: 1.54056 - Hexagonal (Rh) - a 4.93820 - b 4.93820 - c 16.83200 - alpha 90.000 - beta 90.000 - gamma 120.000 - F

86-2334 (A) - Calcite - Ca(CO3) - Y: 97.92 % - d x by: 1. - WL: 1.54056 - Hexagonal (Rh) - a 4.98800 - b 4.98800 - c 17.06100 - alpha 90.000 - beta 90.000 - gamma 120.000 - Primitive - R-3c (167) - 6 -

89-1961 (C) - Quartz low, dauphinee-twinned - SiO_2 - Y: 18.75 % - d x by: 1. - WL: 1.54056 - Hexagonal - a 4.92100 - b 4.92100 - c 5.41600 - alpha 90.000 - beta 90.000 - gamma 120.000 - Primitive - P

Sample: S-232-2-G

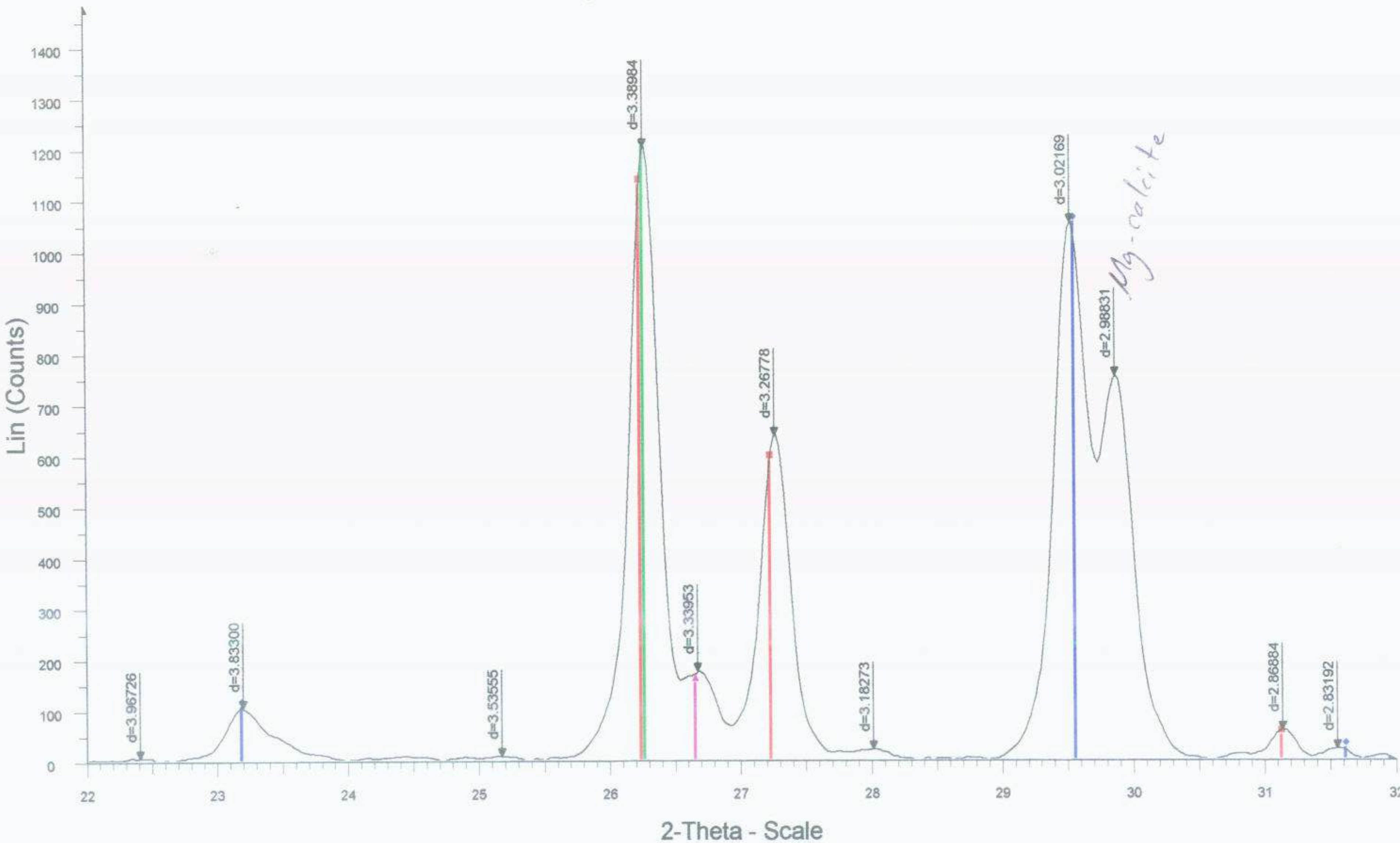

Sample: S-232-2-G - File: Clark-Sherman-26-5-09-S-232-2-G.RAW - Type: 2Th/Th locked - Start: 22.000 ° - End: 32.000 ° - Step: 0.020 ° - Step time: 1. s - Temp.: 25 °C (Room) - Time Started: 16 s - 2-T

Operations: Background 1.000,1.000 | Background 1.000,1.000 | Smooth 0.150 | Import

05-0453 (D) - Aragonite, syn - $CaCO_3$ - Y: 93.75 % - d x by: 1. - WL: 1.54056 - Orthorhombic - a 4.95900 - b 7.96800 - c 5.74100 - alpha 90.000 - beta 90.000 - gamma 90.000 - Primitive - Pmcn (62) - 4

86-2335 (C) - Calcite magnesian - $(Mg_{.064}Ca_{.936})(CO_3)$ - Y: 87.50 % - d x by: 1. - WL: 1.54056 - Hexagonal (Rh) - a 4.96730 - b 4.96730 - c 16.96310 - alpha 90.000 - beta 90.000 - gamma 120.000 - F

87-0703 (C) - Quartz high, syn - SiO_2 - Y: 100.00 % - d x by: 1. - WL: 1.54056 - Hexagonal - a 4.99770 - b 4.99770 - c 5.46010 - alpha 90.000 - beta 90.000 - gamma 120.000 - Primitive - P6222 (180) - 3

86-2237 (A) - Quartz low - SiO_2 - Y: 12.50 % - d x by: 1. - WL: 1.54056 - Hexagonal - a 4.91300 - b 4.91300 - c 5.40400 - alpha 90.000 - beta 90.000 - gamma 120.000 - Primitive - P3121 (152) - 3 - 112.

Sample: S-232-2; < 4-phi

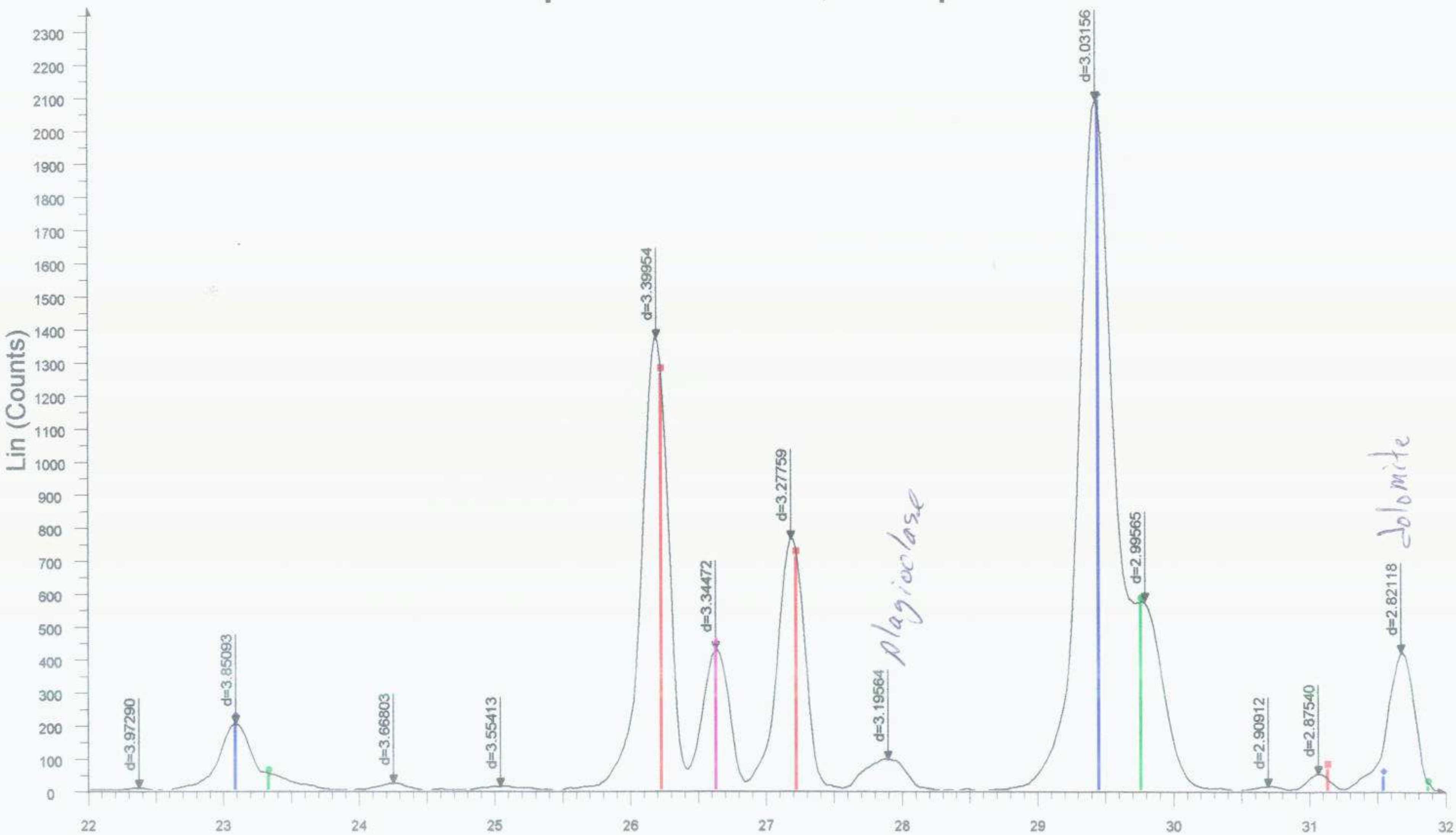

Sample: S-232-2; < 4-phi - File: Clark-Sherman-26-5-09-S-232-2.RAW - Type: 2Th/Th locked - Start: 22.000 ° - End: 32.000 ° - Step: 0.020 ° - Step time: 1. s - Temp.: 25 °C (Room) - Time Started: 16 s -
Operations: Background 1.000,1.000 | Background 1.000,1.000 | Smooth 0.150 | Import

24-0025 (D) - Aragonite - $CaCO_3$ - Y: 60.42 % - d x by: 1. - WL: 1.54056 - Orthorhombic - a 5.74000 - b 4.96100 - c 2.92900 - alpha 90.000 - beta 90.000 - gamma 90.000 - Primitive - Pnma (62) - 4 - 83.

86-2336 (C) - Calcite magnesian - $(Mg_{.129}Ca_{.871})(CO_3)$ - Y: 27.08 % - d x by: 1. - WL: 1.54056 - Hexagonal (Rh) - a 4.93820 - b 4.93820 - c 16.83200 - alpha 90.000 - beta 90.000 - gamma 120.000 - F

72-1652 (A) - Calcite - $CaCO_3$ - Y: 100.00 % - d x by: 1. - WL: 1.54056 - Hexagonal (Rh) - a 4.99000 - b 4.99000 - c 17.00200 - alpha 90.000 - beta 90.000 - gamma 120.000 - Primitive - R-3c (167) - 6 -

88-2487 (C) - Quartz low - SiO_2 - Y: 20.83 % - d x by: 1. - WL: 1.54056 - Hexagonal - a 4.93000 - b 4.93000 - c 5.38500 - alpha 90.000 - beta 90.000 - gamma 120.000 - Primitive - P3221 (154) - 3 - 113.

Sample: S-232-3; < 4-phi

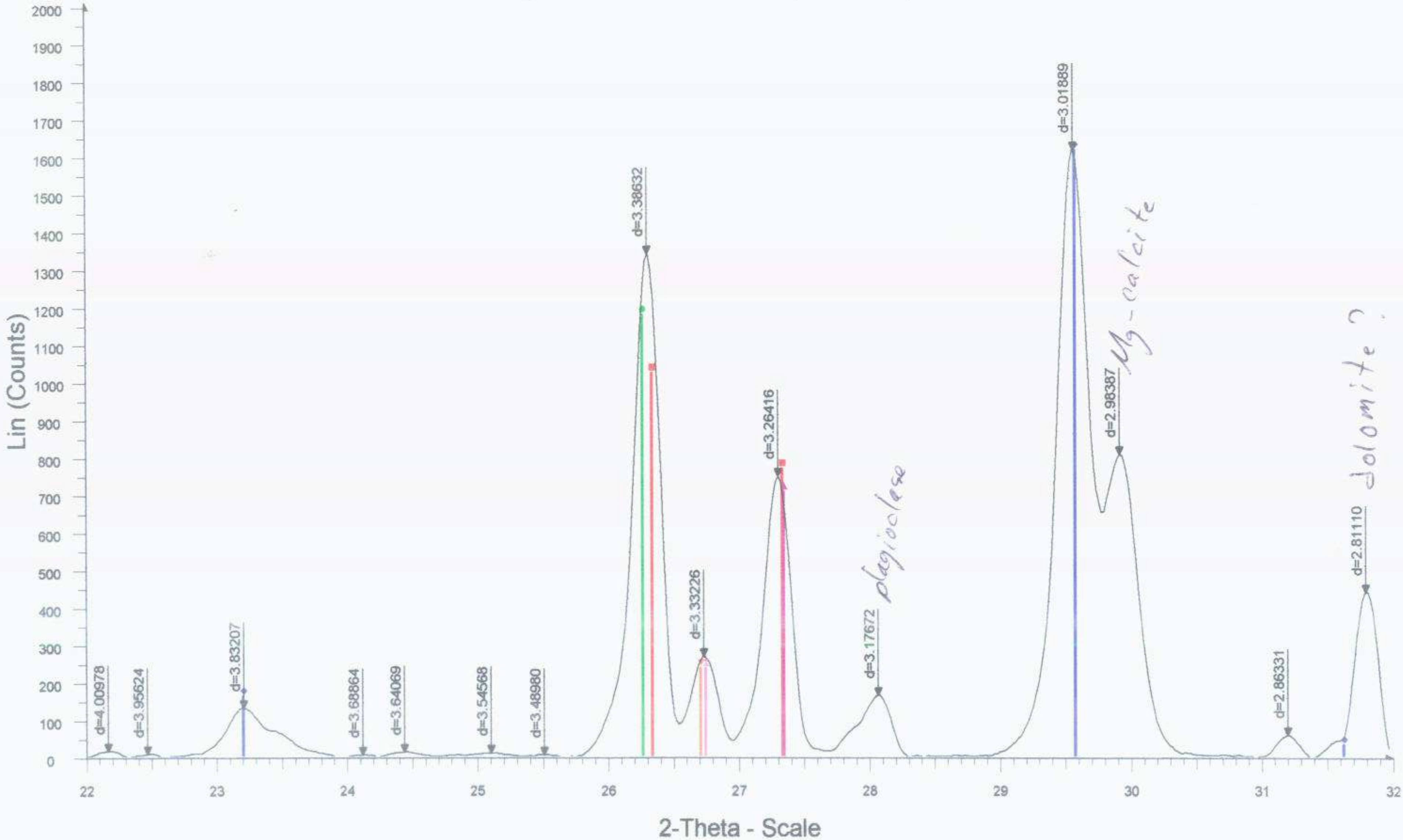

Sample: S-232-3; < 4-phi - File: Clark-Sherman-26-5-09-S-232-3.RAW - Type: 2Th/Th locked - Start: 22.000 ° - End: 32.000 ° - Step: 0.020 ° - Step time: 1. s - Temp.: 25 °C (Room) - Time Started: 16 s -
Operations: Background 1.000,1.000 | Background 1.000,1.000 | Smooth 0.150 | Import

03-1067 (D) - Aragonite - gamma-$CaCO_3$ - Y: 79.17 % - d x by: 1. - WL: 1.54056 - Orthorhombic - a 4.94000 - b 7.94000 - c 5.72000 - alpha 90.000 - beta 90.000 - gamma 90.000 - Primitive - Pnma (62)

89-1305 (C) - Magnesium calcite, syn - $(Mg_{0.06}Ca_{0.94})(CO_3)$ - Y: 100.00 % - d x by: 1. - WL: 1.54056 - Hexagonal (Rh) - a 4.96300 - b 4.96300 - c 16.95700 - alpha 90.000 - beta 90.000 - gamma 120.(

87-0703 (C) - Quartz high, syn - SiO_2 - Y: 72.92 % - d x by: 1. - WL: 1.54056 - Hexagonal - a 4.99770 - b 4.99770 - c 5.46010 - alpha 90.000 - beta 90.000 - gamma 120.000 - Primitive - P6222 (180) - 3

86-1562 (C) - Quartz low - SiO_2 - Y: 43.75 % - d x by: 1. - WL: 1.54056 - Hexagonal - a 4.77360 - b 4.77360 - c 5.30100 - alpha 90.000 - beta 90.000 - gamma 120.000 - Primitive - P3221 (154) - 3 - 104.

85-0865 (A) - Quartz - alpha-SiO_2 - Y: 14.58 % - d x by: 1. - WL: 1.54056 - Hexagonal - a 4.90000 - b 4.90000 - c 5.40000 - alpha 90.000 - beta 90.000 - gamma 120.000 - Primitive - P3121 (152) - 3 - 11

82-0511 (A) - Quartz - SiO_2 - Y: 14.58 % - d x by: 1. - WL: 1.54056 - Hexagonal - a 4.86500 - b 4.86500 - c 5.44300 - alpha 90.000 - beta 90.000 - gamma 120.000 - Primitive - P3121 (152) - 3 - 111.567